Spatial-temporal model to evaluate the system potential of concentrating solar power towers in South Africa

by
Paul Gauché

Dissertation presented for the degree of Doctor of Philosophy in the Faculty of Engineering at Stellenbosch University

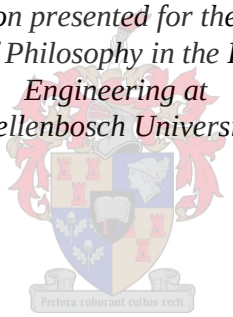

Promoter: Prof Theodor Willem von Backström
Co-promoter: Prof Alan Colin Brent

December 2016

DECLARATION

By submitting this dissertation electronically, I declare that the entirety of the work contained therein is my own, original work, that I am the sole author thereof (save to the extent explicitly otherwise stated), that reproduction and publication thereof by Stellenbosch University will not infringe any third party rights and that I have not previously in its entirety or in part submitted it for obtaining any qualification.

This dissertation includes two original papers published in peer-reviewed journals or books. The development and writing of the papers (published and unpublished) were the principal responsibility of myself and, for each of the cases where this is not the case, a declaration is included in the dissertation indicating the nature and extent of the contributions of coauthors.

December 2016

ABSTRACT

Concentrating solar power (CSP) is a relatively unknown power generation technology entering into the growth phase of its technology life-cycle. The value of CSP is relatively well understood from a state of the art point of view, but its value and potential in a power generation network is not as clear. South Africa potentially offers an accelerated market due to constrained electricity capacity and an excellent solar resource. The objective of this dissertation is to quantifiably evaluate CSP in the electricity system of South Africa and thereby aid national policy. The methodology required the development and validation of a model to predict the performance of central receiver CSP plants in an electricity system.

The Integrated Resource Plan (IRP) of South Africa legislates the definition of the national electricity system with a twenty year horizon and intended updates every two years. The IRP initiated significant renewable energy adoption, but only 1 GW of CSP is officially allocated until 2030, despite several analysis updates recommending increased capacity for CSP in scenarios based on scarcity of resources for fossil or nuclear technologies.

The spatial-temporal CSP model was developed and validated within available means to about 7 % accuracy within a standard deviation of known CSP tower settings. This model permits cascaded allocations of CSP capacity by location, plant configuration and size without being overly prescriptive to technology specification or advancements. The model is, therefore, able to comprehensively evaluate a distributed network of CSP towers within an energy system environment. A deterministic energy system model and a probabilistic economic model were developed to test the behavior of the CSP model in an energy system.

The value of CSP towers was studied in various scenarios, including an emulation of the 2010 IRP, the 2013 proposed IRP Update and scenarios commissioned by the Worldwide Fund for Nature (WWF) in South Africa. The WWF scenario resulted in a renewable-centric proposal for 2030 that includes 8 GW of CSP with 12 storage hours on average. This scenario unexpectedly outperforms other scenarios in terms of cost regardless of resource scarcity. The analysis, however, correlates with other recent research, finding that CSP capacity needs to operate only serving the system to avoid unserved power. In this mode, CSP levelized cost of energy (LCOE) increases due to a drop in capacity factor, but the marginal value of electricity (MVOE) attributable to this operating mode is R 0.48 per kWh. MVOE is introduced as a method to inform tariff policy.

The model successfully demonstrates the importance of technology, space and time within a constrained electricity system in order to fully evaluate the role of CSP towers. The evaluation itself provides initial quantified evidence that CSP has an important role for South Africa and should be pursued by investing more resources in research, planning and implementation.

UITTREKSEL

Gekonsentreerde sonkrag (GSK) is 'n relatief onbekende vorm van kragopwekking wat tans die groeifase bereik in sy tegnologie lewensiklus. Die status van GSK as baanbreker tegnologie word relatief goed verstaan, maar die waarde en potensiaal daarvan in 'n kragopwekking netwerk is onduidelik. Suid Afrika bied potensieel 'n versnelde mark aan as gevolg van beperkte elektrisiteit kapasiteit en 'n uitstekende son hulpbron. Die doel van hierdie proefskrif is om GSK binne die Suid-Afrikaanse elektrisiteitsnetwerk kwantifiseerbaar te evalueer ter ondersteuning van nasionale beleid. Die metodologie het die ontwikkeling en bevestiging van 'n model vereis om die prestasie van sentraal-ontvanger gekonsentreerde sonkragstasies in 'n elektrisiteit stelsel te voorspel.

Suid-Afrika se Geïntegreerde Hulpbronplan (GHP) wet gee die definisie van die nasionale elektrisiteit stelsel met 'n 20 jaar horison en word elke 2 jaar opgedateer. Die GHP het 'n beduidende aanneming van hernubare energie geïnisieer, maar slegs 1 GW van GSK is amptelik toegeken tot 2030 ten spyte van verskeie opgedateerde analises wat groter kapasiteit vir GSK aanbeveel het in raamwerke gebaseer op skaarstes aan hulpbronne vir fossiel of kern tegnologieë.

Die ruimtelike-temporale GSK model is ontwikkel en bewys binne beskikbare hulpbronne tot sowat 7 % akkuraatheid binne 'n standaardafwyking van bekende gekonsentreerde sonkragtoring instellings. Die model laat kaskade toekenning van GSK kapasiteit per ligging, aanleg opstelling en grootte toe sonder om buitensporig voorskriftelik te wees in terme van tegnologie spesifikasies of vooruitgang. Die model is dus in staat om 'n verspreide netwerk van gekonsentreerde sonkragtorings binne 'n energiestelsel omvattend te evalueer. 'n Deterministiese energiestelsel-model en 'n waarskynlikheids-gebaseerde ekonomiese model is ontwikkel om die GSK model gedrag binne 'n energiestelsel te toets.

Die waarde van gekonsentreerde sonkragtorings is bestudeer in verskeie scenarios, insluitend 'n emulasie van die 2010 GHP 2010, die voorgestelde 2013 GHP verbetering en scenarios in opdrag van die Wêreldwye Fonds vir die Natuur in Suid-Afrika. Die WWF scenario het gelei tot 'n hernubaar-sentriese voorstel vir 2030 wat 8 GW van GSK insluit met 'n gemiddeld van 12 uur van stoorkapasiteit. Hierdie scenario presteer onverwags beter as ander scenarios in terme van koste, ongeag hulpbron skaarsheid. Die ontleding stem egter ooreen met ander onlangse navorsing wat bevind dat GSK kapasiteit slegs in diens van die stelsel moet werk ten einde ontoegediende krag te vermy. In hierdie modus, verhoog die vergelykbare elektrisiteitskoste van GSK as gevolg van 'n daling in kapasiteitsfaktor, maar die marginale waarde van elektrisiteit toegeskryf aan hierdie modus van operasie is R 0.48 per kWh. Die marginale waarde van elektrisiteit is ingestel as 'n metode om tariefbeleid in te lig.

Die model slaag daarin om die belangrikheid van tegnologie, ruimte en tyd binne 'n beperkte elektrisiteit stelsel te illustreer ten einde die rol van gekonsentreerde sonkrag torings ten volle te evalueer. Die evaluering self bied aanvanklike gekwantifiseerde bewyse dat GSK 'n belangrike rol vir Suid-Afrika bied en dat dit deur belegging van meer hulpbronne in navorsing, beplanning en implementering nagestreef moet word.

For Ana, my life-partner.

ACKNOWLEDGEMENTS

The following people and entities are acknowledged for their contribution towards this dissertation:

My promotors, Professors Theo von Backström and Alan Brent, for their guidance, patience, availability and motivation. In particular to Theo who taught me the virtue of keeping an open mind and to explore this PhD beyond the boundaries and to Alan who brought systems thinking and collaboration contacts from the start.

Dr Stefan Pfenninger for his collaboration, help and shared enthusiasm. Also to Prof Tony Patt who sparked the collaboration with Stefan and others. Both formerly from IIASA and now at ETH Zurich.

The late Professor Detlev Kröger who provided early guidance and pointed out the need for quantifiable systems knowledge for South Africa's energy future. Prof Kröger had a steadfast vision that the SUNSPOT cycle used in the right way would offer South Africa a cornerstone to a reliable low cost electricity system with many additional benefits.

Professor Wikus van Niekerk for his enthusiasm and dedication to the cause of renewable energy and in supporting the research strengths of his colleagues and predecessors. In particular, for the financial, organizational and advisory support that made it possible to do this work.

My friends in STERG including all my past and present students, staff and colleagues who taught me as they learned and contributed to this work directly or indirectly. Specific appreciation to those having a role in this project. Cebo Silinga, Christina Auret, Sebastian Giglmyr, Leigh Pina and Justine Rudman.

The staff and network of the Sustainability Institute who really helped me see a more complex world. Specifically to the late Professor Paul Cilliers who encouraged a practical way to deliver results rather than hand-wave philosophically.

Saliem Fakir, Louise Scholtz, and Ellen Davies of WWF South Africa for sponsoring and critically reviewing the evaluation of the WWF Renewable Energy Vision. A special note to Megan Sager who provided very useful ideas and for suggesting the evaluation.

Sasol for funding my position allowing for focused CSP research in this project and in my other CSP activities. DST with impending agencies NRF and TIA for their support of CSP. GeoModel Solar for providing the SolarGIS data © 2012 GeoModel Solar s.r.o. and the various sponsors of the Wind Atlas of South Africa.

TABLE OF CONTENTS

LIST OF FIGURES ..... **x**

LIST OF TABLES ..... **xvi**

NOMENCLATURE ..... **xviii**

1 INTRODUCTION **1**

1.1 Background 1
1.2 Objective 3
1.3 Motivation 4
1.4 Delineations and research boundaries 5
1.5 Contributions 8
1.6 Dissertation structure and overview 8

PART 1: FOUNDATION **10**

2 CONCENTRATING SOLAR POWER PRINCIPLES **11**

2.1 Overall process 11
2.2 CSP classifications 12
2.3 Central receiver energy conversion principles 13
2.4 Electricity generation principles 17
2.5 CSP history and outlook 21
2.6 Commercial state of the art 21
2.7 Conclusion 23

3 GENERAL LITERATURE REVIEW **24**

3.1 Solar energy in perspective 24
3.2 The solar resource 25
3.3 The wind resource 27
3.4 Solar and weather resource analysis data types 29
3.5 Energy systems analysis model review 30
3.6 CSP systems and plant analysis model review 31
3.7 CSP in systems analysis studies 31
3.8 Conclusion 34

4 SOUTH AFRICAN ENERGY PROPOSITIONS **35**

4.1 Abstract 35
4.2 Introduction 35
4.3 Conventional and sustainable alternatives 37
4.4 CSP technology for South Africa 42
4.5 Analysis and discussion of alternatives 45
4.6 Conclusion 47
4.7 Epilogue 48

PART 2: ANALYSIS METHOD 49

5 CONCENTRATING SOLAR POWER MODEL 50

5.1 Overall methodology 50
5.2 Overall CSP plant node model 51
5.3 Central receiver definition 53
5.4 Heliostat optics 53
5.5 Receiver energy balance 65
5.6 Thermal energy storage 72
5.7 Heat engine 74
5.8 Other plant considerations 75
5.9 Integration, validation and test cases 76
5.10 Conclusion 82

6 SYSTEM MODEL 83

6.1 Overall spatial-temporal approach 83
6.2 System definition and constraints 85
6.3 Power generation 93
6.4 Result aggregation and cost analysis 100
6.5 Initial scenario testing 102
6.6 Conclusion 103

PART 3: APPLICATION AND SYNTHESIS 104

7 WWF RENEWABLE ENERGY VISION 2030 105

7.1 Background 105
7.2 Objective 105
7.3 Current electricity system and planning 107
7.4 System model 109
7.5 Scenario results 114
7.6 Scenario characteristics 118
7.7 Cost probabilities 122
7.8 Conclusion 125

8 VALUE OF CSP IN THE ENERGY SYSTEM 126

8.1 Introduction 126
8.2 WWF scenario in context 126
8.3 System meaning to research and development 132
8.4 Industrial and economic potential of CSP in Southern Africa 139
8.5 Conclusion 141

9 CONCLUSIONS AND RECOMMENDATIONS 142

9.1 Summary of findings 142
9.2 Conclusions 144
9.3 Summary of contributions 145
9.4 Policy value 146
9.5 Recommendations for future research 146

REFERENCES **148**

APPENDIX A: CONCENTRATING SOLAR POWER MODEL **160**

A.1. Electromagnetic radiation and the sun 160
A.2. Heliostat-receiver attenuation losses 163
A.3. Heliostat field parameters 164

APPENDIX B: NATURE CLIMATE CHANGE ARTICLE **167**

APPENDIX C: POLICY BRIEF **171**

C.1. Background 171
C.2. Analysis and findings 171
C.3. Recommendations 172

LIST OF FIGURES

Figure 1.1: Worldwide long term average annual DNI (Direct Normal Irradiation) (SolarGIS © 2015 GeoModel Solar) 2
Figure 2.1: Basic block diagram of concentrating solar thermal systems (adapted from Stine & Geyer (2001)) 11
Figure 2.2: Schematic layout of a central receiver CSP plant with storage 13
Figure 2.3: Solar and heliostat angles for the CSP model 14
Figure 2.4: Illustrative effect of solar multiple and storage in central receiver CSP plant 17
Figure 2.5: Heat engine Carnot theoretical limit and Novikov practical approximation efficiencies 18
Figure 2.6: Thermal receiver efficiency for various concentration ratios based on one illustrative reference condition where temperature is above ambient 20
Figure 2.7: Basic combined receiver and heat engine efficiency 20
Figure 2.8: Photo of a parabolic trough line in Andasol 3, a 50 MW parabolic trough plant with 7.5 hours of storage (Photo by author) 22
Figure 2.9: Gemasolar CSP plant, a 20 MW central receiver with 15 hours of storage (photo by author) 22
Figure 3.1: Total world energy in 2011 by solar irradiation (left axis) and anthropogenic energy consumption (right axis) (adapted from (de Rosa, 2005) and (IEA, 2013)) 25
Figure 3.2: DNI (minute-averaged and hour-averaged) at the Vanrhynsdorp (VAN) station on 1 May 2014 (source: by author (Brooks et al., 2015)) 26
Figure 3.3: GHI, DHI, wind speed and air temperature (all minute-averaged) at the Vanrhynsdorp (VAN) station on 1 May 2014 (source: by author (Brooks et al., 2015)) 26
Figure 3.4: Accuracy enhanced DNI map of South Africa (Suri et al., 2015) (SolarGIS © 2015 GeoModel Solar) 28
Figure 3.5: Wind resource map for the Western, Eastern and Northern Capes (SANEDI, 2015) 29

Figure 4.1: Capacity and energy supply to 2030 (recreated from IRP2010 and with assumptions on capacity factors to approximate the IRP annual electricity supply model) 37
Figure 4.2: Estimates of long term (ultimate) coal production in Africa (mostly South Africa) showing international survey values as well as historical estimates to the cumulative normal model. Actual and modelled cumulative production is also shown as are all recent Hubbert-style predictions (data and model adapted and used with permission by Dave Rutledge). 38
Figure 4.3: Worldwide ultimately recoverable resources (URRs) of various conventional energy resources adapted from Dale (2012). Grey squares represent mean values and the range represents 5th percentile and 95th percentile; black diamonds represent the median value of the estimates. 41
Figure 4.4: Areas of excellent solar resource (black) and the general area of anticipated shale gas exploration (red) by Meyer *et al.* (2011) 42
Figure 4.5: Photo of the state of the art 20 MWe Gemasolar plant 43
Figure 4.6: Qualitative positioning for all future electricity generation types in 2030. Horizontal axis represents capacity factor characteristics ranging from intermittent to peaking. Vertical axis represents localization potential. Bubble size is approximate annual electricity production. 46
Figure 5.1: Illustrative proportions of a CSP plant with a solar multiple (SM) of 4, 12 storage hours and a 100 MW turbine 50
Figure 5.2: Illustrative definition of nodes for proportioned capacities of CSP 51
Figure 5.3: Overall CSP model structure flow diagram 52
Figure 5.4: Schematic layout of the central receiver CSP plant for the model 53
Figure 5.5: General heliostat-receiver optics illustrated two-dimensionally. Two edge incidence and reflected cones are shown. 54
Figure 5.6: Plan view of heliostat field zones and cells (left) and one heliostat cell (right) 55
Figure 5.7: Principle heliostat blocking parameters 57
Figure 5.8: Comparison of cosine, shading and blocking vs. tower height (defined as midpoint of receiver above heliostat field) 59
Figure 5.9: Net geometric optical efficiency as function of zenith angle and solar azimuth angle for the case reported by Schell (2011) 59

Figure 5.10: Approximation for net geometric optical efficiency with each color marker representing a different solar azimuth angle per Figure 5.9 60
Figure 5.11: Cumulative annual performance impact as a function of wind cutoff speed. Sites indicated use zero cutoff performance of best site as ratio denominator. Wind probability distribution is indicated by respective dotted lines.....61
Figure 5.12: Definition of slant range for atmospheric attenuation.....61
Figure 5.13: Attenuation loss models.....63
Figure 5.14: Central receiver collector performance loss by attenuation 64
Figure 5.15: Generic representation for the receiver energy balance.....65
Figure 5.16: Receiver model correlation for radiation (left) and convection (right).66
Figure 5.17: Typical Northern Cape areas deemed likely suitable for CSP (photos by author): about 25 km west of Pofadder GPS: 29.1 °E, 19.0 °S (top), and in the region of Brandvlei GPS: 30.3 °E, 20.5 °S (bottom).....70
Figure 5.18: Wind speed profile for a reference wind speed of 3 m/s at 10 m and friction coefficients of 0.10, 0.15 and 0.20 70
Figure 5.19: Receiver model correlation for outlet energy (left) and disaggregation by incident irradiation (right) 71
Figure 5.20: Receiver energy balance model disaggregation normalized with logarithmic independent axis.....72
Figure 5.21: Comparison of some ideal and real power plant thermal efficiencies compared with Carnot and Novikov cycle efficiencies 74
Figure 5.22: Normalized annual cumulative energy conversion for a specific site 76
Figure 5.23: Temporal model behavior for various configurations over two days 77
Figure 5.24: Impact of solar multiple and storage capacity.....78
Figure 5.25: Key indicators of two low storage vs. a 15 hour storage tower 78
Figure 5.26: Duration and cumulative generation of gross power curves for storage ratings of 15 hours, 6 hours, 1 hour and a case where the solar multiple is 1 and thermal energy passes through a 1 hour storage system.....79
Figure 5.27: Simplified model of thermal and electric power 80
Figure 5.28: Location of 823 uniformly spaced CSP nodes across all of South Africa. Node grid resolution of 0.375 ° and each node indicated by a red dot. Size of dot has no meaning. (image by S. Pfenninger) 81

Figure 5.29: Model results for representative summer (top) and winter (bottom) days (plots by S. Pfenninger) 81
Figure 5.30: System whole year output for the five cases. The dip in mid-August is due to missing DNI data over that period (plots by S. Pfenninger) 82
Figure 6.1: Overall scenario system model structure and boundaries 84
Figure 6.2: Overall system model process flow 85
Figure 6.3: Annual hourly minimum, average and peak demand for a scenario scaled from the South African 2010 demand shape 86
Figure 6.4: Annual hourly minimum, average and peak demand for a scenario scaled from the South African 2010 demand shape 87
Figure 6.5: Conceptual node definition for the system model overlaid with the Eskom major Transmission Development Plan projects for 2015-2024 (background image (Eskom 2014b)) 92
Figure 6.6: Illustration of sunlight components onto a PV panel (adapted from Auret (2015)) 95
Figure 6.7: Model of five PV configurations over a three day period in early summer near Stellenbosch University 96
Figure 6.8: Behavior of PV plant output for the twelve model nodes containing 100 MW each – seven days of January 97
Figure 6.9: Combined system PV power performance indicators; capacity factor duration curve (as a fraction by ranked hour) and annual cumulative power output (as a fraction by year hour) 97
Figure 6.10: Characteristic and model validation of a wind turbine output based on hub height wind speed 98
Figure 6.11: First week of January at all wind nodes in the system and 500MW of capacity in this example 99
Figure 6.12: Combined system wind power performance indicators; capacity factor duration curve (as a fraction by ranked hour) and annual cumulative power output (as a fraction by year hour) 99
Figure 6.13: Example of the times series result of the model 101
Figure 6.14: Example of cost probability showing binned probability (bar) and cumulative distribution (line) for a scenario 101

Figure 6.15: Map identifying suitable areas for near term peaking support CSP (Silinga & Gauché, 2014) 103
Figure 6.16: LCOE cost as a function of real annual diesel cost inflation (amended from Silinga & Gauché (2014)) 103
Figure 7.1: CSP, PV and wind nodes selected for the model in this report (figure by Rudman & Silinga) 114
Figure 7.2: Typical system based LCOE values for new capacity in the WWF High scenario (and IRP Update in the case of nuclear) 117
Figure 7.3: IRP scenario showing three weeks during summer 118
Figure 7.4: WWF High scenario showing three weeks during summer 119
Figure 7.5: Summer event with poor sun 119
Figure 7.6: Sunny summer days where wind drops 120
Figure 7.7: Transition to winter with higher baseload availability 121
Figure 7.8: Deep winter characteristics 121
Figure 7.9: System pumped storage charge level for the year (WWF High), illustrating the shorter duration but frequent pumped storage usage in winter with exception of two significant winter events 122
Figure 7.10: System pumped storage charge level for the year (IRP), illustrating insufficiency in the system 122
Figure 7.11: Capacity balance for renewable, mid-merit and peaking for all 2030 scenarios 123
Figure 7.12: Annual electricity production balance for renewable, mid-merit and peaking for all 2030 scenarios 123
Figure 7.13: Cost probabilities of the scenarios using simple LCOE. The solid lines are cumulative distributions made up of probability distribution data represented by the dotted lines. Cost values use the simple LCOE technique. 124
Figure 7.14: Cost probabilities of the scenarios using simple LCOE and 50th percentile cost values 124
Figure 8.1: Winter week illustrating CSP in non-forecasting role: WWF High scenario 129
Figure 8.2: LCOE of the CSP fleet and the whole system for CSP plants with 6 or 12 storage hours as a function of system independence (or MDO) 130

Figure 8.3: Helio100 central receiver pilot at Stellenbosch University (photo of SolarPACES 2015 technical tour courtesy of Helio100 project) 132
Figure 8.4 Packed bed concept (Gauché & Louw, 2014) (image courtesy of Allen (Allen et al., 2015)) 133
Figure 8.5: Charging temperature profile of the packed bed concept (legend shows temperature in K) (Louw, 2014) 133
Figure 8.6: Cost estimation of crushed rock thermal storage (Allen et al., 2015) 134
Figure 8.7: Schematic layout of a simplified SUNSPOT CSP plant (own interpretation) 135
Figure 8.8: Results of low cost components in systems scenarios. Left column represents CSP capacity acting independent; right column represents system dependence. Top three rows plot respective LCOE results. Row four plots fulfilment for the WWF scenario. Legend represents turbine size in MW in each case. 136
Figure 8.9: Lowest cost of Big CSP & Gas vs. Big CSP with moderate gas 137
Figure 8.10 Cost probability of Big CSP case (CSP and Gas) compared with the WWF High scenario 138
Figure 8.11 CSP LCOE and Fulfilment in Big CSP case; solid lines represent system operation (MDO = 0), broken lines represent IPP operation (MDO = 1) 138
Figure 8.12: CSP residual duration curves 139
Figure 8.13: Spider diagram for the value of CSP in Southern Africa (Gauché, Brent & von Backström, 2014) 140
Figure A.1: Basic sun – earth relationships (adapted from Duffie & Beckman (2006)) 160
Figure A.2: Solar spectral distribution for extraterrestrial, sea level standard (AM1.5) and blackbody equivalent (adapted from (NREL, 2011e)) 161
Figure A.3: Receiver thermal loss increase as percentage and flux for a 1 °C reduction in surrounding temperature from a 30 °C ambient 162
Figure A.4: CSP model representation of specular and macro reflector behavior ... 163

LIST OF TABLES

Table 2.1: Generally accepted CSP technology types....12
Table 3.1: Primary energy supplies (adapted from de Rosa (2005)) 24
Table 4.1: Summary of Africa peak and ultimate dates and quantities for coal using Hubbert-style analyses....39
Table 5.1: Typical environmental based optical values....60
Table 5.2: Receiver energy balance variable value range settings 67
Table 5.3: Friction coefficients for Hellman exponential law (Bañuelos-Ruedas, Angeles-Camacho & Rios-Marcuello, 2010) 69
Table 5.4: Parameters for a high temperature thermal storage unit....73
Table 5.5: Other parameters of CSP plant model 75
Table 6.1: Solar data specification....93
Table 6.2: Wind data specification 93
Table 6.3: PV model values....95
Table 7.1: The planned capacities for 2030 according to the Base-Case scenarios of the IRP 2010 and IRP Update, as well as the WWF High and Low Demand scenarios (Department of Energy, 2011, 2013b; WWF-SA, 2014)....106
Table 7.2: The existing generation capacity in South Africa; these values are as given in the IRP Update and might differ slightly to those given by Eskom (Eskom, 2011b; Department of Energy, 2013b)....107
Table 7.3: The multiples used to calculate hourly demand for 2030....110
Table 7.4: A summary of costs and technology characteristics for the options included in the proposed WWF scenarios. Sources: (Department of Energy, 2011, 2013b; Black & Veatch, 2012; IRENA, 2012a,b,c; WWF-SA, 2014); Own analysis....111
Table 7.5: Capacity summary for the original scenarios and the resulting cost reduced scenarios 115
Table 7.6: Summary of primary performance and cost....116
Table 8.1: Capacity allocation of the IRP, draft IRP Update and WWF High scenarios 127
Table 8.2: CSP component costs in the WWF vision....127
Table 8.3: Primary CSP model capabilities, behaviors and limitations....128
Table 8.4: Performance and cost indicators for CSP operating mode 131

Table 8.5: CSP component costs for SUNSPOT 135
Table A.1: Combined cosine, blocking and shading efficiencies 164
Table A.2: Shading efficiencies 165
Table A.3: Blocking efficiencies 165
Table A.4: Cosine efficiencies 166

NOMENCLATURE

Symbol	Description	Unit
a	Area (partial)	m^2
am	mean attenuation coefficient	-
A	Area	m^2
A	Availability	-
A_C	Area of cell	m^2
A_{Ch}	Aperture area of heliostat	m^2
B	Angular day of the year	°
B_a	Blocking altitude	m
C	Heliostat cell position	-
C_f	Capacity factor	-
C_p	Specific heat	kJ/kg.K
C_p	Coefficient of performance (wind turbines)	-
C_R	Concentration ratio	-
C_1	3.742 x 10^8	W $\mu m^4/m^2$
C_2	1.4389 x 20^4	μmK
CX	Capital cost	$ or R
CC	Construction cost	$ or R
D	Diameter	m
d	Attenuation decay value	-
d	area weighting or density ratio	-
d	Heliostat density per model cell (usually 1 or 0)	-
d_A	Heliostat aperture density	-
E	Electricity production	Wh
E	Equation of time	hr
F	Fuel cost	$ or R
f	Slant range	m
G	Irradiance	W/m^2
G_{sc}	Solar constant (1,367)	W/m^2
H	Height (mast, receiver, etc)	m
H_d	Heliostat distance to base of tower	m
h	Convective heat transfer coefficient	W/m^2K
I	Solar Irradiation	Wh
I	Investment cost	$ or R
kD	Transmission loss coefficient	-
L	Longitude	°
M	Maintenance cost	$ or R
MF	Fixed maintenance per year	$/yr or R/yr
MV	Variable maintenance per year	$/yr or R/yr
n	Day of the year	year day
P	Power	W
P	Pitch	m
PA	Power availability aggregated over 1 hour	kWh
P_r	Rated power aggregated over 1 hour	kWh
Q	Energy	J
R	Receiver height	m

R	Thermal insulation loss coefficient	$W/m^2.K$
r	Radius	m
r	discount rate	%
S	Slant range	m
SC	System surplus	kWh
SD	System demand	kWh
SU	System shortfall	kWh
$\hat{\boldsymbol{s}}$	Unit vector of incident solar radiation	-
T	Temperature	°C or K
T	Height of tower to midpoint of receiver	m
T_a	Dry bulb ambient temperature	°C
TI	Total interest cost	$ or R
T_w	Wet bulb ambient temperature	°C
t	Time	hr or s
t	Investment time	yr
$\hat{\boldsymbol{t}}$	Unit vector of reflected solar radiation to tower	-
v	Velocity	m/s
UE	Unserved energy	Wh
V	Volume	m^3
W	Receiver width or diameter	m
x	Distance in coordinate field	m
α	Absorptivity	-
α	Friction coefficient for exponential law model	-
α_s	Solar altitude angle	°
α_s	Solar absorptivity	-
β	Slope of surface of interest	°
γ	Surface azimuth angle	°
γ_s	Solar azimuth angle	°
Δ	Difference	-
δ	Declination	°
δ	Temperature correction coefficient	-
ε	Emissivity	-
σ	Stefan –Boltzmann constant (5.67×10^{-8})	$Wm^{-2}\ K^{-4}$
σ	deviation (for attenuation sky clarity)	-
η	Efficiency	-
η_θ	Cosine efficiency	-
η_b	Blocking efficiency	-
η_s	Shading efficiency	-
θ	Angle of incidence and reflection	°
θ_z	Zenith angle	°
λ	Wavelength	m
μ	viscosity	Ns/m^2
ρ	density	kg/m^3
τ	Reflection angle of image to horizontal	°
τ	Transmission loss (Lambert's Law)	m^{-1}
ϕ	Latitude	°
Ω	Cone angle	°
ω	Hour angle	°

Subscript

a	atmospheric (Attenuation)
a	availability
air	air
amb	ambient
at	atmospheric attenuation
au	heliostat aperture per unit
b	beam (direct normal)
b	blocking
B&M	Ballestrín & Marzo
C	Cell
Carnot	Carnot (Thermodynamics)
Ch	cell heliostat aperture
c	cosine
clear	Clear sky (Attenuation loss)
du	Field density
FTR	Full Turbine Rating
H	High (temperature reservoir)
h	hour
hazy	Hazy sky (Attenuation loss)
hm	outermost heliostat (for slant range)
hr	heliostat-receiver
i	incident
i	increment
j	increment
L	Lambert's law (Transmission)
L	Low (temperature reservoir)
m	maximum (cutoff)
m	mean (Attenuation loss)
N	Novikov
net	Net
node	Grouping of capacity by location and technology
o	Baseline
optical	Optical
plant	Individual power plant
power	Power
R	Receiver
Raa	Net attenuation (for attenuation of a tower)
Ro	field receiver intercepted optical component
Roa	Annual weighted field receiver optical component
r	Reflector
r	reflected
ref	reference (condition/specification)
ro	receiver intercepted optical component per cell
rh	Receiver from heliostat
rn	Receiver normal
s	Shading
s	Soiling
s	Storage

s	System
sc	Storage charge
so	Storage out
si	Storage in
st	Standard (time)
spill	spillage
t	time in years (for LCOE)
t	tracking
technology	Type of power generation plant
tu	tower unit
x	x-coordinate
y	year (can be long term average)
y	y-coordinate
z	z-coordinate

Abbreviations

ACC	Air-Cooled Condenser	
AU	Astronomical unit (1.495e11 m)	m
BOP	Balance of Plant	
CA	California	
CAPEX	Capital expenditure	
CCGT	Combined Cycle Gas Turbine	
CDF	Cumulative Distribution Function	
CFD	Computational Fluid Dynamics	
CO_2	Carbon Dioxide	
COUE	Cost of Unserved Energy	
CSIR	Council for Scientific and Industrial Research (RSA)	
CSP	Concentrating Solar Power	
CST	Concentrating Solar Thermal	
CRS	Central Receiver System	
DESERTEC	DESERTEC Foundation (desertec.org)	
DLR	Deutschen Zentrum für Luft- und Raumfahrt (German Aerospace Centre)	
DOE	Department of Energy (RSA)	
DNI	Direct Normal Irradiation	W/m^2
DHI	Diffuse Horizontal Irradiation	W/m^2
ETSAP	Energy Technology Systems Analysis Program	
GCCA	Eskom Generation Connection Capacity Assessment	
GIS	Geographical Information System	
GHI	Global Horizontal Irradiation	
HRSG	Heat Recovery Steam Generator	
HTF	Heat Transfer Fluid	
HX	Heat Exchanger	
IEA	International Energy Agency	
IEP	Integrated Energy Plan (RSA)	
IPP	Independent Power Producer	
IRP	Integrated Resource Plan (RSA)	
IRENA	International Renewable Energy Agency	
KAMM	Karlsruhe Atmospheric Mesoscale Model	

LCOE	Levelized Cost of Energy (or Electricity)	$/kWh or R/kWh
MDO	Minimum Demand Override	
MENA	Middle East and North Africa	
MGT	Micro Gas Turbine	
MVOE	Marginal value of electricity	$/kWh or R/kWh
MTS	Main Transmission System	
NDP	National Development Plan (RSA)	
NOAA	National Oceanic and Atmospheric Administration (USA)	
NPC	National Planning Commission (RSA)	
NREL	National Renewable Energy Agency (USA)	
OCGT	Open Cycle Gas Turbine	
OPEX	Operating expenditure	
OSeMOSYS	Open-Source energy MOdelling SYStem	
PV	Solar Photovoltaic	
PLEXOS	Energy Exemplar Integrated Energy Model	
PDF	Probability Distribution Function	
REIPPP(P)	Renewable Energy Independent Power Producers Procurement Programme (RSA)	
REMix-CEM	Renewable Energy Mix-Capacity Expansion Model	
RSA	Republic of South Africa	
SADC	Southern African Development Community	
SAM	System Advisor Model (NREL)	
SANEDI	South African National Energy Development Institute	
SAURAN	Southern African Universities Radiometric Network	
SAWS	South African Weather Service	
SATIM	South African TIMES Model	
SEGS	Solar Energy Generating Systems	
SLO	Storage Limit Override	
STERG	Solar Thermal Energy Research Group, Stellenbosch University	
SUNSPOT	Stellenbosch University Solar Power Thermodynamic (cycle)	
SM	Solar Multiple	
SWITCH	UC Berkeley Integrated Solar, Wind, Conventional and Hydroelectric Generation and Transmission Planning Model	
TIMES	The Integrated MARKAL-EFOM System	
TMY	Typical Meteorological Year	
TRNSYS	University of Wisconsin transient thermodynamic simulation	
US(A)	United States of America	
US-DOE	United States Department of Energy	
UTC	Coordinated Universal Time	
WASA	Wind Atlas of South Africa	
WM01-10	WASA Wind Masts	
WWF	Worldwide Fund for Nature (World Wildlife Fund)	
WWF-SA	Worldwide Fund for Nature – South Africa	

Other

R	South African Rand (ZAR)
$	United States Dollar (USD)

1 INTRODUCTION

Concentrating solar power (CSP) is a relatively unknown power generation technology entering into the growth phase of its technology life-cycle. The value of CSP is relatively well understood from a state-of-the-art point of view, but its value and potential in a power generation network is not as clear. The complexities arising from a rapid transition in electricity networks towards intermittent energy resources and energy storage compound the need for systems based forecasting and knowledge.

A comprehensive investigation of CSP in a grid-connected system is the subject of this dissertation and is introduced in this chapter. The introduction as with the majority of the text assumes that the global energy, climate and sustainability status quo and outlook are well understood, thus not requiring elaboration. The system value and potential of CSP is investigated for the case of South Africa, but the methods are intended to be generally applicable.

1.1 Background

CSP is a class of power generation technology with several sub-types or variants that are distinctly different, but all share key attributes that label them as CSP technologies. CSP plants are characterized by the concentration of sunlight that is converted to high temperature thermal energy for direct or indirect operation of a heat engine and electricity generator. The initial conversion to thermal energy arguably enables the sensible and intrinsic potential for hybridization, addition of storage and the dual exploitation of electricity and thermal energy (heat).

CSP is a relatively immature technology compared with solar photovoltaic (PV) technology and most other electricity generating technologies. Total worldwide installed CSP capacity exceeded 1,000 MW in late 2011 (IRENA, 2012a). By late 2013, it had more than doubled to around 3,000 MW (NREL, 2013), and it reached almost 4,800 MW at the end of 2015 (REN21, 2016). By comparison, PV has seen continued growth for a longer period of time with the worldwide installed capacity exceeding 67 GW in 2011 (IRENA, 2012b) and reaching about 227 GW at the end of 2015 (REN21, 2016).

A number of interrelated factors are generally attributed to the slower adoption of CSP. Primary amongst these is the historic and contemporary inability to scale modularly due to the thermo-economically driven inverse relationship between generating cost and plant size. The more recent addition of meaningful thermal storage countered by the apparent lack of market need for the benefits of dispatchable power offered by CSP also threatens a cost reduction and growth spiral typical of new technologies (IEA, 2014).

Contemporary South Africa, however, potentially offers an accelerated market

adoption potential due to a confluence of factors, including a need for electricity capacity and the excellent solar resource found in large parts of the country.

South Africa and much of the southern African region experiences a solar resource that can be considered amongst the best worldwide. The amount of direct sunlight, quantified by the Direct Normal Irradiation (DNI) exceeds 2,000 kWh/m² per year in most parts of South Africa with areas in the Northern Cape averaging close to or above 3,000 kWh/m² annually. Figure 1.1 is a long term annual average DNI map derived from satellite data showing most of the world rated on the quality of DNI at the surface (GeoModel Solar, 2015).

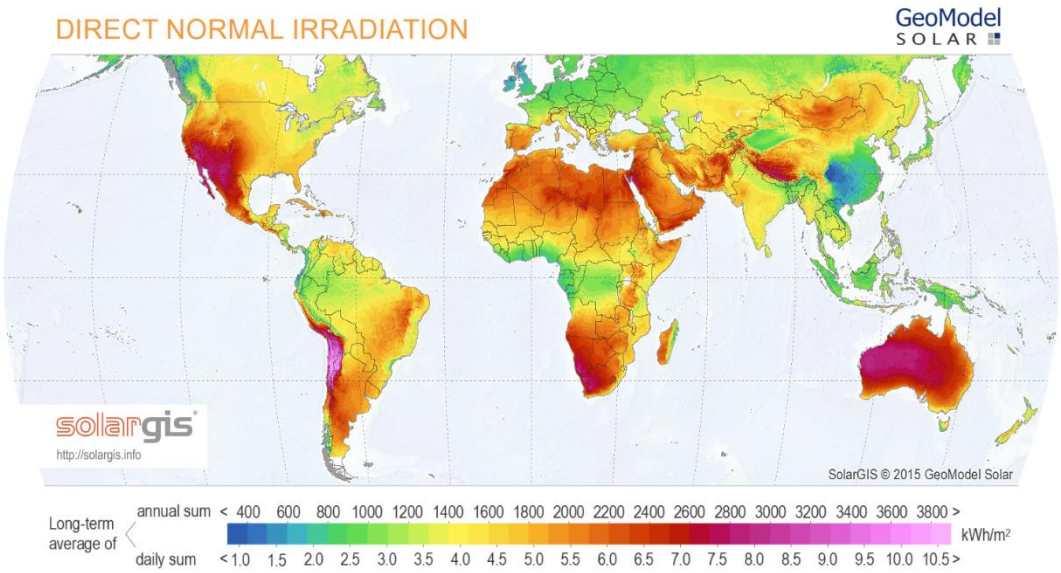

Figure 1.1: Worldwide long term average annual DNI (Direct Normal Irradiation) (SolarGIS © 2015 GeoModel Solar)

Fluri (2009) estimates the short term potential for CSP in South Africa based on an analysis of suitable land near existing transmission infrastructure to be in excess of 500 GW; that is more than an order of magnitude greater than the total generating capacity of Eskom, the South African state utility company.

The secure supply of electricity is considered to be an important component in the nexus that defines the broader transformation of South Africa in the early part of the twenty-first century. A serious effort to deal with poverty, inequality, climate, water, food security and energy security is ongoing and legislated almost continuously. In the energy sector, the Integrated Resource Plan of 2010 (2010 IRP) (Department of Energy, 2011), which sets a twenty year legislated electricity plan and the resulting implementation for renewable power generation, the Renewable Energy Independent Power Producers Procurement program (REIPPPP) (Department of Energy, 2012), is resulting in a rapid evolution of the power generation system.

The added renewable energy capacity since the inception of the REIPPPP has been

welcomed in the wake of the resurfacing electricity capacity crisis since 2014 when rolling power cuts (termed load-shedding in South Africa) became the norm. The Council for Scientific and Industrial Research (CSIR) estimated that renewable energy contributed significantly to the alleviation of load-shedding and resulted in a marginal benefit to the economy of R 800 million after payment of tariffs in the first year that REIPPPP projects started to produce power (CSIR Energy Centre, 2015).

CSP is allocated a relatively small fraction of renewable energy in the 2010 IRP, mostly due to cost and maturity risk (Department of Energy, 2011). Despite this limitation, an acceleration of CSP allocation has occurred, and a two-tiered tariff structure has been established in recognition of the value that CSP is able to produce in the evening peak (Department of Energy, 2013a). At the time of writing, the 2010 IRP has not been officially updated, and CSP allocation remains limited to about 1 GW until 2030 while nuclear power remains prioritized to provide a stable baseload and the majority of South Africa's reduction of greenhouse gas emissions. While CSP is considered by many to be a good match for South Africa, there is insufficient quantifiable evidence to verify the value and potential of the technology.

1.2 Objective

The overarching objective of this dissertation is to develop a method to quantifiably evaluate the value and potential of CSP for South Africa's future electricity system with the intention to provide a better technology perspective for guiding national policy.

The evaluation needs to be appropriately representative of the technology in a grid connected electricity system. The relevant timeframe is from the present to 2030 with limited consideration for the midpoint and end of the current century. While first and foremost a technology based dissertation, a comprehensive investigation of the energy system is needed to make realistic proposals. Accordingly, a survey and investigation in tangential areas such as infrastructure, industrial potential, energy resource and carrier supply, cost and risk are included.

The dissertation, therefore, attempts to holistically evaluate CSP in the system. This is managed by the following methodological sub-objectives:

- Development of a set of propositions for the value of CSP in the South African context through a synthesis of literature relating to CSP, systems analysis and South African energy planning.
- Development and validation of first principle mathematical models to predict the performance of CSP plants. The models should be capable of accurately determining hourly generation of electricity based on any location or high level plant specification. The model needs to have a small number of inputs and solve efficiently in large systems models.
- Identification and testing of scenarios for evaluating the propositions and in seeking optimal use of the technology in the short term and for the future.

- Explore potential limits for the exploitation of CSP in South Africa based on the models, scenarios and regional resources.
- Explore the industrial potential and opportunity for CSP in South Africa. Optionally develop a national R&D strategic plan for CSP including the potential delivery of a CSP pilot or research facility.

1.3 Motivation

South Africa is undergoing multiple transitions simultaneously as a consequence of global constraints such as climate change and the worldwide supply and demand of increasingly scarce resources as well as internal trade-offs between poverty alleviation, economic growth and other priorities resulting from a recent transition to democracy.

The National Development Plan for 2030 (NDP) (National Planning Commission, 2012) acknowledges these challenges and opportunities comprehensively. The NDP is expected to be recognized by more specific plans and in law over time. The provision of renewable energy and electricity is addressed and impacts the majority of challenges, including climate change, creation of jobs, development of skills and infrastructure, environmental sustainability, and resilience.

While CSP has been identified as a viable dispatch based supplier of electricity and other services in an increasing number of publications, the technology is only entering the growth phase of the technology lifecycle (Grobbelaar, Gauché & Brent, 2014). Accordingly, CSP is not well understood not only from a technology point of view but also for its potential role in an electricity and energy system. While CSP is expected to reduce in cost significantly over time, the combination of cost and lack of experience could unnecessarily block an opportunity as articulated by the set of propositions in this research.

The systems analysis therefore seeks to expose the value that CSP may hold for South Africa and, to some degree, for the region. A secondary but not insignificant motivation is that first principle mathematical models should form a foundation of research when a region explores a new technology. While a survey of available methods is necessary and existing models might be applicable, this research explicitly targets the development of a systems based model for CSP in order to contribute to the foundation of knowledge in the region.

Initial factors motivating the CSP propositions that are elaborated in Part 1 are summarized here.

Traditionally low electricity costs have increased steadily in recent years while South Africa has a critically low and diminishing electricity reserve margin in part as a result of public funding priorities elsewhere (Heun et al., 2010). The majority of electricity is produced by large efficient coal power plants adjacent to coal mines. Together with

1 nuclear power plant, the majority of electricity is supplied by large baseload (high capacity factor) power plants that typically do not operate effectively at part-load or reduced capacity factor. The IRP mandates significant new renewable energy capacity to be added to the electricity system. The majority of this is wind and PV that, while more mature than CSP, offers little to no firm capacity (the level of capacity that can reliably be guaranteed at any time) according to the IRP. This implies that almost all renewable energy capacity requires backup generation (Department of Energy, 2011).

The potential for hydro-power and pumped storage is limited in South Africa (Department of Energy, 2011). Coal resource estimates vary considerably but are showing signs of near term supply constraints (Rutledge, 2011). Nuclear power has been prioritized in the 2010 IRP as the primary greenhouse gas alternative. Long lead times and various uncertainties suggest that relying on new nuclear power capacity is a risk factor (Department of Energy, 2013b).

The solar resource in South Africa vastly exceeds the current needs as well as those forecasted, even when factoring in conversion and land use efficiencies for CSP (Fluri, 2009). This is also true for PV, notwithstanding the inability to store energy at large scale. The wind resource of South Africa is intermittent and, in economically viable regions, not sufficient to supply all national needs (Hagemann, 2008).

1.4 Delineations and research boundaries

While the scope of research is comprehensive and has elements of multidisciplinarity, the objectives are constrained sufficiently to enable tangible outcomes in a single dissertation. The overall research method, however, required careful consideration due to the complex nature of the topic and was guided by the following investigations during planning.

1.4.1 Systems dynamics and complexity

The first risk identified in this research relates to the complexity of systems and the related multidisciplinary nature of studying systems.

An exposition of the related disciplines of systems dynamics, complexity and transdisciplinary research is omitted, and these methods are not formally used in this study. The relevance and outcomes of the study, however, are assumed to be more valid and useful with some consideration of these disciplines. This is particularly important for the case where CSP is considered part of a sustainable future given the strong ties between sustainability and holism (Cilliers, 2011).

Elements of complexity theory guided the research method and are introduced in summary in order to clarify a significant delineation in this dissertation.

There is no specific definition for a system that is complex; rather, complexity theory offers a variety of descriptions and attributes. According to Cilliers (1998), complex

systems cannot be expressed by reductionist methods typically used in science and engineering. A corollary of this is that an engineered solution that predictably or deterministically works is not complex, but rather complicated. A CSP plant, for instance, would be considered very complicated but not complex in its design. Complexity exists in biological and social systems; therefore, the choices we make, such as electing to construct a CSP plant instead of an alternative renewable energy system, are not as predictable. In order to understand the extent of CSP in an electricity network in 2030, we would need to simulate a complex system.

Several paradoxes are presented in complexity theory of which two are important for this research method. Firstly, true complexity is impossible to simulate and very difficult to simulate sufficiently well. Secondly, the greater the degree of accuracy in simulating a complex system, the less we actually learn about it. A perfect simulation supposedly ends up being as complex as the system itself and such simulation is neither achievable nor enlightening.

Cilliers (2011) suggested that this study would not benefit from complex models or methods but rather should recognize complexity and address the objectives by using several different analytical approaches. In this way, potentially useful knowledge is tangible rather than the alternative, which would amount to varying degrees of accuracy in methods such as neural network models, none of which would necessarily offer insight regarding validity or reason.

First principle reductionist and behavioral modeling techniques were selected, but additional analysis types such as probabilistic theory, sensitivity analysis, synthesis of multiple sources of data for purposes of validation and understanding were used as appropriately needed. This additionally implies that the research method is centered on engineering and technology. The outcomes of the work are intended to support policy, economics and sustainability, but the research does not include methods in these disciplines.

1.4.2 Maturity and forecast of CSP

For reasons already given, CSP has not fully demonstrated lifecycle value or competitiveness. In Part 1, the state of the art will be clarified in more detail, but the reality is that very little publically available data exists to support the power plant and systems value performance that needs to result from this research.

The validity of the methods, therefore, relies on the degree to which validation can be performed, and this mostly comprises a blend of validating aspects within the integrated technology using various methods and sources. Additionally, three major assumptions are made about CSP technology in the timeframe applicable.

Central receiver systems (CRS) are expected to represent the future of CSP based on popularity amongst the expert community (IEA, 2010; Kolb et al., 2011), at least in the applicable timeframe. Accordingly, the research exclusively focusses on the CRS

CSP technology. CRS are capable of greater efficiency and in combination with other forecast virtues, permit hourly averaged steady-state thermodynamic analysis to be valid in combination with appropriate heat transfer modeling of thermal storage.

Within CRS based CSP, the diversity of solutions in the market is likely to remain significant for some time. For example, a transition from steam turbines to gas turbines or supercritical CO_2 turbines or any combination of combined cycle will probably echo the diversity currently seen in reflector systems, receiver technologies and heat transfer fluids. To satisfy the objective of the study, each component of a CSP system was mathematically set to the lowest common denominator for that component in an agnostic manner. This implies that a heat engine is treated using a practical but generic method only sensitive to the parameters crossing its boundary rather than specifying the heat engine cycle in the model. While this might suggest model limitations, the intention is that the model is able to test fundamental component sensitivities in a systems model context. Similar techniques are applied to the reflector, receiver, storage, generator, environmental and integration components of the model, assuming that the benefits outweigh the drawbacks for systems analysis, which in turn can appropriately guide component choices in more sophisticated models. This flexibility in the model is intended to expose improvements to the technology that would not have been considered rational outside of a systems definition.

1.4.3 Maturity of systems analysis for renewable energy systems

The adoption of renewable energy as a significant share of power production is a fairly recent occurrence in most countries. The rate of adoption of renewable energy in South Africa is unusually high.

Part 1 explores energy systems analysis in some depth. There is no universal model for electricity systems containing significant intermittent renewables. As will be explored later, the model needs to sufficiently address time and space, a capability that does exist in some available modeling systems. It also needs to accommodate for synchronous temporal data and allow for flexible dimensioning of CSP plants within the spatial definition. This combination of capabilities is a firm requirement of the project.

The objective called for a greater understanding of the role of CSP in the system; this resulted in a decision to develop a new model from the start rather than use available systems analysis tools. Additionally, the model needed to be suitable and accurate but simple and fast to compute in order for the model methods to be useful in existing energy systems analysis tools.

1.4.4 Scenario forecasting

Forecasting reasonable outcomes of a complex system is per definition difficult to get right consistently. This dissertation required forecasting of the 2030 electricity

system that may incorporate a technology that we don't know sufficiently enough about at present; nor do we know contingencies for other technologies, resources, policy and implementation. The method needed to be able to handle forecasting scenarios whereby the assumptions and uncertainties of the technologies and the environments that they are in are preferably quantified and handled without loss of the uncertainties. At the same time, modeling of scenarios needed to be fast and reduce results to the fewest number of measures.

1.4.5 Method vs. data and subject accuracy

Satisfying the objective of the study required accuracy in analysis and data. While all efforts were used in the acquisition of good data, the objective required, above all else, an appropriately defined analysis method. The analysis method used is only applicable for systems analysis. While the method could conceptually perform analysis at a single plant level, it is not intended for CSP plant design.

1.5 Contributions

Two primary contributions were expected from this dissertation. Firstly, the development of an analysis method capable of determining the systems impact of a central receiver CSP. This impact needed to account for the temporal, spatial, dimensioning, incentivizing and cost consequences of CSP. These consequences needed to be measurable in order to quantify the propositions made in the study.

The second primary contribution was to evaluate the value and potential of CSP for South Africa leading to 2030 by means of the analysis method in combination with a comprehensive assessment of the economic opportunity. This evaluation should contribute quantifiable knowledge to the South African public and policy community through appropriate peer review publications.

1.6 Dissertation structure and overview

The dissertation is a compilation of published peer review journal articles, conference proceedings, contracted research and original chapters. In the case of chapters based on publications, formatting, content and language changes have been made to improve the consistency and flow of the dissertation. In order to offer better structure, this compilation is divided into three parts.

Part 1: Foundation

Chapter 2 introduces CSP technology with a short overview of the basic principles, classifications, history and outlook.

Chapter 3 presents a general literature review, mostly covering literature relating to the state of the art in systems analysis relevant to CSP and other review matter not covered in other parts.

Chapter 4 presents a published work on the propositions made in this dissertation. A review of the energy system of South Africa is comprehensively covered.

Part 2: Analysis model

Chapter 5 summarizes the CSP model developed for this dissertation and presents early applications.

Chapter 6 summarizes the systems model developed to test the dissertation propositions. This chapter also includes a summary of models for other technologies used in the system model.

Part 3: Application and synthesis

Chapter 7 presents the primary systems analysis conducted for the research. The chapter is primarily an abbreviated version of a report prepared for the Worldwide Fund for Nature (WWF).

Chapter 8 presents derivative investigations of the WWF systems analysis to explore the behavior and challenges of CSP in energy systems.

Chapter 9 summarizes the dissertation findings, conclusions, contributions and recommendations for future research. The chapter also introduces a policy brief.

PART 1: FOUNDATION

Part 1 of the dissertation provides a contextual basis for the method in Part 2 and the application and synthesis in Part 3.

The principles of CSP are introduced in order to explore the technology, the state of the art and the constraints of the technology.

The literature review more specifically covers the state of the art in analysis methods for CSP plants and energy systems analysis.

Part 1 concludes with a more comprehensive exploration of the value proposition of CSP in the South African context, which sets the tone for the choices made in the rest of the dissertation.

2 CONCENTRATING SOLAR POWER PRINCIPLES

This chapter presents the high level principles of CSP with specific reference to the central receiver technology applicable to the model described in Part 2. These principles and a brief review of the history and outlook of central receivers is also intended to provide context to the remainder of Part 1.

2.1 Overall process

Solar thermal energy systems is a broad technology category involving the conversion of sunlight to thermal energy in order to supply thermal energy, electricity or both. Concentrating solar thermal (CST) energy is a classification within solar thermal energy characterized by the increase of solar radiation flux density in order to achieve higher temperatures and efficiencies. Figure 2.1 illustrates the basic elements and conversions involved from source to demand in CST.

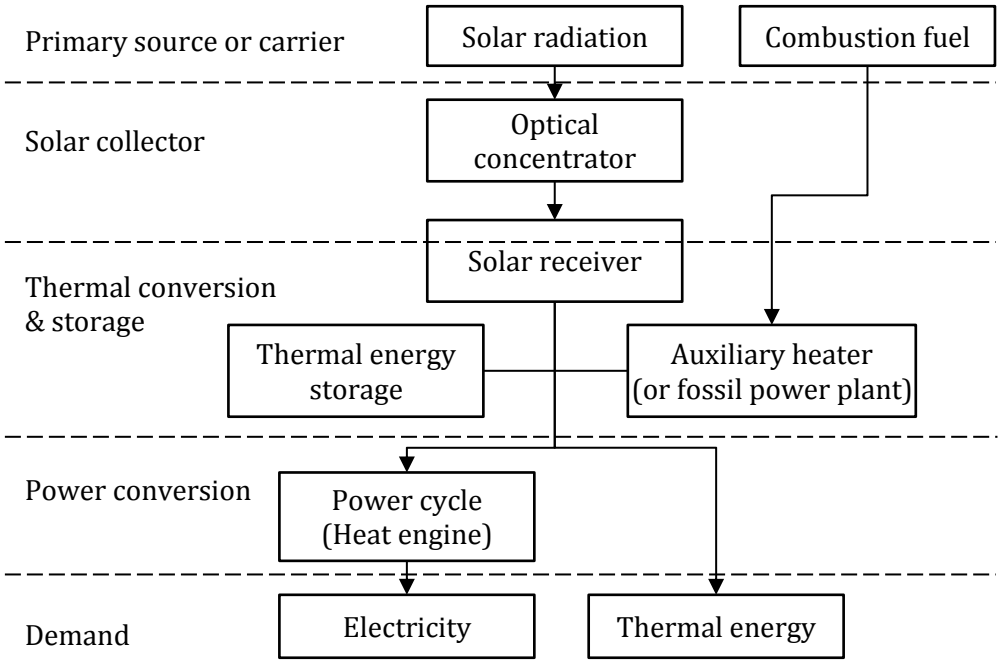

Figure 2.1: Basic block diagram of concentrating solar thermal systems (adapted from Stine & Geyer (2001))

There is no consensus regarding the definition or use of names in solar thermal energy systems. For the remainder of this dissertation, CSP is the term that defines such concentrating solar technologies that are intended mostly for the generation of electricity. Several key characteristics can be observed from the basic elements in the source-to-demand process in CSP.

CSP has a relatively high number of distinct components, making it a complicated

technology. While this is a drawback, the technology offers versatility in application to suit demand.

The conversion initially to thermal energy differentiates CSP from the other major renewable energy technologies such as hydropower, wind power and PV. This conversion process offers intrinsic compatibility with thermal hybridization and thermal storage as illustrated in Figure 2.1. Hybridization can take the form of auxiliary fossil fuel heating in CSP plants or augmentation of solar energy in existing or future conventional power plants. These various combinations allow for sharing of components or resources, theoretically offering cost advantages (IEA, 2014).

Thermal storage takes place prior to power conversion, thus enabling a cost tradeoff between the storage and downstream components which include the heat engine, generator and transmission equipment. This implies that storage does not proportionally add to the cost of a CSP plant, it can actually reduce the cost of power production in the case where the thermal storage is increased in exchange for a smaller turbine and generator.

2.2 CSP classifications

There are four generally accepted CSP technology types, characterized by the method of concentrating sunlight and summarized in Table 2.1.

Table 2.1: Generally accepted CSP technology types

	Focus type	
Reflector type	Line focus (single axis, 2D concentrating)	Point focus (2 axis, 3D concentrating)
Continuous (continuously curved to axes)	**Parabolic trough** 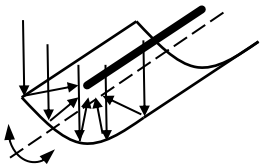	**Parabolic dish** 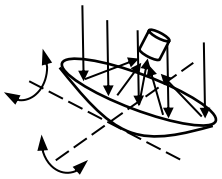
Discrete (multiple, near flat)	**Linear Fresnel** 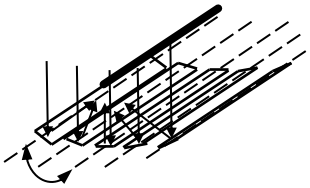	**Central receiver** 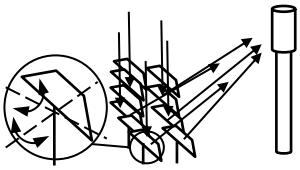

Line focus CSP collectors focus concentrated sunlight on a linear receiver, typically a steel tube with an evacuated glass cover for insulation. The parabolic trough line focus system is to date the most commonly found CSP technology in operation. The simpler tracking of the sun and efficient use of the curved parabolic mirrors are clear advantages that have not been significantly challenged by the proposed alternative

for line focus, the linear Fresnel reflector system. Line focus technologies have fundamental limits, particularly relating to the theoretical concentration ratio of 212 (Duffie & Beckman, 2006).

Point focus types are able to achieve far higher concentration ratios but require proportionally more effort in tracking accuracy. A continuously tracking paraboloid shaped reflector provides the highest concentration ratio and is theoretically the most efficient concentrator type maintaining high levels of efficiency at all times of the day. To date, no large scale or scalable technologies have been developed to exploit this advantage commercially (REN21, 2016). Parabolic dish concentrators with Stirling engines have been successfully demonstrated and used for several decades, but lack of energy storage, cost and long term reliability are some of the reasons for the ideal solar concentrator not in regular use.

The central receiver system using multiple tracking mirrors called heliostats approximates a point focus. While not able to achieve the highest efficiencies, this system is able to scale in size allowing for the use of efficient thermal storage and utility sized turbines operating at superheated levels (IEA, 2014). Figure 2.2 illustrates the basic layout of a state of the art central receiver system with a two-tank molten salt storage system and steam cycle.

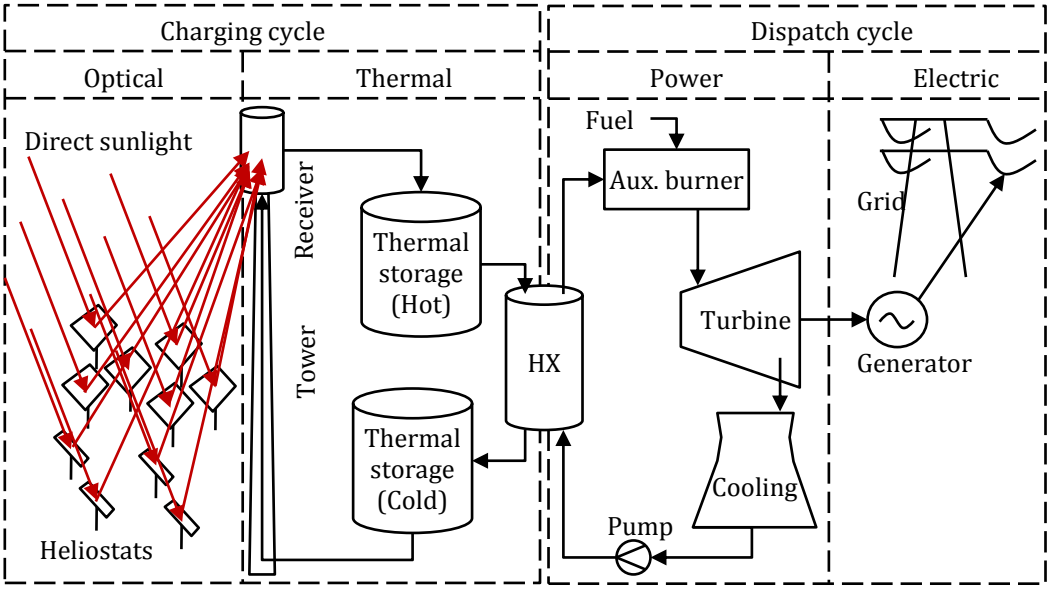

Figure 2.2: Schematic layout of a central receiver CSP plant with storage

2.3 Central receiver energy conversion principles

The central receiver system as illustrated in Figure 2.2 is the reference for the CSP model and serves to describe overall principles of the energy conversion process. The system can be divided into a charging cycle and a dispatch cycle, where the only significant dependency between these two cycles is the charge level of the thermal storage.

The optical component is a solar collector system containing a field of heliostats that reflect incident DNI to a thermal receiver in the form of concentrated solar irradiation. The thermal receiver converts the optical energy to thermal energy, which is then stored in a high temperature container. Thermal energy is transferred by a heat exchanger to the dispatch cycle, which is generally a standard superheat steam cycle.

2.3.1 Optical conversion

The performance of the optical system is dependent on the DNI quantity and the position of the sun relative to the location of the system. The model uses the empirical and geometric relationships of Duffie & Beckman (2006). These relationships are found to be suitable for energy systems analysis and are valid for all solar collector types used in the systems analysis model.

All heliostat field angles are described in Figure 2.3 and relate the position of the sun relative to time, location and the angular position of a heliostat.

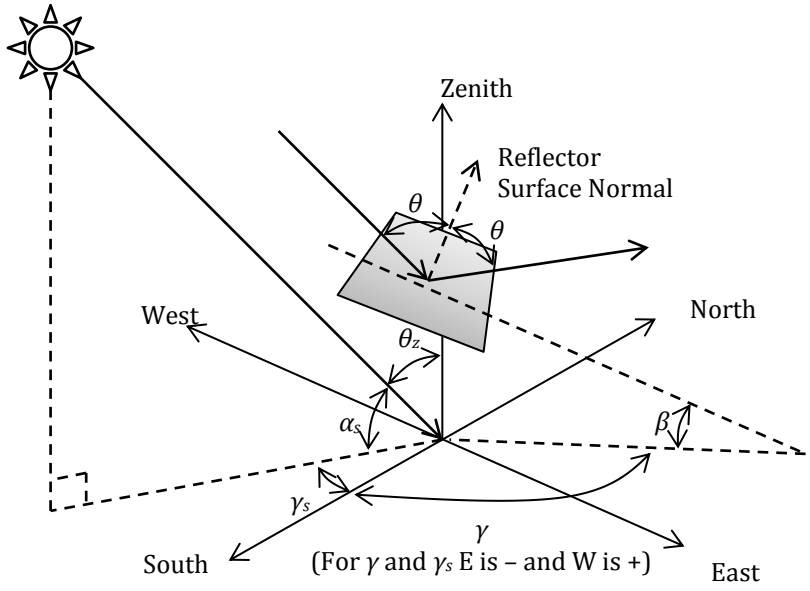

Figure 2.3: Solar and heliostat angles for the CSP model

The position of the sun is given by two components: Zenith angle (θ_z), the angle of the sun relative to vertical. The compliment of this is the solar altitude angle (α_s) and solar azimuth angle (γ_s), the latter of which is the angle of the projection of the sun's rays relative to south. The position of the sun with respect to the observer can be determined with latitude (ϕ), date and solar time. Two terms relating to seasons and time remain: declination angle (δ), the angle of the zenith relative to the equator due to the tilted rotation axis of earth; and hour angle (ω) based on solar time, a conversion of solar time to an angle where 24 hours = 360 ° and solar noon is 0 °.

Zenith angle is given as

$$\cos\theta_z = \cos\phi\cos\delta\cos\omega + \sin\phi\sin\delta \tag{2.1}$$

and solar azimuth is given as

$$\gamma_s = \text{sign}(\omega)\left|\cos^{-1}\frac{\cos\theta_z\sin\phi - \sin\delta}{\sin\theta_z\cos\phi}\right| \tag{2.2}$$

An approximation for the declination angle is given as

$$\begin{aligned}\delta = {} & 0.006918 - 0.399912\cos B + 0.070257\sin B \\ & - 0.006758\cos 2B + 0.000907\sin 2B \\ & - 0.002679\cos 3B + 0.00148\sin 3B\end{aligned} \tag{2.3}$$

where B converts the day of the year to an angular value.

$$B = \frac{(n-1)360}{365} \tag{2.4}$$

Solar time accounts for the difference in longitude between the observer longitude (L_{loc}) and the longitude on which the local standard time (L_{st}) is based. Each 1 ° difference accounts for 4 minutes and the perturbations in the earth's rate of rotation. The sum of these two components is described by the equation of time (E)

$$\text{Solar time} = \text{Standard time} + 4(L_{st} - L_{loc}) + E \tag{2.5}$$

where the equation of time (E) is given as

$$\begin{aligned}E = {} & 229.2(0.000075 + 0.001868\cos B - 0.032077\sin B - \\ & 0.014615\cos 2B - 0.04089\sin 2B)\end{aligned} \tag{2.6}$$

Information about the heliostat surface is contained in these components: slope of heliostat (β); surface azimuth (γ), the direction of the slope relative to south; and angle of incidence and reflection (θ). A generalized equation for the position of the sun relative to the plane of interest is given as

$$\begin{aligned}\cos\theta = {} & \sin\delta\sin\phi\cos\beta - \sin\delta\cos\phi\sin\beta\cos\gamma \\ & + \cos\delta\cos\phi\cos\beta\cos\omega \\ & + \cos\delta\sin\phi\sin\beta\cos\gamma\cos\omega \\ & + \cos\delta\sin\beta\sin\gamma\sin\omega\end{aligned} \tag{2.7}$$

which can be more conveniently represented by the zenith angle and solar azimuth angle by

$$\cos\theta = \cos\theta_z\cos\beta + \sin\theta_z\sin\beta\cos(\gamma_s - \gamma) \tag{2.8}$$

The CSP model performs an hourly averaged (h) energy conversion, and the optical energy collected is a function of DNI, reflector aperture area and the efficiency of the

reflector system based on time of day and the given relations to sun position.

$$Q_{optical(h)} = I_{b(h)} A_{optical} \eta_{optical(h)} \quad (2.9)$$

where I_b is the hourly averaged DNI, and subscript *optical* refers to the optical system. This conversion process is described in detail in Chapter 5.

2.3.2 Storage and solar multiple

Thermal energy storage permits a CSP plant to operate more flexibly at higher efficiency and a higher capacity factor. To do this, the solar field needs to be some multiple of that needed to get the turbine to its full rating on an ideal summer day. Even CSP plants with no thermal storage or auxiliary heating generally require an oversized solar field in order to allow the turbine to operate at its rated output for reasonable periods of time. The oversizing of the solar field is commonly referred to as the solar multiple (Trieb et al., 2009; IEA, 2010). The ability to size and optimize the solar multiple is considered an additional advantage in an electricity system (IEA, 2010).

Figure 2.4 illustrates a number of basic concepts for variations of the central receiver technology using outputs of the model developed for this dissertation. Three primary variables impact the utilization of the cycle.

1. Collector size and rating: This is the optical component in the described cycle and refers to the effective aperture area of the reflector system and the associated rating of the receiver, which, if not sized appropriately, can limit full use of the reflector system.
2. Thermal storage rating: This is the thermal storage component, which is usually specified in multiples of full load turbine hours utilizable.
3. Turbine rating: This is the power component, the gross (or net) size of turbine power.

Hourly aggregated DNI is indicated relative to the collected thermal energy per unit area of heliostat field for cases ranging from no storage to 15 storage hours over a two day period.

In a system with no storage, energy needs to be used directly by the turbine. A solar multiple of unity means that the turbine can use all of the collected energy but will only do so under ideal conditions. This means that in reality it will always underperform, thereby underutilizing the capital investment of the turbine. Any solar multiple greater than unity will cause curtailment of the optical system, thus capping the energy potential as shown by the red line for the “no storage” case. All energy above this line will be unutilized. An increasing solar multiple will, therefore, result in a transfer of underutilization from the turbine to the optical (or collector) system. For efficient and practical operation, CSP plants without storage usually have solar multiples ranging from 1.1 to 1.5.

In a system with storage that never restricts the optical or power components, utilized energy is still capped, but all additional energy is stored for use when the need exceeds the collection. A short-duration example can be seen in Figure 2.4 where performance on day two continues when solar irradiation dips for the case of a 1 hour storage plant. The 15 hour storage case shows continuous performance and would have a solar multiple of about 3 to 4. In a hypothetical case in which the energy storage has no constraints, all other capital is fully utilized.

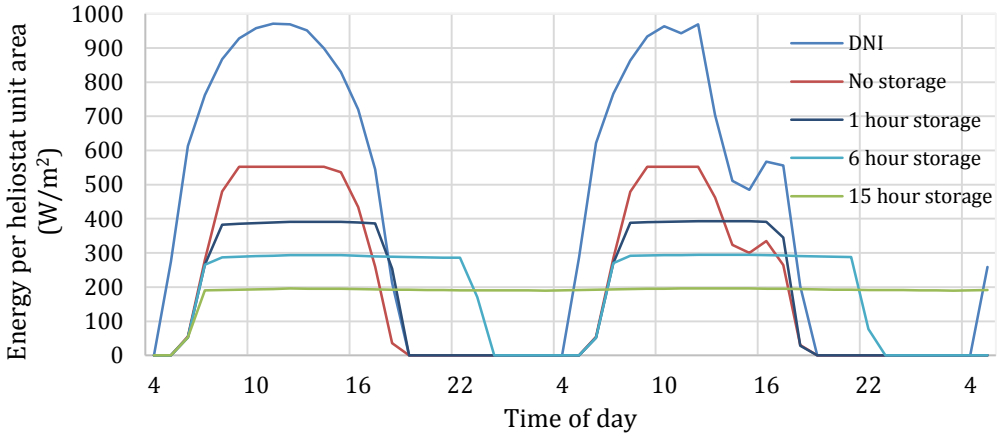

Figure 2.4: Illustrative effect of solar multiple and storage in central receiver CSP plant

In reality, energy storage cannot be unbounded due to the diurnal cycle whereby residual energy storage carried over to the next day results in another capital utilization constraint. In the event that the marginal cost of energy storage is lower per kWh of delivered energy relative to the cost of the turbine, initially an increase in energy storage in exchange for turbine size will result in a lower cost of electricity. The rate of cost reduction will reduce at the point when residual storage starts to lead to curtailment of the collector system. From this point, marginal cost derivative will be positive, and the cost of energy will grow beyond the optimal storage size. These tradeoffs have been well studied at an individual plant level (Denholm et al., 2012; Jorgenson et al., 2013).

2.4 Electricity generation principles

CSP plant integration principles and primary performance indicators of the CSP model of Chapter 5 are discussed using a simplified annual yield example.

A basic first order assessment can be performed to determine the capacity factor, efficiency, output and space needed of a CSP plant that utilizes its collector system at all times due to the inclusion of sufficient thermal energy storage.

$$C_f = \frac{E_{plant(y)}}{P_{net} \times 8{,}760} \tag{2.10}$$

where C_f is the capacity factor of the plant defined by the actual annual electricity produced (E_{plant}) from solar energy divided by the amount of power the plant is capable of delivering if it ran at net output (P_{net}) all year (8,760 hours). Subscript y denotes year.

$$E_{plant(y)} = I_{b(y)} A_{ref} \eta_{plant(y)} \tag{2.11}$$

where I_b is the long term average annual DNI, A_{ref} is the concentrator aperture area of the plant and η_{plant} is the total annual plant efficiency.

$$\eta_{plant(y)} = \eta_{optical(y)} \eta_{receiver(y)} \eta_{power(y)} \tag{2.12}$$

where $\eta_{optical}$, $\eta_{receiver}$, and η_{power} are the respective process efficiencies for collecting and concentrating sunlight, its conversion to thermal energy and its net conversion of power production, which incorporates the efficiency of thermal energy storage.

In general, power conversion efficiency is related to the quality of energy, and thus temperature, of the thermal energy supply. Power conversion efficiency is limited theoretically by the Carnot efficiency and represented reasonably well in adapted form, referred to as the Novikov cycle (Novikov, 1958; Curzon & Ahlborn, 1975) shown in Figure 2.5.

$$\eta_{power} \approx \eta_N = 1 - \sqrt{\frac{T_L}{T_H}} \tag{2.13}$$

where T_L is the ambient temperature and T_H is the operating temperature entering the turbine.

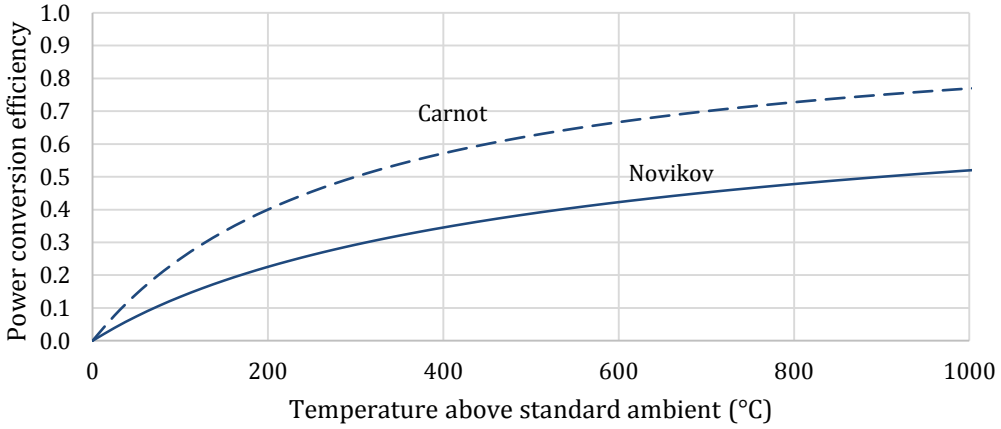

Figure 2.5: Heat engine Carnot theoretical limit and Novikov practical approximation efficiencies

As an example, a thermal power plant that operates at a working fluid temperature peak of 600 °C can operate at about 40 % efficiency.

Conversion of sunlight to high quality thermal energy requires efficient solar thermal collectors. Solar thermal collectors are always exposed to the environment and will incur energy losses super-linearly to the increase in collector temperature output, all other things equal. Losses occur due to reflection, glazing absorption, convective heat transfer and thermal radiation – the latter terms being somewhat or significantly non-linear to the collected temperature. The use of insulating techniques such as selective absorption coatings, glazing and evacuation can help to a point.

The single most effective method in getting to very high temperatures is to substantially reduce the exposed receiving area of the collector (receiver). This is achieved by concentrating sunlight from a large primary aperture (usually a collection of reflector surfaces) to the receiver. Receiver efficiency can also be represented by temperature (Figure 2.6) analogous to the heat engine efficiency shown in Figure 2.5, in this case for a specified reference condition relating to the receiver qualities, which will be covered in more detail in Chapter 5.

Using the same example, a receiver delivering 600 °C to the heat engine needs to have a concentration ratio (C_R) of almost 500 in order to achieve an efficiency of 80 %.

The annual effective optical efficiency is not linked to temperature in the same way and requires consideration of the specific design; this will also be covered in more detail in Chapter 5. For purposes of the example, an average annual optical efficiency of 60 % will be assumed.

Figure 2.7 plots the combined receiver and heat engine efficiency for this case. The first observation is that the two efficiencies trade off against each other leading to optimal operating temperatures, all other things equal. The second important observation is that concentration ratio always increases plant efficiency, all other things equal.

Following the previous example, the optimal concentration ratio for a 600 °C receiver is about 280 resulting in a combined efficiency, $\eta_{plant} = 0.193$.

$$\eta_{plant} = 0.6 \times 0.76 \times 0.422 = 0.193 \tag{2.14}$$

For a CSP plant containing 1,000,000 m^2 of reflector surface in a location with a long term average annual DNI of 2,800 kWh per m^2 per year, the annual solar-only power generation is

$$E = 2{,}800 \times 1{,}000{,}000 \times 0.193 = 539{,}975{,}335 \text{ kWh} \tag{2.15}$$

If this CSP plant has a 100 MW output rating and produced this amount of power, the plant would have a capacity factor of

$$C_f = \frac{539{,}975{,}335}{100{,}000 \times 8{,}760} = 61.6\ \% \qquad (2.16)$$

A capacity factor of 61.6 % represents a CSP plant with a significant amount of storage, typical of a small number of CRS plants representing the state of the art. If such a plant were also hybridized, it would represent a firm baseload power plant for a utility company. Such a plant would occupy about 5 km² of land, assuming typical current land usage for CRS plants (Ong, Campbell & Denholm, 2012; NREL, 2013). In a hypothetical scenario where such a plant is replicated in a distributed power network and is able to supply 81.4 TWh of electricity per year (20 % of annual demand in 2030 per one scenario (WWF-SA, 2014)) at that capacity factor, 151 plants would be required, occupying 754 km² of land. This would represent 0.062 % of South Africa's land surface.

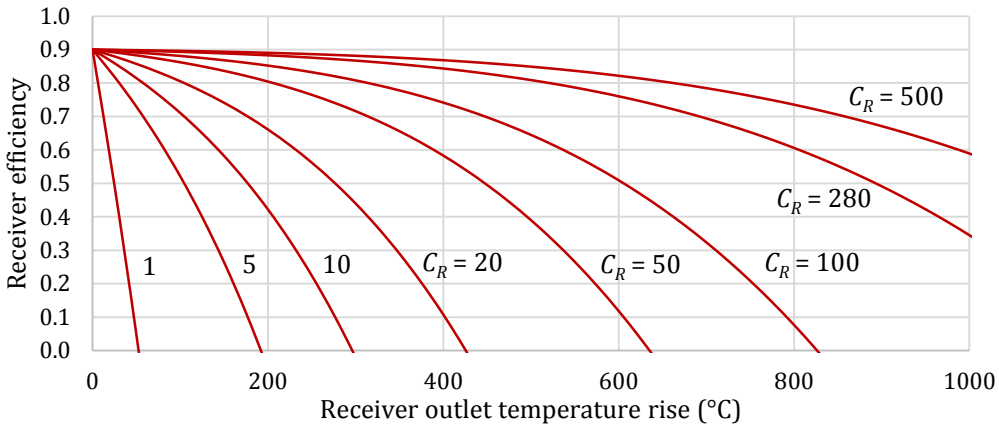

Figure 2.6: Thermal receiver efficiency for various concentration ratios based on one illustrative reference condition where temperature is above ambient

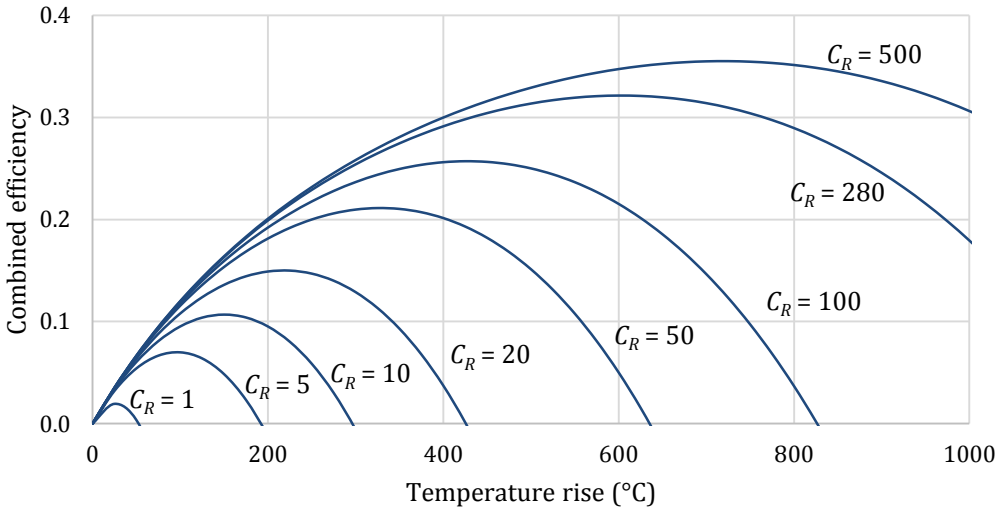

Figure 2.7: Basic combined receiver and heat engine efficiency

2.5 CSP history and outlook

While the history of CSP at least by demonstration goes back to before the turn of the twentieth century, it is a series of 9 parabolic trough plants with a combined capacity of almost 400 MW in California commissioned in the late 1980s that has provided the only proof of lifecycle performance to date. Most of these plants, known as the Solar Energy Generating Systems (SEGS) I - IX, are known to be still operating today. The SEGS formed the reference for many more plants deployed mostly in Spain and the USA in recent times. (IEA, 2010, 2014). While the installed capacity of CSP increased by a factor of six over a four year period to the end of 2013, the growth rate of the technology is lagging expectations.

Despite the slower adoption, CSP is considered strategically important for future energy systems in several countries, particularly Israel, France, Spain, Germany, USA, China, Australia and now South Africa. For example, the United States Department of Energy (US DoE) SunShot program provides competitive grants for CSP research aimed at reducing the cost of flexible baseload electricity from CSP to $ 0.06 per kWh by 2020 (Gary, Turchi & Siegel, 2011; USA Department of Energy, 2012). The US DoE awarded $ 335 million to this program from 2007 to 2015 (USA Department of Energy, 2015).

The SunShot program vision (USA Department of Energy, 2012, 2015) has placed particular emphasis on supercritical CO_2 power cycles for central receivers, but this concept has already faced challenges as pointed out by Cheang *et al.* (2015). Parametric analysis of CSP components such as heliostats (Blackmon, 2013; Emes, Arjomandi & Nathan, 2015; Larmuth, Landman & Gauché, 2015) suggests that central receivers have tangible and significant prospective advances without radical new ideas. How or if CSP realizes the SunShot goal is particularly difficult to forecast due to the maturity of the technology and the variety of types that exist. CRS are currently favored to succeed parabolic trough systems, but advancements continue to occur and certain applications and regions might always favor the parabolic trough. For very different reasons, the parabolic dish (usually with Stirling engines) and the linear Fresnel type have not succeeded in the market, but these concepts may still emerge in time.

2.6 Commercial state of the art

The two CSP types that are dominant in the market are the parabolic trough (Figure 2.8) and the central receiver (Figure 2.9).

The majority of CSP plants in operation are of the parabolic trough type. Parabolic trough plants brought into operation in the twenty-first century closely resemble the still operating SEGS plants with the exception of the addition of thermal energy storage. While proven and bankable, the state of the art parabolic trough technology has a practical operating temperature of around 390 °C and uses three working fluids. Thermal oil is used as the heat transfer fluid, molten salt is used for thermal storage

and water is used for the power cycle.

The first operating CSP plant in South Africa, KaXu near Pofadder, is a 100 MW system with 3 hours of storage. Two other parabolic trough plants are in construction or commissioning (NREL, 2014).

Figure 2.8: Photo of a parabolic trough line in Andasol 3, a 50 MW parabolic trough plant with 7.5 hours of storage (Photo by author)

The state of the art central receiver based plants operate using two working fluids. Molten salt is both heat transfer and storage medium, and the power cycle is a superheated steam Rankine cycle as illustrated in Figure 2.7. The first commercial plant of this type is the Gemasolar plant in Spain, first operated in 2011. The receiver outlet temperature is 565 °C and the storage capacity is rated to 15 hours (NREL, 2011a). The higher operating temperature enables more compact and, hence, larger capacity storage. To date, only one other tower of this type has entered operational status, the 100 MW Crescent Dunes plant developed by SolarReserve (NREL, 2015a). A similar SolarReserve plant, called Redstone, is in advanced planning (NREL, 2015b).

Figure 2.9: Gemasolar CSP plant, a 20 MW central receiver with 15 hours of storage (photo by author)

2.7 Conclusion

CSP is entering its growth phase with over 3 GW of capacity installed. The central receiver type is regarded as the technology that will enable affordable high capacity factor power generation, but projects of this type are only starting to operate. The propositions, analysis and findings of this dissertation assume that such high storage capacity central receiver plants, or equivalent derivatives, will fulfill lifecycle promises as it is only now starting to be the case with parabolic trough technology without storage.

Basic analysis suggests that immediately commissioning about 10 central receiver plants per year sized to the Redstone project could result in the generation of about 20 % of South Africa's baseload power needs by 2030.

3 GENERAL LITERATURE REVIEW

This chapter presents a summary review of energy systems and the state of energy systems analysis relevant to the objective and not covered in other chapters.

3.1 Solar energy in perspective

Solar energy is the source of most of Earths ongoing primary energy supply as tabulated in Table 3.1. It is also the original energy source for most electrical power generation with the exception of nuclear power, geothermal and tidal based power generation.

Table 3.1: Primary energy supplies (adapted from de Rosa (2005))

Source of energy	Amount (TW)
Solar	**173,000**
Direct reflection (Albedo)	52,000
Conversion to heat	78,000
Evaporation of water	39,000
Wind & waves	3,600
Photosynthesis	40
Tides	**3**
Geothermal	**32**

Total global production of electricity in 2011 was 22,126 TWh (IEA, 2013). How this compares with global anthropogenic consumption of energy and annual solar energy irradiation is represented by Figure 3.1.

Electricity consumption represents about one fifth of anthropogenic energy consumption, which in turn is about 5 orders of magnitude lower than non-reflected solar energy irradiation. A review of most conventional energy resources is the subject of the final chapter of Part 1. This review considers global and South African energy resources, suggesting that conventional energy resources are likely to reach extraction peaks fairly soon despite growing demand (Gauché, von Backström & Brent, 2013). Multiple reasons are argued for these extraction peaks. Provided solar power is valued and competitive, it offers the potential for energy and electricity far in excess of our needs.

Trieb *et al.* (2009) assess the global CSP potential at almost 3,000,000 TWh per year, more than 130 times the 2011 world electricity production. The analysis considered areas where DNI exceeded 2,200 kWh/m^2 annually and excluded areas used for other purposes or that were not suitable due to vegetation, water or terrain. The suitable areas add up to about 25,000,000 km^2. Just the very sunniest regions where DNI exceeds 2,700 kWh/m^2 per year provides a potential for about 46,000 TWh per year, or 20 times the 2011 world energy production.

In the case of South Africa, Fluri (2009) assesses the potential of CSP in the short term to be in excess of 500 TWh per year. This study had many similar exclusions and also considered only the suitable areas within 20 km of the existing transmission network.

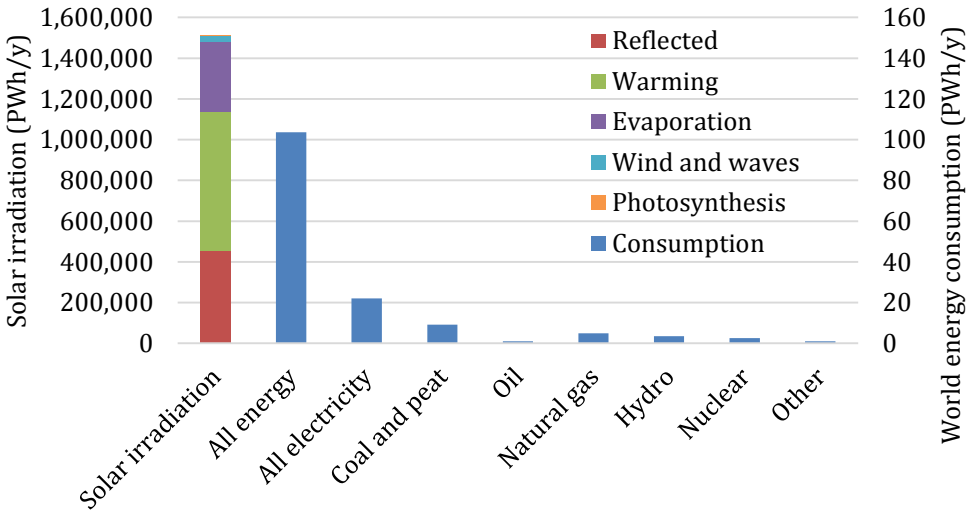

Figure 3.1: Total world energy in 2011 by solar irradiation (left axis) and anthropogenic energy consumption (right axis) (adapted from (de Rosa, 2005) and (IEA, 2013))

3.2 The solar resource

Increasingly accurate knowledge of the solar resource is a fundamental requirement – if not a pre-requisite – to an increasing installation rate of solar energy. This is particularly true for CSP, which, still in its infancy, has a high capital cost relative to most alternatives. CSP relies exclusively on DNI sunlight, which is historically more difficult to measure than global horizontal irradiation (GHI) (NREL, 2011b; Suri et al., 2015).

The solar resource at any location is intermittent and impacted by many factors relating to time, location, environmental and atmospheric conditions. For solar energy conversion, the commonly used measures are GHI and DNI, measured per unit area per unit of time at ground level (Duffie & Beckman, 2006).

The only way to accurately determine the solar resource at any location is by ground measurement using broad spectrum solar resource instruments. Typically a pyranometer for GHI and tracking pyrheliometer for DNI give the highest accuracy. Ground measured solar resource data has the drawback of being relevant to specific point locations. Stations around the world have varying degrees of reliability, and not all stations make data available publically. The World Radiometric Network maintains a database of about 1,200 stations and provides monthly and daily values (Cros & Wald, 2003).

Solar and weather resource measuring and monitoring activities have substantially

increased with the more recent mandated introduction of renewable energy in South Africa. A multi-institutional effort has resulted in a publically accessible database of measurement stations capable of accurately measuring data relevant for CSP. The Southern African Universities Radiometric Network (SAURAN) was launched in 2014 and serves as an academic and public reference (Brooks et al., 2015).

Figures 3.2 and 3.3 demonstrate examples of DNI and all other measurements respectively over the span of 1 day for one SAURAN measurement station. DNI is plotted for minute-averaged and hour-averaged values, an important distinction in energy systems analysis.

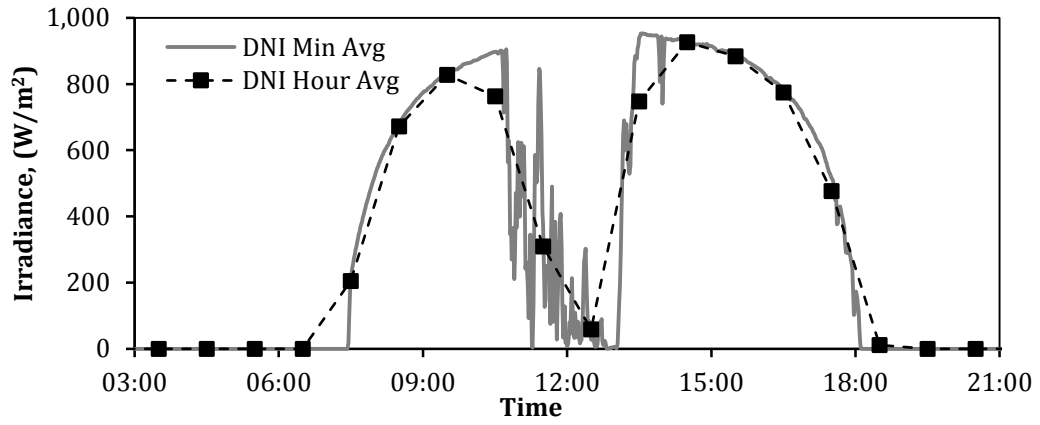

Figure 3.2: DNI (minute-averaged and hour-averaged) at the Vanrhynsdorp (VAN) station on 1 May 2014 (source: by author (Brooks et al., 2015))

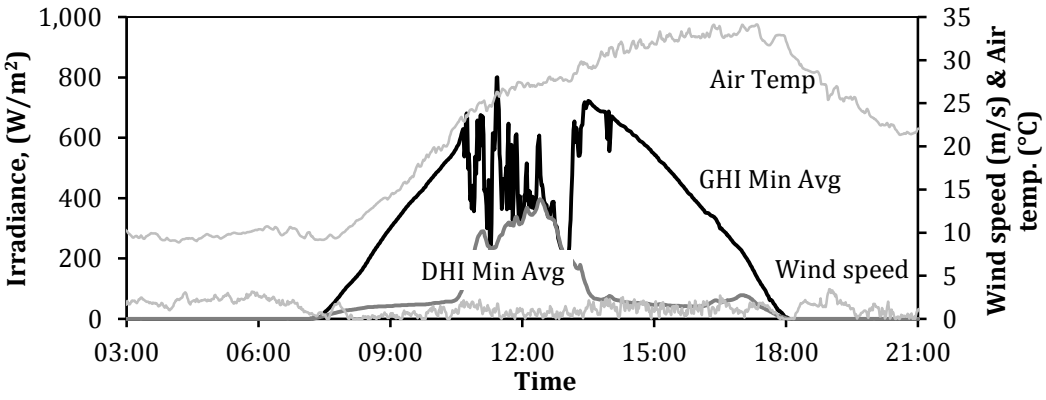

Figure 3.3: GHI, DHI, wind speed and air temperature (all minute-averaged) at the Vanrhynsdorp (VAN) station on 1 May 2014 (source: by author (Brooks et al., 2015))

To overcome the spatial limitations of ground measurements, satellite derived solar and weather resource methods are used. Satellite instruments cannot directly measure ground based solar and weather parameters. Algorithms that are becoming more reliable are used to derive these values based on available sensors. For Europe and Africa, the Meteosat satellites are used (GeoModel Solar, 2012a; Ineichen, 2013). These are geostationary satellites scanning the visible and infrared spectrum every

30 minutes (first generation) in lines east to west from south to north. Other sensors measure aerosols, water vapor and ozone. Second generation satellites scan every 15 minutes. Spatial resolution ranges from 3 to 7 km for the electromagnetic spectra to 35 km for water vapor and 125 km for aerosols.

A variety of commercial and free sources of satellite derived data exists. Each supplier typically has proprietary methods, and the best satellite derived data is generally able to predict the solar resource with small hourly to annual bias and reasonable standard deviation. Third party evaluations have been performed to assess various data sets. Ineichen (2013) reports on a detailed analysis of 6 suppliers comparing data with 18 ground measurement stations. While satellite models for GHI are fairly accurate, DNI values are prone to error, particularly at shorter intervals. The GeoModel SolarGIS DNI results show the highest accuracy but with a mean bias deviation of 7.5 %.

More recently, GeoModel Solar performed an accuracy enhancement to the southern African SolarGIS data set, using amongst others the SAURAN network (Brooks et al., 2015). Data from fourteen meteorological stations was used to compare with and improve the SolarGIS model. The model adaptation process is aimed to reduce bias, randomness frequency distribution error by optimizing algorithm coefficients on a regional basis. This results in an improvement of the mean bias from -3.9 % to 0.2 %. In South Africa's sunny western region, the SolarGIS enhanced long term dataset shows DNI levels typically 5 to 10 % higher than previously reported (Suri et al., 2015).

The twenty year improved high resolution DNI of South Africa is shown in Figure 3.4. The vast majority of land surface has an annual average DNI exceeding 2,000 kWh per year, and about 2,500 km^2 mostly located near Springbok and Calvinia have long term average annual DNI values exceeding 3,100 kWh per year.

3.3 The wind resource

Wind is the primary resource for wind power and needs to be accurately known due to power production being proportional to the cube of the wind speed at the hub height of a wind turbine. Wind also plays a minor but positive role in cooling PV panels, which leads to improved efficiency. Wind conditions impact cost and performance of all renewables but particularly for CSP where reflector systems can be damaged and performance degraded from loss of optical or thermal energy. Similarly, wind turbine performance needs to be curtailed or halted depending on the severity of wind gusts.

The additional dimension of height or altitude makes wind resource mapping particularly challenging. Wind height profiles are a function of local topography, weather patterns and a range of other environmental factors. Bañuelos-Ruedas *et al.* (2010) investigate the suitability of the Hellman exponential law and the logarithmic wind profile law in urban and rural case studies, finding that these wind profiles are overly simplistic and do not account for environmental complexities. The authors

recommend more suitable locations for measurements in combination with more detailed wind modeling. It should be noted that these conclusions are based on the need for wind turbine performance and that results typically were within 10 % between the two models and measurement.

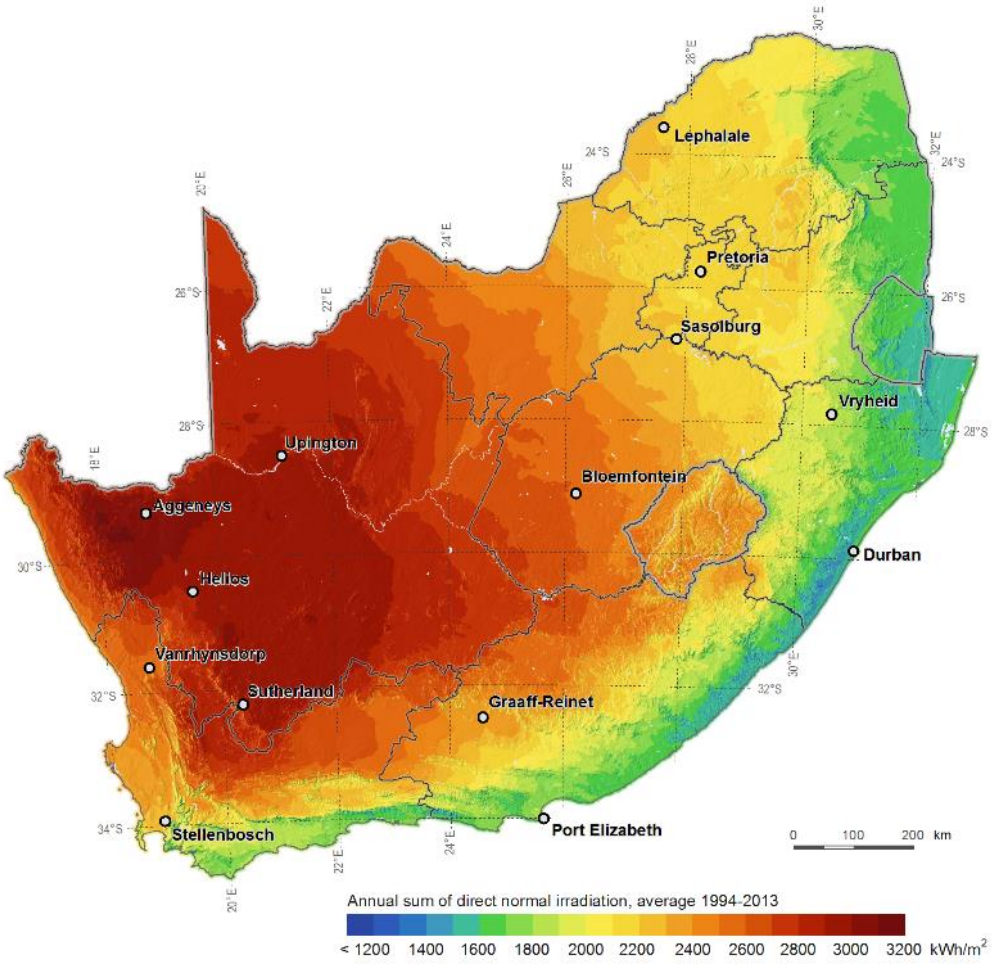

Figure 3.4: Accuracy enhanced DNI map of South Africa (Suri et al., 2015) (SolarGIS © 2015 GeoModel Solar)

Hagemann (2008) provides what is understood to be the first mesoscale wind atlas of South Africa with the intention of supporting wind power deployment. The model uses a fifth generation mesoscale modeling methodology and 17 South African Weather Service meteorology stations with most anemometers placed at a standard height of 10 m.

A more recent and substantially updated wind atlas project was undertaken by the South African Department of Energy and supported by several international entities. The Karlsruhe Atmospheric Mesoscale Model (KAMM) is used and described by Hahmann *et al.* (2014). The project utilizes 10 strategically located 60 m high wind masts in the key wind regions of South Africa (Mortensen et al., 2012).

Figure 3.5 is the 2014 WASA mean wind speed map showing the location of the 10 wind masts (WM01 to WM10) and average wind speed modelled at a height of 100 m. A high spatial resolution dataset of hourly averaged wind speed over many historical years is freely available for download from the project website (SANEDI, 2015).

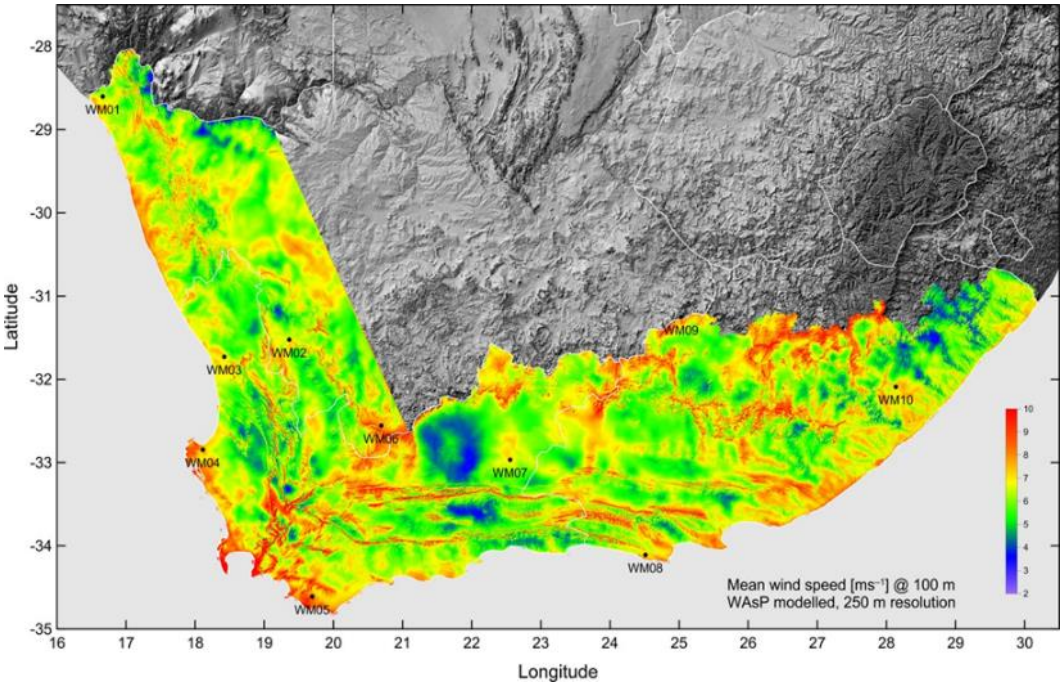

Figure 3.5: Wind resource map for the Western, Eastern and Northern Capes (SANEDI, 2015)

3.4 Solar and weather resource analysis data types

For solar and wind energy system modeling and plant design, information about the resource needs to be sufficiently granular to factor in time of day changes. Solar data in increments of 1 hour is used as a standard for energy systems analysis with significant renewable energy capacity and for individual projects. Due to significant annual deviations in actual conditions, a timeframe of typically thirty years is considered necessary for reliable modeling, particularly for bankability of expensive projects. It is difficult to obtain information for longer terms and also usually too computationally intensive. The typical meteorological year (TMY) method, in which twelve statistically representative chronological months are stitched together for a specific location (Wilcox & Marion, 2008), is the standard used for producing a typical year of meteorological data that enables more convenient analysis. For large renewable energy projects, lenders require expert analysis to understand the output of plants for typical and extreme years. TMY P50 and P90 are datasets to test the probability that a plant will deliver a certain annual output 50 % and 90 % of the time (Vignola, Grover & Lemon, 2011; Dobos, Gilman & Kasberg, 2012).

3.5 Energy systems analysis model review

Pfenninger *et al.* (2014a) present a comprehensive review of energy systems modeling relevant to the needs emerging in the twenty-first century. The review is centered on energy systems modeling for national and international energy policy.

Energy systems modeling emerged during the second part of the twentieth century to primarily focus on energy security and cost. The more recent emphasis on climate change and the resulting interest in renewable resources for the provision of energy has led to challenges relating to the intermittent nature of renewable technologies. Greater temporal and spatial information is needed in modeling, which was not previously a concern in energy systems.

The TIMES (The Integrated MARKAL-EFOM System) model platform, developed as part of the IEA-ETSAP (Energy Technology Systems Analysis Program) (Loulou & Labriet, 2008), is a widely used modeling platform that has been broadly adapted and emulated from open source versions such as OSeMOSYS (Howells et al., 2011) to the commercially sold PLEXOS power systems platform (Energy Exemplar, 2015).

The TIMES model uses a so-called bottom-up approach whereby technologies in the system are described in as much detail as needed in order to optimize energy systems over time. The primary drawback is that complexity in the models cause very long computation times. This is often resolved by simplifying the model and also simulating only single or several representative time slices. The ability to deal with forecasting, scenarios and contingencies add to the computational burden in such physically-described models.

Fouché and van Niekerk (2014) report on plans for an energy modeling alliance for South Africa that incorporates the current state of energy systems modeling in South Africa. The South African TIMES Energy Model (SATIM) has been developed and maintained by the Energy Research Centre (ERC) at the University of Cape Town (ERC, 2013). The SATIM has contributed to the NDP (National Planning Commission, 2012) and the 2010 IRP of South Africa (Department of Energy, 2011). The 2013 draft IRP Update (Department of Energy, 2013b) switched to the PLEXOS platform.

Pfenninger (2014a) categorizes four challenges of emerging approaches in energy systems analysis. Firstly, resolving time and space is becoming increasingly important and requires improved models but also better access to spatial-temporal information. Secondly, addressing uncertainty and the future requires that scenario analysis emphasize predictive methods rather than technical accuracy in order to achieve better predictions. The remaining challenges relate to handing optimization across scales and incorporation of behavioral and social factors.

Pfenninger and Keirstead (2015) have developed a new energy systems platform called Calliope that aims to address many of the shortcomings of existing platforms. The focus is on flexibility, high spatial and temporal resolution and open-source

transparency with clear separation of model and data.

3.6 CSP systems and plant analysis model review

Ho (2008) provides a comprehensive review of CSP system and component analysis methods and models used by Sandia Laboratories, illustrating a fairly long history of modeling capabilities built up in the USA. Most of these models focus on detailed aspects of CSP technology, and many of the codes have been superseded or are used mostly in the Sandia Laboratory environment. The Solar Advisor Model (SAM), now called the System Advisor Model (Gilman & Dobos, 2012), is listed as the remaining CSP system modeling tool used by Sandia Labs and National Renewable Energy Laboratory (NREL).

SAM is free to download and use for any purpose and has been used extensively in the analysis of CSP plants and energy systems including CSP plants around the world. SAM performs technical and financial simulations of many renewable technologies and comprehensively covers CSP technology variants. It uses hourly solar and weather data and is able to perform parametric and optimization simulations. SAM uses the TRNSYS (Klein, 2010) (Fiksel & Thornton, 1995) transient thermodynamic simulation algorithm developed at the University of Wisconsin in 1975. It also incorporates several older models reported in Ho (2008).

SAM has several limitations. The first is that it is not developed to be a systems simulation tool and needs to be used in conjunction with other tools for energy systems analysis. While it is free to use worldwide, its algorithms are largely proprietary or not directly accessible making it difficult to use with confidence.

Bode and Gauche (2012) review available CSP optical modeling methods and software, and find no single optical method to evaluate the detailed optics of CSP plants for systems analysis or optimization. Generally, methods are published that can investigate optical details for limited cases, or systems models make use of simplified or analytical approximations of the optics.

Numerical ray tracing methods, typically using Monte Carlo methods to fully describe individual or multiple optical elements, give the most detailed results but require longer computational time. Two freely available ray tracing tools are the proprietary SolTrace (NREL, 2011c) and open source Tonatiuh (Blanco, 2011).

Heliostat field performance prediction and optimization has traditionally been done by simpler analytical or hybrid methods. Delsol 3 (Sandia, 2009), developed by Sandia National Laboratories, is one of the most sighted tools using analytical approximations and is also used as the heliostat field optimization tool in SAM.

3.7 CSP in systems analysis studies

Beyond the most popular energy and CSP systems models, a high number of methods have been published in some form, particularly during the last decade. This section

covers key studies where CSP has been included to some degree in systems analysis.

The global potential of CSP has been expressed using a wide range of model detail. Trieb *et al.* (2009) use a spatial-GIS approach, suggesting that CSP can potentially supply 3,000,000 TWH per year, vastly exceeding the world electricity consumption. More recently, the value of CSP has been tested using an hourly spatial-temporal method to determine the optimal contribution in four key world regions. Pfenninger *et al.* (2014) use the CSP model developed for this dissertation and report that well configured systems can satisfy baseload needs with little to no backup generation at costs approaching $ 0.06/kWh by 2030.

Fluri (2009) reports on the South African CSP potential using a similar method to Trieb *et al.* (2009) but limited to locations close to the existing transmission system. This study confirms that the short term potential vastly exceeds the current and future electricity needs of South Africa.

Several studies under the banner of the DESERTEC project (Viebahn, Lechon & Trieb, 2011; Trieb et al., 2012) present a case for solar electricity imports from the Middle East and North Africa (MENA). The authors claim that less than 0.2 % of suitable CSP land is sufficient to supply 15 % of the 2050 European electricity demand. The referenced studies are spatial-GIS based, but multiple agencies have considered the DESERTEC concept or parts thereof using linear programing with varying degree of spatial and temporal resolution.

REMix-CEM (Renewable Energy Mix-Capacity Expansion Model) by the German Aerospace Centre (DLR) appears to be one of the first models to transcend the energy systems domain of linear optimization, employing CSP in some detail in the case of Jordan (Trieb, Fichter & Moser, 2013; Fichter, Trieb & Moser, 2014). The CSP model is quite detailed and incorporates part-load and environmental impacts to performance. Cost is optimized for the entire energy system containing capital and operating costs for all technologies. The outcome is that a significant amount of CSP in a renewable mix results in Jordan continuing its economic growth while becoming energy secure.

Mileva *et al.* (2013) present simulation results that demonstrate the value of reaching SunShot (Gary, Turchi & Siegel, 2011; USA Department of Energy, 2012) cost goals for solar energy technology. The authors use a multi-nodal abbreviated time series model called SWITCH, developed by Fripp (2008), for energy systems modeling in California. SWITCH comprehensively considers multiple demand areas, technologies, transmission, costs and reliability. The model relies on SAM to perform the CSP simulations, perhaps explaining why the CSP plant configurations are limited in the publication.

Multiple studies have been conducted by NREL to evaluate the potential of CSP in the USA, particularly in the Southwest. Almost without exception, SAM is used to provide CSP modeling for a limited number of CSP configurations into linear modeling.

Nevertheless, the studies point to clear advantages of CSP when cost are realized and PV saturation starts to occur (Denholm & Hand, 2011; Denholm et al., 2012).

Several South African policy driven energy systems analyses have incorporated CSP over the last decade. The majority of these use a variant of TIMES modeling (Department of Energy, 2011, 2013c; Miketa & Merven, 2013). Most, if not all, energy systems models use simplified capacity factor based assumptions for technologies, stochastic single-node environmental parameters and typical time slices for intra-week or seasonal behavior. No references to full spatial-temporal models have been found for South African energy planning.

Ummel (2013a,b) performs wind, PV and CSP spatial-temporal modeling for a future South African energy system and uses SAM to produce the outputs of a set CSP plant configuration with 6 hours of storage replicated in a detailed spatial distribution. The performance of the CSP fleet appears to be exogenous to the system model, which in turn is simplified to a single node aggregation. Ummel suggests that improved spatiotemporal efforts will result in significant economic gain.

A multi institutional German-South African project considered the highly urbanized region of Gauteng in a holistic study that assumed energy to be the key element in its sustainable transformation (Eltrop & Annegarn, 2013). Within this project, CSP was included endogenously using a comprehensive and fairly detailed self-developed CSP model applied in a TIMES model for the greater project and reported in various publications (Telsnig et al., 2013; Tomaschek et al., 2015). As with most TIMES models, time slices were used, but it seems that greater emphasis was placed on the use of temporal solar resource data than has been applied in other South African TIMES models. A key limitation of this study seems to have been access to good solar and weather data with only two sites used, one of which was outside of the study region (Upington) and one in Gauteng.

Recent spatial-temporal research, using self-developed methods that are related but not part of this dissertation, have studied cases for South Africa. Giglmayr *et al.* (2013a; 2015) present an analysis of the first two rounds of the South African REIPPP program showing the virtues of PV, wind and CSP that have been allocated and are mostly now in operation. Auret (2015) developed a spatial-temporal model of the South African electricity system based on the 2010 IRP and several scenarios proposed in the 2013 draft IRP Update. This bottom-up model treats the operation of all power generation technologies and plants endogenously based on system and IPP operator tariff structures and behaviors. Annual demand is based on the IRP and shaped hourly based on the 2010 Eskom demand data. Auret (2015) is critical of CSP's ability to deliver on the promise that the proponents of the technology usually suggest; this is due primarily to current tariff structures, not technology limitations.

Giglmayr *et al.* and Auret benefited substantially from the availability of validated high spatial resolution hourly solar and weather data. The value of high spatial-temporal resolution solar and weather data in energy systems analysis is illustrated

by Suri *et al.* (2014a). The authors show that PV electricity production in South Africa becomes increasingly predictable when more widely distributed. The hypothetical case illustrates that the 15 minute rate of change in production over a multiple year period drops from the range of 15 % to 40 % for a single location to a range of 2 % to 6 % for 225 locations in a 500 km x 500 km area.

3.8 Conclusion

The review leads to three key observations or conclusions that have relevance to this dissertation. Firstly, a lot of effort seems to have gone into energy modeling at all scales, from energy systems to components within a technology, as renewable energy has become more commonplace. A high degree of variation exists in the methods, and at almost every level, computational resources restrict analysis by simplifications in time or by other constraints. Secondly, the availability of good quality spatial and temporal data has prevented better outcomes in many studies, particularly in large energy systems analyses. Lastly, care is needed in forecasting, particularly with respect to factors not directly related to technology. Models that forecast need to account for a potentially high number of contingencies, and the computational burden of this needs to be considered and traded off with the bottom-up detail in the model.

4 SOUTH AFRICAN ENERGY PROPOSITIONS

This final chapter of Part 1 presents propositions regarding the value and potential of CSP in South Africa based on a review of energy resources and technologies applicable in the 2010 IRP. The chapter is a reproduction of a peer reviewed journal article: Gauché, P., von Backström, T. W., & Brent, A. C. (2013). A concentrating solar power value proposition for South Africa. Journal of Energy in Southern Africa, 24(1), 67–76. The objective, research and findings of this article are attributable to the author of the dissertation, and the article has been edited for style and cohesiveness.

4.1 Abstract

Concentrating solar power (CSP) offers the potential for a high degree of localization and an alternative strategy to meet electricity demand for South Africa in a future of uncertain conventional resources. The integrated resource plan (IRP) makes strides to introduce renewables to the electricity generation system by 2030, but we argue that the proposed energy mix is too reliant on resources that are not only unsustainable but also at risk in the short to medium term. Coal and other conventional resources may be more limited than originally anticipated, which if true requires action to be taken soon.

CSP is currently the only sustainable and dispatchable energy technology that could domestically supply a significant portion of South Africa's electricity needs. A balanced mix of PV, wind and CSP can provide the energy supply needed in South Africa, but steps are required soon to take advantage of the localization potential and excellent sustainable energy resources.

4.2 Introduction

A CSP value proposition for South Africa is proposed as follows: CSP is the ideal future dispatchable power technology for South Africa in the broadest context because it can dispatch power in response to demand and can enable a very high degree of local inclusion. The value of such a technology at a macro level is described and argued here. While several specific propositions are made, each will be addressed in greater detail in future.

The South African public know through experience of two related indicators about the current provision of electricity. Firstly, the cost of electricity per kWh is increasing dramatically with little end in sight. In 2011, Eskom began planning the next phase of price increases, applying to the regulator for annual increases in the 25 % to 30 % range until 2016 (Creamer, 2011). Secondly, generation capacity is stretched thin, and the public has been put on standby for rolling power cuts.

The electricity crisis experienced by the public is paralleled with the underlying polycrisis faced in South Africa for the provision of electricity and energy in general. This polycrisis is so-named due to the impact of multiple environmental constraints

and limits that constrain economic development. This problem is particularly acute in South Africa where economic development is strongly resource coupled and considered unsustainable (Heun et al., 2010).

South Africa learned lessons during the previous fifteen years during which the country had to deal with a major political transition while being confronted with pressure to change its electricity generation profile away from being coal dominant. The integrated resource plan (IRP) arose at the end of the first decade of this century and it appears to be a robust system. The twenty year horizon with updates every two years, the legal mandate, and a plan with rigorous stakeholder input should be the right way forward (Department of Energy, 2011).

The IRP already recognizes a reduction of electricity from coal. After the current coal power stations are constructed, which will add about 10 GW to the grid, only another 6.3 GW will be added until 2030. The reasons for limited coal growth may vary, but this paper elaborates on some reasons why this is believed to be a step in the right direction.

The IRP is generous towards renewable and sustainable electricity technologies (hereon "renewables"). This includes 8.4 GW wind, 8.4 GW photovoltaic technologies (PV) and 2.6 GW of imported hydro. In addition, nuclear capacity dramatically increases by 9.6 GW. Both government and Eskom are committed to the nuclear expansion despite tougher regulatory, cost and public pressure. The primary argument is the need for a solid baseload for future electricity generation, and the IRP acknowledges the prioritization of nuclear over renewables for this reason. Figure 4.1, derived from the IRP, illustrates how nuclear will aim to replace some coal, particularly in terms of energy supplied.

CSP is allocated 1.2 GW during the next twenty years. This capacity represents a little over 1.3 % of the generating capacity in 2030 and less in terms of energy supplied. The other 17 GW of domestic renewables are intermittent by nature, and all three types have lower capacity factors that diminish their role when viewed in terms of energy supplied vs. capacity installed. The IRP recognizes this limitation and can be seen in the differences between the two plots in Figure 4.1.

What the IRP may not fully account for at this stage is the consequence of the lower capacity factors due to intermittency for wind and PV when they represent a significant portion of the total capacity. Both require potentially 100 % backup capacity either in the form of alternative generation or storage. The cost and/or availability of storage options for these technologies are barriers in the South African context, at least at this point in time. It may be that imported hydro (indicator 2 in Figure 4.1) and significant open cycle gas turbine (OCGT) capacity (indicator 1 in Figure 4.1) offer this backup. The former appears significantly accounted for in energy supplied, and the IRP acknowledges the downside risk of hydro due to deployment risk and severe drought. The cost of running OCGTs is downplayed by a low capacity factor. If these plants need to provide backup to both at-risk hydro and renewable

intermittency, the almost negligible OCGT component on the right side of Figure 4.1 would need to grow, but in doing so it would add considerable cost to energy supplied as these are linked to diesel and gas prices.

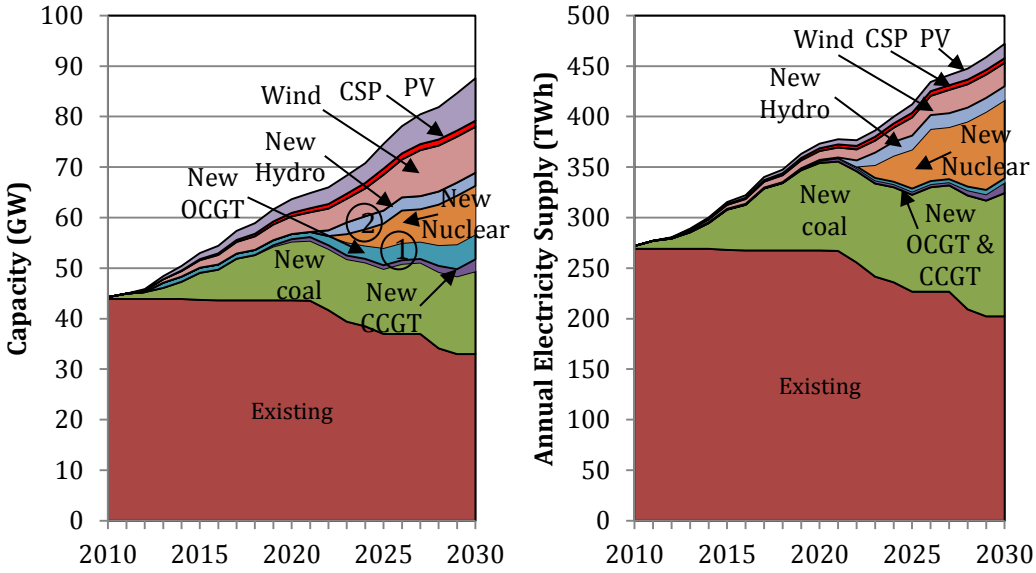

Figure 4.1: Capacity and energy supply to 2030 (recreated from IRP2010 and with assumptions on capacity factors to approximate the IRP annual electricity supply model)

CSP offers a solution to the intermittency of renewables. This study argues for a balanced mix of renewables when they form a significant portion of electricity production. Whereas CSP could theoretically supply 100% of South Africa's electricity, this is acknowledged to be unnecessary, costly and risky at this time.

The methodology comprises primarily a survey and analysis of the alternatives available to South Africa during the next twenty years. A description of CSP is presented, followed by a review of the state of the art of this technology and what it may mean in the local context.

4.3 Conventional and sustainable alternatives

The following considers each major source of practically available energy for electricity production in South Africa over the IRP period.

4.3.1 Coal

Coal has long been the staple of the South African energy supply. Although coal capacity will decrease to a lower fraction of the mix from about 2020, it still represents a large amount of the electricity supplied through 2030. The IRP is influenced by climate change mitigation goals, but it also recognizes what it calls a "peak-oil-type" increase risk in fuel prices as a motivation to prioritize a large nuclear fleet that begins to replace coal.

A number of recent international publications have looked at coal reserves worldwide and for Africa (mostly South Africa) specifically. The authors use Hubbert style forecasting, which has proved reliable at predicting peak and ultimate production of oil in mature or depleted regions. Hubbert analysis uses historical production information fitted to a normal distribution curve or similar. If sufficient production has occurred, particularly at the point where the rate of production increase starts to wane, peak and ultimate production quantities and dates are predictable with higher accuracy than geological exploration estimates predict (Hubbert, 1956).

Rutledge (2011) developed a model that uses the better of a logistic or cumulative normal model for all coal regions and the world as a whole. Rutledge (Rutledge, 2013) makes his data and models available to others, and the results have been re-processed in Figure 4.2. Patzek and Croft (2010) use a multi-Hubbert cycle analysis to determine a global coal production forecast. Mohr and Evans (2009) also perform Hubbert style analysis on world coal incorporating an iterative supply and demand method in an attempt to replicate real world conditions. Locally, Hartnady (2010) worked on a similar model which examines the (South) African coal resource question in detail. Hartnady (Hartnady, 2012) revised his estimate based on updated data from Rutledge. All of the authors' current ultimate estimates are shown in Figure 4.2 indicated using symbol "×".

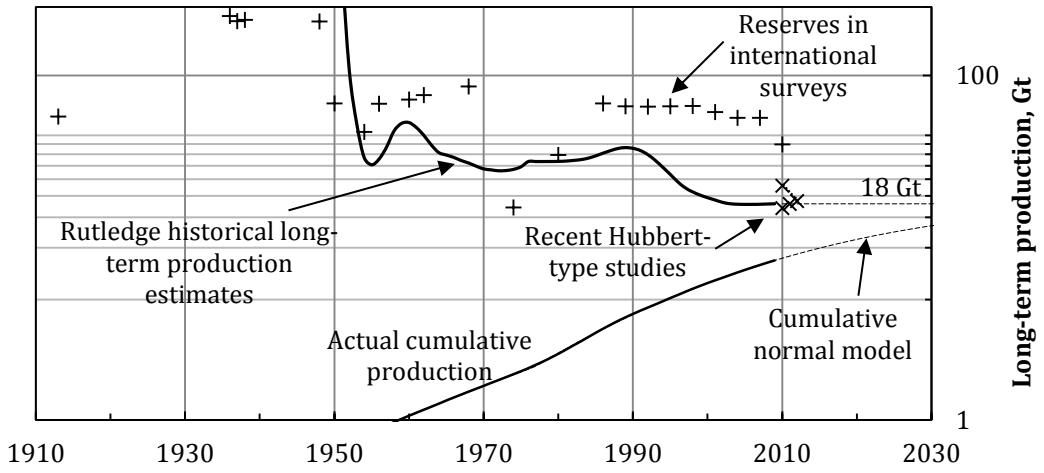

Figure 4.2: Estimates of long term (ultimate) coal production in Africa (mostly South Africa) showing international survey values as well as historical estimates to the cumulative normal model. Actual and modelled cumulative production is also shown as are all recent Hubbert-style predictions (data and model adapted and used with permission by Dave Rutledge).

It should be noted that besides the actual and modelled cumulative production lines, all plot data refers to the ultimately recoverable resource estimated by surveys at a particular date or the result of the Rutledge model based on actual production data prior to a particular date. Peak production and year as well as 90 % depletion date estimate and ultimate production quantity are summarized in Table 4.1.

When examining these models for exhausted coal or oil regions there is little doubt that they predict peak and ultimate production more accurately than geological estimations do. These models show predictability when other regions can make up for demand, but it is not known how the models will behave for world production or production of later maturing regions as there may be no motivation to cease production of sub-economic resources. On the other hand, this hindsight model is indifferent to supply and demand mechanisms and even handles significant occurrences well such as war and cartel interference. In the event of approaching sub-economic resource levels, one would speculate that alternatives would by then have succeeded to enter the market, fulfilling the prophesy.

Table 4.1: Summary of Africa peak and ultimate dates and quantities for coal using Hubbert-style analyses

Source	Peak year (and peak production)	90% year (and/or total cumulative extraction)
Mohr & Evans (2009)	2012 (258 Mt/y)	(18.6 Gt)
Rutledge (2011)	Similar to others but prefers not to comment due to peak year volatility	2048 (18 Gt)
Patzek & Croft (2010)	2007 (based on energy, not mass)	(478.6 EJ calculated as 17.15 Gt)
Hartnady (2010, 2012)	2020 (284 Mt) 2012/2013 (254.3 Mt/yr)	(23 Gt) (18.675 Gt)

Unlike oil or uranium, coal markets tend to be regional with only 15 % of world coal production exported (Rutledge, 2011). If there is any merit to the estimates, then while the world sits on peak oil, South Africa is simultaneously perched on peak coal. At peak, production is generally incapable of increasing to demand, and we begin to experience a significant change in price elasticity as reported recently for oil (Murray & King, 2012). Murray and King correlate price of oil to daily oil production and to demand and are making the assertion that world oil is on peak based on the data.

Hartnady (2010) suggests that the peak will not be a smooth curve just as all parts of the real production curve are bumpy. We are as likely to have years that exceed estimates as we are likely to have years that fall short around the peak itself. From as soon as late 2012 or 2013, we could experience a production dip that for the first time fails to meet demand.

Eskom consumed 124.7 Mt of coal to produce roughly 230 TWh of electricity in 2011 (Eskom, 2012). This represents about half of current coal production in South Africa. By 2030, the models suggest that the same coal consumption will represent about two thirds of production, yet the amount of electricity from coal is not below today's level between now and 2030.

The theme of this section is intentionally focused on reserves of conventional energy sources. Combustion of coal and other fossil resources leads to an increase in the level of CO_2 in the atmosphere. This in turn leads to global warming by the greenhouse

effect, according to the consensus of climate scientists. This important debate as well as the true cost of climate change is far more established than a discussion on fossil resources and is therefore omitted from this paper. If the reported resource estimates are accurate, the world soon will be responding to a crisis of similar proportion without choice.

4.3.2 Uranium

Similar models for uranium were not found, and it seems that the decrease in new plant deployment worldwide since the 3 Mile Island incident and leading to the rapid economic growth in China has made it more difficult to make these estimates. Popular perception is that nuclear energy is carbon free and sustainable. While the former is mostly true, the latter is problematic. With conventional once-through nuclear technology, economically extractable fissile uranium turns out to be a far more limited resource than popularly believed.

Recent work by Knapp *et al.* (2010) looks at the potential for the remaining reserves of uranium to reduce carbon emissions by 2065. Knapp estimates that by using all remaining recoverable reserves by once-through technology, carbon emissions will reduce 39.6 % by this year. The year 2065 has no significance to uranium and was only selected as a date for the analysis. Knapp does suggest that this gives some indicator of time to build sufficient safety into fast-breeder reactors to mitigate nuclear terrorism. If this is possible and notwithstanding the other long term and operational risks of nuclear power, fast breeder technology would be able to sustain the power needs of Earth for a very long time. An alternative is the use of thorium as nuclear fuel, which is more abundant then uranium. Thorium will require considerable R&D investment before it can be considered a cost-effective replacement to uranium (World Nuclear Association, 2011).

Dale (2012) reports a meta-analysis of all major non-renewable sources. The methodology includes statistical analysis on a large set of resource estimates the author was able to obtain. Figure 4.3 is a re-creation of the results, and as would be expected in such work, the range on each type is large. Ranges are not shown for unconventional oil and gas due to insufficient estimates.

The purpose of showing this data is primarily to expose the fact that the upper estimates on fissile material are lower than the lower estimates on coal. Uranium has a worldwide market, and South Africa will (and does) compete for new plants and fuel. The NDP 2030 (National Planning Commission, 2012) urges reconsidering a potentially costly nuclear build, and Eskom has on several occasions been warning of the difficulty to meet IRP requirements to deploy 9.6 GW on time and within budget.

4.3.3 Other fossil sources

Figure 4.3 also illustrates best known estimates on unconventional fossil energy sources. Murray and King (2012) state that the oil sands of Canada and Venezuela will peak at around 6.7 million barrels per day, well short of daily needs. Shale gas seems

to be an immense resource both worldwide and in South Africa. Besides evidence of environmental harm caused by hydraulic fracturing, recent reports suggest that these gas wells experience rapid annual declines and become sub-economic within a few years. Shale gas exploration is being planned for South Africa in the region shown in Figure 4.4. This map also shows the best solar resource region of South Africa. The potential gas reserves on the east coast of Africa could also be considerable (Brownfield et al., 2012), and these sources need to be tracked closely as alternatives to coal or nuclear.

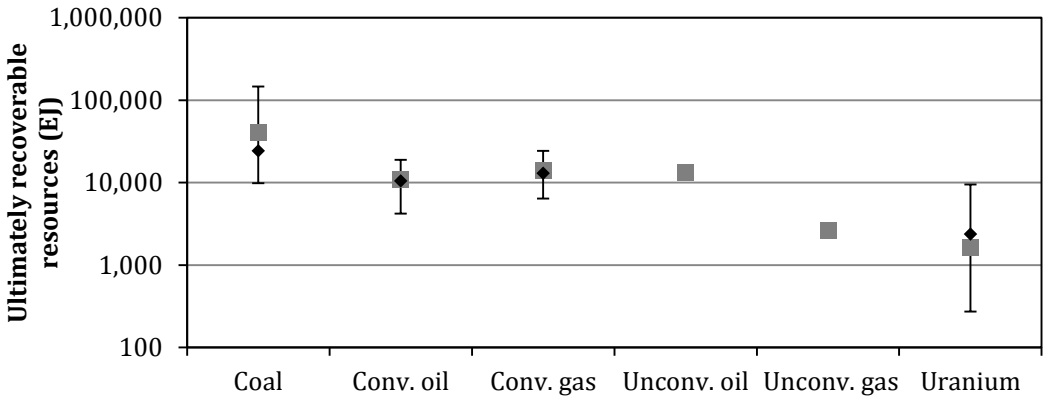

Figure 4.3: Worldwide ultimately recoverable resources (URRs) of various conventional energy resources adapted from Dale (2012). Grey squares represent mean values and the range represents 5th percentile and 95th percentile; black diamonds represent the median value of the estimates.

4.3.4 Other renewable and sustainable sources

Referring to Figure 4.1, the resources that impact all current (and majority to 2030) generating capacity have been discussed. The remaining sources in South Africa's IRP, hydro, solar and wind, are covered here only peripherally to provide context to CSP.

South Africa is largely dependent on new hydro imports for the hydro component, and these contain risk of project completion and drought (Department of Energy, 2011). In general, hydro power is an excellent source of electricity if available and is capable of baseload electricity.

PV technology is well established at small distributed scale in many countries. There are larger PV plants operating or under construction, but these plants can experience sudden production changes with weather. No utility scale electricity storage technologies exist at this time to moderate supply. PV is supported as a vital component in the future supply of electricity in South Africa due to the cost advantages of this technology and the ability to generate clean energy. For simplicity it was assumed that the potential for PV in South Africa is similar to that of CSP at a capacity factor of 0.2 based on the IRP. This amounts to over 800 TWh for the same assumptions as made by Fluri (Fluri, 2009) for CSP potential. This exceeds the total energy needs of South Africa in 2030 but with intermittent supply.

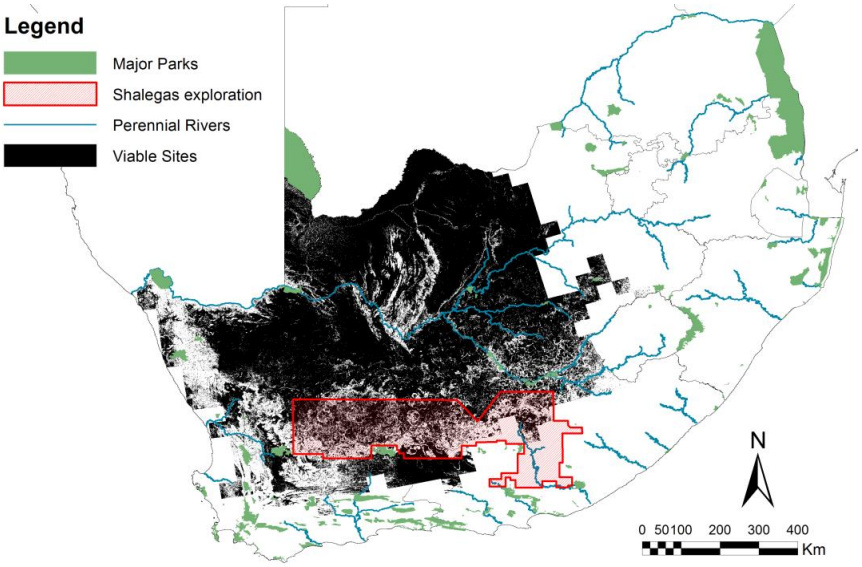

Figure 4.4: Areas of excellent solar resource (black) and the general area of anticipated shale gas exploration (red) by Meyer *et al.* (2011)

Wind energy experiences similar intermittency, and as electricity is produced immediately, the lack of large scale storage again prevents supply moderation. A capacity factor of 30 % is considered good for wind. A recent report by Young (2011) provides statistics of UK wind production. This report breaks many assertions of wind potential including the ability for wind to generate reliably in a distributed system as well as its potential to support pumped energy storage systems with sufficient capacity for low wind times. As with PV and despite the drawbacks, wind is believed to play an important role in South Africa's future. Hagemann (2008) produced a detailed mesoscale wind atlas of South Africa. He determined a realistic wind potential of South Africa to be just over 80 TWh at a capacity factor of 30 % with high sensitivity to capacity factor.

4.4 CSP technology for South Africa

4.4.1 Solar and other resources

South Africa benefits from one of the best solar resources worldwide. The majority of the country receives annual DNI values in excess of 2,100 kW/m^2 per year (representing good Spanish conditions), and parts of the Northern Cape reach 3,000 kW/m^2 per year (GeoModel Solar, 2012b). Fluri (2009) and Meyer and van Niekerk (2011) show short to long term viable suitable land for CSP, and even the most constrained short term suitable sites show a potential of more than 500 GW.

The key constraints for CSP at suitable sites are water and transmission limits. South Africa is a water stressed country, and suitable regions are particularly dry. With low density populations and little significant economic activity, suitable regions also currently have limited capacity to remove electricity.

4.4.2 CSP technology summary

In order to assess the value of CSP, a brief look at the anatomy of a CSP plant is presented. Four primary CSP plant types exist, with the parabolic trough type as the most mature and bankable. Two different departures to the parabolic trough are the central receiver type, as shown in Figure 4.5, and the linear Fresnel type, similar to the parabolic trough. Both of these alternatives offer the potential for further cost reduction. The fourth type is the parabolic dish concept, which potentially has the highest efficiency but remains commercially unproven (IEA, 2010). The remainder of this discussion focuses on the central receiver type.

The 20 MWe Gemasolar CSP plant by Torresol Energy, shown in Figure 4.5, represents the state of the art for CSP technology due in part to its record breaking 15 hour storage system. Marker 1 shows part of the heliostat field, which covers 195 Ha of land and is by far the most extensive part of the plant. The heliostat field is made up of steel structures, glass mirrors, motors, gearing and control systems representing roughly a third of the cost of the plant.

Marker 2 shows the tower with its 120 MWt molten salt receiver near the top. In this image, the receiver is fully operational as evidenced by the brightness of the receiver and the concentrated rays of sunlight incident to the receiver. The receiver, tower and heliostats are collectively termed the collector system, representing about half the cost of the plant. This tower is constructed of concrete, but lattice steel structures are also used for similar plants. Marker 3 points to the location of the rest of the plant, which forms an island with the surrounding heliostat field. A traditional steam turbine with wet cooling system is coupled to a large two-tank molten salt storage system via heat exchangers.

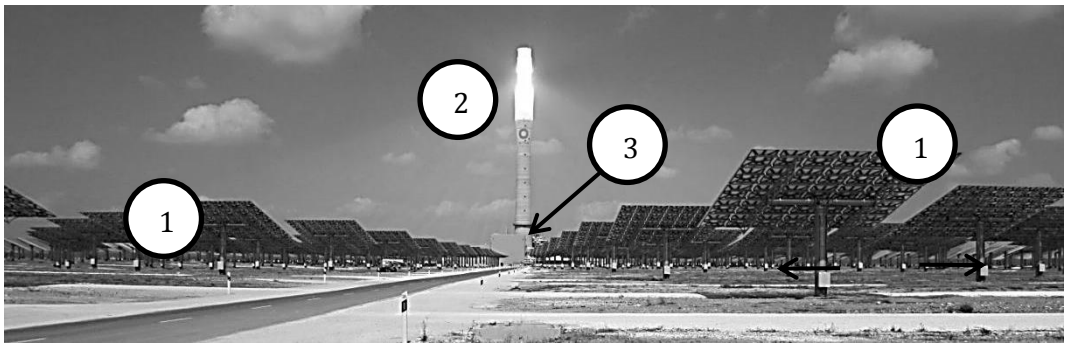

Figure 4.5: Photo of the state of the art 20 MWe Gemasolar plant

Wet cooling is used due to the availability of water. This plant's operating temperature is limited to the turbine rating of 565 °C, making its thermodynamic efficiency and water use similar to conventional coal power. As a result of this operating temperature, the plant is capable of dry cooling with similar cost and efficiency implications compared to the existing dry cooled plants in South Africa. This is an important development in CSP because regions identified for this technology are typically those where water is particularly scarce.

The relatively small turbine at 20 MWe is capable of a relatively fast start-up, which makes the plant ideal to offer dispatch power, and thus its usage can be considered similar to that of a peaking station. The Gemasolar plant is only the fourth commercially operating central receiver plant worldwide but has already demonstrated full-load power 24 hours per day in its first summer. The plant operators expect it to run continuously at full-load for most of the summer (Torresol Energy, 2011).

The central receiver type is just entering the growth phase of the technology life-cycle and as such offers significant scope for technical and cost improvements. In particular, the central receiver should be capable of achieving much higher temperatures, which will lead to the following benefits:

- Combined cycle plants with very high efficiency, thus smaller heliostat fields
- Efficient dry cooling
- Greater storage capacity due to increased efficiency
- Inline hybridization to provide efficient auxiliary capability

The cost target of electricity from large coal plants is in the region of $ 0.06 per kWh. CSP costs are currently in the low $ 0.20 per kWh range and are benefiting from a learning rate typical of developing technologies.

A last note on the auxiliary capability of CSP relates to Figure 4.4 where overlap between the proposed prospecting sites for shale gas and sunny regions is shown. In the event that shale gas is discovered and exploited, CSP offers the opportunity to limit the consumption of this energy source if hybridized CSP were to be used for power generation.

4.4.3 Propositions regarding CSP in South Africa

Although CSP is untried in South Africa, it is quite well proven in the USA where nine CSP plants, called Solar Energy Generating Systems (SEGS), were constructed from the mid to late 1980s. All of these plants are still in operation, illustrating lifecycle competence, and they have provided invaluable learning for the current generation of plants. Spain and the USA compete for deployed CSP capacity. Worldwide, capacity exceeded 1 GW in 2011.

Based on the alternatives presented, the following list of propositions is being put forward:

- CSP is the ideal sustainable and dispatchable power method for South Africa in the longer term when fossil fuels approach depletion. Although the cost of CSP needs to drop before wider adoption can occur, system wide costing needs to account for the dispatch capability which compliments other generation types.
- CSP components, skills and operation risks are a good match for the resources,

skills and infrastructure of South Africa.

- South Africa has a relatively short period of time to adapt to and benefit from a large scale rollout of CSP. The cost of the rollout will be a significant portion of the GDP, but it presents an equivalent opportunity should the country adapt and embrace the technology. The variable nature of the energy source makes CSP design and operation more complicated. On the other hand, the technology is relatively safe compared with other existing and future dispatchable energy sources. South Africa will benefit by taking appropriate small steps towards building capacity and industry regardless of the scale plans of international technology providers. As such, it is vitally important that there be a national effort to construct smaller scale pilot plants and research facilities in order to maximize the opportunity.
- The key CSP type for utility power generation in the longer term will be scalable point focus types. At this time, this is represented by the central receiver plant type. Although more complicated, this type will be more efficient (in terms of land area and cost) and it will consume significantly less water.
- CSP types that are less complicated to construct and operate will remain appropriate in the longer term for a variety of applications including on and off grid community power and heat, pre-heat augmentation to utility power plants as well as process heat.
- CSP technology in combination with a good solar resource is suited to a distributed power generation model, which could have many benefits including lower transmission risks and increased local value.

4.5 Analysis and discussion of alternatives

The propositions and statements in this paper, particularly about future events, cannot be validated. Instead, a synthesis is presented of the aforementioned alternatives for future South African power production capacity.

Several criteria can be used to measure the alternatives available to South Africa for the period between now and 2030. The list could include: Resource size, demand matching, cost, learning rate, technology risk, resource availability risk, national security risk, environmental risk, localization potential, local participation, industrialization and export potential. These should be explored in detail, but for this study an analysis of three is presented:

- Resource size
- Localization potential
- Demand matching

The result can be represented using a bubble plot where bubble areas represent resource size and the other two parameters are qualitatively judged on the horizontal and vertical axes. Figure 4.6 shows this plot for the 2030 timeframe. Conventionals

are shown constrained to the IRP allocation assuming all prior arguments justify this to be the upper bound. Renewables are shown constrained only by short term (twenty year) infrastructure limitations except where otherwise indicated.

Coal as a resource is sized to the IRP, which is marginally larger than the current capacity. Coal provides a solid baseload supply through efficient, reliable, large utility plants. The localization potential for coal has been established and mainly exists on the periphery of the plant capital cost and the full extent of fuel and operations. It thus positions in the center of the plot at about 300 TWh per year.

Nuclear, combined cycle gas turbines (CCGT), hydro and OCGT are IRP sized, assuming that they are constrained by cost, resource, safety or foreign reliance. All of these offer moderately poor to poor localization potential. Hydro would offer local potential had the resource existed locally. All of these sources offer reliable electricity supply for baseload or dispatch. The items in the "shrinking conventionals" bubble all represent conventional energy resources that were previously described as peaking and at risk of depletion far sooner than previously forecasted.

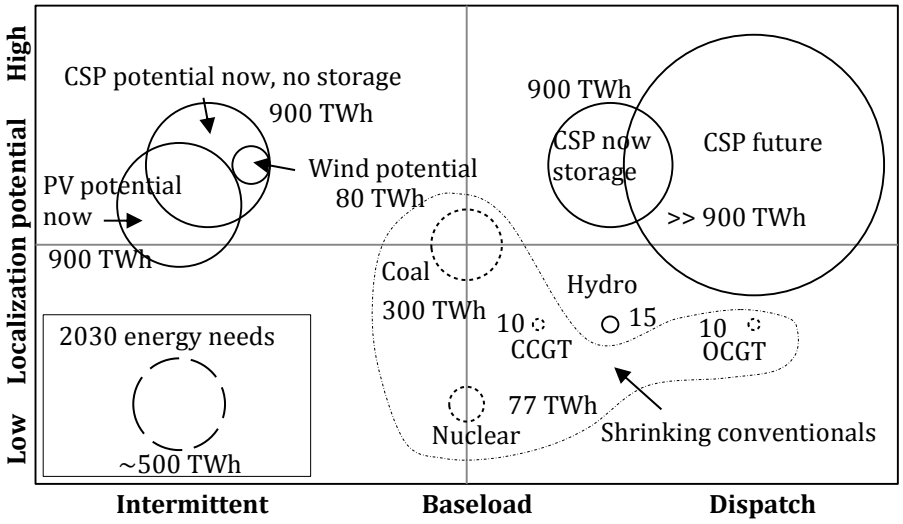

Figure 4.6: Qualitative positioning for all future electricity generation types in 2030. Horizontal axis represents capacity factor characteristics ranging from intermittent to peaking. Vertical axis represents localization potential. Bubble size is approximate annual electricity production.

PV offers huge potential and is better at localization than the conventional types for construction and operations, but PV cells and perhaps large inverters may be sourced more economically from abroad. The full potential for PV in the future was not included here because of the uncertainty of utility scale electrical storage or legislation for household/commercial feed-in policy. Wind is similarly positioned with perhaps slightly higher localization potential and intermittency that may improve with a distributed system. This resource is far more limited but is an important independent energy source. CSP without storage offers similar localization

as PV and wind. It offers a slight advantage over PV from the intermittency point of view due to thermal inertia of plants, which allows for brief solar irradiation interruptions. CSP with storage swings it to the dispatch side of the plot as this creates fast start-up ability and efficient thermal storage systems. The potential of CSP will continue to grow in the future since the technology offers electricity production potential, localization and dispatch as the rollout grows and the transmission system is in place.

When drawn in this way, two additional observations can be made:

1. While there doesn't seem to be a shortage of energy sources, the future electricity supply system appears vulnerable to meeting demand. With the current focus of the IRP on risk avoidance in the short to medium term, the alternatives to baseload and peaking mostly fit in the shrinking conventionals group, with some reliance on imported hydro. This suggests that the risk mitigation is paradoxical in the event that the forecasts discussed in this work are accurate.
2. CSP appears to be the ultimate solution. While the technology is a contender for post-fossil energy supply, for now, cost and maturity are limitations. In particular, a system of CSP plants could be deployed with reasonable certainty of supplying all energy needs, but the cost would be considerable (Gauché et al., 2012). A cost optimal energy system with similar certainty would probably comprise all three renewable types in similar proportion.

4.6 Conclusion

South Africa is embarking on an electricity generation transition to reduce reliance on coal. Coal is still viewed as a considerable resource, but recognition is given to CO_2 emissions and the risk associated with resource prices inflating in peak fossil scenarios.

For this reason, the IRP generously mandates a significant portion of future capacity for renewables, but it prioritizes a significant nuclear program to reduce risk. The renewable mix has a high degree of intermittency, and less than 1 % of produced electricity is CSP by 2030.

A significant portion of capacity in 2030 will come from plants yet to be constructed. When the degree of localization potential in renewables is compared with nuclear as well as the potential to produce to demand, a better short and long term picture is presented, and the country moves toward a sustainable path sooner.

Adding recent updates to world and South African supplies of fossil and fissile sources, it appears that immediate action is required, and a more drastic turn to renewables is essential. The analysis in this paper suggests that continued reliance on coal together with the choice of nuclear to provide a most stable baseload option could be a paradoxical choice. The environmental risks of the nuclear option were put

aside here due to the ad-hoc nature of catastrophic events now and an inability to agree on the long term consequence of nuclear power. What is more tangible from this analysis is the prospect of energy uncertainty in an age of supply limited conventional energy sources. A scenario can be imagined where significant plant capital investments are made and followed by unstable and escalating energy prices without guarantee of delivery. A later switch to renewables will take time and will be more economically challenging if existing conventional plants need to be written off or continue running at high cost.

In any scenario where we decide to prioritize renewables or where we have no choice, this basic analysis shows significant risk for both baseload and dispatch or peaking energy supplies. Assuming that the storage potential offered by CSP will remain the most efficient and economical storage for utility scale power generation, an optimal mix of CSP with other renewables will be essential.

4.7 Epilogue

At the time of writing, the 2010 IRP had only recently become law and the REIPPP program had not yet been implemented. In review, the majority of the work and the propositions made remain relevant. The outlook for nuclear power and the exploitation of gas both remain uncertain (Department of Energy, 2013b). Coal and oil prices have plummeted (IEA, 2015), and world leaders are increasingly concerned about the impact and cost associated with climate change caused by anthropogenic production of CO_2.

Heun and de Wit (2012) argue that clearly diminishing energy return on energy invested (EROI) trends need to be taken as a warning. During times of oversupply and low costs, this places pressure on resource companies. Regardless of price, other factors such as the dramatic reduction in cost of renewables (REN21, 2016) will reduce demand for conventional energy resources, reinforcing the point made by Rutledge (2011) that a high confidence forecast using his method is indifferent to the cause.

Part 3 of the dissertation evaluates the state of the 2010 IRP and the propositions made in this chapter.

PART 2: ANALYSIS METHOD

Part 2 of the dissertation describes the analysis methods developed to address the objectives.

The core of the method is the development of a central receiver CSP model that sufficiently resolves hourly power production for fast solution times and the ability to test primary component techno-economic sensitivities.

The system model which incorporates other power generation technologies and a cost method is complementary to the CSP model. The system model is developed to validate the application of CSP in an energy systems analysis and to test the value of CSP in South Africa.

5 CONCENTRATING SOLAR POWER MODEL

This chapter describes the CSP model developed for the dissertation. The model has been described (Gauché, von Backström & Brent, 2011; Gauché et al., 2012) and used (Silinga & Gauché, 2013, 2014; Pfenninger et al., 2014) in several peer review publications. The CSP model is a primary contribution based on the identified need for a simple, yet sufficiently sensitive treatment of CSP in energy systems analysis as outlined in Part 1.

An exhaustive description of the model is not practically possible. Instead, all items specifically relevant in terms of developing a suitable systems analysis CSP model are described. Generally understood methods and relationships of interest that support this chapter are included in Appendix A.

5.1 Overall methodology

An overriding principle in developing such a model is that it needs to capture the performance of a specified capacity of CSP that is spatially placed, based on that capacity's solar multiple and storage size proportioning. It could be that a given location (spatial position) is occupied by groups (hereon referred to as nodes) of CSP capacity differentiated by proportion of the primary components as illustrated for a single plant in Figure 5.1.

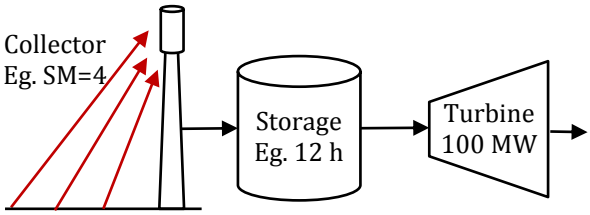

Figure 5.1: Illustrative proportions of a CSP plant with a solar multiple (SM) of 4, 12 storage hours and a 100 MW turbine

Figure 5.2 illustrates the concept for two geographically separated solar parks; one has two nodes of differently proportioned CSP capacity, and the other has only one node because of the same proportioning despite the variations in plant size. The consequence is that besides proportioning of each node, the size and technology specification per unit is to be immaterial. While this is intended to result in a much simpler analysis, the challenge is to capture the behavior of the technology as best as possible without compromising model accuracy. The model development approach to achieve such an analysis is by deconstruction of the technology down to a generic but first principle level as far as possible without prescription of how the technology manifests.

Validation of what constitutes sufficient model accuracy is not possible based on measurement due to the nature and scope of the model. Accordingly, various means

are used including piece-wise validation of referenced CSP plants and components, parameter and variable sensitivity analysis, and energy balance testing for components, component integration, temporal steps and temporal aggregation.

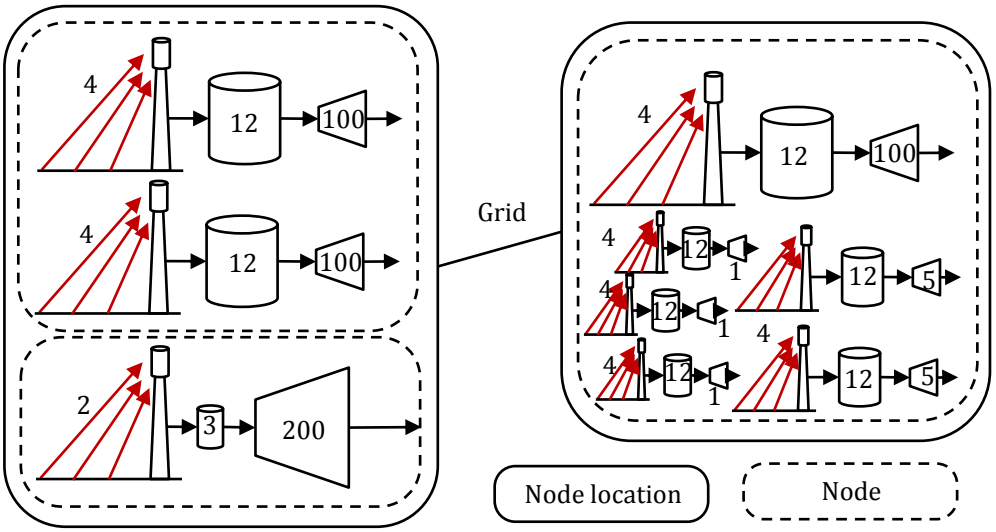

Figure 5.2: Illustrative definition of nodes for proportioned capacities of CSP

The overall assumptions and simplifications are summarized here. While the simplified model structure is type-agnostic to accommodate any variant of CSP technology, only the central receiver type is addressed, assuming that it is the CSP technology type of choice for the immediate future.

Operating choices are based on optimal running of nodes. Thus, it does not make sense to judge the performance of a single plant; rather, it is assumed that individual plants run at their optimal points and are otherwise in a standby mode instead of all plants running under part-load conditions.

CSP plants in the future will strive for highest efficiency, and how this is achieved is likely to be diverse in the market. Techno-economic performance is linked to the peak working fluid temperature, and learning rates are applied to components within the model in order to correctly account for the size and cost relationships within the technology. What is not as obvious are the decisions relating to the advances in CSP over time in achieving improved techno-economic performance. Accordingly, the assumptions around the technology require clarification in the applied scenarios.

An energy balance based, hourly, steady-state, modeling process with specific treatment of thermal inertia and thermal storage is assumed valid for energy systems analysis.

5.2 Overall CSP plant node model

The CSP node model predicts hourly power output based on configuration and

operating environment supplied or prescribed. Any part of the model that can be omitted from the hourly prediction, such as the heliostat field behavioral model, is processed prior to the temporal analysis. The overall process flow of the temporal model is shown in Figure 5.3.

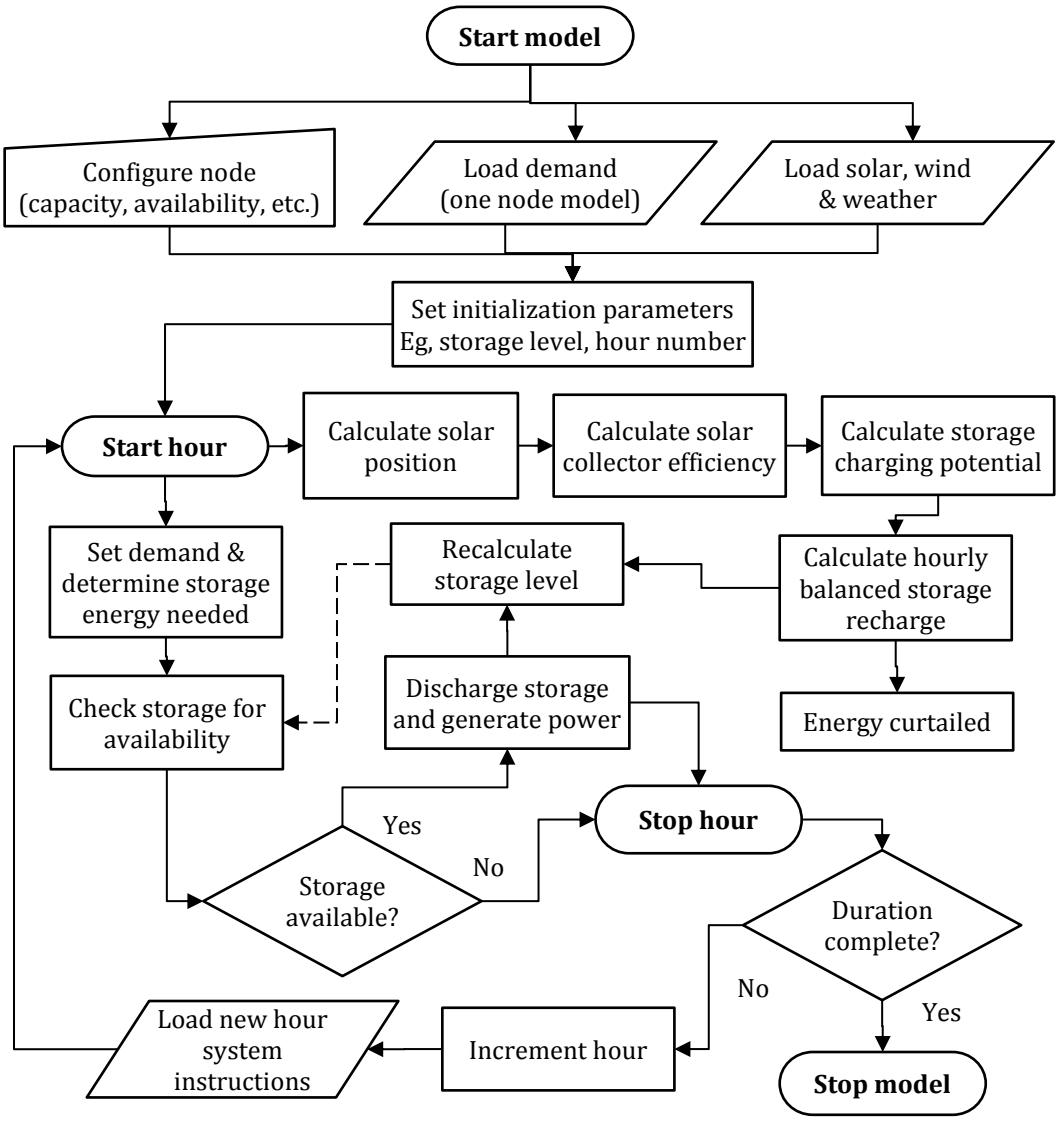

Figure 5.3: Overall CSP model structure flow diagram

The model is configured with all necessary node configuration ratings and limitations such as number of units, turbine rating per unit, system operating temperature, heliostat field model, storage rating per unit and availability. Any time dependent parameters are either supplied at the start or linked in by the systems model at the commencement of a time step. Each component of the model is described, primarily by physical principles, in the following sections.

5.3 Central receiver definition

The CSP plant process in the node model is based on the process of the state of the art system as elaborated in Chapter 2. Figure 5.4 illustrates the basic process.

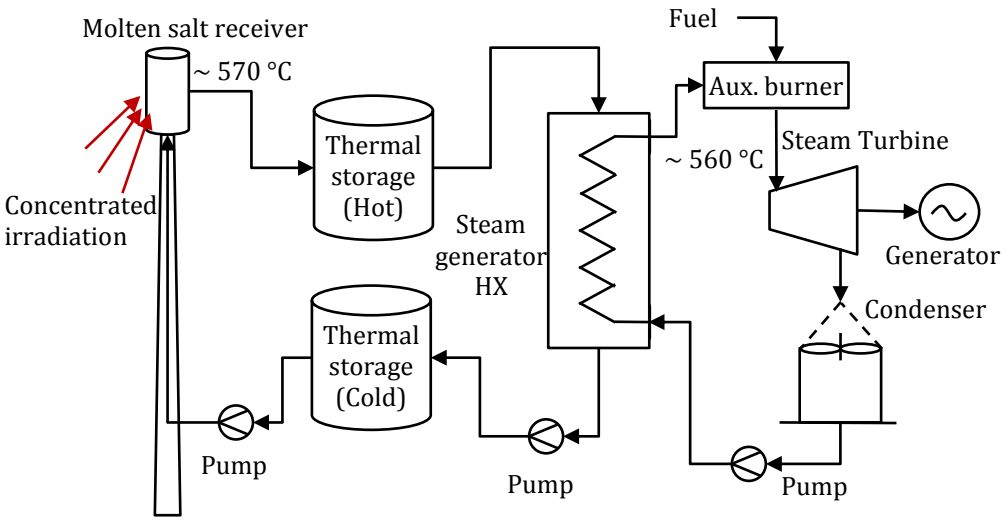

Figure 5.4: Schematic layout of the central receiver CSP plant for the model

The system operates using two working fluids. The charging loop working fluid is both heat transfer and storage medium. The power loop is a superheat steam power generation cycle. The model can be represented by any working fluids, such as the air-water cycle in Chapter 8, but always follows the process flows as indicated.

5.4 Heliostat optics

The concentrating system performance in the overall CSP model is determined by a correlation to the position of the sun and the relationship between the reflector system and receiver. The geometric components (cosine, blocking, shading and receiver spillage) are characterized by a reduced field performance model such as the commonly used azimuth/zenith efficiency table. This reduced model can be obtained by several means such as by ray-tracing or the use of convolution methods described by Bode and Gauché (2012). A compact cone optic field performance model intended for satisfying the needs of energy systems analysis was developed for this dissertation. Temporal and environmental conditions such as wind stowing and attenuation are treated in the temporal loop.

The geometric relations in Chapter 2 define all general geometric relationships in this chapter.

5.4.1 Reflector system energy balance

Optical energy analysis is simplified to single beam cone optics for one heliostat or a group of heliostats. Since only intercepted energy is of interest, no treatment is given

to image flux distribution or aiming as is found in more sophisticated convolution models such as Delsol (Kistler, 1986) or HFLCAL (Schwarzbözl, Pitz-Paal & Schmitz, 2009).

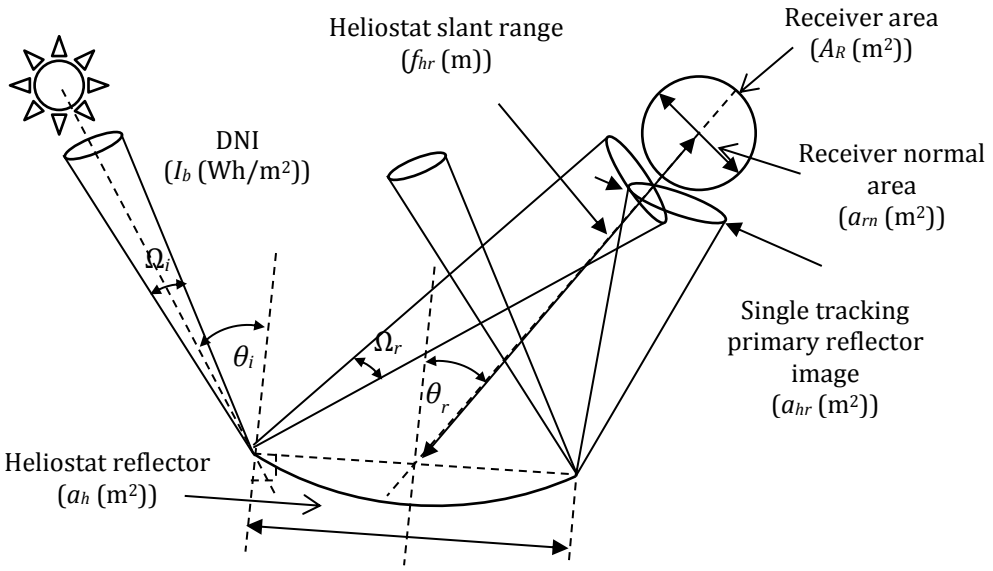

Figure 5.5: General heliostat-receiver optics illustrated two-dimensionally. Two edge incidence and reflected cones are shown.

The total incident optical energy on the receiver is the sum of optical energy from each heliostat or group of heliostats.

$$Q_R = \sum_{i=1}^{n} Q_{rh(i)} \tag{5.1}$$

where subscript R is receiver and $rh(i)$ is receiver intercepted energy per heliostat.

$$Q_{rh(i)} = I_b a_h \eta_r \eta_b \eta_s \eta_a \eta_s \eta_\theta \eta_{at} \eta_{spill} \tag{5.2}$$

where a_h is heliostat aperture area. Subscripts: r is reflector, b is blocking, s is shading, a is availability, s is soiling, θ is cosine, $spill$ is spillage, and at is atmospheric attenuation.

The reflected image cone angle (Ω_r) is the summation of the sun angle, effective tracking error and the effective beam quality of the heliostat.

$$\Omega_r = \Omega_i + \varepsilon_t + \varepsilon_r \tag{5.3}$$

where $\Omega_i = 9.3$ mrad is the sun angle, $\varepsilon_t = 1$ mrad is the tracking error, and $\varepsilon_r = 2$ mrad is the reflected beam quality including surface slope error, specularity and astigmatism.

$$a_{hr} = \pi\left(\frac{f_{hr}\Omega_r}{2}\right)^2 \tag{5.4}$$

where f_{hr} is the slant range to the receiver, thus assuming a uniform circular normal image. Spillage per heliostat is therefore linearly related to the intercepted normal projection area of the receiver relative to image size.

$$\eta_{spill} = \begin{cases} \frac{a_{rn}}{a_{hr}}, & a_{rn} < a_{hr} \\ 1, & a_{rn} \geq a_{hr} \end{cases} \tag{5.5}$$

where a_{rn} is the effective normal receiver intercepted area slant range normal receiver area such that the effective receiver area relative to the heliostat is scaled to the cosecant of the vertical term of the heliostat reflected unit vector $\hat{\boldsymbol{t}}_z$ from equation 5.13, and the intercepted area is simplified to the intercepted bounding box. While this is conservative per heliostat, its impact is marginal for the integrated field, and the assumption allows for the case where the receiver becomes a circular aperture.

5.4.2 Heliostat field efficiency

The geometric components of the net receiver optical efficiency, including cosine, blocking, shading and receiver spillage, are approximated by grouping heliostats into discretized cells as illustrated by Figure 5.6.

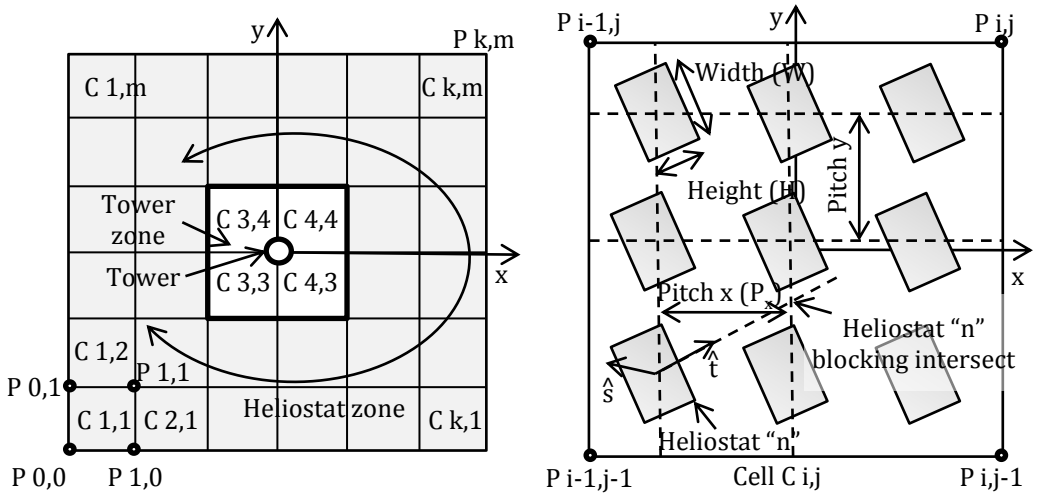

Figure 5.6: Plan view of heliostat field zones and cells (left) and one heliostat cell (right)

The field shown is rectangular with a tower zone in the center, but by cell weighting, any heliostat field can be approximated. Each zone (or cell) has multiple heliostats, although all heliostats in a cell are treated identically based on the center location of the cell. Figure 5.6 (right) schematically shows the principle dimensions needed or produced in the analysis. The geometry of only one heliostat is determined, and the impact of shading and blocking is done for heliostat "n" on itself.

$$\eta_{ro} = \eta_\theta \, \eta_b \, \eta_s \eta_{spill} \tag{5.6}$$

where η_{ro} is the receiver optical efficiency for a single cell.

$$\eta_{Ro} = \frac{\sum_{i,j=1}^{k,m} \left(d_A A_C \eta_\theta \, \eta_b \, \eta_s \eta_{spill}\right)_{(i,j)}}{\sum_{i,j=1}^{k,m} (d_A A)_{(i,j)}} \tag{5.7}$$

where η_{Ro} is the combined receiver optical efficiency, and each cell is weighted by the cell heliostat aperture density d_A.

$$d_A = \frac{A_{Ch}}{A_C} \tag{5.8}$$

where A_{Ch} is the heliostat aperture area, and A_C is the cell area.

The annual combined efficiency used by Schell (2010, 2011) is weighted by DNI for every hour.

$$\eta_{Roa} = \frac{\sum_{h=1}^{8760} \left(\eta_{Ro(h)} I_{b(h)}\right)}{\sum_{h=1}^{8760} I_{b(h)}} \tag{5.9}$$

where η_{Roa} is the annual combined optical efficiency.

The position of the sun and the receiver relative to the cell center determines the cosine efficiency. For convenience, Euclidean space is used to determine these relationships. Firstly, unit vectors (direction cosines) are determined from the cell center to the sun ($\hat{\boldsymbol{s}}$).

The vertical (z) component is represented by the cosine of the zenith angle.

$$\hat{\boldsymbol{s}}_z = \cos \theta_z \tag{5.10}$$

The other two terms (x, y) are represented by the compliment of the vertical and the solar azimuth angle.

$$\hat{\boldsymbol{s}}_x = -\cos \gamma_s \sin \theta_z \qquad \hat{\boldsymbol{s}}_y = -\sin \gamma_s \sin \theta_z \tag{5.11}$$

The reflected beam unit vector ($\hat{\boldsymbol{t}}$) is unique for each heliostat but only needs to be determined once assuming a stationary receiver. The slant range is given as

$$f_{hr} = \sqrt{T^2 + {C_{i,j,x}}^2 + {C_{i,j,y}}^2} \tag{5.12}$$

where T is the tower height, $C_{i,j,x}$ is the x position of a heliostat cell relative to the

tower, and $C_{i,j,y}$ is the y position of a heliostat cell relative to the tower.

$$\hat{\boldsymbol{t}}_z = \frac{T}{f_{hr}} \qquad \hat{\boldsymbol{t}}_x = \frac{-C_{i,j,x}}{f_{hr}} \qquad \hat{\boldsymbol{t}}_y = \frac{-C_{i,j,y}}{f_{hr}} \tag{5.13}$$

Having defined the incident ($\hat{\boldsymbol{s}}$) and reflecting ($\hat{\boldsymbol{t}}$) unit vectors, the heliostat incidence angle can be determined.

$$\theta_i = \frac{\cos^{-1}(\hat{\boldsymbol{s}} \cdot \hat{\boldsymbol{t}})}{2} \tag{5.14}$$

The heliostat shading and blocking efficiencies are based on the configuration shown in Figure 5.6 (right) and are approximations based on general geometric considerations. The blocking and shading methods are the same with the exception of the unit vectors used. The first step involves determining which heliostats block the heliostat of interest. Referring to Figure 5.7, the reflecting heliostat "n" is blocked by the heliostat or heliostats at the intercept of the unit vector $\hat{\boldsymbol{t}}$ and the line representing a particular row or column of heliostats for a rectangular arranged set of heliostats.

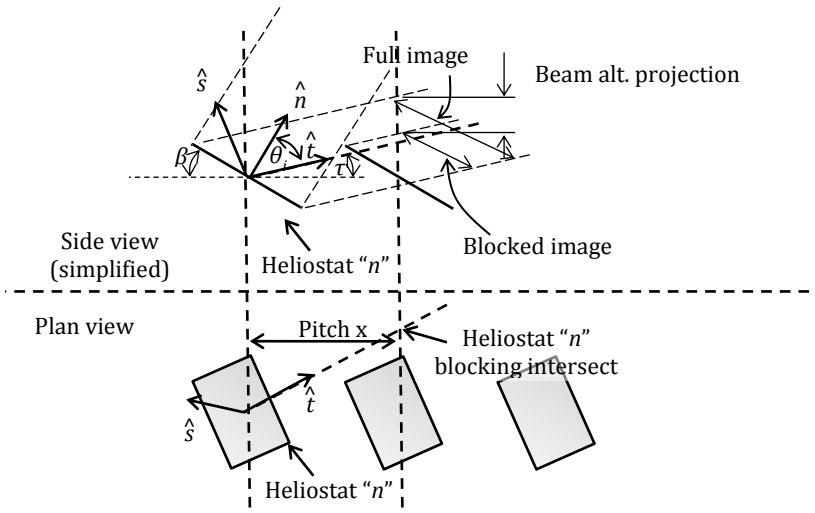

Figure 5.7: Principle heliostat blocking parameters

Because a cell contains a group of heliostats, all heliostats in the cell assume the same direction vectors as a virtual heliostat at the center of the cell. The intercept is used only to determine the horizontally projected reflected light path length to the intercept and the elevation of the beam at the intercepting heliostat(s). For a rectangular array, if

$$\frac{|\hat{\boldsymbol{t}}_x|}{P_x} > \frac{|\hat{\boldsymbol{t}}_y|}{P_y} \tag{5.15}$$

then the blocking is caused by the heliostat row one line over in the x direction.

Otherwise the blocking is caused by the adjacent heliostat row one line over in the y direction.

For the case where the above "if" test is true, the resultant "beam altitude projection" (B_a), the height of the image from the heliostat projected at the distance of the pitch of the intercepting heliostat(s) is defined as

$$B_a = \hat{\boldsymbol{t}}_z \frac{P_x}{|\hat{\boldsymbol{t}}_x|} \tag{5.16}$$

This value determines the vertical component of the non-blocked image. The equation is similar for the false "if" result. The blocking efficiency is a ratio of the reflection cosine of B_a to the angle of incidence cosine of the full image with a modification for the gaps between the blocking heliostats based on the ratio of the heliostat width (W) to pitch (P). The blocking efficiency reduces to

$$\eta_b = \frac{B_a \cos(\tau)}{H \cos(\theta_i)} \frac{P}{W} = \frac{B_a \, \hat{\boldsymbol{t}}_z}{H \cos(\theta_i)} \frac{P}{W} \tag{5.17}$$

This simplified expression shows that maintaining a constant area but changing the dimensions (H, W) of a heliostat makes no difference to the result. The shading efficiency uses the same method but uses the incident unit vector instead of the reflected one.

$$\eta_s = \frac{B_a \, \hat{\boldsymbol{s}}_z}{H \cos(\theta_i)} \frac{P}{W} \tag{5.18}$$

5.4.3 Net field optical results and validation

Schell (2011) reports that an in-house ray tracing algorithm predicts an annual efficiency of 70.1 % for the eSolar SierraTowers system with tower height at 50 m. The NREL SolarPACES reference indicates that these towers are 55 m (NREL, 2011d). For the 50 m configuration, the model predicts 62.3 % and 64.8 % for Lancaster and Upington (South Africa) respectively. For a 55 m tower, the model predicts 67.2 % and 69.9 % respectively as shown in Figure 5.8, which shows the result as a function of tower height. Interestingly, per the result, a 55 m tower is located near the inflection point where shading and blocking is no longer a significant factor in the performance of the plant.

For the same case, Figure 5.9 is a surface plot of the net geometric optical efficiency as a function of sun position. The result indicates that optical performance is mostly a function of the zenith angle and correlates with other models such as reported by Leonardi and D'Aguanno (2011).

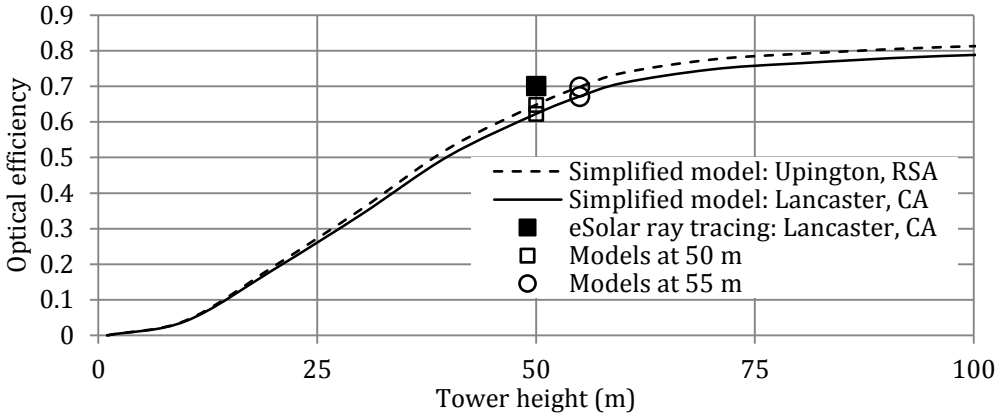

Figure 5.8: Comparison of cosine, shading and blocking vs. tower height (defined as midpoint of receiver above heliostat field)

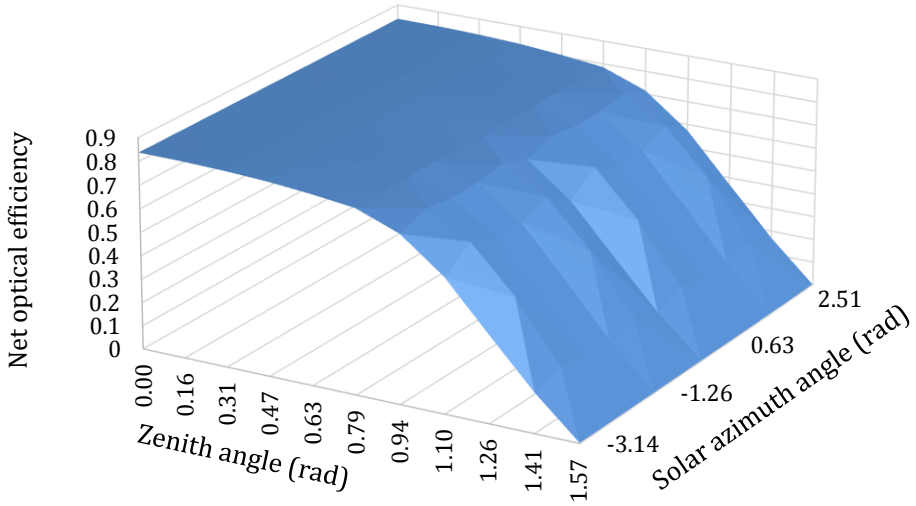

Figure 5.9: Net geometric optical efficiency as function of zenith angle and solar azimuth angle for the case reported by Schell (2011)

The net, blocking, shading and cosine geometric optical efficiency values of this case are tabulated in Appendix A. The tabulated data provides efficiency values in increments of zenith and solar azimuth angles in the lookup table format used by other CSP simulation tools such as the generic CSP model in SAM (Gilman & Dobos, 2012). While using such a lookup table offers convenience and flexibility, the predictability of the surround heliostat field allows for further simplification to zenith angle interpolation of the average solar azimuth angle efficiencies or the use of a curve fit of the average shown by Figure 5.10 and equation 5.19.

$$\eta_{Ro} = 0.4254{\theta_z}^6 - 1.148{\theta_z}^5 + 0.3507{\theta_z}^4 + 0.755{\theta_z}^3 - 0.5918{\theta_z}^2 + 0.0816\theta_z + 0.832 \quad (5.19)$$

Equation 5.19 is used in the model, and it is assumed representative of a state of the

art system with a ± 0.02 efficiency deviation on an annual basis.

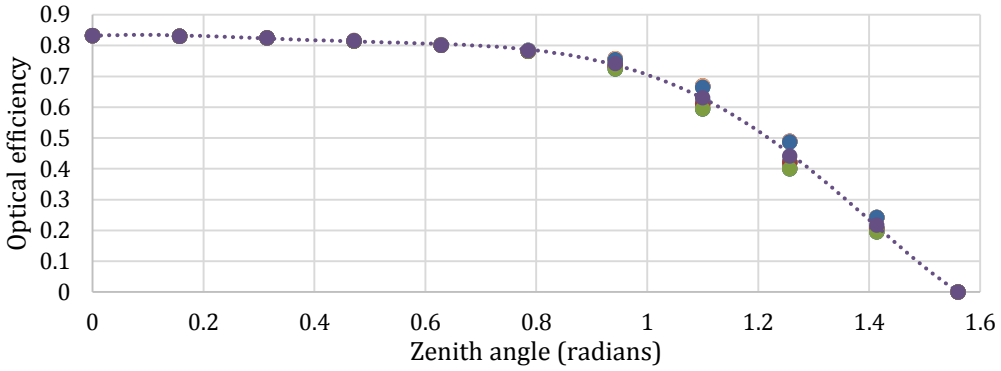

Figure 5.10: Approximation for net geometric optical efficiency with each color marker representing a different solar azimuth angle per Figure 5.9

5.4.4 Heliostat-receiver environmental losses

Environmental heliostat–receiver performance efficiencies are treated independently from the geometric optics and include mirror reflectivity, heliostat availability, mirror soiling, high wind cutoff, and atmospheric attenuation. Except for atmospheric attenuation, most of these are simple parameters and set as a matter of design choice. Typical values used are given in Table 5.1.

Table 5.1: Typical environmental based optical values

Parameter	Efficiency	Deviation
Mirror reflectivity	0.95	± 0.01
Heliostat availability	0.99	± 0.01
Mirror soiling	0.95	-
Atmospheric attenuation	0.95	± 0.04
High wind cutoff	1.0 (v_m < 15 m/s) 0.0 (v_m ≥ 15 m/s)	± 0.00 (± 5 m/s)

Two environmental parameters show a high degree of sensitivity and are discussed in more detail. Firstly, the choice of wind cutoff speed has an impact on annual plant performance at a specific location as indicated in Figure 5.11.

Wind properties vary considerably by location and local climate. Annual performance at two South African locations, Welkom (approximately 26.775 °E, 27.975 °S) and south of De Aar (approximately 23.625 °E, 31.425 °S), show the impact of cutoff limits relative to no cutoff limit at the better site, thus also indicating performance of weather in general. Welkom is characterized by summer storms or cloudy conditions leading to lower annual DNI but lower wind speeds in clear conditions. The site near De Aar is more typical of a high DNI dry region but generally windy.

The simple Boolean model using hourly averaged wind speed is a matter to be

revisited due to wind-based stowing being a function of intra-hour wind behavior. It is also noted that the choice of wind cutoff is likely to have a significant impact on heliostat field cost, the highest cost component in a CSP plant (Emes, Arjomandi & Nathan, 2015). In this way, it is conceivable that a fully optimized plant in Welkom could have a lower cost of electricity production.

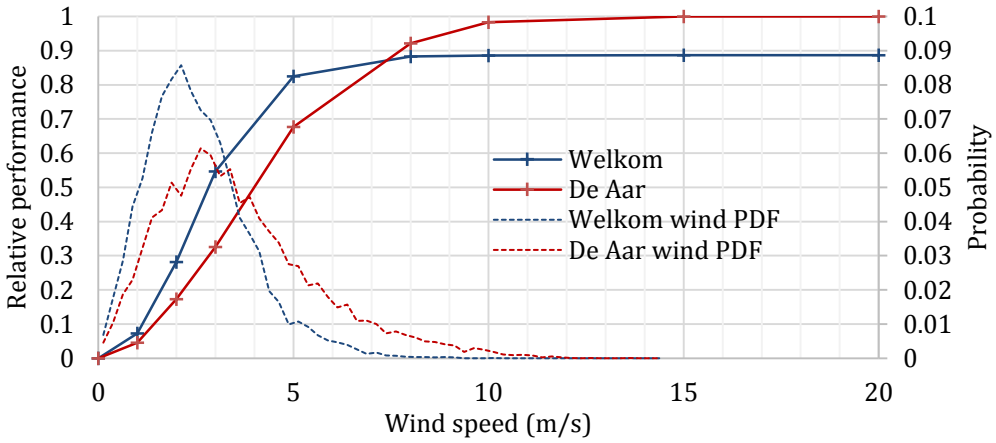

Figure 5.11: Cumulative annual performance impact as a function of wind cutoff speed. Sites indicated use zero cutoff performance of best site as ratio denominator. Wind probability distribution is indicated by respective dotted lines.

The second sensitive environmental parameter is atmospheric attenuation. Illustrated in Figure 5.12, atmospheric attenuation for central receivers is the loss of energy due to attenuation of the reflected beam between heliostats and receiver. While attenuation is included in the ground measurement of DNI, it needs to be added for this additional distance of beam travel. Attenuation can be high in the final 250 m of atmosphere and can result in significant energy loss; this needs to be accounted for in a central receiver model.

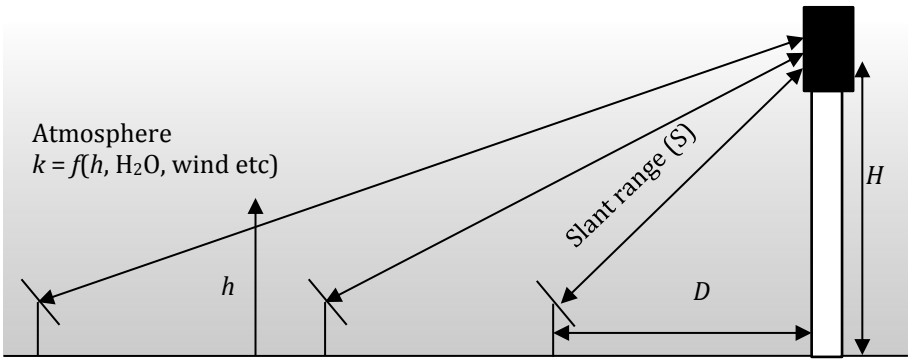

Figure 5.12: Definition of slant range for atmospheric attenuation

Quantifying, measuring and modeling the solar weighted optical depth and attenuation is difficult as it is a function of numerous variables and cannot easily be measured. At this time, there is no agreed measuring standard and various research

institutions are investigating methods to accurately do so (Ballestrín & Marzo, 2012; Sengupta & Wagner, 2012). As a result of very little good data and no standard measurements or standard methods to derive attenuation from solar and weather resource data sets, it is not possible to study the integrated effect of attenuation in this dissertation. The approach taken is to explore the sensitivity of attenuation on the heliostat field performance through re-analysis of existing data and models, assuming that the data and its impact are valid.

Ballestrín & Marzo (2012) perform an analysis of attenuation for a specific site by mathematically separating the monochromatic spectral distributions of measured transmitted irradiance over various transmitted distances including the spectral qualities of a mirror and the solar spectrum. The authors found discrepancies between most models but achieved good correlation with the Pitman & Vant-Hull five variable physical model adjusted to the selected site (Pitman & Vant-Hull, 1984). In a similar manner to most other heliostat field attenuation models, the result is approximated using a third order polynomial valid up to 4 km.

$$\text{Loss}(\%) = 0.29544 + 15.22128\,S - 1.8598\,S^2 + 0.15182\,S^3 \qquad (5.20)$$

representing clear sky (23 km) visibility.

$$\text{Loss}(\%) = 0.77941 + 55.49083\,S - 14.78875\,S^2 + 1.53718\,S^3 \qquad (5.21)$$

representing hazy sky (5 km) visibility.

Other approximations reported and used are provided in Appendix A. These models do not satisfy the need to achieve greater reduction of physical parameters for this dissertation, and a simple yet more fundamental relationship is explored here. The Beer-Bouguer-Lambert law (hereon, Lambert's law) describes transmission through a medium.

$$\tau_L = e^{-kDL} \qquad (5.22)$$

where kD is the transmission loss coefficient in a transmissive medium, and L is the distance of transmission. The longer range data fit of Leary & Hankins (1979) suggests that this law might be appropriate for approximating attenuation in general. The physical model of Pitman & Vant-Hull (1984) suggest that attenuation is a function of five explicit variables (site elevation, water vapor, scattering coefficient, tower height and slant range), three implicit variables (time of year, climate and elevation above ground) and the qualities of the heliostat relative to the solar spectrum. Assuming the transmission loss coefficient is applicable, then Lambert's law approximates atmospheric attenuation

$$\tau_a \approx e^{-am\,S} \qquad (5.23)$$

where am is a data fitted mean attenuation coefficient, and S is slant range.

Figure 5.13 shows that this approximation leads to a flatter curve, suggesting that the effective attenuation coefficient changes over distance. Presumably, this is why previous authors have fitted data and models using third order polynomials, particularly for the region within the first km.

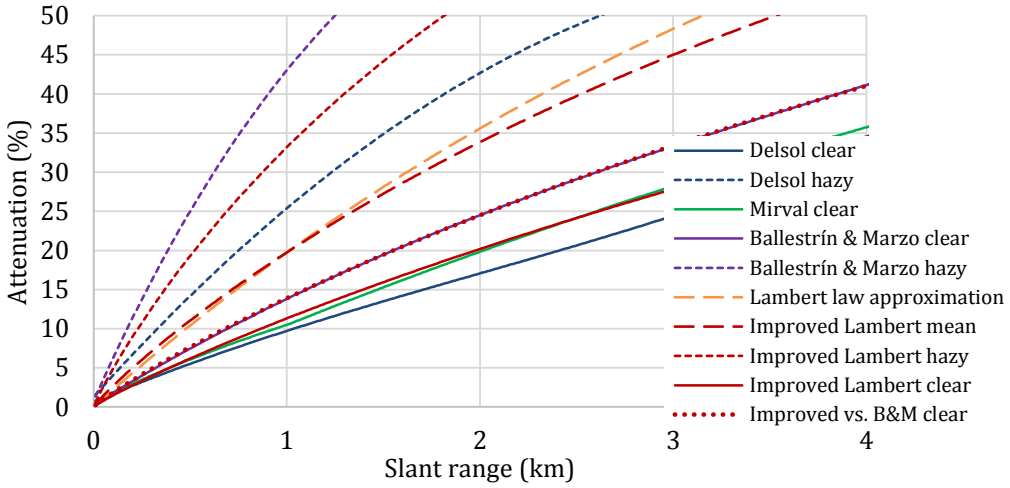

Figure 5.13: Attenuation loss models

The transmission modeling of Ballestrín & Marzo (2012) suggests that the region of transmission between heliostat and tower has varying rational monochromatic transmission decay effects that would not behave to Lambert's law when integrated. To accommodate the effect of varying rates of decay, a distance based decay is proposed for the attenuation coefficient.

$$\tau_a \approx e^{-am\, S^d} \tag{5.24}$$

where *d* is a distance decay power factor between 0 - 1. A deviation factor for handling the range from clear to hazy skies is also introduced.

$$\tau_a \approx e^{-am^{(1+dev)}\, S^d} \tag{5.25}$$

where *am* is a data fitted mean attenuation coefficient and *dev* is a deviation term such that

$$Loss(\%)_m = 100\left(1 - e^{-am^1\, S^d}\right) \tag{5.26}$$

$$Loss(\%)_{clear} = 100\left(1 - e^{-am^{(1+\sigma)}\, S^d}\right) \tag{5.27}$$

$$Loss(\%)_{hazy} = 100\left(1 - e^{-am^{(1-\sigma)}\, S^d}\right) \tag{5.28}$$

where subscripts *m*, *clear* and *hazy* represent median, clear sky and hazy conditions respectively. σ is a deviation representing the departure of clear and hazy skies from

the median. The values

$$am = 0.22 \quad d = 0.91 \quad \sigma = 0.4 \quad \sigma_{B\&M} = 0.255 \tag{5.29}$$

provide a good range from clear to hazy skies and comparison to Ballestrín & Marzo clear sky ($\sigma_{B\&M}$) shows excellent correlation over slant range.

This measurement provides a single fundamentally based reduced expression that is a function of slant range and sky clarity only and is not prone to extrapolation error.

Figure 5.14 illustrates an example of the integrated collector loss per unit based on circular heliostat fields. The example assumes that a 100 MW unit with 12 hours of storage occupies 5 km² of land. Using a similar method to the geometric optical model, the area is discretized, and the area weighted losses are aggregated.

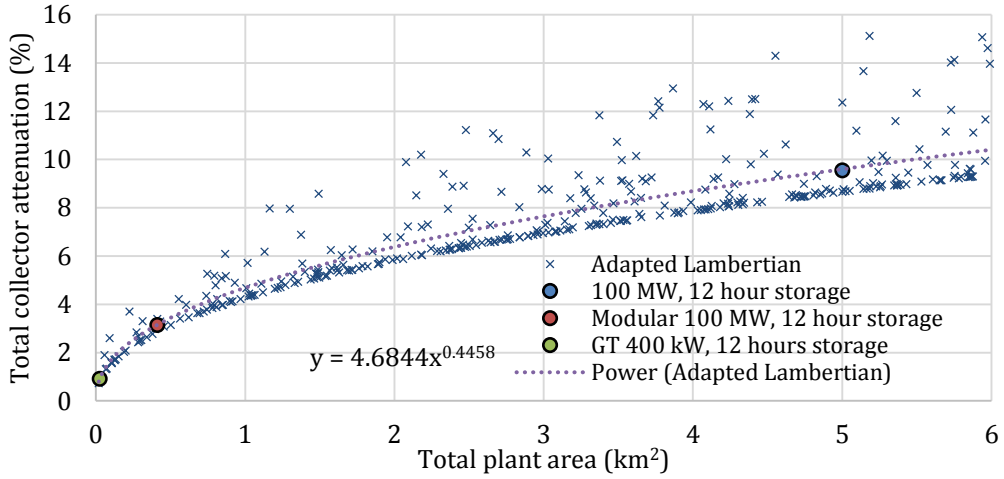

Figure 5.14: Central receiver collector performance loss by attenuation

Assuming that CSP plants will be located in clear-sky areas, a power law weighting is used to bias attenuation towards clear sky conditions in a probabilistic simulation, resulting in a unit (single tower) based loss as a function of plant total area. The result is represented by the power law curve fit shown in Figure 5.14 and Equation 5.30. Three point configurations of central receiver plants are indicated on the trend-line. A hypothetical 400 kW solarized gas turbine unit with 12 hours of storage will result in a loss of 1 % by attenuation. A 100 MW plant also with 12 hours of storage using modular towers as proposed by eSolar (Tyner & Wasyluk, 2014) will result in a loss slightly above 3 %, and a large single unit plant of similar rating will lose about 9 %.

$$\eta_{Raa} = 1 - 0.046844\ {A_{tu}}^{0.4458} \tag{5.30}$$

where η_{Raa} is the net attenuation efficiency for a tower unit occupying an area A_{tu} in units of km². The area occupied can be approximated by the field optical area and density.

$$A_{tu} = \frac{A_{au}}{f_{du}} \approx \pi {d_{hm}}^2 \tag{5.31}$$

where A_{au} is the heliostat field aperture area in km², and f_{du} is the field density relative to all land occupied by the tower unit including road access and power plant. A further approximation is based on the distance of the mean slant range of the outermost heliostats, d_{hm}.

Due to uncertainty, the assumptions made and the indifference to plant size in the CSP model, attenuation is not an explicit function variable. The model assumes that in the near future, an equal proportion of plant unit sizes are used, but a larger model deviation (± 0.04) is assumed for the sensitivity analysis, implying the range from very small to very large units can occur.

5.5 Receiver energy balance

The receiver model is one dimensional and reduces to only the most elementary parameters considered necessary to offer sufficient accuracy and tolerance to technology variation: inlet temperature, outlet temperature, total incident solar flux, effective view factors for convection and radiation losses, and surface radiation properties. Figure 5.15 illustrates the energy balance of the receiver generically.

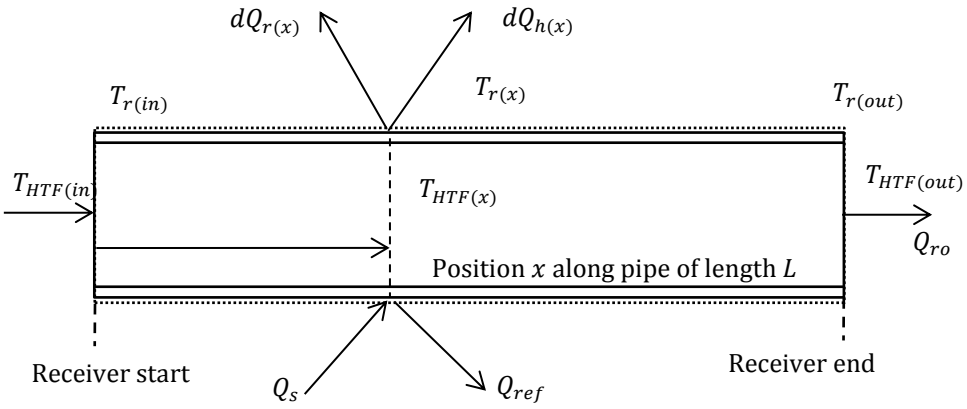

Figure 5.15: Generic representation for the receiver energy balance

The overall reduced hourly-averaged energy balance is

$$Q_s = Q_{ref} + \int_{x=0}^{L} Q_r dx + \int_{x=0}^{L} Q_h dx + Q_{ro} \tag{5.32}$$

representing incident and reflected concentrated irradiation by

$$Q_s - Q_{ref} = \alpha_s Q_s \tag{5.33}$$

and where subscripts *s* is incident irradiation, *r* is thermal radiation, *h* is convective heat transfer, *ref* is reflected irradiation, and *ro* is energy transferred to the heat transfer medium (*HTF*).

A basic radiation loss model that considers only the average receiver temperature and environment is given as

$$Q_r = \sigma \varepsilon_r A_r F_r \left(\overline{T_r}^4 - T_{ra}{}^4 \right) \tag{5.34}$$

where $\overline{T_r}$ is the simple average between inlet and outlet and T_{ra} is ambient temperature T_a.

Appendix A.2. summarizes a sensitivity study on the choice of the environment radiant temperature; this suggests that the radiant surrounding is well represented by ambient temperature (T_a), which is a blend between the radiant sky temperature and ground temperature. The average receiver temperature radiation model, however, does not compare well with radiation calculated in a discretized non-linear model of the receiver, as indicated by the 'Basic radiation' correlation of the left plot in Figure 5.16. While relatively inconsequential in the overall system performance, as characterized by high concentration levels, it turns out that an easy improvement is possible and implemented to ensure validity for lower concentration cases.

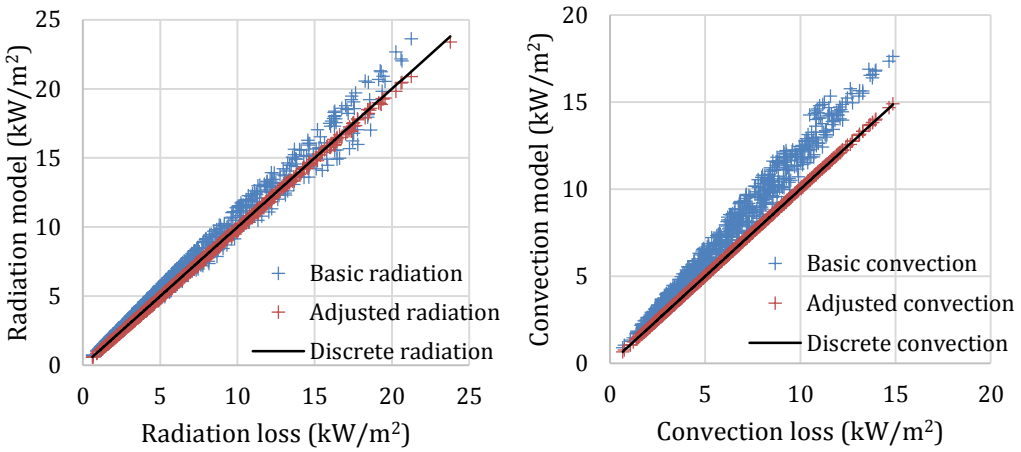

Figure 5.16: Receiver model correlation for radiation (left) and convection (right)

The radiation loss in the discretized receiver model assumes a constant irradiation flux and predictable sensible heating, assuming this is valid to remain technology indifferent. For a receiver with a given flow length (L), radiant loss at a position (x) along the length is represented by

$$dQ_{r(x)} = \sigma \varepsilon_{r(x)} F_{r(x)} \left(T_{r(x)}{}^4 - T_{ra}{}^4 \right) dA \tag{5.35}$$

Assuming that the surface emissivity (ε_r) and view factor (F_r) are not a strong function of position or temperature, the radiation losses integrate to

$$Q_r = \sigma \varepsilon_r F_r \int_{x=0}^{L} \left({T_{r(x)}}^4 - {T_{ra}}^4 \right) dA \tag{5.36}$$

and are discretized into sections of the receiver represented by

$$Q_r \approx \sigma \varepsilon_r F_r \sum_{i=1}^{n} A_{(i)} \left({T_{r(i)}}^4 - {T_{ra}}^4 \right) \tag{5.37}$$

With a key assumption that the receiver inlet and outlet temperatures are set and controlled by heat transfer fluid flow rate, determination of discretized surface temperatures needs to be done iteratively and in combination with reflection and convection losses. A probability analysis of the discrete model using a broad range of values for the primary influence variables of the receiver model was performed. The variable value ranges are given in Table 5.2.

Table 5.2: Receiver energy balance variable value range settings

Variable	Unit	Default	High	Low
External receiver outlet temperature	°C	590	1,000	300
External receiver inlet temperature	°C	290	600	27
Concentration ratio	-	-	3,000	5
Receiver solar reflectivity	-	0.9	0.95	0.8
Receiver thermal emissivity	-	0.9	0.95	0.8
Wind speed	m/s	-	15	1
Radiant view factor	-	1.0	1.0	0.3
Ambient temperature	°C	25	-	-

All solutions able to meet the receiver outlet setting predictably demonstrated a temperature rise and temperature rate variance in the flow direction. This suggests that the mean receiver temperature would be better approximated using a temperature bias and, in the case of radiation, a temperature extremity approximation. The receiver is therefore represented using two temperatures related to the inlet and outlet temperatures with two fixed coefficients (δ_1 and δ_2) representing adjustment for temperature extremity and bias respectively. Each temperature represents half of the receiver such that

$$\begin{aligned} Q_r \approx \sigma \varepsilon_r A_r F_r \Big(& 0.5\left(273.15 + T_{r(in)} + \delta_1 \Delta T - \delta_2 \Delta T\right)^4 \\ & + 0.5\left(273.15 + T_{r(out)} - \delta_1 \Delta T - \delta_2 \Delta T\right)^4 - {T_{ra}}^4 \Big) \end{aligned} \tag{5.38}$$

where

$$\Delta T = T_{r(out)} - T_{r(in)} \tag{5.39}$$

$$T_{ra} = 273.15 + T_a \tag{5.40}$$

and values $\delta_1 = 0.137$ and $\delta_2 = 0.18$ resulted in the improved correlation shown in Figure 5.16.

The acceptability of the radiation loss model can also be assessed on the annual cumulative energy yield on the receiver. For one typical configuration, a linear change to radiation, due typically to a change in surface emissivity or view factor, results in a -0.63 % variance in annual performance for a 10 % variance of that factor when the receiver is operating at a maximum external temperature of 590 °C. The high temperature approximation model variance is similarly 0.18 % for a 10 % variation in δ_1, and the ambient variance is 0.0011 % per 1 °C change in the radiant environment temperature.

Convective heat transfer from the receiver presents a difficulty in that a large number of factors influence convective heat transfer. As this model needs to be generic enough to reasonably represent any CSP plant, those parameters that are known for the decision are (1) Flow is external and typically around cylindrical objects. (2) Flow rates and length scales imply that the flow is mostly turbulent. (3) The model uses hourly data for wind, and in the majority of cases there is sufficient wind to classify it as forced. A very simple and general external flow forced convection heat transfer relationship is used (Mills, 1995; Duffie & Beckman, 2006) because of the very weak sensitivity that convective losses indicate in the model, besides the inability to be prescriptive.

$$Q_h = hA_r(T_{hr} - T_a) \tag{5.41}$$

where *hr* denotes receiver convection and

$$h = 2.8 + 3v \tag{5.42}$$

Using a simple average or receiver temperature results in a significant positive bias, typically exceeding 20 %, in results when compared with the discrete model. A bias coefficient, similar to that used in the radiation model is added.

$$T_{hr} = \frac{T_{r,out} + T_{r,in}}{2} - \delta_3 \Delta T \tag{5.43}$$

with the bias coefficient $\delta_3 = 0.13$ resulted in the improved correlation shown in the right plot of Figure 5.16. The difference between δ_2 and δ_3 leaves the correlations appearing somewhat arbitrary. Associating the coefficients geometrically produces the same result ($\delta_3 = 0.131$), so only two independent correction coefficients exist for the radiation and convection model.

$$\delta_3 = (1 - 2\delta_1)\delta_2 \tag{5.44}$$

The generality of Equations 5.38, 5.43 and 5.44 was tested by exposing the receiver to zones of different flux densities in order to test the ability to model receivers that handle phase change. In all cases, the probability parameter correlation produced similarly accurate results, provided the coefficients were adapted. In non-extreme cases, such as 60 % of the area exposed to double the flux density of the remaining 40 %, the default coefficients remained valid.

Air velocity has a linear impact on convection losses, and due to the generally significant height of receivers it needs appropriate treatment. Wind speed data is typically available for a specified height of 10 m above ground unless it is data specifically intended for other purposes such as wind turbine performance prediction. The Hellman exponential law is a commonly used model and simple to use. Banuelos-Ruedas *et al.* (2010) suggest that with so many factors influencing wind speed at different heights, extrapolation should be used with care, particularly if only one wind speed height is available.

$$v = v_0 \left(\frac{H}{H_0}\right)^{\alpha} \tag{5.45}$$

By using appropriate friction coefficients and with an understanding that convection losses are of a second order of importance, unlike in wind turbine analysis, extrapolation in this manner is considered appropriate based on results. Table 5.3 lists typical friction coefficients.

Table 5.3: Friction coefficients for Hellman exponential law (Bañuelos-Ruedas, Angeles-Camacho & Rios-Marcuello, 2010)

Landscape type	Friction coefficient (α)
Lakes, ocean and smooth hard ground	0.10
Grasslands (ground level)	0.15
Tall crops, hedges and shrubs	0.20
Heavily forested land	0.25
Small town with some trees and shrubs	0.30
City areas with high rise buildings	0.40

Selection of a friction coefficient is based on observation of areas in South Africa where CSP plants are most likely, namely areas that have high annual DNI and are already relatively flat. Some representative landscapes are shown in Figure 5.17.

A median value of α = 0.15 has been chosen to represent the range from hard flat surfaces to areas adjacent to agricultural crops. As the wind data used in this study pertains to the land in its current state, it is assumed that the addition of expansive heliostat fields (or other reflector types) will reduce wind speeds near ground level and increase the friction coefficient, leading to the same wind speed at greater heights. Accordingly, no adjustment for the optical field is considered necessary.

Figure 1.18 shows a simple sensitivity analysis on friction factor that indicates that wind speed estimation on a 200 m tower will vary by about 14 % with a change in friction factor of 0.05. This in turn has a variance of 0.52 % on annual receiver output at a typical site for a receiver operating at 590 °C.

The overall receiver energy balance model is assessed based on its performance compared with the discretized model using a probability analysis based on the

variable range of Table 5.2. Receiver outlet performance is an indicator of the combined model and shows excellent correlation to the discrete model as presented in Figure 5.19 (left).

Figure 5.17: Typical Northern Cape areas deemed likely suitable for CSP (photos by author): about 25 km west of Pofadder GPS: 29.1 °E, 19.0 °S (top), and in the region of Brandvlei GPS: 30.3 °E, 20.5 °S (bottom)

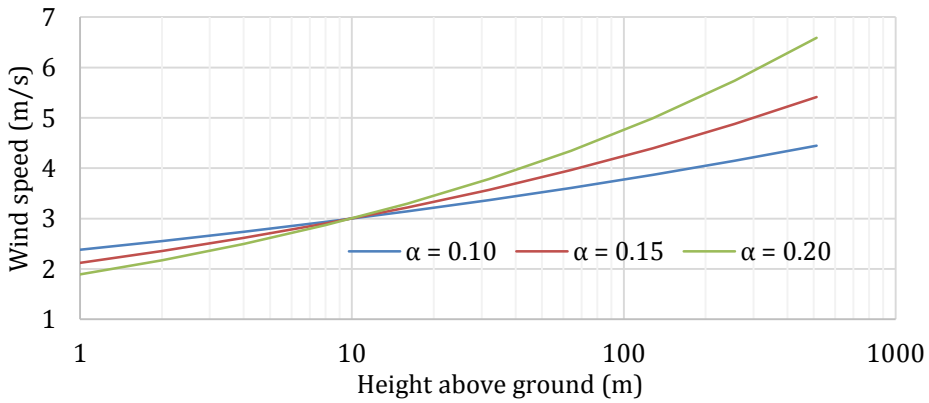

Figure 5.18: Wind speed profile for a reference wind speed of 3 m/s at 10 m and friction coefficients of 0.10, 0.15 and 0.20

This good correlation is not unexpected as it only demonstrates validity of the model

based on a discretized iterative analysis with the same assumptions. Before further validation is conducted using other data sources, the sensitivity of the variables in the model can be used to argue the model's validity.

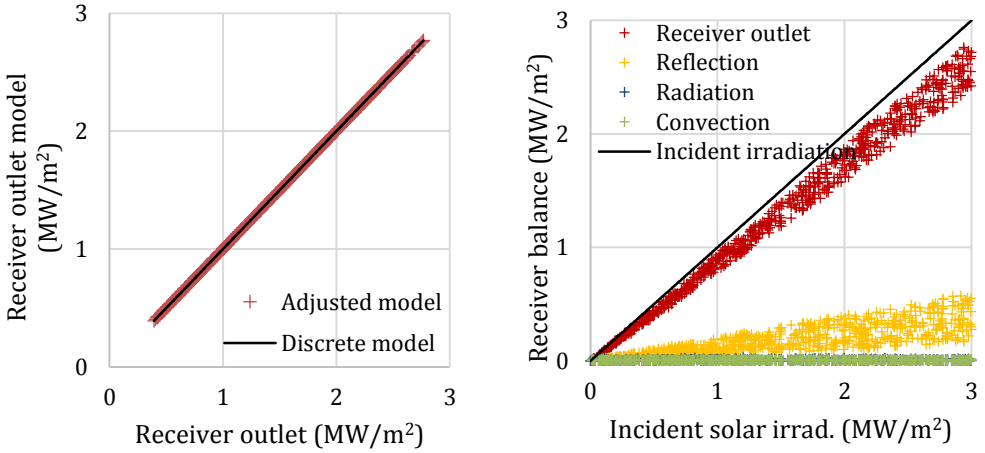

Figure 5.19: Receiver model correlation for outlet energy (left) and disaggregation by incident irradiation (right)

The range of variables in Table 5.2 represents most conceivable central receiver designs expected in future in an equality wide ranging set of environments. It is argued that these ranges will produce results exceeding variances that can be expected for more precisely defined plants in the environments in which they will be placed. In this way for instance, a high temperature receiver for a solarized gas turbine plant is represented by forcing a high temperature and varying receiver efficiency by concentration ratio, receiver reflectivity and view factor, the latter two being proxy variables for glazed receivers. If the receiver is unable to reach the operating temperature, no energy is delivered. Model parameter sensitivity is demonstrated by plotting each energy balance component from the probability analysis, as shown in Figure 5.19 (right) and Figure 5.20, using a logarithmic independent variable axis.

Typical receiver outlet energy (and variance) correlates almost linearly with effective concentration ratio and incident irradiation flux density. Similarly, most energy is lost due to light reflection, and this is increasingly the case at higher concentration ratios. Convection and radiation losses are not significant contributors, and neither component is linked to concentration ratio as is expected. The proportional contribution of these losses increases with diminishing concentration to the point where the receiver cannot reach operating point, thus yielding no output energy.

Above a concentration ratio of 200, receiver efficiency typically has a variance of less than ± 0.10 and an R^2 value of 0.988 with a linear correlation to an effective concentration ratio. The variance drops below ± 0.01 when receiver reflectivity is not varied. Assuming that the variable range results exceed the model accuracy, the model is considered sufficient and a model variance of ± 0.02 is assumed.

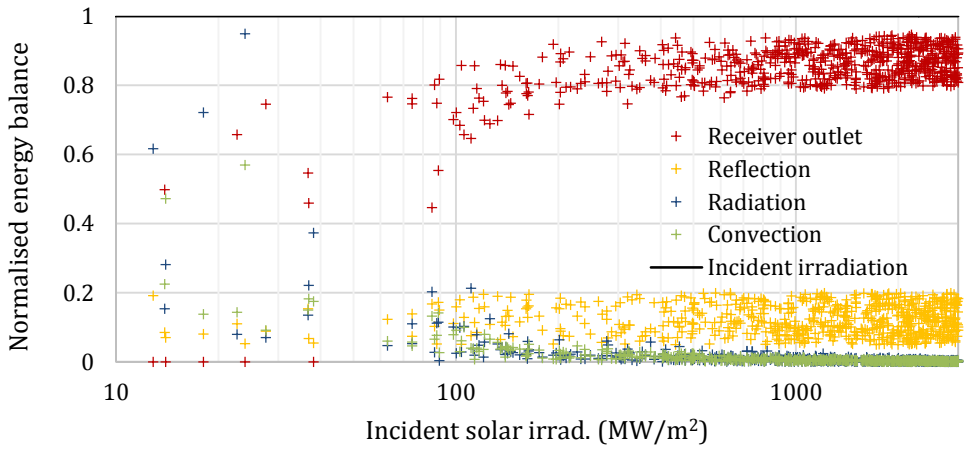

Figure 5.20: Receiver energy balance model disaggregation normalized with logarithmic independent axis

5.6 Thermal energy storage

The thermal energy storage model consists of three lumped parameter components that have associated energy transfer efficiencies and limitations: (1) energy transfer to storage, (2) storage capacity, and (3) energy transferred out of storage. The model transfers all energy received from the collector system to storage regardless of time of day, thus energy transfer conversion efficiencies are always encountered.

The primary specification for the storage is the capacity, specified as hours at full turbine rating (H_{FTR}). This specification is used as it is a popular specification rather than a technical one and is in keeping with the use of the model. The amount of energy in a fully charged storage system is determined from the specifications and typical operating conditions of the turbine.

$$Q_{s(full)} = \frac{H_{FTR} P_{FTR}}{\eta_{t(ref)}} \tag{5.46}$$

where $\eta_{t(ref)}$ is based on the turbine efficiency at reference conditions. The amount of energy in storage is determined at each hour.

$$Q_{s(t)} = \eta_s Q_{s(t-1)} + Q_{s(i,t)} - Q_{s(o,t)} \tag{5.47}$$

where (t) is the current time step, $(t-1)$ is the previous time step, η_s is the thermal storage efficiency per hour and set to 99.8 % (per hour), i is storage inlet from receiver, and o is storage energy dispatched for power generation.

$$Q_{s(i,t)} = \eta_{sc} Q_{r(o,t)} \tag{5.48}$$

η_{sc} is the storage charging efficiency and set to 99 %. $Q_{r(o,t)}$ is thermal energy from the receiver at that time step.

$$Q_{s(o,t)} = \frac{Q_{he(i,t)}}{\eta_{sd}} = \frac{E_{g(t)}}{\eta_{N(t)}\eta_{sd}} \tag{5.49}$$

η_{sd} is the storage dispatch efficiency also set to 99 %. $Q_{he(i,t)}$ is the thermal energy required by the heat engine for gross power (E_g) where η_N is the efficiency of the heat engine.

Storage charging and dispatch are governed by a number of system parameters and constraints not covered here. Principally, the storage needs to always fall within useful storage limits.

$$Q_{s(full)} \leq Q_{s(t)} \leq 0 \tag{5.50}$$

Within an hour, if the storage is full or approaching full, it can fully charge, at which time charging is governed by dispatch needs; this allows storage to remain full at the end of the hour.

Assuming sensible heating, temperature drops as a consequence of heat exchange. Therefore, thermal energy exiting the storage will be at a reduced temperature, thus reducing heat engine performance further. A simple lumped parameter analysis of a typical molten salt storage system, its parameters described in Table 5.4 (Gil et al., 2010), suggests very small temperature fluctuations. The model assumes an efficiency based temperature reduction from receiver to turbine as is shown in Table 5.5.

Table 5.4: Parameters for a high temperature thermal storage unit

Parameter	Unit	Value
Hot tank temperature (T_h)	°C	560
Height (H_T)	m	20
Diameter (D_T)	m	30
Specific heat (C_p)	KJ/kg.K	1.214
Density (ρ)	Kg/m^3	1794
Thermal insulation loss coefficient (R)	W/m^2.K	0.4
Ambient temperature (T_a)	°C	25

Heat loss is approximated as one dimensional through the thermal insulation of the tank sides.

$$\dot{Q}_T = RA_T(T_h - T_a) \approx R\pi D_T H_T(T_h - T_a) = 403 \text{ kW} \tag{5.51}$$

resulting in heat loss over 24 hours

$$Q_{T(24h)} \approx 34.85 \text{ GJ} \tag{5.52}$$

and the corresponding temperature drop for that volume of storage

$$\Delta T_{24h} \approx \frac{Q_T}{\rho V C_p} = 1.13\ ℃ \tag{5.53}$$

This temperature drop represents the temperature drop of an idle storage. The corresponding theoretical sensible heat storage efficiency is 99.5 % over 24 hours and 99.98 % in 1 hour.

In the integrated sensitivity model discussed in section 5.9.1, the annual thermal energy lost exceeds 10 %. About half of this loss is due to the inability of the storage to accept energy when full (i.e. due to curtailment) and half due to thermal losses. The storage efficiency setting of 99.8 % per hour is likely conservative by 1 order of magnitude but is a placeholder for heat transfer losses in the system not otherwise accounted for. A deviation of ± 0.02 is assumed for non-curtailment storage losses but noting that this might still be conservative.

5.7 Heat engine

In keeping with the objective, the power generation model is not prescriptive, and no thermodynamic cycles are modeled. Rather, it is assumed that the Novikov heat engine is a suitable practical representation of present and future power generation technologies. As a result, the model assumes a heat engine is applicable in CSP in the future and that advances in CSP technology will allow for ever increasing operating temperatures, thereby increasing plant performance as show in in Figure 5.21.

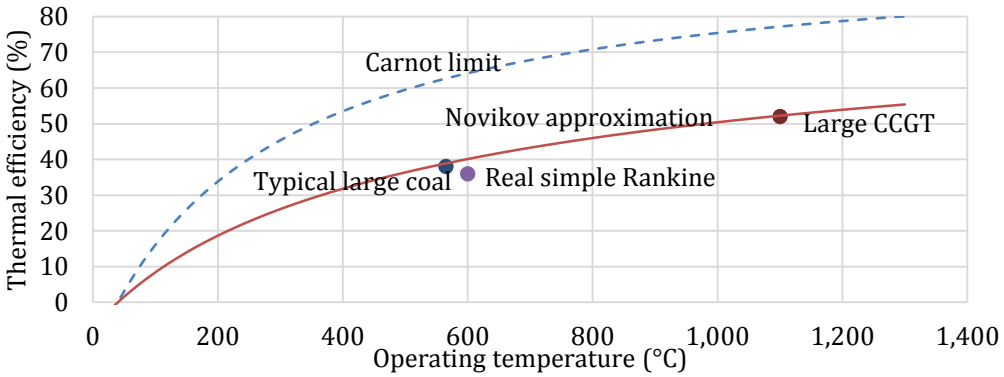

Figure 5.21: Comparison of some ideal and real power plant thermal efficiencies compared with Carnot and Novikov cycle efficiencies

The original derivation from Novikov (1958) led to the name – Novikov engine or cycle. The Novikov cycle fits within a branch of thermodynamics called endoreversible thermodynamics where internally reversible cycles make use of more realistic assumptions regarding heat transfer. It has been derived in several ways since and shown to represent real power plants well (Curzon & Ahlborn, 1975; USA Department of Energy, 2012).

$$\eta_N = 1 - \sqrt{\frac{T_L}{T_H}} \tag{5.54}$$

The cycle assumes no evaporative cooling; therefore, power production at each hour is defined by

$$T_{L(t)} = 273.15 + T_{a(t)} \tag{5.55}$$

where

$$T_{H(t)} = 273.15 + \eta_{rt}\left(T_r - T_{a(t)}\right) + T_{a(t)} \tag{5.56}$$

in which η_{rt} is a temperature derating coefficient accounting for the temperature drop from external receiver outlet to turbine inlet.

Gross power generation per hour is, therefore

$$E_{g(t)} = \eta_{N(t)} Q_{s(o,t)} \tag{5.57}$$

The reference condition for the model is a turbine rated at 562 °C, running at its rating, thus achieving a gross efficiency $\eta_{N(ref)} = 0.402$. Deviations not considered elsewhere in the model such as the allocation of part-load within nodes and technology advances are handled by a deviation of ± 0.03 in the model sensitivity assessment. Advances in combined cycle plants using gas turbines or supercritical CO_2 cycles are amongst the candidates for future but are not expected in the shorter timeframe at the desired efficiency or cost levels (Cheang, Hedderwick & McGregor, 2015).

5.8 Other plant considerations

Remaining assumptions, parameters and considerations of significance for the integrated CSP node model are provided in Table 5.5.

Table 5.5: Other parameters of CSP plant model

Parameter	Value	Dev
Generator efficiency	0.98	-
Plant parasitic electricity as a fraction of gross electricity produced while operating	0.05	-
Plant parasitic electricity needs when idle as a fraction of nameplate rating	0.01	-
Auxiliary heating	-	-
Temperature drop from receiver outlet to turbine inlet as a fraction of receiver outlet temperature to ambient temperature	0.05	-
Thermal inertia in charging loop	-	-
Grid connection efficiency	0.98	-

The model assumes that auxiliary or parasitic energy needs, particularly during non-operating times, is minimal as a result of technology advances in central receiver plants. The model has also been developed for a direct steam receiver with thermal inertia, but this variant is only used for validation. All application of the model assumes the model as described in this chapter. Power generation can ramp following nameplate ramping capabilities, assuming that heat transfer from storage to turbine is not a limiting factor.

5.9 Integration, validation and test cases

The integrated CSP node model is tested for energy balance, parameter sensitivity, comparison with other sources and initial performance for its purpose in energy systems analysis.

5.9.1 Integrated energy balance

Figure 5.22 presents the component and cumulative energy conversion efficiencies of the overall model for a central receiver system configured to the Gemasolar plant specifications (NREL, 2011a) with minor adjustments for the higher site DNI. In this instance, the plant produces the maximum possible electricity at each hour for a full year and results in a net generation efficiency of 15.2 %. The capacity factor of this plant is 69.3 %, and the annual DNI of the site is 2,762 kWh/m².

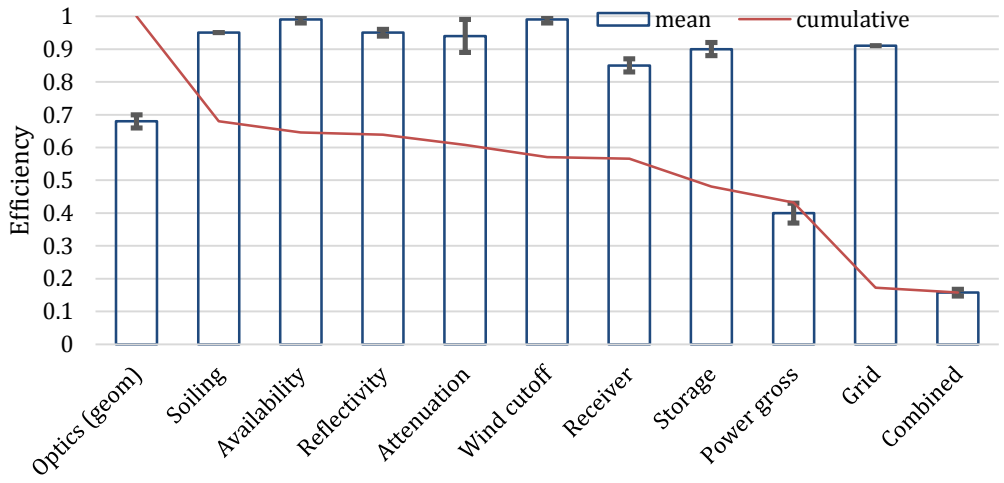

Figure 5.22: Normalized annual cumulative energy conversion for a specific site

Model validity can be broken into two major components. The first is implicit in terms of its use in a systems analysis and comprises all modeling choices and simplifications that generally would not be changed either due to lack of data or lack of technology definition. Significant examples of this component include atmospheric attenuation, technology configuration that is not part of the three proportion settings (Figure 5.1) and technology advancement enabling higher efficiency high temperature cycles. An estimate of the implicit validity of the model for the next decade based on probability

analysis results in a standard deviation of 0.01. For the case described, this translates to a standard deviation of 6.58 % on electricity served to the grid. The associated component deviations are added to the case as shown in Figure 5.22.

The second component of model validity relates to all aspects that explicitly define a node of CSP capacity, site, resource, environment, cost and usage. The validity of the model to explicit parameters is largely dependent on the validity of external data and is accordingly dealt with in later parts.

5.9.2 Hourly performance behavior

Figure 5.23 presents a time series representing two days of performance during summer near Pofadder, South Africa. Thermal energy in this example is scaled relative to the DNI of that hour, thus providing a direct sense of the thermal efficiency of the various configurations.

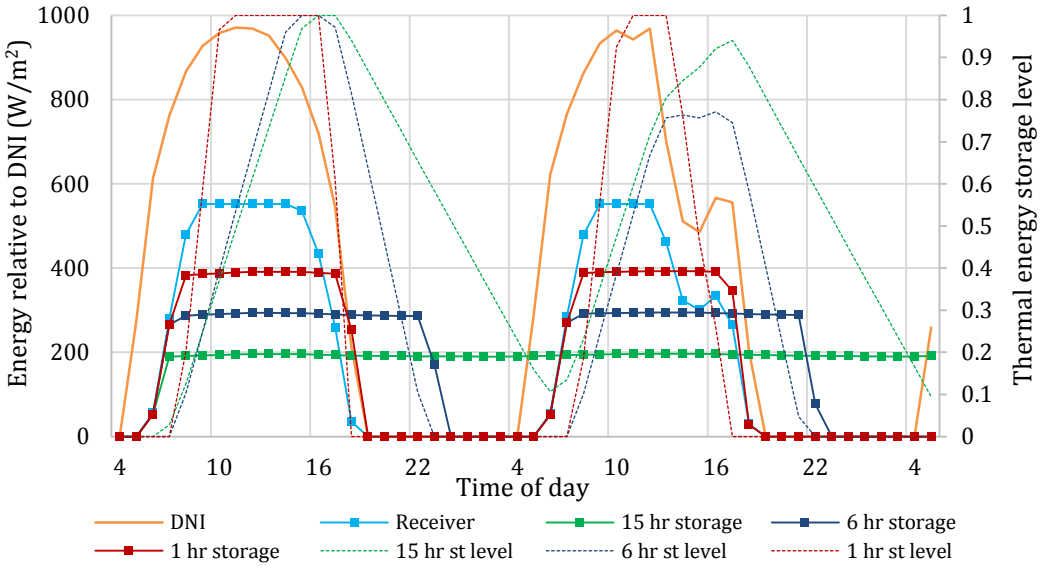

Figure 5.23: Temporal model behavior for various configurations over two days

Dotted lines represent the storage level for the color associated thermal markers. Receiver output is the same in all cases and itself represents a case with zero storage. In this case, the receiver output is governed by a receiver performance limit as can be seen by the performance cropping at around 550 W/m². Thermal output duration is generally inversely proportional to thermal output level, provided that storage is utilized. The 1 hour storage case shows an example of a poorly configured node. An undersized storage or turbine is causing excessive curtailment. Figure 5.24 and Figure 5.25 illustrate sensitivity to plant dimensioning.

Increasing the turbine size from 46 MW to 52 MW, all other things equal, the storage level takes longer to fill, indicating better pass-through. On a good day, curtailment is still experienced, but on a less sunny day, the storage never completely fills.

Nonetheless, a smoother thermal performance is experienced. Annual performance of these tradeoffs can be assessed using a capacity factor, relative annual performance (dimensionless annual energy produced) and LCOE, which will be defined in Chapter 6. Using the 2011 Sandia Power Tower Roadmap reference costs (Kolb et al., 2011), Figure 5.25 shows relative indicators for this site for the two 1 hour storage cases and compared with a well configured 15 hour storage node.

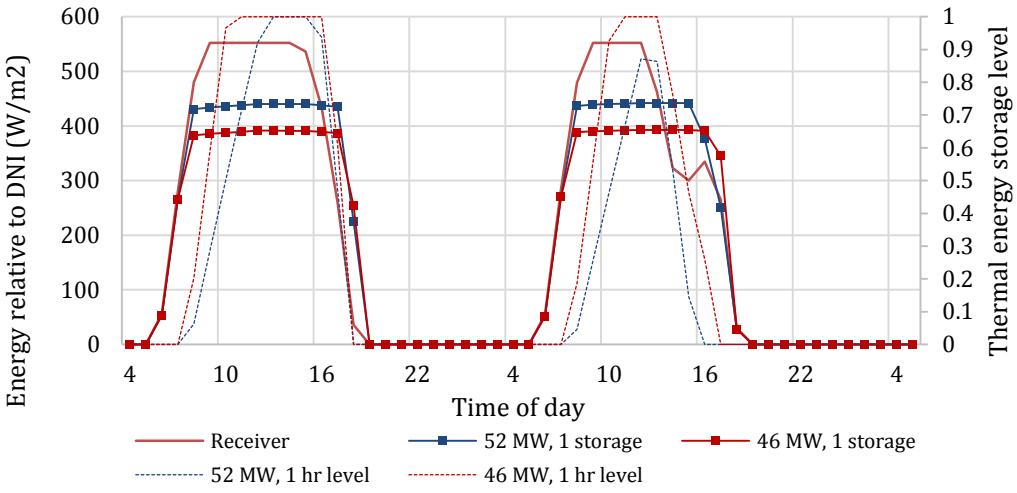

Figure 5.24: Impact of solar multiple and storage capacity

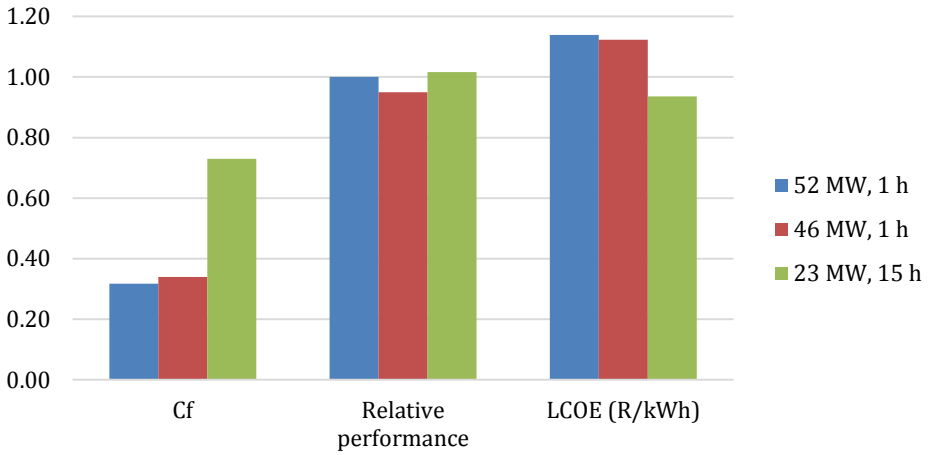

Figure 5.25: Key indicators of two low storage vs. a 15 hour storage tower

While the larger turbine results in a lower capacity factor, it does produce more power annually. Despite this, the LCOE is higher. For all indicators, a 15 hour storage node is superior. Figure 5.26 shows a comparison between the various storage options of the same example using a gross power duration curve (gross hourly power output ranked from highest to lowest for a year) and cumulative gross power generation (dotted line with secondary vertical axis).

The table-top shape is a consequence of thermal storage configured in series, which

enables consistency for power generation and the lack of system instruction for dispatching, which enables the node to deliver at its rating until it can no longer do so in an hour. The slope and the end of the duration curve indicate the drop in hourly cumulative capacity running at rating during that hour.

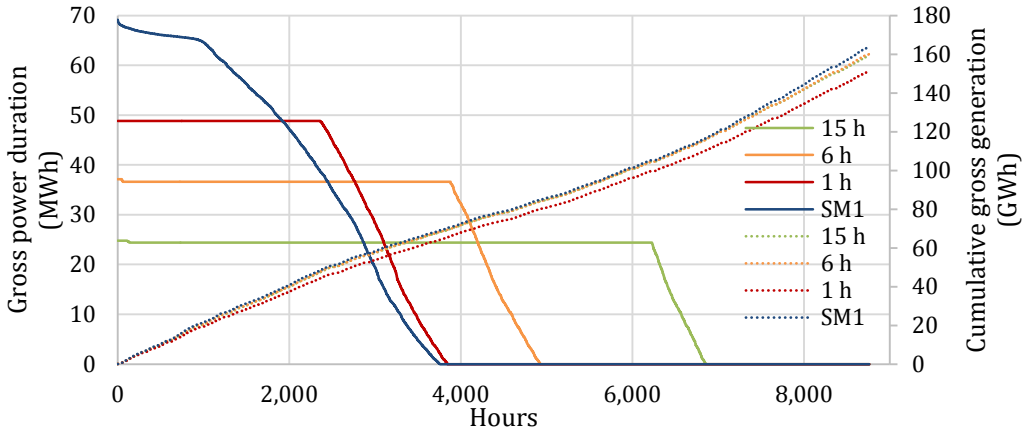

Figure 5.26: Duration and cumulative generation of gross power curves for storage ratings of 15 hours, 6 hours, 1 hour and a case where the solar multiple is 1 and thermal energy passes through a 1 hour storage system

Cumulative annual gross power illustrates the effectiveness of storage configurations to maximize power output. The 1 hour storage case, the lower cost version indicated in Figure 5.25, is unable to dispatch all potentially collected energy. The gradient of cumulative gross power indicates the combined impact of seasonal variations in DNI and optical system efficiency.

5.9.3 eSolar SierraTowers

Meduri, Hannemann, & Pacheco (2010) report on measured performance of the SierraTowers receivers over several different days. Besides comparing with Lancaster in California (34.7 ° latitude) (NREL, 2011b), results are also determined for Upington, South Africa (-28.4 ° latitude). The model was adjusted to the SierraTower configuration (Schell, 2011), and the results are shown in Figure 5.27.

Results for thermal power show good agreement with both simulated and measured data from Meduri *et al.* at about 16 MW_{th} at noon. The model predicts a similar slower start in the morning compared with measured results due to setting a lumped capacitance (inertia) based on commonly known startup times of CSP plants. A sensitivity test showed a high degree of sensitivity to solar absorptivity and a low sensitivity to thermal emissivity. Electrical power correlates well to the 5 MW rating of the plant, but Meduri *et al.* report significantly lower measurements and predictions on the turbine for reasons that might relate to the specific condition of the turbine unit.

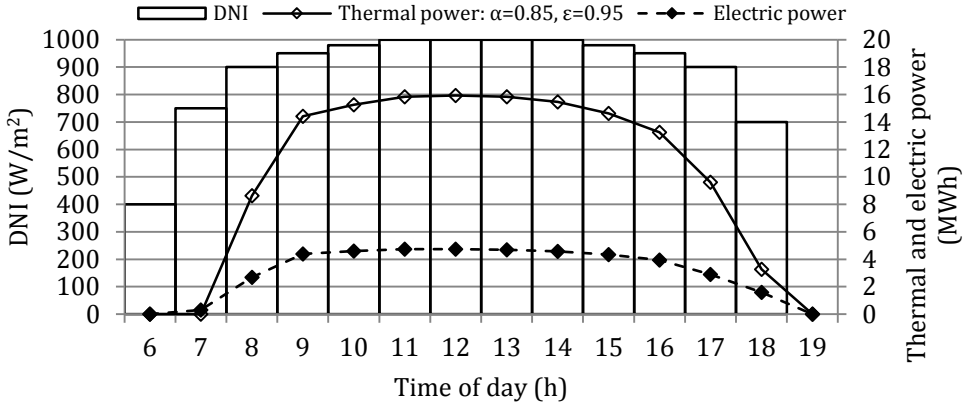

Figure 5.27: Simplified model of thermal and electric power

5.9.4 South African baseload test

The first application of the CSP nodal model prior to integration into a systems model tested the model parameters for all logic, energy balance and analysis speed. The details of this application are published (Gauché et al., 2012) and summarized here.

The Gemasolar plant of Torrasol Energy formed the reference for this test and was adapted in the model to permit a higher capacity receiver (175 MW vs. 120 MW) for nodes that experienced higher DNI due to excessive curtailment in such cases. The Gemasolar plant is rated to 19.9 MW gross electrical generation, 15 hours of full-load storage and planned annual electricity production of 110 GWh per year based on the sites average annual DNI of 2,172 kWh/m^2. (NREL, 2011a). The model was tested in a case with similar DNI (2,175 kWh/m^2) and latitude conditions, resulting in the annual production of 115 GWh per year. This production results in a DNI weighted difference of +4.4 % comparing the model to the reference.

The baseload test has 823 nodes spaced in a grid with a resolution of 0.375 ° attitudinally and longitudinally as shown in Figure 5.28. Each node has hourly averaged DNI, ambient temperature and wind speed for the full year of 2005. The model generates power as the only output per node per hour, which results in processing of 21.6 million inputs and 7.2 million outputs for an annual simulation. A single sweep of the country takes about 30 minutes on a 2011 Apple laptop running the code in Python, noting that data extraction and loading data to memory per node is the primary time consumer.

The Gemasolar plant is replicated at each node, and the model tested the following variations: (1) model run with default parameters as outlined in the method section above, (2) power block size reduced to 10 MW but with the same solar field and storage size as in run (1), (3) power block size reduced to 10 MW and storage size reduced by half with the solar field remaining the same size, (4) power block size reduced to 5 MW but with the same solar field and storage size as in run (1), (5) power

block size reduced to 5 MW and storage size reduced by three quarters. All nodes operate as independent power producers with a single tariff and, therefore, dispatch power as soon as possible. Results are shown in Figure 5.29 for representative summer and winter periods and in Figure 5.30 for the whole year.

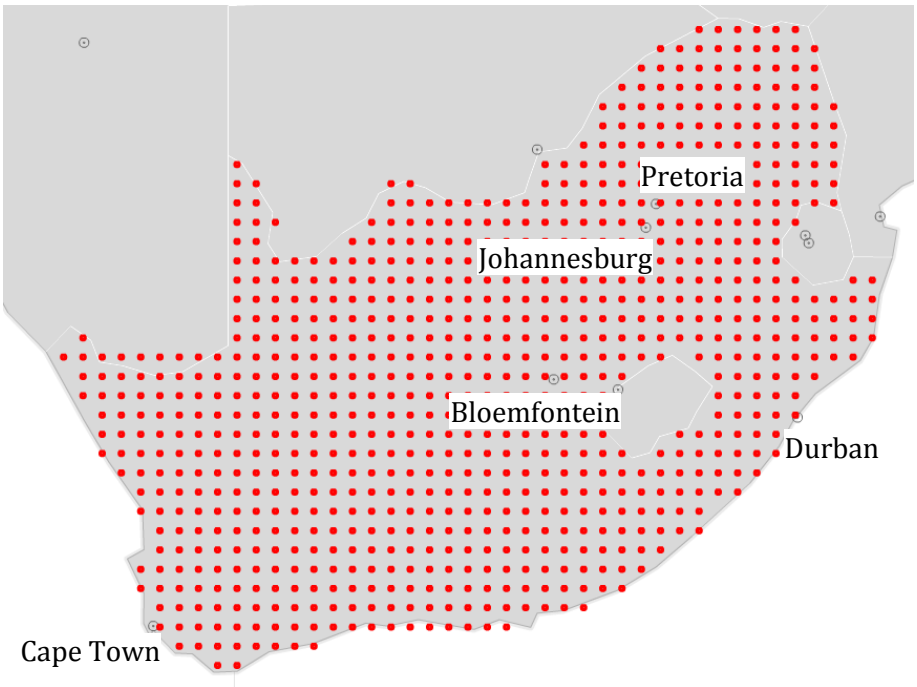

Figure 5.28: Location of 823 uniformly spaced CSP nodes across all of South Africa. Node grid resolution of 0.375 ° and each node indicated by a red dot. Size of dot has no meaning. (image by S. Pfenninger)

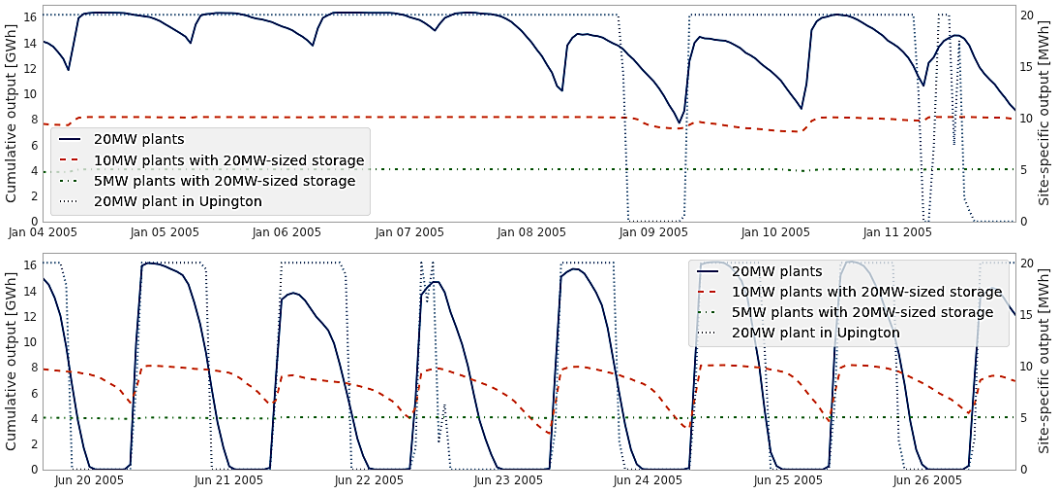

Figure 5.29: Model results for representative summer (top) and winter (bottom) days (plots by S. Pfenninger)

The value of distributing CSP capacity spatially is demonstrated by the lack of

production for periods of time for the node near Upington while the aggregation of power for the distributed system shows continued performance. A discussion of the merits of the proposal are out of scope and can be found in Gauché et al (2012).

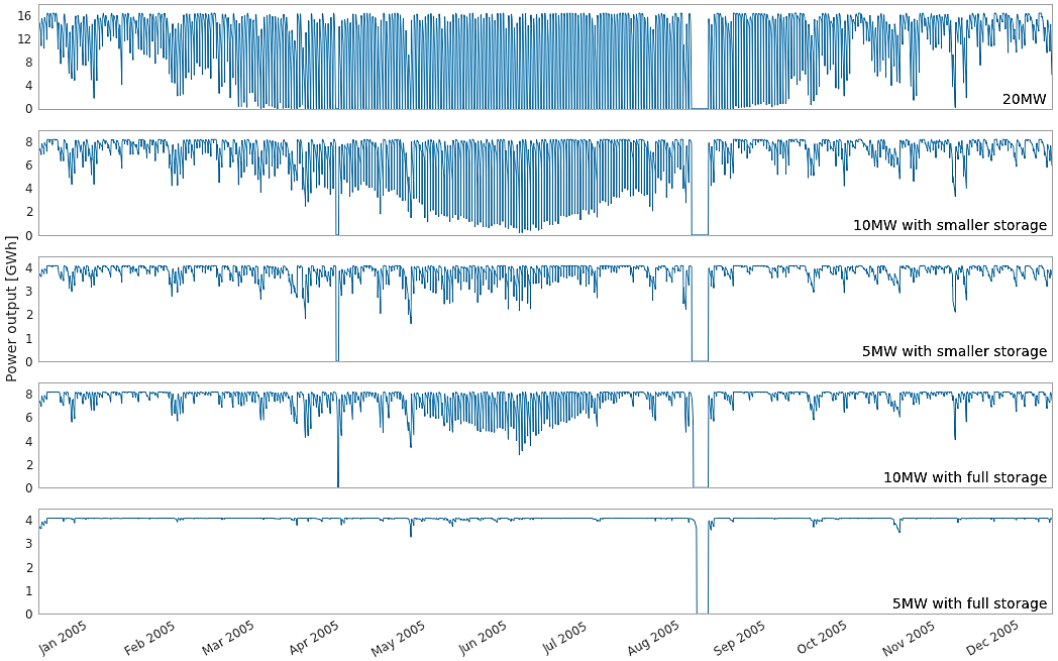

Figure 5.30: System whole year output for the five cases. The dip in mid-August is due to missing DNI data over that period (plots by S. Pfenninger)

A model data sensitivity was also performed showing that DNI is (expectedly) the primary input parameter, but the degree of sensitivity to ambient temperature and wind in the integrated system was minimal (less than 1 %) when a single reference ambient temperature and wind speed was used. While not exhaustively tested, this suggests that energy systems analysis of CSP could be substantially simplified by using regionally relevant average ambient conditions.

5.10 Conclusion

The CSP node model represents behavioral characteristics within a state of the art central receiver technology to a level of abstraction considered suitable for the specific purpose of performing efficient systems analysis. With very limited operational time, let alone published performance data of baseload central receiver plants, much of the model is based on principles and validated with the means at hand. Accordingly, the implicit definition of the model “is what it is” and is assumed to represent that definition to a standard deviation of about 7 %.

Technology advances that are expected in the future as part of the technology learning rate can be accommodated by treating any default implicit value as explicit. The ability to simulate a high number of uniformly spread nodes independently is the first step towards the use of the model in a system analysis model.

6 SYSTEM MODEL

The overall system model used in Part 3 is described in this chapter. The system model is purpose-developed to satisfy the objective of the dissertation and is accordingly not intended to represent generalized energy systems analysis capabilities. The simplified system model provides a convenient framework to test the original propositions and to evaluate the CSP model for use in other energy systems analysis tools capable of performing spatial-temporal analyses.

The CSP model has been used and demonstrated effectively through collaborative research in energy systems analysis, most notably in the following publication, which is provided in Appendix B: Pfenninger, S., Gauché P., Lilliestam, J., Damerau, K., Wagner, F., & Patt, A. (2014). Potential for concentrating solar power to provide baseload and dispatchable power. Nature Climate Change, 4(8), 689–692. The methods used are parts of a new generation of energy systems analysis (Pfenninger & Keirstead, 2015) for which this CSP model is intended.

Additional early use and testing of the CSP model in this limited system model has been performed and published by Silinga and Gauché (2014) and referenced in the IEA 2014 CSP roadmap (IEA, 2014). The proposition made and the model for the work is attributable to this dissertation and will be described as an example in this chapter.

6.1 Overall spatial-temporal approach

The overall system model follows a bottom-up approach. The cost model provides a proxy for top-down elements of energy systems analysis by using probability analysis.

Figure 6.1 illustrates the overall model structure. The system is defined and constrained per scenario in terms of time, location, technology scope, forecast cost ranges, system (operator) rules and synchronous hourly definition of demand and resource availability.

The systems model specifically includes all South African power generation types of any significance to the extent that the CSP model is sufficiently tested; these include PV, wind, CSP, coal, nuclear, hydro, OCGT, CCGT and pumped storage.

Once established, the system power generation model runs sequentially in the time domain and is endogenous in terms of satisfying criteria for hour and scenario duration. No optimization occurs, but the model attempts to satisfy each time step at the lowest cost and with minimal curtailment or shortfall.

Once the scenario duration is complete, all supply, curtailment and shortfall is aggregated, and key metrics such as technology or node capacity factors are calculated.

The output of the aggregated results are inputs to the system cost forecasting model,

a Monte Carlo type cost model. The final step is the reduction of the scenario to a cumulative distribution function with a mean and standard deviation for the system cost.

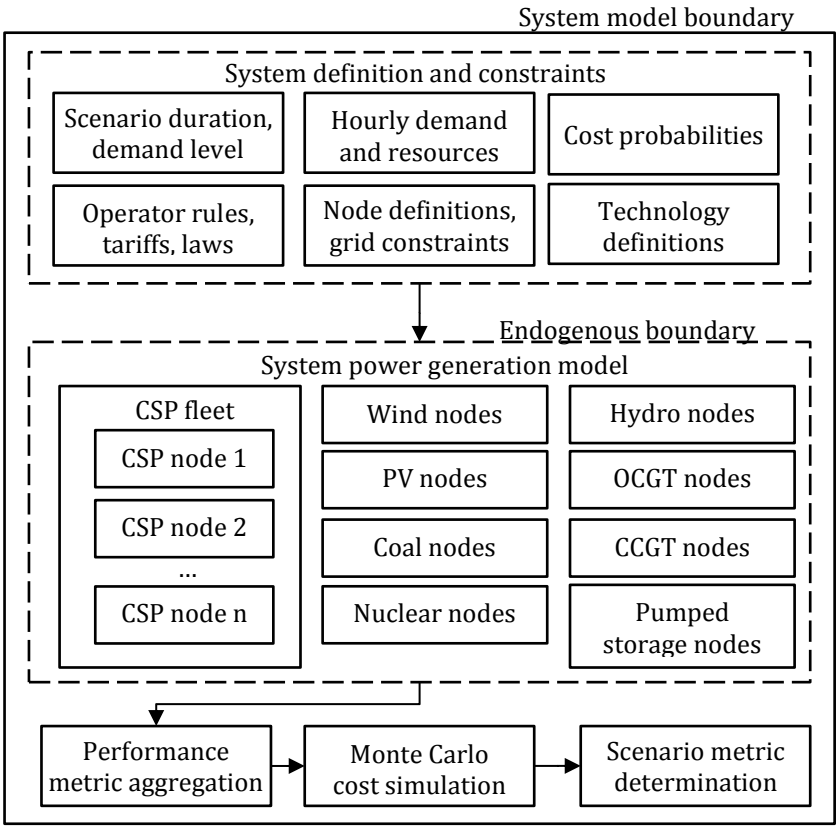

Figure 6.1: Overall scenario system model structure and boundaries

The area described within the endogenous boundary is the power generation model, summarized in Figure 6.2.

At each time step, the model attempts to satisfy demand for that time step by cascading through each technology, node and defined power plant as need be. At the end of each hour, the model aggregates the amount of power delivered, curtailed and unmet. The aggregated power and the power generated per node and technology is cumulatively tallied for post processing at the end of the time period.

As each hour proceeds, the model cascades through the ranked order of merit of technologies and nodes and determines if capacity is available based on conditions of the node at the end of the previous hour and the ability in the present hour only. No scheduling is done and no attempt is made to forecast demand or resources. The model has limited capabilities for intra-hour ranking and prioritizing between technologies and nodes.

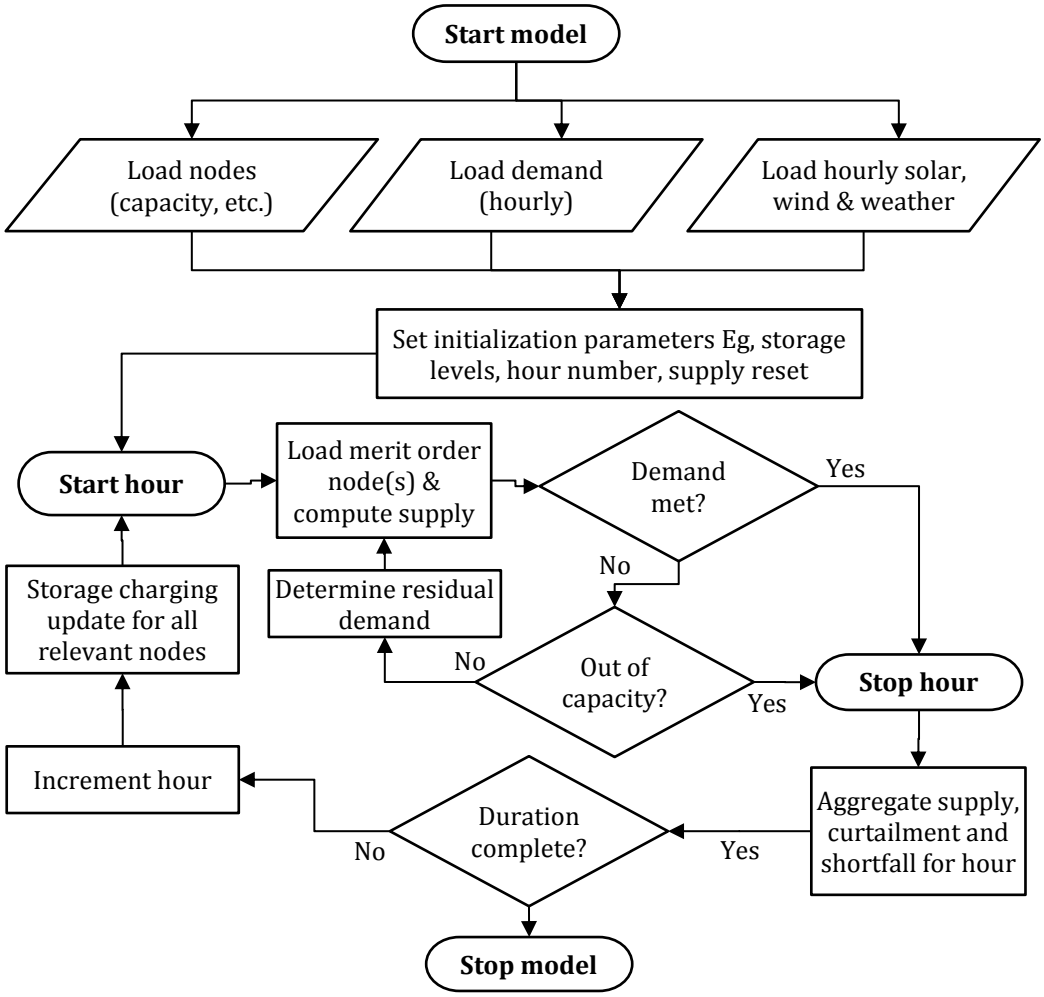

Figure 6.2: Overall system model process flow

6.2 System definition and constraints

6.2.1 Demand

Demand is treated as a single node in this model, meaning that the model assumes that all generation serves a single time step demand requirement. This treatment makes only the most elementary transmission constraint modeling possible, but it simplifies the validation of the objective.

The CSP model has been developed partly considering the likely importance of dependence between all nodes at all times in order for covariance in the system to be correctly detected and acted upon. In short, the model should use a definition for hourly demand linked to the behaviors and resources for that hour. The easiest way to do this is to use real historic demand and resource data from the same time period.

Not only does this largely obviate the use of stochastic assumptions for time and space, but the use of time slices or TMY data sets is also not desirable. For example, a

large low pressure system during summer will result in higher than average temperatures, clearer skies, less wind and a higher demand for cooling. In order to capture this reality, all nodes need to observe their respective synchronized environments correctly.

Real historical electricity demand for South Africa is available for the entire year of 2010 in hourly increments (Eskom, 2011a) and adapted for all scenarios described in the rest of the dissertation. Figure 6.3 presents a summary of the daily shape of the 2010 demand where each hour is represented by that hour's annual minimum, average and maximum for the year. Figure 6.4 presents the shape of the daily minimum, average and peak for the calendar year.

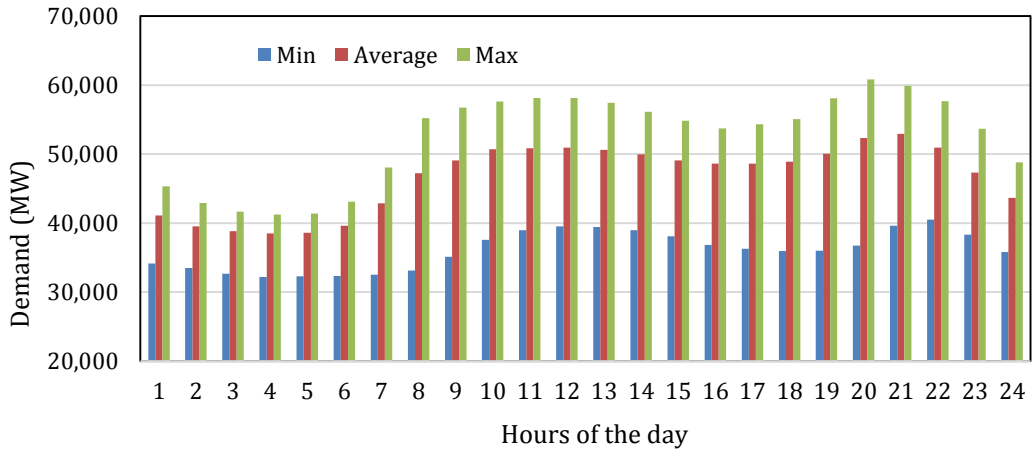

Figure 6.3: Annual hourly minimum, average and peak demand for a scenario scaled from the South African 2010 demand shape

The hourly profile shows the characteristic nature of the South African electricity demand with a mid-morning to mid-afternoon high demand and an evening peak demand.

The annual profile demonstrates the higher peak demand in winter, the lower weekend demand and the very low demand in the few days around Christmas, New Year and Easter. Specific time period demand profiles will be discussed in Part 3.

No attempts are made to predict the nature of future demand shapes. Instead, the model uses referenced annual demand forecasts for the scenarios of Part 3 and linearly scales the demand of each hour of the 2010 demand.

$$m_s = \frac{SD_s}{SD_{2010}} \tag{6.1}$$

where m_s is the scenario multiplier, SD_s is the scenario annual system demand, and SD_{2010} is the annual system demand of 2010.

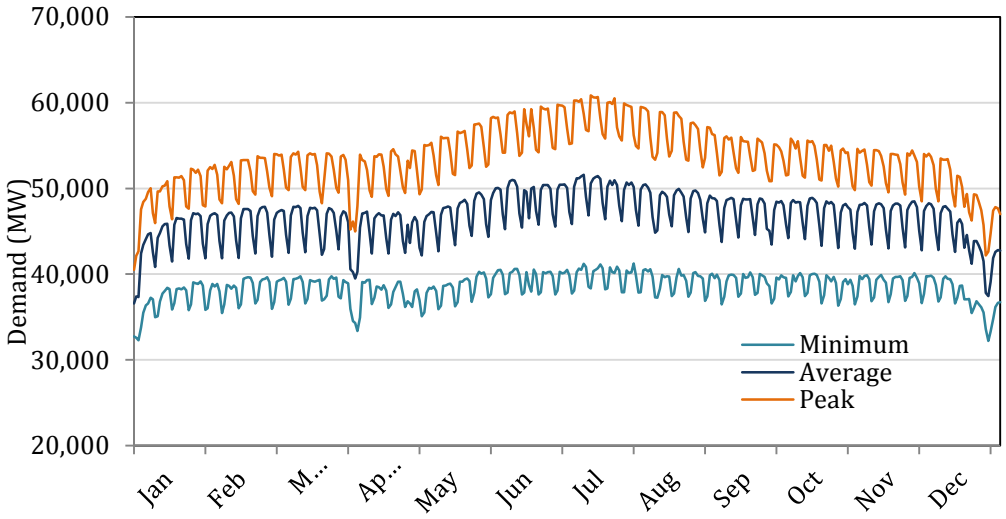

Figure 6.4: Annual hourly minimum, average and peak demand for a scenario scaled from the South African 2010 demand shape

System power demand at each hour.

$$SD_{s(h)} = m_s SD_{2010(h)} \tag{6.2}$$

where subscript *h* represents the hour.

6.2.2 System generation response and merit order

The model is specified and constrained by a number of parameters based on the realities of the existing power system, the tariff structures of the REIPPPP and the likely near-term implementation of the IRP. Generalized examples of such specifications and constraints are summarized.

Most power plants, particularly those that operate using a heat engine, have limited abilities to increase or decrease production rates. Each technology or node in the system accommodates prescribed ramp rates. The consequence is that the system risks forced overproduction or under supply when the available capacity in the system is unable to respond in time to residual demand changes. Ramp rates are applicable at the node or technology level as appropriate.

Similarly, large thermal plants and other turbine based plants have limited part-load capabilities. Below the specified part-load limit, certain nodes are set to zero. This is not applied across the system model due to the non-discrete nature of how capacity is allocated.

Wind and PV are uniquely treated with high priority in the model due to the nature of the technology and the existing tariffs, which compel the operator to purchase power. All generated electricity is, therefore, accounted for in an hourly system aggregation and can contribute to a system surplus, which is measured and would likely cause

curtailment of these technologies.

Nuclear power is given baseload priority and is the last in the order to reduce or curtail. Coal and hydropower follow in the baseload merit order.

CSP and CCGT capacity play a twinned role in mid-merit power generation, aiming to generally satisfy demand before peaking and emergency generation is required. Either technology can have its roles independently adjusted to serve as baseload, dispatch power or a combination of both at a system or node level.

OCGT and pumped storage serve as last-resort generation. In the case of pumped storage, charging is prioritized based on the charge level of the upper reservoirs. In normal periods, charging will be done when excess renewable generation otherwise would trigger ramping down of coal power. At critical thresholds, charging will be done by any available generator.

Availability (A) is defined as the fraction of time when a node or technology is not in maintenance and is capable of producing power at full rating. Availability is averaged over the time period or averaged over intervals of the time period in order to simplify the model. Available node capacity is the product of the technology availability, node capacity and a governing term based on multiple constraints from the system such as the amount of supply requested and from the technology such as ramp rates and turndown limits.

$$PA_{r(node)} = G_{(node)} A_{technology} P_{r(node)} \tag{6.3}$$

where $PA_{r(node)}$ is available node capacity, $G_{(node)}$ is the system and technology governing term, $A_{technology}$ is the average availability and $P_{r(node)}$ is the rated capacity of the node.

Capacity factor (C_f) is not a constraint of the model, rather it is implicitly resolved in the solution and is an important and interesting measure of the system nodes and technologies.

$$C_{f(node)} = \frac{\sum_{hours} P_{(node,hour)}}{8{,}760\ P_r} = A_{technology} \frac{\sum_{hours} P_{(node,hour)}}{8{,}760\ PA_r} \tag{6.4}$$

and

$$C_{f(technology)} = \frac{\sum_{nodes} \sum_{hours} P_{(node,hour)}}{\sum_{nodes} 8{,}760\ P_{r(node)}} \tag{6.5}$$

Moving forward, nodes and technologies can be viewed somewhat interchangeably. System generation is the aggregation of generation of all nodes for all technologies.

$$
\begin{aligned}
SG_{s(h)} = \eta_g \sum_{PV-nodes} PA_{PV(node)} + \eta_g \sum_{W-nodes} PA_{W(node)} \\
+ \eta_g \sum_{H-nodes} PA_{H(node)} \\
+ \eta_g \sum_{N-nodes} PA_{N(node)} \\
+ \eta_g \sum_{C-nodes} PA_{C(node)} \\
+ \eta_g \sum_{CSP-nodes} PA_{CSP(node)} \\
+ \eta_g \sum_{CC-nodes} PA_{CC(node)} \\
+ \eta_g \sum_{OC-nodes} PA_{OC(node)} \\
+ \eta_g \sum_{PS-nodes} PA_{PS(node)}
\end{aligned}
\tag{6.6}
$$

where η_g is the efficiency of the connection to a distribution line.

System shortfall is the amount of unserved power in each hour and aggregated over the year. Shortfall can occur due to ramp rate or available capacity limitations.

$$
SU_{s(h)} = \begin{cases} SD_{s(h)} + SP_{s(h)} - SG_{s(h)}, & SG_{s(h)} < SD_{s(h)} + SP_{s(h)} \\ 0, & SG_{s(h)} \geq SD_{s(h)} + SP_{s(h)} \end{cases} \tag{6.7}
$$

where $SU_{s(h)}$ is the system scenario shortfall, and $SP_{s(h)}$ is the system pumped storage charging needs. Pumped storage charging usually doesn't occur during shortfall hours but theoretically remains valid in the model to accommodate for ramp rate of pumped storage nodes, which might not be able to respond to sudden changes.

Annual system shortfall is the aggregation of shortfall at each hour.

$$
SU_s = \sum_h SU_{s(h)} \tag{6.8}
$$

System surplus is the hourly curtailed energy in the system due to the inability of defined generators in the system to ramp down when demand drops and/or when these generators are unable to drop below turndown limits. This does not include constraints within a plant that lead to curtailment, such as defocusing of heliostats when the receiver thermal limit is reached. It can include power generated by CSP when CSP nodes are permitted to dispatch electricity to avoid curtailment when thermal storage is full.

$$
SC_{s(h)} = \begin{cases} SG_{s(h)} - SP_{s(h)} - SD_{s(h)}, & SG_{s(h)} > SD_{s(h)} + SP_{s(h)} \\ 0, & SG_{s(h)} \leq SD_{s(h)} + SP_{s(h)} \end{cases} \tag{6.9}
$$

Annual system shortfall is the aggregation of shortfall at each hour.

$$SC_s = \sum_h SC_{s(h)} \tag{6.10}$$

Shortfall and surplus can be determined at a technology and node level in a similar way in order to assess the value or role of that technology or node. This concept is used in Part 3 for the case of CSP.

6.2.3 Cost model

The standard method to determine the cost of alternative power generation technologies is by the levelized cost of energy (LCOE) (IRENA, 2015).

$$\text{LCOE} = \frac{\sum_{t=1}^{n} \frac{I_t + M_t + F_t}{(1+r)^t}}{\sum_{t=1}^{n} \frac{E_t}{(1+r)^t}} \tag{6.11}$$

where the investment cost is in year t, M_t is the operating and maintenance cost in year t, F_t is the fuel cost in year t, E_t is the electricity produced in year t, r is the discount rate, and n is the lifetime of the plant.

Newer technologies such as CSP are expected to have lower LCOE values as the cumulative installed capacity grows due to technology improvements and high volume manufacturing. This trend is accurately represented by the learning rate for most technologies and defined as the rate at which a technology reduces cost per doubling of the installed capacity.

Scenarios in this systems analysis model do not account for the year of construction of new capacity; this limits costing analysis to a simpler, non-discounted LCOE model.

LCOE is calculated for each node (or technology), enabling cost comparison between nodes and technologies.

$$\text{LCOE}_{node} = \frac{I_{node} + MF_{node} + MV_{node} + F_{node}}{E_{node}} \tag{6.12}$$

where MF is the fixed annual maintenance cost, and MV is the variable annual maintenance cost.

More importantly, LCOE is calculated for the entire system, including the sum of all nodes and the impact of the cost of unserved energy. By incorporating the latter term, all scenarios can be comparatively rated by a single cost regardless of the system ability to deliver the power demanded.

$$\text{LCOE}_{scenario} = \frac{\sum_{p,o=1}^{n}\left(MF_{(p,o)} + MV_{(p,o)} + F_{(p,o)}\right) + \sum_{p,n=1}^{m}\left(I_{(p,n)} + MF_{(p,n)} + MV_{(p,n)} + F_{(p,n)}\right) + UE_u}{E_d} \quad (6.13)$$

where subscripts *p,o* represents all older power capacity, and *p,n* represents all power capacity with outstanding investment debt; U is the economic cost of unserved electricity per kWh, E_u is the annual cumulative unserved electricity (kWh), and E_d is the annual system demand (kWh).

The annual investment cost is the cost of repayment for the project cost, which includes finance costs during construction and finance costs during the repayment term during operation. In the model, it is assumed that all new capacity is fully debt funded and repaid in equal proportions during the repayment period.

$$I_{p(n)} = \frac{CX_{p(n)} + CC_{p(n)} + TI_{p(n)}}{d} \quad (6.14)$$

where CX is the capital cost, CC is the construction cost, and TI is the total interest over the financing period d.

Because system cost is the ultimate output of the system model and because the objective of the dissertation is to provide a reliable CSP model for systems analysis, the cost breakdown needs to be sensitive to the three major parameters of the CSP node model: (1) collector size, (2) storage hours, and (3) turbine rating. CSP node capital cost is, therefore, a function of the cost of the various components that define the makeup of the node.

$$CX_{CSP(n)} = \left(A_h CX_h + Q_{th} CX_r + H_s Q_{th} CX_s + E_g CX_t + E_g CX_g\right)\left(1 + BOP_f\right)_{(n)} \quad (6.15)$$

where A_h is the aperture area of the collective heliostat system, Q_{th} is the thermal rating of the receiver, H_s is the full-load hour rating of the thermal storage, E_g is the gross power rating of the turbine, and BOP_f is a factor to account for the balance of plant.

6.2.4 Nodes, transmission and resource

The degree of predictability in renewable energy networks is a function of the physical (spatial) distribution of capacity within the system (Pfenninger et al., 2014; Silinga & Gauché, 2014; Suri, Cebecauer & Skoczek, 2014b). It is assumed that a small number of distributed spatial nodes, where a node represents a region based on a latitude and longitude coordinate, and a defined radius will suitably represent a continuum of spatial choices.

Figure 6.5 illustrates the concept of spatial and virtual nodes in the energy system model. The system hub links the nodes and is also the point of demand in the system.

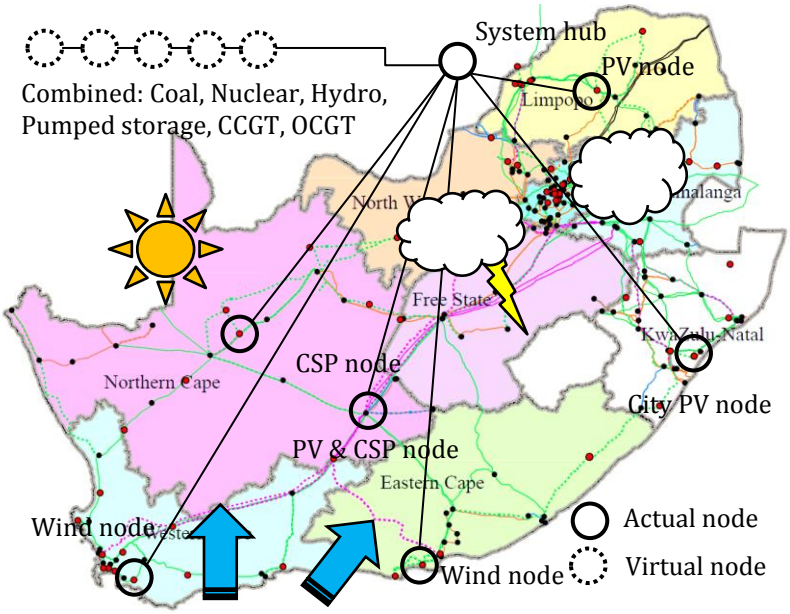

Figure 6.5: Conceptual node definition for the system model overlaid with the Eskom major Transmission Development Plan projects for 2015-2024 (background image (Eskom 2014b))

The connection between a node and the hub is only represented by a distribution connection efficiency (98 % in all cases). Node and regional capacity evacuation limit flags can be set but do not govern capacity limits at a node.

All actual nodes are represented by locational and temporal data. Solar and weather data was supplied by GeoModel Solar for all nodes used for CSP or PV capacity. Table 6.1 summarizes the data specification available (GeoModel Solar, 2012a).

For all wind power nodes, the WASA wind time series atlas was used (Mortensen, Hansen & Kelly, 2014). Besides being acknowledged as a better wind time series, the value of the WASA wind atlas is the fact that it is generated for and validated at wind heights relevant to wind turbines. Table 6.2 summarizes the wind data specification available.

The availability of these data sets allowed for selection of nodes at close proximity to the point of interest, and both data sets included all data for 2010, thereby allowing for synchronization with the Eskom demand dataset.

Table 6.1: Solar data specification

	Reference	Unit	Quality
GeoModel Solar: SolarGIS Database	Version 1.8		
Direct normal irradiation (DNI)	hourly aggregated Meteosat derived	Wh/m^2	Good
Global horizontal irradiation (GHI)	hourly aggregated Meteosat derived	Wh/m^2	Good
Air temperature at 2 m	NOAA NCEP, ground validated	°C	Reasonable
Relative humidity		-	Poor
Wind speed at 10 m		m/s	Poor
Time reference	UTC		
Data years available	2008 – 2010		
Spatial resolution	3	Arc-minutes	
Spatial range: Longitude	20 to 25	°	
Spatial range: Latitude	-25 to -30	°	

Table 6.2: Wind data specification

	Reference	Unit	Quality
Wind Time series for WASA domain, South Africa: DTU Wind Energy, UCT and CSIR	April 2014		
Spatial resolution	9 km x 9 km		
Time reference	UTC		
Wind speed		m/s	High
Wind height	Third model level (.FNg=0.9913) ~ 66 – 76 m		
Data years available	1990 – 2012		
Temporal definition	Hourly, data 15 minute averaged at the hour		
Spatial range:	Northern Cape, Western Cape, Eastern Cape		

6.3 Power generation

Power generation at the node level is governed based on the cascaded demand from the system and by technology constraints. This section summarizes technology constraints and behaviors to place the CSP node model in context.

6.3.1 CSP operating and control logic

Two levels of operating and control logic are applicable in the system model but outside of the definition of a plant, specifically for CSP.

The first relates to the operating and control within a node, independent of other

nodes. CSP nodes can be set to run independently, assuming a single IPP based tariff and maximum profit implies the maximum possible dispatchable power in any hour. CSP nodes can also be fully constrained by system instructions that limit a node based purely on system demand. The latter implies that CSP serves pure system availability and likely lower capacity fraction operation. Two mechanisms allow for a degree of system dependence.

1. Operating CSP nodes when node storage is full and would otherwise result in curtailment if not demanded by system. This setting leads to improved economic performance of the CSP node and risks system curtailment elsewhere.
2. Setting a minimum dispatch level for CSP to enable more continuous production of power. This emulates a baseload profile and allows a CSP node to operate more uniformly over time. The higher the minimum threshold, the more independent a node becomes, thus reducing its potential system value, particularly when availability is required in the morning.

Both mechanisms can be used at the same time. The impact of these node controls will be discussed in more detail in Part 3.

At the system level, CSP nodes are controlled by ranking each node at each hour by the level of full-load storage capability. This assumes that a system of CSP plants is most optimally utilized in the system by using plants (nodes) that have the highest level of storage first. Doing so preserves the highest level of available capacity in the system at the next hour. Such ranking results in a special loop performed by the system model as conceptually illustrated by the CSP system block containing CSP node blocks in Figure 6.1.

6.3.2 PV

A PV model was developed for this study using the principles from Stine and Geyer (2001) and generally sharing the principles of the solar and weather resource used in the CSP model. The PV model has been validated (Giglmayr, 2013b) and used to assess the utility scale PV power outlook for South Africa (Giglmayr et al., 2015).

The PV model assumes no storage and accordingly dispatches to the grid immediately. Gross hourly averaged power per node is a function of the collective effective sum of panels using the same basic configuration and the effective total irradiation during that hour. Figure 6.6 illustrates the relevant terms.

$$P_{PV-node} = \sum_{plant} \eta_{plant}\eta_{panel}\eta_T\eta_I A_{t,plant} I_{t,plant} \qquad (6.16)$$

where η_{plant} is the intra-plant efficiency accounting for shading, soiling, breakage and other O&M factors, η_{panel} is the nameplate panel efficiency, η_T is a temperature derating modifier, η_I is an irradiation level modifier, A_t is the effective net plant

aperture area, and I_t is the total incident solar irradiation on an unshaded panel. The model assumes the values given in Table 6.3.

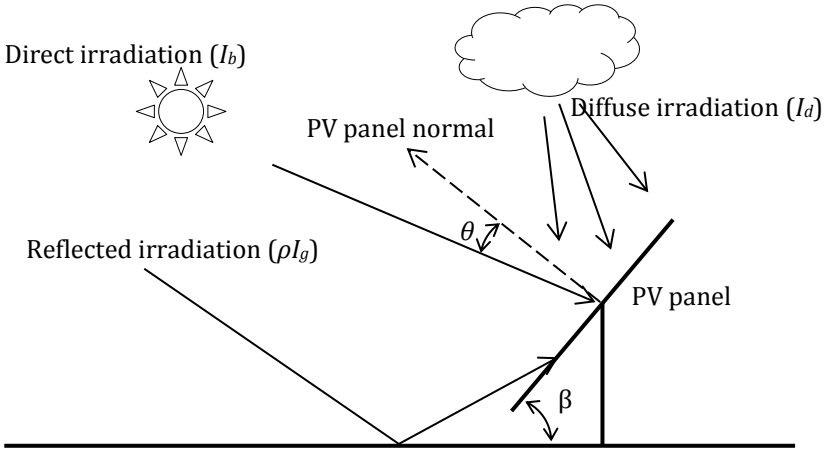

Figure 6.6: Illustration of sunlight components onto a PV panel (adapted from Auret (2015))

Table 6.3: PV model values

Parameter	Unit	Value
Intra-plant efficiency (η_{plant})	-	0.98 (zero shading) 0.0 (partial or full shading)
Net panel efficiency (η_{panel})	-	0.15
Irradiance efficiency (η_I)	-	1.0 – (I_t – 1,000)0.000125 (for deviation from reference irradiance)
Temperature efficiency (η_T)	-	1.0 - (T_a – 25)0.005 (deviation from reference ambient temperature)
Ground reflectivity (ρ)	-	0.1 (assumes reflection blocking in large installations)

The total incident irradiation for a PV panel per Stine and Geyer (2001) is

$$I_t = I_b \cos\theta + \left[I_d \left(\frac{1 + \cos\beta}{2} \right) + \rho I_g \left(\frac{1 - \cos\beta}{2} \right) \right] \tag{6.17}$$

following the same notation in the CSP model and where ρ is the effective ground reflectivity. All PV tracking types are conveniently handled by standard derivations based on the relationships in Appendix A.

The collective power at a node is an aggregation of each type and size of plant based on the following types:

1. Fixed tilt, either latitude (automatic) or manually set.
2. Declination angle tilt (modelled to continuously follow declination angle).
3. Single-axis tracking (horizontal).

4. Two-axis tracking for full two-axis or single-axis tracking with seasonal adjustment of secondary axis.
5. Concentrated PV (CPV).

The concentrated PV (CPV) net irradiation is reduced to the DNI component only.

$$I_t = I_b \tag{6.18}$$

An example of five hypothetical PV installations near Stellenbosch over three days in early January 2010 is plotted in Figure 6.7.

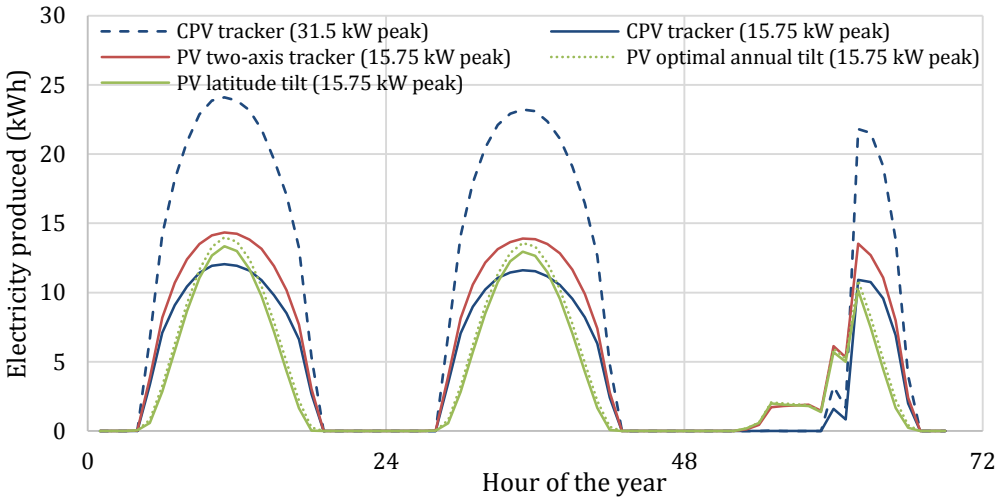

Figure 6.7: Model of five PV configurations over a three day period in early summer near Stellenbosch University

The single site example shows the virtues of the various PV types. Stationary PV has a sharp peak at solar noon and is improved when the tilt angle is adjusted. A two-axis PV tracker yields more, particularly early and late in the day, resulting in a better capacity factor. CPV performs almost as well provided there is direct sunlight. The 31.5 kW CPV system has the same panel size as the standard PV cases and yields more power due to the high efficiency cells using in CPV. All other cases have the same peak rating.

It is worth pointing out that while PV output at a single node is not highly predictable, the authors reached similar conclusions as those by Suri *et al.* (2014a), who show that distributed PV systems increase output predictability and decrease output fluctuation. A test of twelve utility PV nodes with equal capacity of stationary PV at each shows integrated behavior for seven days of January in Figure 6.8. Predictability is high for most of the year, and Figure 6.9 illustrates this using a cumulative power production curve. Besides predictability at any point of the year, the lower production rate in winter is noticeable. The PV model results in a system-wide capacity factor of 19 % for utility power plants. This closely correlates with the assumption in the IRP Update, thus serving as system analysis validation.

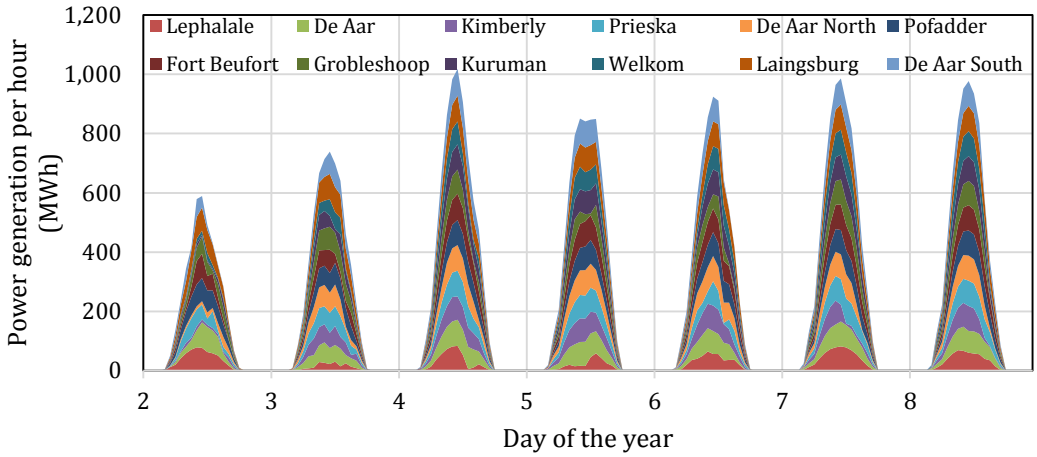

Figure 6.8: Behavior of PV plant output for the twelve model nodes containing 100 MW each – seven days of January

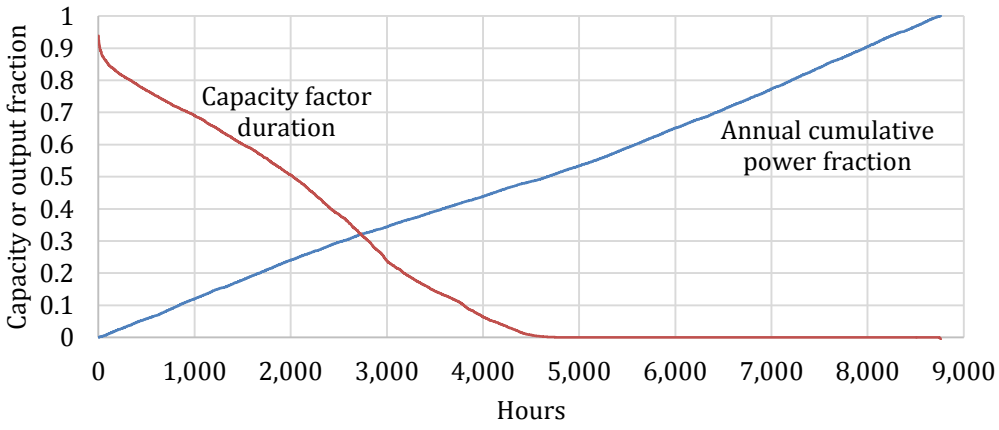

Figure 6.9: Combined system PV power performance indicators; capacity factor duration curve (as a fraction by ranked hour) and annual cumulative power output (as a fraction by year hour)

6.3.3 Wind

Wind power is modeled using an adapted version of a generic wind turbine performance model in order to be generally used.

$$P_{w-unit} = \begin{cases} \frac{1}{2}\rho A_{swept} C_p v^3, & v_l \leq v \leq v_r \\ \frac{1}{2}\rho A_{swept} C_p {v_r}^3, & v_r < v \leq v_{co} \\ 0, & v < v_l \; and \; v > v_{co} \end{cases} \quad (6.19)$$

where v is the hub-height wind speed (calculated using the log law based on available wind speed data), v_l is the minimum operating wind speed, v_r is the rated wind speed, v_{co} is the cut-out wind speed, ρ is the air density, A_{swept} is the swept area of the wind

turbine, and C_p is the coefficient of performance, which is based on the theoretical Betz limit of 0.59 (Ayodele et al., 2012).

Using the reported performance of a 3.3 MW commercial wind turbine, a constant coefficient of performance was found to over-predict at the wind speed limits or under-predict at the rated wind speed. A simple modifier was introduced to replicate this trend assuming that it would be rational to optimize a wind turbine for its rated wind speed.

$$C_p = 0.755 - 0.1 \times \cos\left(\frac{v - v_l}{v_r - v_l} \times \pi\right)^2 \tag{6.20}$$

This results in a reduction from the theoretical Betz limit of between 0.05 and 0.15, and the correlation to the commercial unit is shown in Figure 6.10.

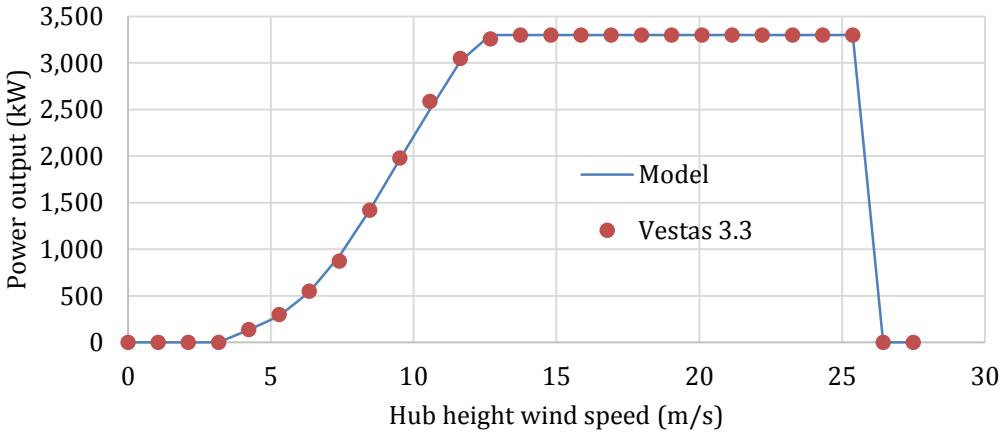

Figure 6.10: Characteristic and model validation of a wind turbine output based on hub height wind speed

Wind power plant capacity factors tend to range from 0.3 to 0.4. These plants tend to contain many turbine units, at times exceeding 100. Due to variances in placement and downstream impacts, plants are expected to generate less than the performance at the optimal point at a site. Without adjustment, the model developed for this work indicated nodes where capacity factors exceeded 0.5. While there are new wind farms in South Africa that are observing capacity factors exceeding the norm, these numbers have not been confirmed. It was agreed that the model sufficiently captures the behavior of wind power plants by suppressing the wind speed linearly such that all nodes have capacity factors in the anticipated range.

An example of ten distributed wind nodes for the South African model is shown by the stacked plot in Figure 6.11 for a week of production and in Figure 6.12 by annual performance. An elaborated discussion of distributed wind is beyond scope here, but the following were observed about wind power in such a case.

- In some instances, distributed nodes show independence, in others not, as is the case early during day 2 of the year when all nodes simultaneously stopped most production within 1 hour.
- Wind is fairly unpredictable and intermittent intra-week, particularly in winter.
- In a distributed system, wind appears to be predictable cumulatively and compliments solar power due to increased winter cumulative performance.

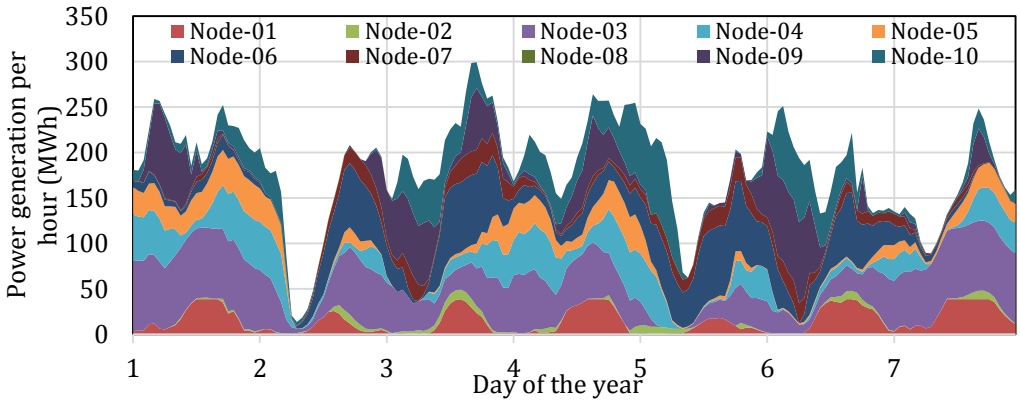

Figure 6.11: First week of January at all wind nodes in the system and 500MW of capacity in this example

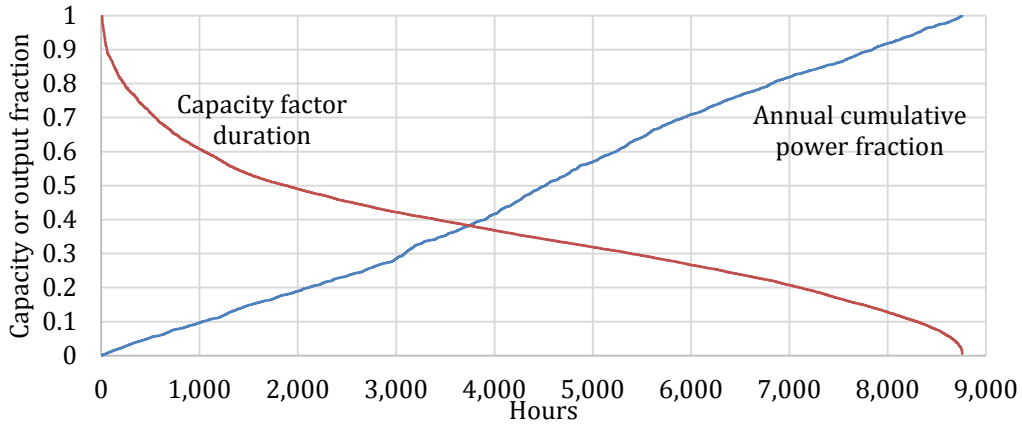

Figure 6.12: Combined system wind power performance indicators; capacity factor duration curve (as a fraction by ranked hour) and annual cumulative power output (as a fraction by year hour)

6.3.4 Other

In isolation of the system, all other power generation technologies are given very simple treatment. The other technologies are

- Thermal plants: Nuclear, coal, OCGT and CCGT.
- Hydropower: Run of the river and pumped storage.

The performance of these is also nodal and based on energy conversion efficiencies. In the system, the performance is additionally governed by constraints such as

- Energy conversion efficiency from energy carrier: This is mostly used in the event that energy carrier consumption rate and cost is of interest as the plant performance is given by plant rating.
- Ramp rate: The rate ability for a plant to increase or decrease output based on demand.
- Turndown limit: The lowest level at which a plant can operate before it has to shut down.
- Availability: the fraction of a year that a plant of a technology category is likely to be operating and not in scheduled or unscheduled maintenance. Availability is averaged across technologies and no treatment is given to discrete maintenance events.

6.4 Result aggregation and cost analysis

The power generation model is deterministic and will always reproduce the same results for the same model settings and constraints. The hourly aggregated results can be plotted as a time series per the example in Figure 6.13. In all of the time series plots, the purple line represents demand for that scenario.

Figure 6.13 reveals key features of the system model behavior. Aggregation is represented by stacking power generation by system merit. Wind and PV are at the bottom due to tariff structure. Nuclear, hydro and coal are then loaded where coal has the greatest ability to ramp. CSP and CCGT capacity have a twin role in mid-merit generation. Pumped storage and OCGT generation occurs as last resort. During day 25, poor sun and a high load during the day lead to exhausted baseload and mid-merit capacities, resulting in the use of pumped storage and OCGT capacity. Small amounts of OCGT capacity are shown to exceed the demand line during the 26th day and the following evening due to the critically low threshold of pumped storage capacity. From day 28, lower cost generators resume replenishment of the pumped storage system.

Once a simulation period is complete, the node and technology capacity factors are produced as defined earlier. At this point, the cost analysis is performed for each technology and for the overall system as defined earlier. For scenarios forecasting the future, knowledge of cost is not possible and is usually handled by considering alternative scenarios that account for limited specified contingencies. The South African IRP for instance considers scenario derivatives based on higher than expected nuclear costs or exploitation of larger quantities of low cost gas. The resulting system configurations vary significantly, and recommendations are made to monitor such contingencies in future updates (Department of Energy, 2013b).

An alternative approach is recommended here in an attempt to adhere to the practical approach to forecasting a complex system. While technology modeling can be

reasonably represented deterministically, forecasting the cost and availability of technologies and resources is too complex and would be better represented on a probability basis. Rather than selecting a small number of contingent scenarios to configure or optimize, it is recommended to run many scenarios based on a range of possible futures and configure the system based on the lowest cost system under a reasonable probability of occurrence.

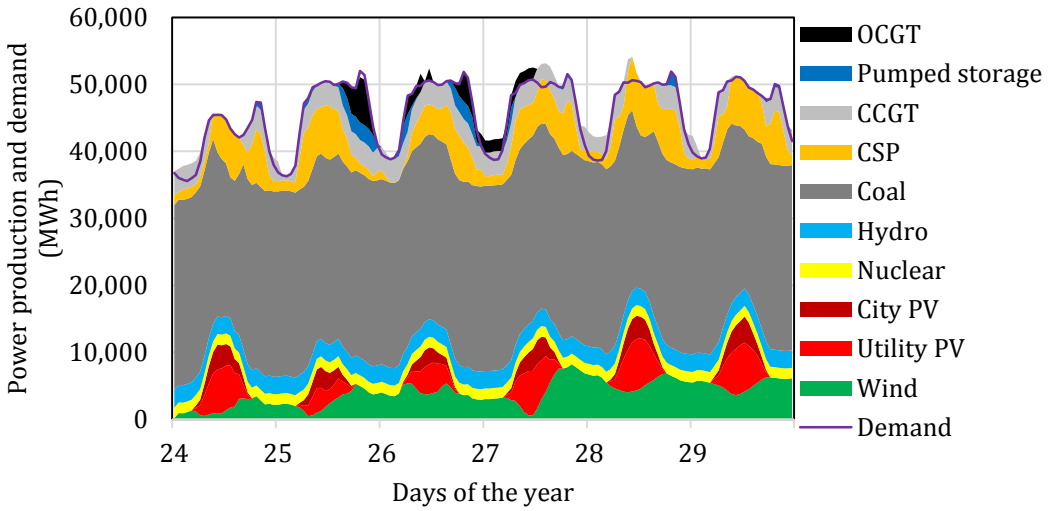

Figure 6.13: Example of the times series result of the model

A simple implementation of this kind of modeling is done by setting a range on each cost element in the cost model based on cost ranges from a variety of sources. With a high and low cost for each cost component and a statistical distribution function (in this case, constant), a randomized cost is produced for each variable, and the cost model is run enough times to produce a probability distribution on cost as shown by the example in Figure 6.14.

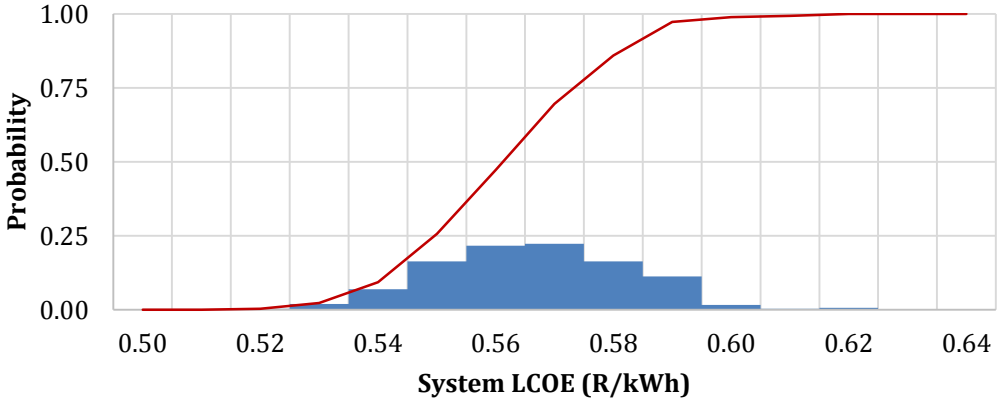

Figure 6.14: Example of cost probability showing binned probability (bar) and cumulative distribution (line) for a scenario

A good example of a considerable range in cost estimates in the South African case is the cost of running OCGT and CCGT systems. No publically available national planning publications indicate any certainty regarding the availability, quantity or cost of gas in the 2030 timeframe, and the consequence of this is significant in terms of the allocation of capacities per technology as indicated in the draft IRP Update (Department of Energy, 2013b).

On the one hand, abundant low cost gas could result from a combination of importing or exploitation by hydraulic fracturing. On the other hand, most if not all gas turbine capacity could still need to rely on expensive diesel at a cost almost an order of magnitude higher. Rather than speculate, the entire range of fuel cost could be represented by the extremes.

Another aspect about this approach is the ability to reduce all future scenarios to a mean (average) system cost with a standard distribution. In this way, the cost and the associate cost variance is understood by two simple derived measures, allowing an easy manner to select a robust (resilient) solution for the future rather than an optimized scenario of the future. For the example in Figure 6.14, the mean and standard deviation are

$$LCOE_{mean} = \text{R } 0.56 \text{ per kWh} \tag{6.21}$$

$$\sigma_{LCOE} = \text{R } 0.0165 \text{ per kWh} \tag{6.22}$$

meaning that if cost estimates for the scenario were realistic, then the system will have a high likelihood of generating power below R 0.58 per kWh.

6.5 Initial scenario testing

Elements of the system model were tested initially with simplified scenarios. One such study was a test of a distributed set of CSP plants optimized to perform a supporting role in the provision of peak electricity in the near term to avoid the excessive use of diesel in the capacity constrained South African power grid (Silinga & Gauché, 2014).

Assuming that all capacity of such a fleet would serve as availability to generate power when daily demand capacity exceeded 90 % of daily peak, the result is that the addition of 3.3 GW of CSP capacity would offset 80 % of diesel consumed if the alternative was all diesel. Assuming current CSP costs, the marginal cost of providing peak power is plotted in Figure 6.16.

The proposed concept significantly lowers the cost of peaking power only when CSP capacity is distributed along the indicated high capacity transmission line. When distributed, it offers both a lower cost of peaking and a higher resilience to fluctuations in the cost of diesel.

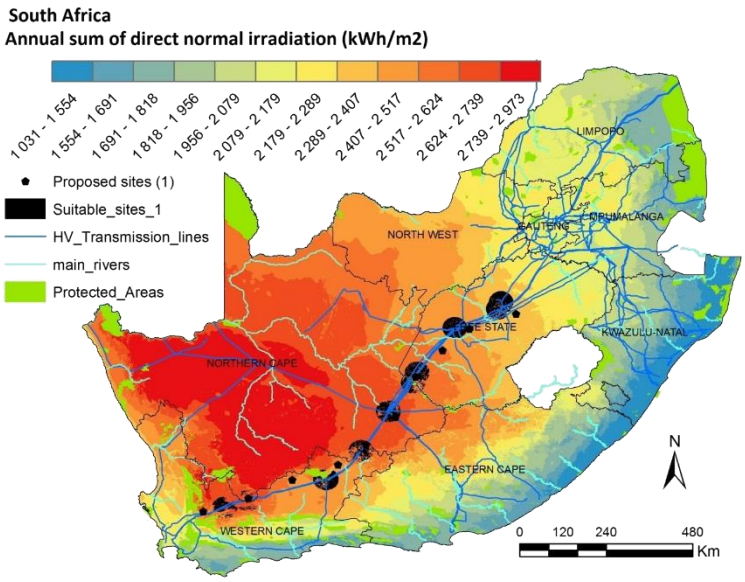

Figure 6.15: Map identifying suitable areas for near term peaking support CSP (Silinga & Gauché, 2014)

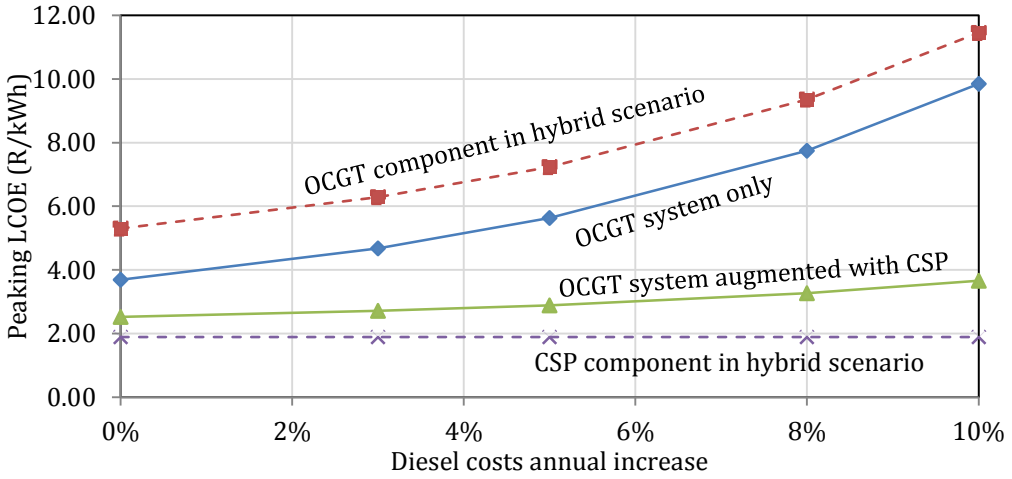

Figure 6.16: LCOE cost as a function of real annual diesel cost inflation (amended from Silinga & Gauché (2014))

6.6 Conclusion

Initial evidence of the relevance of covariant spatial-temporal analysis for the case of CSP is presented in this chapter. The CSP model is supported with validated reliable solar and wind data, hourly models for all other significant power generation technologies and a proposed cost forecasting methodology that reduces an energy systems analysis to an average and variance estimate for cost. Assuming that the various technologies making up the present and future South African electricity system are reasonably representative and that the system definition is adequate, the value of CSP in the electricity system can be tested thoroughly.

PART 3: APPLICATION AND SYNTHESIS

Part 3 covers the application, synthesis and conclusions of the dissertation.

WWF-SA commissioned a spatial-temporal study to investigate the feasibility of a renewable centered alternative to the IRP. This study serves as the systems analysis for the dissertation and is used to evaluate CSP per the objective of the dissertation.

The evaluation of CSP is centered on the WWF scenario. Techniques such as sensitivity analysis and marginal value analysis are used to interpret the results of the systems models in order to reach conclusions and propose recommendations.

7 WWF RENEWABLE ENERGY VISION 2030

This chapter represents the implementation of the methods presented in Part 2 and is substantially a summary of a report prepared for and published by the South African branch of the Worldwide Fund for Nature (WWF) (Gauché, Rudman & Silinga, 2015).

The objective of this chapter is to present the viability of a renewable energy prioritized way forward for South Africa. Accordingly, it does not emphasize CSP or the CSP node model, but it does provide context for the remainder of Part 3 where the value of CSP is presented.

7.1 Background

WWF identified the continued reliance on coal to generate more than two-thirds of the country's electricity as a threat to natural resources such as land and water, which are critical to the agricultural sector and will consequently present increased challenges in terms of the food-energy-water nexus. As a result of this concern, WWF proposes an increase in the percentage of renewable energy generation capacity into the South African system to achieve 11-19 % of generation capacity from renewable sources as opposed to the 6-9 % share as proposed in the IRP 2010 Update for 2030 (Department of Energy, 2013b). This proposal is published as The WWF Renewable Energy Vision Report for 2030 (WWF-SA, 2014) and referred to hereon as the WWF Vision.

This study uses the WWF Vision as a starting point to test the technical and cost (techno-economic) feasibility and merits of the scenarios that it proposes. The intention is to assess the viability, cost, risk and reliability of the national generating system that aims to provide 20 % of annual electricity by renewable resources, excluding hydropower. Scenarios are conceptually designed and compared to the IRP 2010 and its draft update of 2013. Key concerns are energy and economic security, which are gauged by scrutinizing the ability to meet electricity demand for every hour of the year coupled with the likely costs of each scenario representing South Africa's 2030-electricity system. The study assumes that only a direct economic argument will drive change and excludes analysis on the cost and impact of climate change and other externalities.

7.2 Objective

The WWF Vision proposes amending the draft IRP Update Base-Case scenario to scenarios prioritizing renewable energy technologies. Hereafter, this is referred to as "the WWF scenario(s)". A high demand and a low demand scenario are considered and typically abbreviated as "WWF High" and "WWF Low" respectively. Table 7.1 summarizes the scenarios investigated.

Both WWF scenarios propose that besides environmental benefits, a combination of

renewable energy capacity, storage and flexible gas-turbine generation offers South Africa a far more flexible energy system at a time of uncertainty regarding future electricity demand.

Table 7.1: The planned capacities for 2030 according to the Base-Case scenarios of the IRP 2010 and IRP Update, as well as the WWF High and Low Demand scenarios (Department of Energy, 2011, 2013b; WWF-SA, 2014)

Energy technology	IRP 2010 Base Case	IRP Update Base Case	WWF High Demand	WWF Low Demand
	Capacity (MW)			
Solar	9,600	13,070	18,884	9,334
Wind	9,200	4,360	16,134	8,184
Hydro	4,809	3,690	3,690	3,690
Existing coal	34,746	36,230	36,230	36,230
New coal	6,250	2,450	-	-
Nuclear	11,400	6,660	1,860	1,860
Open cycle gas	7,330	7,680	7,680	6,720
Combined cycle gas	2,370	3,550	3,550	1,420
Pumped storage	2,912	2,900	2,900	2,900
Other	915	760	760	640
Total	89,532	**81,350**	**91,688**	**70,978**
Expected 2030 demand (TWh)	454.4	**409.1**	**407**	**358.1**
% Expected 2030 Renewable Energy generation contribution	9 %	**9 %**	**19 %**	**11 %**
% Renewable Energy capacity in system	21 %	**21 %**	**38 %**	**25 %**

The objective of this study is to use the WWF scenario as a starting point to test the technical and cost (techno-economic) feasibility and merits of the proposed scenarios. More specifically, the feasibility and merits of targeting 20 % annual electricity generation by 2030 are tested by performing a spatial-temporal analysis on the complete electricity system of South Africa. While the WWF scenarios define and delineate the work in general, the analysis is confined neither to the proposed system makeup nor to prescribed technology performance characteristics. An intended outcome of this work is to validate the general idea and refine a conceptual electricity system for 2030. Scenarios are compared using a single metric (i.e., cost of electricity in Rand per kilowatt-hour (R/kWh)) in order to reach this objective, and this cost is tested against various demand forecasts.

WWF's proposal acknowledges that there are certain limits and constraints associated with the country's transmission network and that grid expansions will be necessary in order to realize a large rollout of renewable capacity in this timeframe. A starting constraint in this work is an assumption that economic realities in South Africa and in Eskom will result in limited grid expansion expenditure. As an independent study, the ability to accurately quantify and define grid constraints and

costs is not possible. The study does attempt to minimize the cost burden of the transmission system to be somewhat comparable to other scenarios that can fulfil the same future demand.

7.3 Current electricity system and planning

The most prominent characteristic of the current Eskom-owned electricity supply is that the generation system is dominated by coal power, generating around 93 % of electricity and supply baseload alongside the country's only nuclear power station, Koeberg. Of the thirteen coal power stations in operation, three are return-to-service stations; these are stations that have been re-commissioned to supply the growing demand for electricity after being mothballed in 1990. The two new supercritical coal-fired power stations, Medupi and Kusile, are the only new coal generation capacities currently under construction (Eskom, 2011b; Department of Energy, 2013b). The generation capacity that is now in operation and owned by Eskom is summarized in Table 7.2.

Table 7.2: The existing generation capacity in South Africa; these values are as given in the IRP Update and might differ slightly to those given by Eskom (Eskom, 2011b; Department of Energy, 2013b)

Generation type	Generation technology	Capacity (MW)	New Capacity (MW)
Eskom owned			
Baseload	Coal	35,980	9,564
	Nuclear	1,860	
Peak demand	Hydroelectric	600	
	Small hydroelectric	61	
	Pumped storage	1,400	1,332
	Gas turbines	2,460	
Renewable energy – new build	Concentrating solar power		100
	Wind	Not operational	100
	Total Eskom owned	**42,361**	**11,096**
Non-Eskom generation			
	Various	3,330	1,258
	Total generation capacity	**45,691**	**12,354**

Arguably, the aging fleet of coal-fired power stations are associated with further risks and implications relating to reliability. Since the electricity supply shortage in 2008, demand has apparently been met by not complying with standard maintenance schedules on the coal fleet. As a result, the fleet has been subject to deterioration, and where the expected annual performance was thought to be 86 % in 2010, the actual performance was reportedly below 80 % (Department of Energy, 2013b). Due to the small-to-non-existent reserve margin, any unexpected event at a coal power plant results in load-shedding; this was the case in November 2014 when a coal silo collapsed at the 4,110 MW Majuba plant, the youngest of Eskom's coal-fired stations. There are, however, an array of incidents that can occur as a result of dwindling maintenance practices, affecting not only the individual consumer but also business

owners and industries with an ultimate effect on the economy (Department of Energy, 2010).

7.3.1 Integrated resource plan (IRP)

This section expands on the IRP process in Part 1, noting that at the time the 2010 IRP had just been legislated (Gauché, von Backström & Brent, 2013).

The National Energy Act of 2008 set the objective for a long term Integrated Energy Plan (IEP) (Department of Minerals and Energy, 2008). Although the IRP was published as a subset of the IEP with the intent to be governed by the IEP, the IRP was promulgated in 2011, a year before the release of the draft IEP (Department of Energy, 2013c). A final IEP still has not been released at the time of this report. Resource availability and uncertainties associated with demand growth in the IRP and IEP draft are considered in several scenarios using a stochastic programming approach. The anticipative method is included as one of the scenarios, where decisions can be made by the user before uncertainty is observed. The objective of all models is to minimize costs, but other constraints with regards to investment, load and generation are all inputs under which simulations are conducted (Fouche & van Niekerk, 2014).

Regardless of delays in the IEP, a draft IRP Update was released in 2013 but not finalized (Department of Energy, 2013b). The Update was necessary in terms of the following aspects: renewed technology and fuel options, changes related to electricity demand and the relationship thereof with economic growth, possibilities for carbon mitigation and the price of electricity along with the associated impact on demand and supply after 2030.

In the IRP Update, the CSIR Green Shoots demand forecast is considered for the Base Case scenario, causing the demand projection for 2030 to decrease from 454 TWh to closer to 345-416 TWh. The Green Shoots forecast plans for a 2.7 % annual electricity demand growth up to 2030, and an aspirational average economic growth rate of 5.4 % is considered as suggested in the NDP. This growth rate is in line with poverty alleviation and a shift towards a less energy intensive economy, and the risks associated with overbuilding generation capacity should this growth rate not be realized are recognized.

The modelling parameters that were changed in the IRP Update are summarized in the IRP report and pertain to instantaneous reserves, fuel price merit order, maximum load factors, unit commitments, minimum stable generation levels, capacity profiles and modelling updates for the demand, and PV and wind profiles. In addition to the Base Case, several other demand forecasts, sensitivities regarding learning rates, fuel availability and costs, new build options and combinations of these parameters have resulted in fourteen other scenarios in the IRP Update.

The IRP of 2010 is still recognized as the official plan of the government, but the IRP

Update proposes seemingly valuable changes with the aim of improving the next formal iteration of the IRP.

7.3.2 REIPPP programme

To date, renewable energy capacity is predominantly the result of the REIPPPP (Department of Energy, 2012). Launched in 2011, the REIPPPP is an initiative of the DOE that awards bids to applicants according to allocations set per technology. Initially, the total allocation to renewable generation was 3,725 MW. By the end of 2012, an additional 3,200 MW was allocated, and this is expected to be online by 2020. At the time of writing, three rounds of allocations have been concluded. Financial closure for the Round 3 projects has not yet been reached due to complications beyond the control of the IPPs such as issues relating to grid connectivity. Round 3.5 was added to allocate extra CSP capacity, and preferred bidders were announced in late 2014. Round 4 preferred bidders were announced in early 2015.

The tariffs allocated to REIPPPP projects have become increasingly competitive with each bidding round and are, in instances, better than the expected generation costs for Medupi and Kusile. In the third bidding window, wind power projects had the lowest tariffs at R 0.66/kWh, PV followed at R 0.82/kWh, and CSP at R 1.46/kWh. These tariffs were lowered even further with approximately R 0.10/kWh for both wind and PV in the fourth bidding window. The exception to the tariff structure for CSP lies in the benefit of receiving 270 % of the standard tariff when a plant generates electricity during the evening peak demand hours. Despite this adjusted tariff for what is currently the most expensive renewable energy technology, this tariff is already cheaper than the cost of OCGTs currently used as a last resort to serve peak demand hours as per the IRP Update and also according to analyses by Silinga and Gauché (2013).

7.4 System model

7.4.1 System demand characteristics

The model accounts for four demand scenarios in 2030. Hourly demand in 2030 is assumed to take much the same form as is experienced now, with morning and evening peaks, weekend and public holiday dips and higher winter daily peaks. A complete hourly set of 2010 Eskom demand was used, and every hour was simply scaled with the ratio of annual 2030 scenario demand to total 2010 demand. No efforts were made to account for changes in behavior or technology advances that aim to improve time-of-day demand balancing that might exist in the system in 2030. Accordingly, the 2010 shape of annual demand was assumed to be representative enough, likely more challenging to meet than a future demand-side managed system, and a level playing field for all scenarios.

For simplicity and to reiterate that this study does not aim to replicate or validate the analysis of the IRP, annual demand for each scenario is taken “as-is” and no

discounting is performed for efficiency measures that might occur in future. Demand in this study needs to be satisfied by power generation only. The ratio multiples are given in Table 7.3, and in particular it should be noted that WWF High and the IRP Update Base Case scenarios are practically the same.

Table 7.3: The multiples used to calculate hourly demand for 2030

Annual demand (TWh)	Scenario	Multiples
250	2010	n/a
358	WWF Low	1.430
407	WWF High	1.625
409	IRP Update	1.634
454	IRP 2010	1.816

7.4.2 Technology characteristics

The performance characteristics and behavior of each technology – and where possible, each known plant – needs sufficient and fair definition in the model. These characteristics are a function of many variables including technology, local conditions, trends and forecasts. Additional complexity results from data sources that have differing definitions, contradicting characteristics or missing information. Power generation characteristics in the model result from a distillation of many sources requiring many assumptions.

Table 7.4 summarizes the technologies included in the proposed WWF scenario, and the following paragraphs outline key motivations for the choices made.

Ranges given for the costs of the various technologies aim to allow for variations from predicted costs in terms of learning rates, exchange rates and resource availability. The values given as upper and lower bounds are drawn from various sources but predominantly the IRP Update and Black & Veatch (2012).

Capital costs given are estimates for the year 2022 in 2014 ZAR, the midpoint year for the years leading up to 2030. Technology costs in 2022 were assumed to represent an average for the duration in real terms.

Investment (or project) capital costs were used rather than 'overnight' capital costs, accounting for cost of capital during the construction phase. In the case of coal power, only technologies that do not include carbon capture and sequestration (CCS) were taken into account on the assumption that cost and maturity risks are too high for South Africa in the next fifteen years. The range for nuclear power was based on the IRP Update on the low end (R 60,000 /kW) and on other sources for the high end (under R 90,000 /kW). No decommissioning or other externality costs were factored into the analysis.

Table 7.4: A summary of costs and technology characteristics for the options included in the proposed WWF scenarios. Sources: (Department of Energy, 2011, 2013b; Black & Veatch, 2012; IRENA, 2012a,b,c; WWF-SA, 2014); Own analysis

Technology	CAPEX R/kW	Fixed OPEX R/kW/a	Variable OPEX R/MWh	Fuel Costs R/GJ	Avail-ability	Turn-down limit	Ramp rate (%/min) *	Max life Span (years)**
PV Fixed tilt	13,115	484	0	0	90 %	NA		25
	11,210	208	0	0				
CSP – 6h TES	37,610	573	29	0	90 %	0	6 %	30
	36,726	573	0	0				
CSP – 9h TES	43,259	573	29	0	90 %	0	6 %	30
	42,242	573	0	0				
Wind	19,463	400	0	0	90 %	NA		20
	14,502	310	0	0				
OCGT	5,738	78	0.2	500	90 %	0	22.2 %	30
	5,615	78	0.2	92				
CCGT	8,708	163	0.7	92	90 %	0	5 %	30
	8,524	163	0.7	70				
Nuclear	87,754	1,017	29.5	10	90 %	0.80	5 %	60
	60,000	532	29.5	6.8				
Coal (PF with FGD)	34,938	552	79.8	22-35	80 % - 85 %	0.40	2 %	60
	34,894	368	51.2	17.5				
Pumped storage	56,846	333	0	0	90 %	0	50 %	60
	23,973	247	0	0				
Imported Hydro	28,341	344	13.9	0	66.7 %	0	2 %	60
	12,044	80.2	0	0				
Domestic hydro	28,341	344	13.9	0	96.6 %	0	2 %	60
	12,044	80.2	0	0				
	* Represents spin ramp rate for baseload and intermediate load technologies and quick start rate for peaking technologies as per Black & Veatch (2012). **The maximum life span includes life extension plans for the coal-fired power plants.							

The CAPEX range for CSP is represented for fixed plant configurations as typically found in the relevant literature, but the model uses a more detailed breakdown in order to correctly account for scaling the size of storage, turbine rating and collector field.

Operational costs are as given by the sources for the respective year; the reference year is 2012 for most of the technologies. Gas costs are according to the predictions made about gas acquisition in the IRP Update. A high degree of uncertainty notably exists around the availability of gas for the large additional capacity of OCGTs and CCGTs, and the following assumptions were made:

The significant new planned CCGT capacity will play a mid-merit to peaking role due to their characteristics. In instances where a scenario is underserved, the CCGT fleet will be permitted to operate as baseload. Accordingly, higher capacity factors were expected than for the OCGT fleet. Economically, it will be important that these plants run on gas, and therefore it was assumed that all CCGT plants will run on gas. The fuel cost range was based mostly on costs given in the IRP Update.

The even higher reliance on an OCGT fleet is a different matter. Assuming that the

OCGTs could span the range from only relying on gas to only relying on diesel due to uncertainty around sourcing gas for all gas turbines suggests that a range of costs warrants consideration. What must be kept in mind is that a fleet of CCGTs running only on gas will already significantly increase gas infrastructure needs. The upper value assumes super-inflationary diesel costs between now and 2030, and the lower value is given with the anticipation of higher gas availability in South Africa within the next ten years. This scenario is similar to what is described as the 'Big Gas Scenario' in the IRP Update. This means that in this model, the average outcome is that half the OCGT plants use diesel and half use gas.

In addition to capital, operational and fuel costs associated with the various technology options, there is a cost to bear when electricity cannot be supplied due to limited generation capacity. This cost is known as the COUE, which encourages the system planner to balance the incremental costs of supplying the energy that was not served with the total COUE. The COUE is not a parameter that can be measured directly and varies greatly between customer sectors according to load segments and timing of unplanned electricity outages (Department of Energy, 2010). The current COUE estimation ranges from R 10/kWh (based directly on the relationship between GDP and total demand) to R 150/kWh (based on many other factors linked to the disruption in the provision of power). The IRP Update assumes R 75/kWh, but given that cost is handled probabilistically, the extent of the IRP Update data range is simply used. On average, this study's result is similar to the assumptions in the IRP Update.

The initial reason for accommodating the COUE is that this model simulates a complete year of generation and reflects all over- and under-generation. In scenarios with insufficient capacity, varying levels of unserved electricity were observed. In order to compare or improve scenarios using a single cost metric, COUE was added in all cases.

The technology characteristics in Table 7.4 are used as part of the performance definition in the model and are briefly explained here in context of the choices made.

Availability: Plant or technology availability requires explicit definition in this model as this is primarily driven by choices and realities regarding the reliability and maintenance of plants. Most values are typical, perhaps with the exception of coal power. 80 % was chosen for coal plants prior to Medupi and 85 % for all new builds based on assumptions made in the IRP Update as well as what was understood to be the harsh reality of the ageing coal power fleet. While 80 % is low for such units, there was no basis to justify higher numbers. This has serious implications for the results.

Capacity factor: This was not provided as input. The model calculates these values and provides them as outputs.

Turndown limit: Turndown limits are relevant mostly to coal and nuclear, but other technologies have built-in rules governing lower limits to performance that are not useful at a plant level. It was assumed that nuclear plants can operate down to 80 %

of rated performance based on the way that Eskom manages the Koeberg plant. While modern nuclear plants as described in the references can apparently turn down to 50 %, it was assumed that on a usage basis, predictable and maximum operation would be preferred. Regardless, none of the scenarios required much nuclear turn down, and assuming a lower value would not have changed the results much.

Ramp rate: It was necessary to govern how quickly a power plant can adjust its output at the request of the system. In the event that the system of plants cannot respond fast enough to changes in demand or changes elsewhere in the system (such as a very sudden system-wide drop in wind power), the model would simply be forced to under- or over-produce. The ramp rate values used are typical, and no noteworthy events were found in any scenarios.

7.4.3 Node selection

Defining the location and limitations of renewable energy capacity for the WWF scenario is the final step in defining the system. No single analytical method was used to synthesize all assumptions and definitions. Rather, a selection of nodes were chosen in order to attempt a practical and fair balance given all constraints. Key factors in this selection include:

- Locating very close to the existing transmission system in order to comply with the assumption that this will reduce the cost burden of transmission, particularly in the near term.
- Experience gained in prior work to confirm that distributed renewable energy generation can be cost-effective and meet demand.
- Selecting locations that have good-to-excellent renewable resources whilst also offering resource independence.

The generation areas (nodes) for PV, CSP and wind selected for this study are shown in Figure 7.1.

These points are consistent with the five corridors mentioned in the draft IRP Update (Department of Energy, 2013b) with the exception of three points in the eastern and north-eastern region of the country that were selected at points of consumption. Each node is located at or close to an existing Eskom substation in order to satisfy the assumption on cost. Although recognized that the substations themselves are generally not sufficient now to attach new capacity, the model relies on an assumption that the regional transmission line capabilities are not a major constraint within the definition of the main transmission system (MTS). Additionally, the nodes must be able to accommodate additional renewable power within a 20 km radius of the substation in order to contain the additional cost of low voltage lines between the plant and substation.

Node capacities are constrained based on the MTS connection limits of the Eskom Generation Connection Capacity Assessment (GCCA) for 2016 (Eskom, 2014). The

limits set out in the 2016 GCCA are respected at the regional extraction levels in the model. Beyond this, the model contains no further definition of the transmission or connection system.

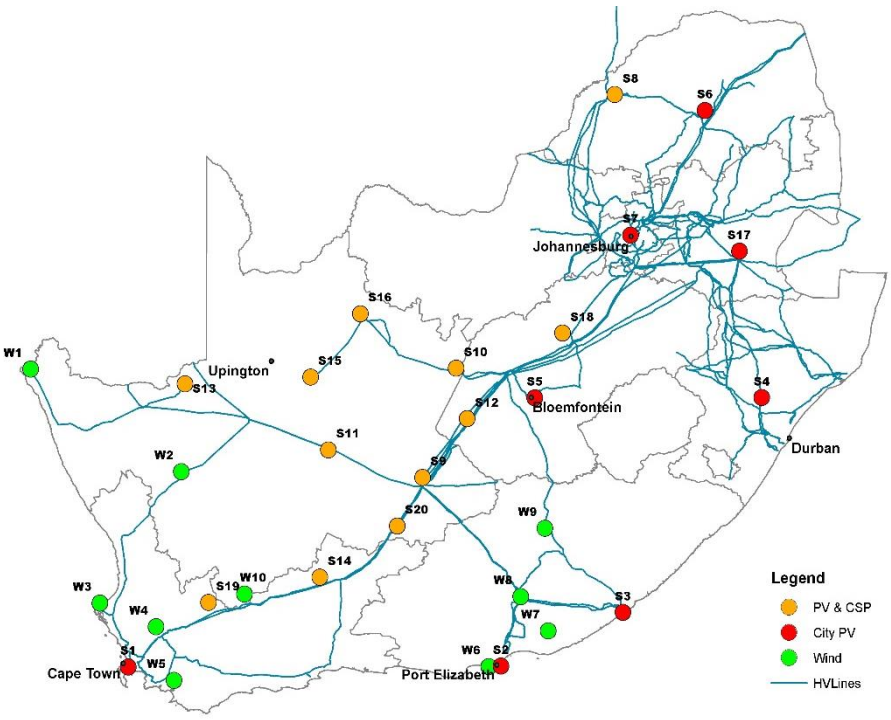

Figure 7.1: CSP, PV and wind nodes selected for the model in this report (figure by Rudman & Silinga)

7.5 Scenario results

Scenarios for the IPR, draft IRP Update and WWF scenarios were constructed after which, the WWF scenarios were tuned by trial and error to achieve lowest cost. High level results are presented first followed by a more thorough review of choices made and the behavior of the scenarios.

The final WWF scenarios are summarized in Table 7.5 and shown relative to the two IRP variants and the two WWF Vision study starting points.

The system definitions of the IRP and the draft IRP Update were kept intact, and there is little deviation between their definition and performance at a plant level. In both cases, the amount of power delivered per unit (and hence capacity factors) by renewable energy was well validated. In order to match well to the CSP capacity factor in this model, storage needed to be set to around 6 hours full-load on average. This appears to be consistent with the original and draft update documents.

Table 7.5: Capacity summary for the original scenarios and the resulting cost reduced scenarios

	IRP Capacity	IRP Update Capacity	WWF High Final	WWF High Initial	WWF Low Final	WWF Low Initial
Wind	9,200	4,360	14,000	16,134	9,000	8,184
PV	8,400	9,770	10,000	11,884	7,000	6,334
City PV	0	0	7,000	0	3,000	0
CSP	1,200	3,300	8,000	7,000	4,500	3,000
Coal	40,995	38,680	36,230	36,230	36,230	36,230
Nuclear	11,400	6,660	1,800	1,860	1,800	1,860
CCGT	2,370	3,550	4,000	3,550	3,000	1,420
OCGT	7,330	7,680	7,680	7,680	6,720	6,720
Pumped storage	2,900	2,900	2,900	2,900	2,900	2,900
Hydro	4,809	3,690	3,690	3,690	3,690	3,690
Other	915	760	760	760	640	640
Total	**89,519**	**81,350**	**96,060**	**91,688**	**78,480**	**70,978**

Notable points regarding the system capacities are summarized:

- The starting WWF capacities did not differentiate solar PV from CSP; this was left to the authors to configure.
- City PV is essentially a demand-side matter and could have been applied in some measure to the IRP and IRP Update; due to stated assumptions, it was not.
- The IRP Update Base Case is somewhat comparable to the WWF scenarios and formed the basis on the WWF Vision study assumptions.
- CSP capacity on its own is misleading. The IRP and IRP Update models assume 6 hours of storage while the optimal storage levels in the proposed WWF scenarios tended to exceed 12 hours.
- The WWF High and WWF Low capacities for solar increased, and wind remained similar, pushing the overall system capacity up in both cases.
- Results showed that a marginally higher capacity was required for CCGT in the WWF scenarios. Because it is generously assumed that gas will be available under all cost probability assumptions, this might seem like a violation in the parity rule. Parity for the CCGT and OCGT fleet does need monitoring, but this is measured by actual use rather than capacity. As will be demonstrated, the WWF scenarios use significantly less gas than the scenarios representing the IRP and IRP Update.
- A more generalized point regarding capacity is that all initial scenarios fall short in expectation when tested against what might be considered a grueling demand curve. In combination with the assumed availability of coal power, other changes and assumptions and the use of a system-wide spatial-temporal approach, it is perhaps not unexpected that this occurred.

Table 7.6 summarizes the performance and system cost metrics. The resulting WWF scenarios have been tuned for lowest cost, which automatically tends to mean that the level of unserved energy would be very low and that last resort generators using diesel would be used sparingly. When renewable capacities are well balanced, which includes a significant capacity of high storage CSP, low cost and low levels of unserved electricity were achieved.

The high amount of unserved electricity in the IRP is likely mostly attributable to the reduced availability assumption in this study, but it may also be a consequence of the full spatial-temporal modeling method. It is not difficult to reconfigure the IRP or the draft IRP Update to avoid unserved electricity, but within the constraints of the system and technology definitions, lower cost always results in the addition of renewable energy capacity. Cost continued to drop until the annual renewable energy generation fraction approached 25 %, significantly exceeding the WWF target.

Table 7.6: Summary of primary performance and cost

	IRP		**IRP Update**		**WWF High**		**WWF Low**	
	Annual power (TWh)	**Share**	**Annual power (TWh)**	**Share**	**Annual power (TWh)**	**Share**	**Annual power (TWh)**	**Share**
Annual demand	454.7	0.99	409.1	0.98	407.0	0.99	358.0	0.99
Wind	26.2	0.06	12.4	0.03	39.9	0.10	25.6	0.07
Utility PV	14.3	0.03	16.6	0.04	17.0	0.04	11.9	0.03
City PV	0.0	0.00	0.0	0.00	10.8	0.03	4.6	0.01
CSP	4.5	0.01	11.9	0.03	36.1	0.09	17.9	0.05
Renewable supply	**45.0**	**0.10**	**40.9**	**0.10**	**103.8**	**0.25**	**60.1**	**0.17**
Hydro	29.2	0.06	22.8	0.05	22.8	0.06	22.8	0.06
Coal	245.2	0.53	254.6	0.61	245.7	0.60	246.2	0.68
Nuclear	93.0	0.20	54.3	0.13	14.7	0.04	14.7	0.04
CCGT	15.1	0.03	21.5	0.05	19.0	0.05	13.7	0.04
OCGT	25.3	0.06	16.4	0.04	2.1	0.01	1.5	0.00
Pumped storage	6.6	0.01	5.6	0.01	3.1	0.01	2.9	0.01
Annual actual	**459.4**		**416.0**		**411.1**		**361.9**	
Shortfall	4.1		0.6		0.0		0.0	
Surplus	0.0		0.0		0.0		0.0	
System cost high (R/kWh)	**R 2.32**		**R 1.04**		**R 0.67**		**R 0.61**	
System cost low (R/kWh)	**R 0.59**		**R 0.49**		**R 0.48**		**R 0.44**	

Why the renewable energy favored WWF scenario results in lowest cost is not explicitly obvious. The difficulty in an explicit understanding may be due to the model approaching characteristics of a complex system with a high number of variables, constraints and a domain with a reasonably significant number of endogenous

variable in the model. Analysis by sensitivity studies and by other means does provide insight.

Taking care not to violate constraints and assumptions regarding resource availability and cost, typical LCOE values for the technologies were extracted from the WWF High scenario (and in the case of nuclear, from the IRP Update). These are presented in Figure 7.2.

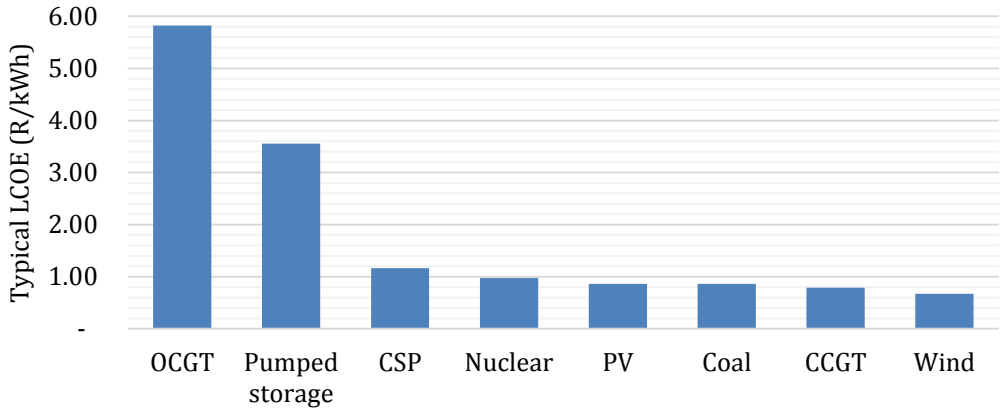

Figure 7.2: Typical system based LCOE values for new capacity in the WWF High scenario (and IRP Update in the case of nuclear)

The complexities of the system make it difficult to fully understand the trade-offs, let alone explain them. Nonetheless, some high-level explanations are argued here. In a capacity constrained system, any new capacity helps directly, so the lowest cost options would benefit the system.

Additional CCGT capacity does help, but care is needed to maintain parity. If gas resources do not support additional capacity, the marginal cost will increase. The CCGT capacity in the WWF High scenario was indeed increased, and because more would be needed if renewable capacity was removed, this is not something that the authors would advocate. While this model does not adjust for this marginal cost, it is still not expected that the cost will drop with significant additional CCGT capacity in exchange for renewables.

A reason for this might be the care that was taken to balance wind, PV and CSP, noting that CSP in this case plays a sacrificial availability role. When renewable capacity is reduced, the system relies more heavily on OCGT capacity to meet demand. Had CSP been used as a baseload option, LCOE for CSP would be about 20 % lower and thus competitive with nuclear. The aforementioned balancing of wind, PV and CSP is a particular virtue of the spatial-temporal method.

Nuclear simply cannot lower LCOE under any condition when added at the expense of renewables. CSP automatically takes on the role of baseload capability in a marginal sense when compared to nuclear and coal power. Neither can compete with CSP, and

this characteristic of CSP value and cost is intrinsic to the model. This occurs despite the likely underestimation of the real costs of new nuclear power plants in this work.

After several attempts to try different configurations it was found that by trying to reduce cost further, something else would "pop" – i.e. the marginal cost elsewhere in the model would rise. What stood out was the impact of the availability of existing coal power capacity. Assuming that better maintenance management of the existing coal fleet is cost-neutral (the higher cost of proper maintenance offset by the cost of wear-and-tear from poorly maintained plants), increasing availability to normal levels leads to a lower system cost. More importantly, the system shows improved availability, and this is reflected in the high probability end of the cost values. While the objective and scope of this study do not deal with management of the Eskom coal power fleet and while the authors do not advocate for more coal power emissions, it would be remiss not to point out this significant finding. Two corollary implications are also worth mentioning. Firstly, it may be marginally more cost effective to reduce the size of the coal fleet to ensure improved maintenance of the best plants, resulting in the same available capacity level. Secondly, capacity loss due to the decommissioning of existing coal plants will result in a rise in system cost regardless of the configuration of new capacity.

7.6 Scenario characteristics

It is increasingly clear that nothing is more damaging to the full cost of the system than a shortfall in available capacity. The IRP scenario experiences close to 800 hours of load-shedding in which a load-shed hour is defined as an equivalent hour where 10 % of average system demand is unmet. Figure 7.3 illustrates such an example over a period of roughly three weeks in summer.

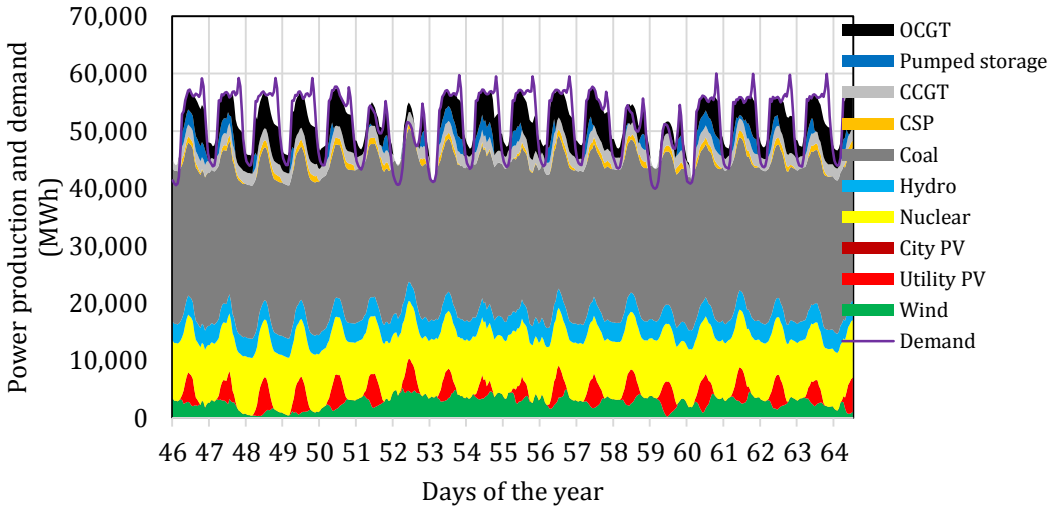

Figure 7.3: IRP scenario showing three weeks during summer

The contribution to cost in the system due to unserved energy in addition to the very

high utilization of high cost OCGT plants are the key contributors to the very high cost of the system. The same timeframe in the WWF High scenario is shown in Figure 7.4. Despite no new nuclear or coal capacity and noting the difference in demand, this period of time never reflects any shortfall.

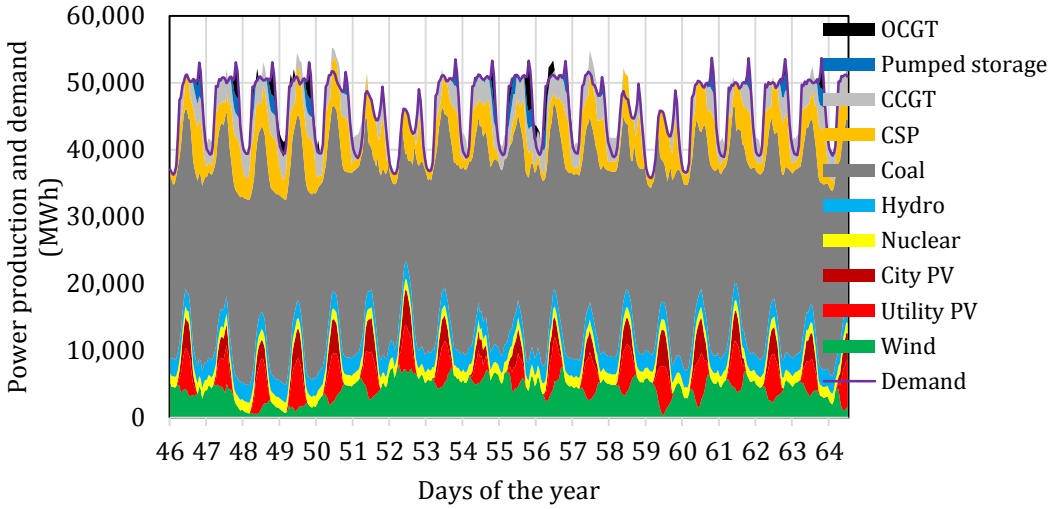

Figure 7.4: WWF High scenario showing three weeks during summer

A somewhat surprising outcome of the study was the degree to which the WWF scenario, with all its associated constraints, could be configured for a high degree of complementarity between technologies. This outcome relied on the assumption that the coal power fleet availability was 10% lower in summer than in winter while maintaining an overall fleet availability. Figure 7.5 illustrates the near-daily predictability of wind complementing solar during summer periods. Additional examples are shown for interesting characteristics of the WWF High scenario.

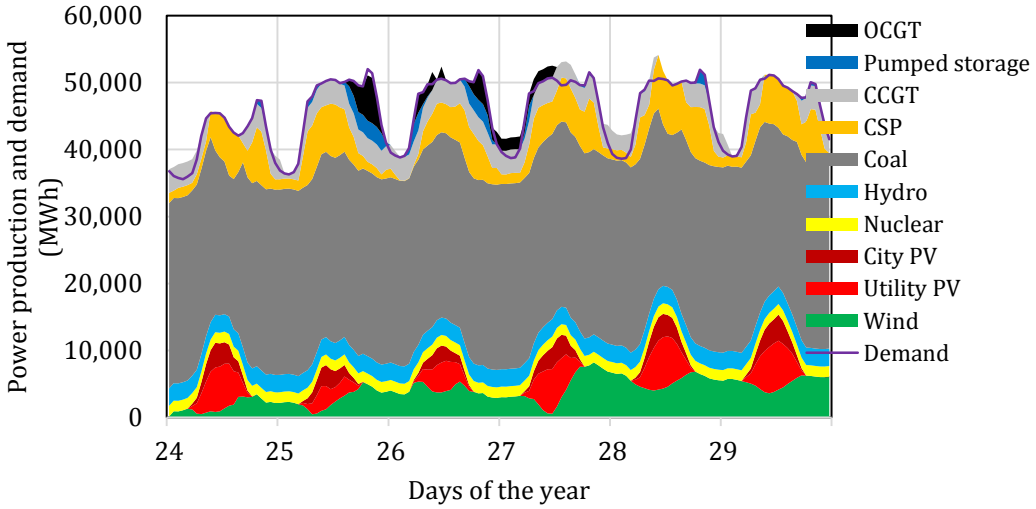

Figure 7.5: Summer event with poor sun

Large weather systems occur periodically during the summer where usually sunny skies in the arid region are affected by significant cloud cover. Figure 7.6 illustrates two days in the series where reduced PV output and depleted CSP storage results in significant use of pumped storage and OCGTs. During this period, the pumped storage capacity is depleted to the point that the system chooses to use all spare generators to re-charge overnight on the second day of decreased sunlight. This pumped storage charging continues into the next day when possible and eventually is replaced with solar energy on the fourth day of the start of the event.

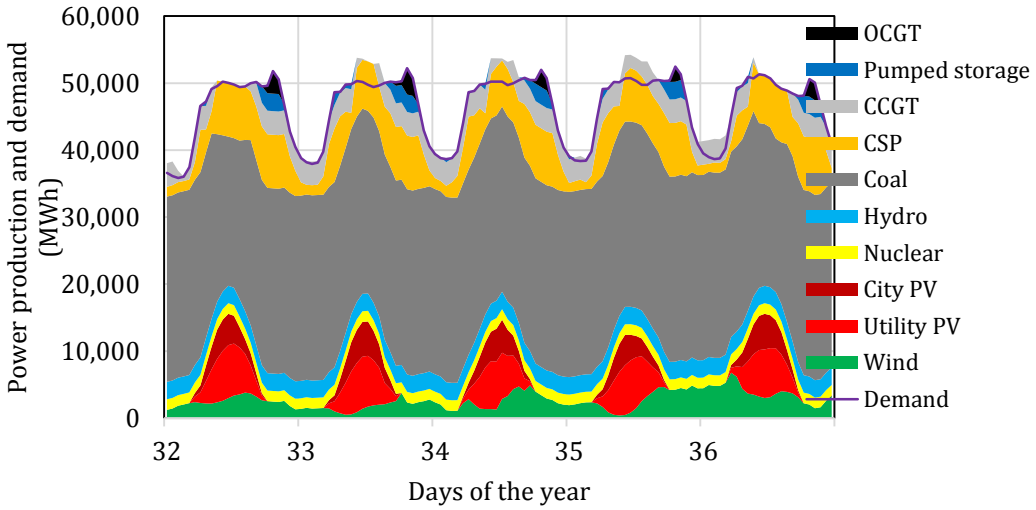

Figure 7.6: Sunny summer days where wind drops

Figure 7.7 illustrates an event of lower than average wind across the country during a summer period. Wind is not supportive on the fringe of the day requiring a significant CCGT capacity, but during the day, solar power is produced in excess since it is utilized to recharge pumped storage. Given that there is very little suppression of coal output, this apparent excess of solar power is not considered as excess since it only recharges the pumped storage. CSP remains supportive during evening peak, but OCGT, pumped storage and OCGT capacity are required during all evenings during peak.

Figure 7.8 illustrates the time around Easter where, coincidentally, coal power availability increased in the model. This very early winter stretch demonstrates excess renewable power that causes coal power to frequently ramp down and back up. During this period, the system experiences no excess renewable power (as with all scenarios at all times).

The model was set to use CCGT capacity as mid-merit and this allowed these plants to immediately recharge pumped storage used during the previous very high peaks. The frequent ramping of the coal fleet does not exceed the ramping that the current Eskom fleet needs to manage based on the majority of power presently generated by coal and nuclear.

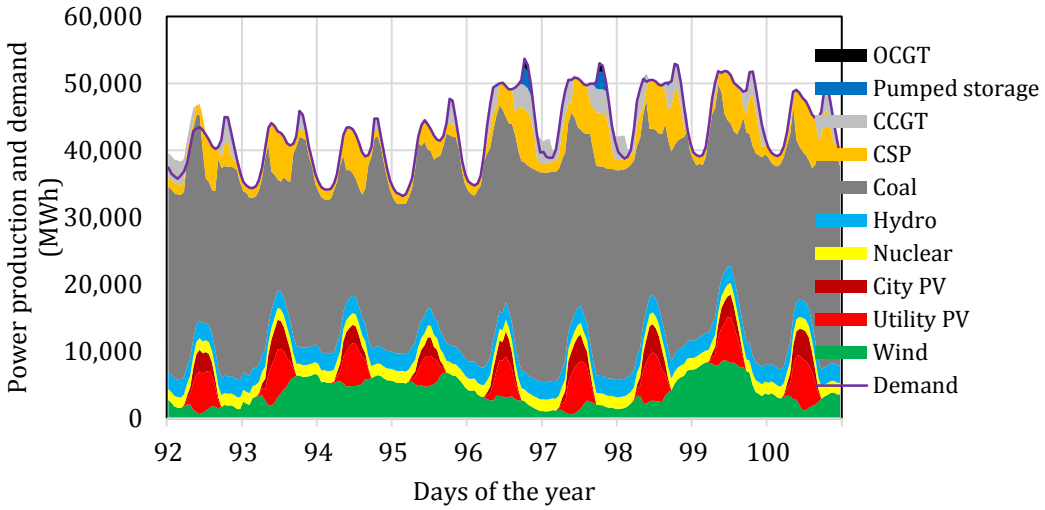

Figure 7.7: Transition to winter with higher baseload availability

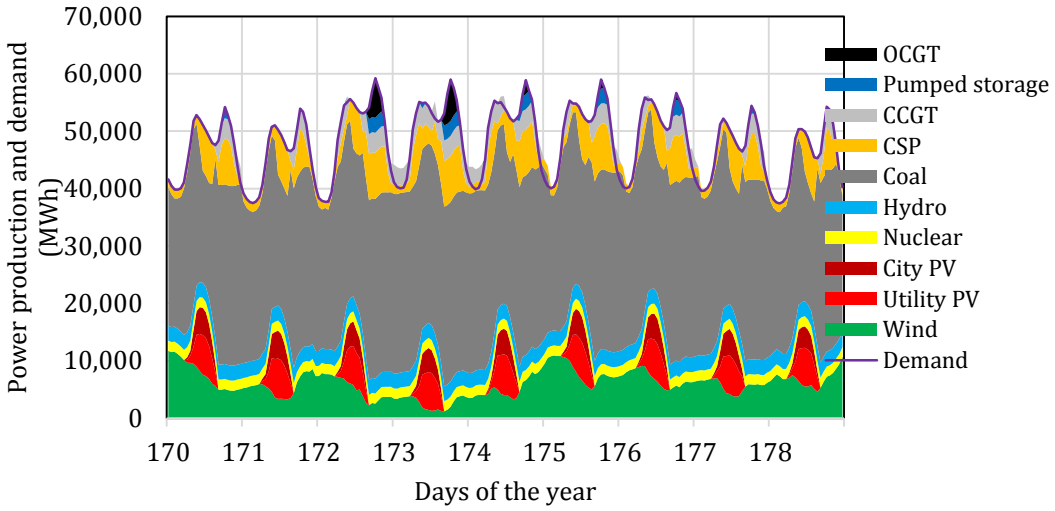

Figure 7.8: Deep winter characteristics

Figure 7.9 is a plot of the system pumped storage charge level for the WWF High scenario. Besides the variation between seasons, a key attribute that stands out is the degree to which the pumped storage system is available throughout the year. The pumped storage charge level appears to be a good indicator in the model for total system capacity sufficiency. When pumped storage tends to start showing good availability, the system cost is low.

Figure 7.10 is the IRP scenario version of the system pumped storage level illustrating system insufficiency. An interesting observation is that the South African pumped storage system does not appear to be insufficient for a well-planned, high renewable scenario in the future. Increased pumped storage capacity would certainly be advantageous, but it only supports a system as a capacitor. In a high renewable case,

the model outcome suggests that once the Ingula pumped hydro project is complete, the total reservoir capacity is very good and perhaps only limited by turbine rating.

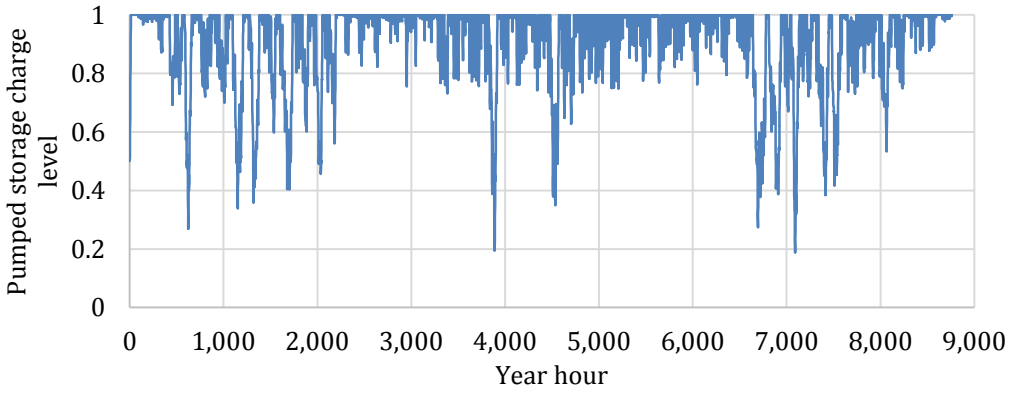

Figure 7.9: System pumped storage charge level for the year (WWF High), illustrating the shorter duration but frequent pumped storage usage in winter with exception of two significant winter events

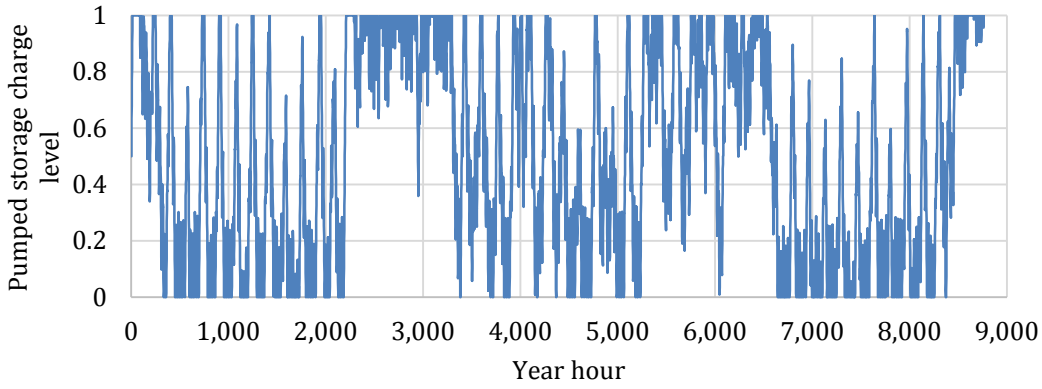

Figure 7.10: System pumped storage charge level for the year (IRP), illustrating insufficiency in the system

Analysis of the results indicated that special attention is needed between the intermittent performance of PV and wind, and the blend between the mid-merit and peaking solutions of CSP, CCGTs, pumped storage and OCGTs.

Figure 7.11 and Figure 7.12 are plots of the capacity and output balances, respectively, between the renewable, mid-merit and peaking options in the four scenarios. The balanced provision of renewables, including 8 GW of high storage capacity CSP, results in a very significant reduction of OCGT and pumped storage use.

7.7 Cost probabilities

Once each scenario model has been defined, there is a switch to the cost probability model. The cost method produces a probability distribution for each scenario, and it has been argued this could potentially provide a better way to make decisions for a

more resilient system. This is perhaps best illustrated by looking at the combined cost result shown in Figure 7.13.

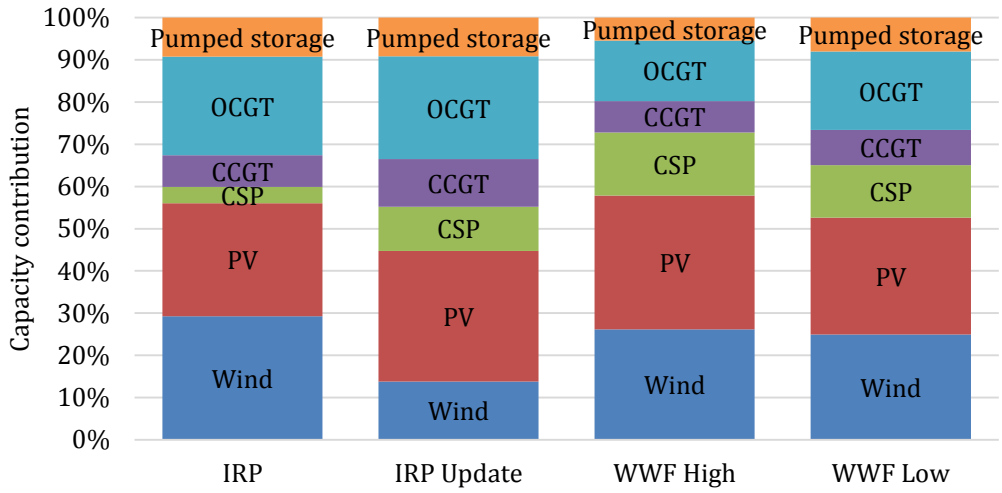

Figure 7.11: Capacity balance for renewable, mid-merit and peaking for all 2030 scenarios

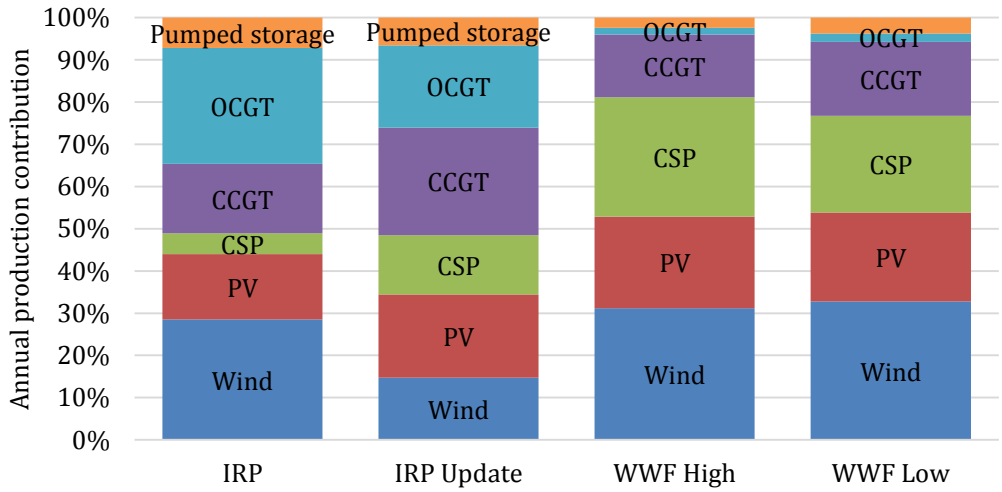

Figure 7.12: Annual electricity production balance for renewable, mid-merit and peaking for all 2030 scenarios

The cumulative distribution function (CDF) plot of the four scenarios uses the simple LCOE method as described in Part 2. Key assumptions for the cost model include:

- Capacity brought online prior to 2014 is paid for. All new capacity requires full investment budgeting.
- No cost has been included for grid expansion.

The steep cumulative distribution curves for the WWF scenarios are in part explained

by the lower reliance on fuel costs, particularly the cost of diesel. The significant deviation, particularly of the IRP scenario, is largely attributable to the cost of unserved energy. Because the scenarios were defined for different annual demand levels, each scenario was then subject to all demand forecasts to test for resilience. The mean cost for each case is shown in Figure 7.14.

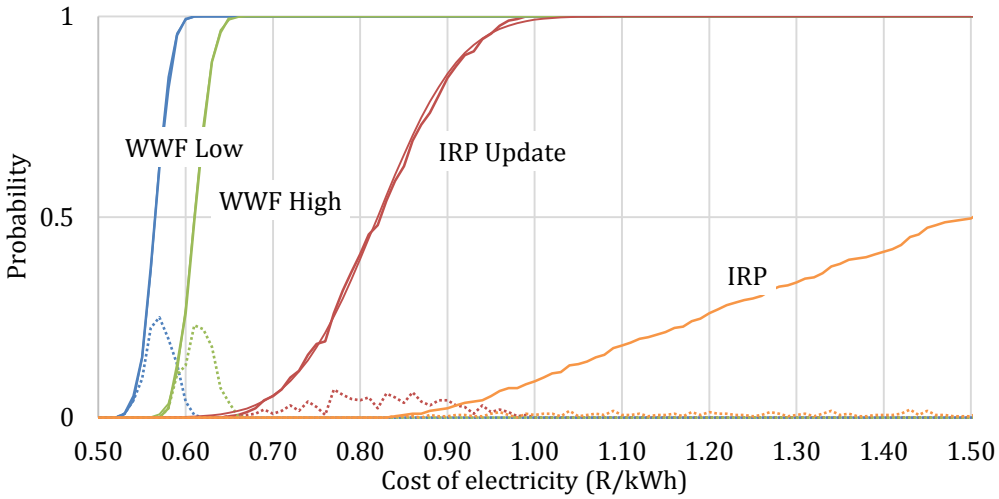

Figure 7.13: Cost probabilities of the scenarios using simple LCOE. The solid lines are cumulative distributions made up of probability distribution data represented by the dotted lines. Cost values use the simple LCOE technique.

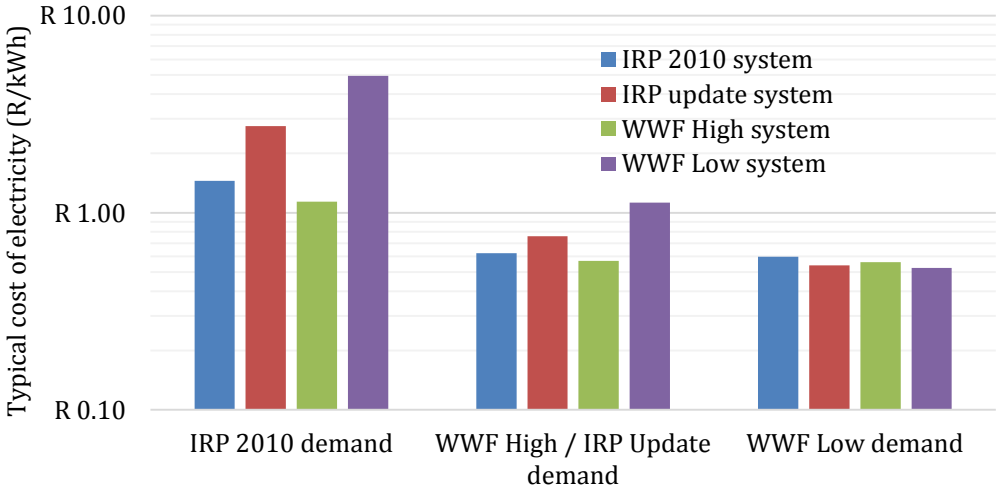

Figure 7.14: Cost probabilities of the scenarios using simple LCOE and 50th percentile cost values

It was anticipated that the WWF High scenario would benefit from the balanced system described earlier but not to the extent to which it offered robustness in the results. Unexpectedly, the result shows that the WWF High system outperforms the IRP system for the high (IRP) demand case. The IRP Update struggles with the high

demand case, as was expected, while the WWF Low is the worst performer. On the low demand side, the scenarios largely collapse with similar outcomes for the WWF Low and IRP Update. Interestingly, the cost of the WWF High scenario is not much higher than the lowest cost options. This scenario benefits from fuel savings, hence the slight decrease in cost compared with the medium demand.

A renewable-centric system is one that can add capacity at short notice, even at utility scale. Given this definition, which is conceptualized for low dependence on system needs from a demand response point of view, the WWF High and WWF Low are essentially variants of the same overall WWF scenario. Accordingly, the WWF scenario outperforms in every case by a considerable margin, making it highly resilient to changes in demand, fuel cost uncertainty and technology cost uncertainty.

7.8 Conclusion

The results and insights from this study reinforce the proposition that spatial-temporal analysis is valuable and important as renewable energy becomes a larger fraction of the electricity system.

While the system model lacks detailed treatment of the costs and implications of the required transmission system for each scenario, the method is demonstrated, noting that it can be used in context of a more detailed energy systems analysis where these details are available. With the simplification assumptions noted, the WWF study does offer evidence to the value of a well-defined renewable based electricity network expansion.

This study suggests that the WWF scenario is not only viable, it is economically advantageous to accelerate the fraction of power generation beyond the proposed 20 % threshold by 2030. The benefit of the lower cost WWF scenario is directly demonstrated in this analysis, but other benefits of a higher fraction renewable system were also encountered. While a balanced system needs significant backup generation capacity, the inexpensive CCGT and OCGT capacities are very sparingly used, which reduces the availability and cost uncertainty of gas and diesel. The double-benefit of the WWF scenario in providing resilience to changing demand and in being responsive to additional capacity implies that the provision of electricity should not hold up the economy. Based on the success of the REIPPPP to date, it will also add to the economy in the participation of adding and maintaining renewable power.

8 VALUE OF CSP IN THE ENERGY SYSTEM

This chapter presents a more specific evaluation of the value of CSP in the near term South African energy system, following the WWF Vision study outcome. The system analysis findings with reference to other work is used to explore the opportunities, challenges and needs for the technology and for the system.

The chapter includes abbreviated content from a published peer review paper titled: CSP Opportunity and Challenges in a National System: The WWF Renewable Vision for a 2030 South African Electricity Mix (Gauché et al., 2015); and a published journal article titled: Concentrating solar power: Improving electricity cost and security of supply, and other economic benefits (Gauché, Brent & von Backström, 2014).

8.1 Introduction

The implementation of the two-tiered tariff structure for CSP in South Africa was considered a landmark for the technology as it demonstrated recognition of the ability to deliver power in the peak demand period of the early evening (IEA, 2014). Through similar spatial-temporal analysis, Auret (2015) found that beyond a certain level of adoption, the two-tier tariff structure negatively impacts system adequacy measures such as reserve margin and system cost. This is resolved in such scenarios by converting a fraction of the CSP capacity to serve as flexible baseload power. The work concludes that CSP dispatch flexibility is technically feasible but will not benefit the system without changing the incentive structure.

This chapter firstly explores primary technical, cost and operational sensitivities, using the methods developed for the dissertation, and commences from the WWF Vision study. Research, development and industrial strategy with consideration to the methods are also proposed.

8.2 WWF scenario in context

The CSP model in the WWF study is by a considerable measure the most detailed of the various technology models. This is partly due to the emphasis of this research, but also arguably a consequence of the technology's inherent definition and its potentially complicated role in a grid connected system. The WWF study does not, however, have a CSP emphasis. Rather, the study aims to offer fairness to all technologies in order to determine the most reliable system as the lowest cost for 2030. In other words, the WWF Vision proposes a techno-economically sensible, lowest cost electricity system for South Africa.

The assessment of CSP commences from the WWF High scenario presented in Chapter 8 and is summarized in Table 8.1. Direct and marginal values of CSP are investigated recognizing that these virtues are a function of the system definition. The goal is to provide an initial assessment of how CSP can be positioned in terms of guiding policy and economic activity.

Table 8.1: Capacity allocation of the IRP, draft IRP Update and WWF High scenarios

	IRP (MW)	IRP Update (MW)	WWF High (MW)
Wind	9,200	4,360	14,000
PV	8,400	9,770	17,000
CSP	1,200	3,300	8,000
(Storage hours)	(~6 assumed)	(~6 assumed)	(12)
Coal	40,995	38,680	36,230
Nuclear	11,400	6,660	1,800
CCGT	2,370	3,550	4,000
OCGT	7,330	7,680	7,680
Pumped storage	2,900	2,900	2,900
Hydro	4,809	3,690	3,690
Other	915	760	760
Total	89,519	81,350	96,060

8.2.1 Performance and cost parameters

The CSP node model requires that cost be a function of the three primary proportions in the model, namely the collector size, storage rating and turbine rating. The CAPEX cost ranges used in the WWF study are used as reference values to re-correlate reference costs from the 2011 Sandia Power Tower Roadmap (Kolb et al., 2011) and other sources. The CSP model was run in an IPP single tariff mode in order to find a correlation for the cost values, which are presented in Table 8.2. For simplicity, only the optical component was varied to find a correlation to the 2022 cost forecast range as scaling components will result in corresponding cost scaling, and most costs are linked to the size of the heliostat field.

Table 8.2: CSP component costs in the WWF vision

	Unit	Sandia reference	WWF Cost high	WWF Cost low
Optical	$/m^2	200 - 120	105	90
Receiver	$/kW$_{th}$	200 - 170	120	120
Thermal storage	$/kWh$_t$	30 - 20	30	30
Power plant	$/kW$_e$	1,000 – 800	900	900
Steam generator	$/kW$_e$	350 - 250	300	300
Balance of plant	-	-	10	10

The primary capabilities, behaviors and limitations of the CSP model are highlighted in Table 8.3. These limitations guide the extent to which the CSP model can be used to evaluate the technologies behavior in the system.

The worst period for the WWF scenario occurs in deep winter. This period of time is helpful in clarifying how CSP behaves in the model and is shown in Figure 8.1. This period of time shows several hours where demand could not be fully satisfied. Presumably, the lowest cost solution permits this occurrence as a result of the marginality of additional capacity to serve these isolated hours.

Table 8.3: Primary CSP model capabilities, behaviors and limitations

Item	Description
CSP type	Central receiver with state-of-the-art two tank molten salt storage
Dimensioning	Per node, the following can be set • Total node capacity [MW] • Unit (plant) rating [MW] • Optical field size [aperture m^2] • Storage size [Hours at full rating]
Operating modes	All nodes can collectively operate based on combinations of the following • Supply to demand only: "Sacrificial availability" mode forcing CSP to play mid-merit to peaking role. • Minimum demand override (MDO): Capacity factor based threshold forcing demand above that value. E.g., MDO = 1 would enable CSP plants to generate at all times possible. • Storage limit override (SLO): Enables CSP plants to generate above demand when storage is fully charged to avoid excessive curtailment.
CSP network supply	At each hour, each node is ranked in order of the storage charge level of that node. To preserve the maximum amount of availability in the system, CSP nodes dispatch in order of that ranking.
Forecasting and incentives	The needs and limitations of the system are summarized by the following • System is purely demand-driven and seeks lowest cost; therefore, there are no time-of-day tariffs or a determination of revenue. • No multi-hour demand or supply forecasting. Forecasting and response is hourly.

The plot is set up to graphically represent a somewhat simplified merit order. For this reason, wind and PV power is plotted first because of those technologies' lack of dispatch control. Nuclear, hydro and coal are plotted next based on those technologies' ability to ramp. CSP is assigned a mid-merit role together with CCGT and some coal. Pumped storage and OCGT provide backup and peaking generation. The purple line represents demand. Unmet demand is shown as a white gap, and energy required to charge pumped storage reservoirs is shown as generation exceeding demand. Excess generation and unmet demand can occur as a result of ramp rate limitations, but such events were negligible in all tested scenarios. The six day period illustrates the following additional aspects of CSP in a system context.

When significant CSP capacity is applied and storage hours are high (with associated scaling down of turbine size or larger solar multiples), CSP successfully demonstrates a moderating function between demand and the rest of the system. The shift in CSP generation towards the end of the day compliments PV generation most of the time, illustrating a positive contribution to evening peak.

Days 161 and 162 are poor for both wind and solar power. CSP storage reserves are depleted completely, and all emergency generators are used. The lack of forecasting is most visible during this period. Had the system known how to optimally dispatch

the CSP fleet, there would have been less need for last resort generators, and there would have been no unmet demand in this case.

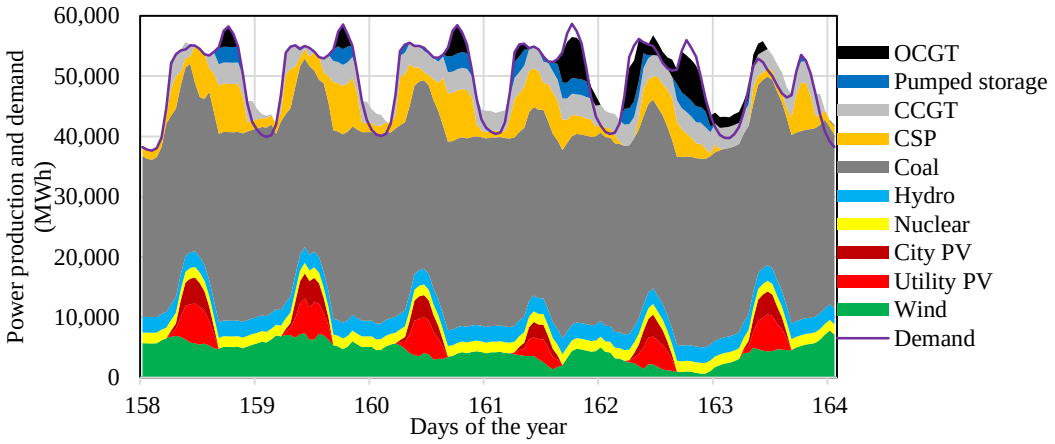

Figure 8.1: Winter week illustrating CSP in non-forecasting role: WWF High scenario

CSP and CCGT capacities work well together, jointly covering the mid-merit role. This implies that gas is an important fuel in the future where currently there are no reserves for such a fleet. It was observed, however, that a well-balanced renewable scenario relies less on annual gas (and diesel) consumption than other scenarios.

8.2.2 Testing value of CSP

As mentioned in Chapter 7, the complexity of the model prevents a direct understanding of why the WWF scenario resulted in lower cost. A better understanding of the scenario can be achieved by subjecting the model to sensitivity analyses and by breaking down cost and cost margins within the scenario to draw conclusions.

Of interest in this study, the LCOE of CSP is higher than expected in the fifteen year period to 2030. At around R 1.20/kWh, it is higher in cost than nuclear power, yet when substituted by nuclear in our tests, the system LCOE increased. As described earlier, CSP in this scenario plays a "sacrificial availability" role. All CSP plants operate based only on system need with the exception that CSP plants can utilize the storage limit override (SLO) without penalty to the system. To explore this further, a sensitivity analysis of the cost of the CSP fleet and the related cost of the system is possible by varying the minimum demand override (MDO) operating feature of the CSP node model. MDO in this case is a CSP node independence parameter ranging from zero to one.

Figure 8.2 plots two variants of the WWF scenario. All other things equal, the 8 GW of CSP capacity is equipped with either six or 12 hours of storage on average. The turbine rating is slightly altered in each case for improved usage of the collector field, but no substitute generation is added in the system for the lower storage case. From a system point of view, the higher storage hour case (12 hours at rating) almost always results

in lower cost and is less sensitive to the degree of dependence of the CSP fleet. When the CSP fleet serves the system needs, the system LCOE is about R 0.57/kWh. This increases to about R 0.61/kWh when the CSP fleet serves its own needs (assuming uniform tariffs). The "sacrificial" nature of the CSP fleet can be observed in the LCOE trend of the CSP fleet (dotted lines). Thus, within the system model as defined, the overall WWF scenario leads to a low cost system as reported in the WWF validation report (Gauché, Rudman & Silinga, 2015), and within that, CSP appears to play a surprisingly important role.

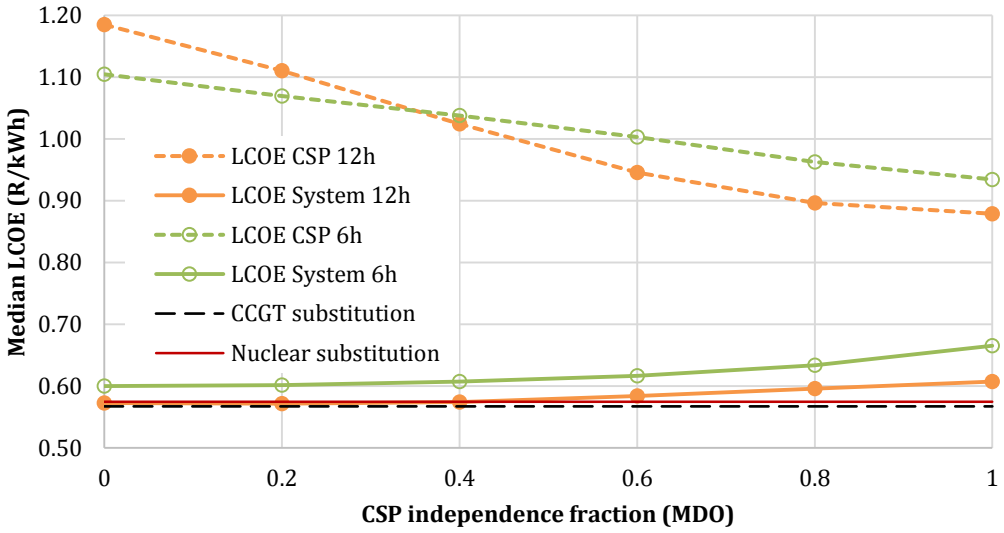

Figure 8.2: LCOE of the CSP fleet and the whole system for CSP plants with 6 or 12 storage hours as a function of system independence (or MDO)

One possible argument for an alternative would be to substitute CSP capacity for additional CCGT capacity. For this to be considered, risks associated with a substantial increase of gas supply or increased reliance on diesel to power these units would need to be considered. This risk would likely take the form of a higher marginal fuel cost, which in turn would result in a system cost increase. While fuel cost is probabilistically treated, adjusting the marginal cost is beyond scope in this study. Accordingly, a simple test was performed whereby CSP capacity is substituted for CCGT capacity without adjusting the fuel cost range in order to assess arguably the best case substitution. The same test was performed for additional nuclear capacity substitution. In both instances, 1,000 MW of the substitute were added, and a capacity factor weighted equivalent of CSP was removed. As shown in Figure 8.2, the CCGT substitution showed an insignificant marginal reduction in median system cost while the nuclear substitution showed an insignificant marginal increase in median system cost and an increase in the cost range (not shown), seemingly due to an increase in the amount of unserved power, probably due to the substitution difference between capacity and capacity factor.

When considering the consequences of the value of CSP in the system, two cost factors

come into play. Firstly, the increased LCOE of CSP is a result of the decreased capacity factor. This inverse proportionality could play a role in valuing CSP in tariffs in order to find parity revenue.

$$\frac{LCOE_{CSP(MDO=1)}}{LCOE_{CSP(MDO=0)}} \propto \frac{C_{fCSP(MDO=0)}}{C_{fCSP(MDO=1)}} \tag{8.1}$$

Secondly, the marginal value to the system can be expressed as a marginal value of energy (MVOE) between two scenarios.

The system annual cost is obtained from the system LCOE and capacity factor

$$SAC_{(scenario)} = LCOE_{system(scenario)} E_{system(scenario)} \tag{8.2}$$

where the subscript *scenario* represents the defined system. Two scenarios can then be compared to evaluate the MVOE attributable to the component that differentiates the scenarios; in this case, the operational behavior of CSP. The MVOE is given as

$$MVOE_{CSP(scenario\ 2)} = \frac{SAC_{(scenario\ 1)} - SAC_{(scenario\ 2)}}{E_{CSP(scenario\ 2)}} \tag{8.3}$$

The primary performance and cost measures of CSP dependence in the WWF scenario are tabulated in Table 8.4. Fully system dependent CSP has an MVOE of R 0.479/kWh when compared with the IPP mode in this scenario. The implication is that from a system point of view, the lower usage and correspondingly higher cost CSP also has a corresponding marginal value attributable to the generation of CSP leading to an apparent lower CSP LCOE of R 0.706 /kWh. MVOE could be used to inform tariff structures for CSP in the future recognizing the system contribution per measured output of a generator.

Table 8.4: Performance and cost indicators for CSP operating mode

	Unit	IPP (Independent)	System dependent
MDO value	-	1.0	0.0
LCOE (system)	R/kWh	0.607	0.572
LCOE (CSP)	R/kWh	0.878	1.185
Capacity factor (CSP)	-	0.628	0.466
Annual power generation (system)	TWh	413.254	411.203
Annual power generation (CSP)	TWh	43.995	32.640
MVOE (CSP)	R/kWh	-	0.479
"Apparent" LCOE (CSP)	R/kWh	-	0.706

The spatial-temporal method applied to these scenarios presents a case for CSP to play a significant role in the evolving electricity system of South Africa. According to the analysis, a reliable, resilient and cost effective system can be realized, providing CSP capacity is well distributed, and this capacity serves system needs. The key risks for such a system relate to the maturity of the technology and the manner in which it is incentivized. The risks of the substitutable technologies are factors relating to the

availability and security of their fuel sources and, in the case of nuclear power, the unknowns about cost and the time it takes to commission new capacity.

8.3 System meaning to research and development

The methods developed to evaluate CSP in a system are applicable to assist and evaluate strategic priorities in research and development. An optional objective of this dissertation included the development of a national research and development (R&D) strategy for CSP and delivery of a CSP pilot or research facility. These objectives have substantially been achieved through the formation and coordination of the Solar Thermal Energy Research Group (STERG), Stellenbosch University, and the strategically focused R&D centered on the Stellenbosch University Solar Power Thermodynamic cycle (SUNSPOT) of Kröger (2011). What is of interest here, is the progress of the research in terms of value in the future electricity system using the methods developed in Part 2.

Two key areas of progress in the SUNSPOT research focus area are the development of low cost heliostats and thermal storage using crushed rock. The Helio100 project is a national flagship project of the South African Department of Science and Technology (Stellenbosch University, 2014). The Helio100 project, the pilot shown in Figure 8.3, aims to develop a very low cost heliostat system for solarized gas turbines and is making progress towards achieving a cost target of $ 85/m^2 by 2020 (Larmuth, Landman & Gauché, 2015).

Figure 8.3: Helio100 central receiver pilot at Stellenbosch University (photo of SolarPACES 2015 technical tour courtesy of Helio100 project)

The Helio100 concept is developed around principles supporting small heliostats. The parameter analysis of Blackmon (2013) indicates that lowest cost asymptotes favor small heliostats, provided fixed costs such as control are reduced. Low cost is further promoted by autonomy and lack of anchoring, thus saving the costs of cabling, connectors, trenching and foundations.

In a similar timeframe, the crushed rock thermal storage concepts reported by Allen *et al*. (2015) could achieve cost of below $ 10/kWh$_{th}$. The lowest cost concept is presented in Figure 8.4 and Figure 8.5 with cost estimates in Figure 8.6.

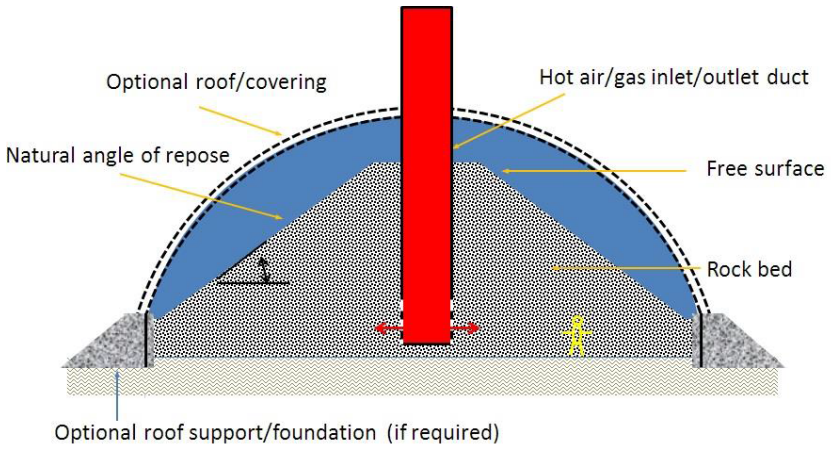

Figure 8.4 Packed bed concept (Gauché & Louw, 2014) (image courtesy of Allen (Allen et al., 2015))

The low cost packed bed concept has several defining features that are proposed in order to achieve a very low lifecycle cost. A conical naturally packed bed surrounds a vertical air vent used to charge and discharge the bed. Charging occurs from the core of the bed with the intention of avoiding heat transfer losses to the environment, which further enables the use on uninsulated covers. The natural repose conical shape of the rock pile is intended to reduce ratcheting, but it also allows for convenient removal of the crushed rock if performance is impacted by thermal cycle damage. Figure 8.5 presents a porous model CFD analysis by Louw (2014) of a storage system designed to contain 30 hours of discharging energy for a 100 MW Rankine cycle. This requires a conical packing with a radius of 68 m and height of 48 m. The temperature profile indicates two distinct temperature regions, the charge temperature and ambient, divided by a relatively thin thermocline.

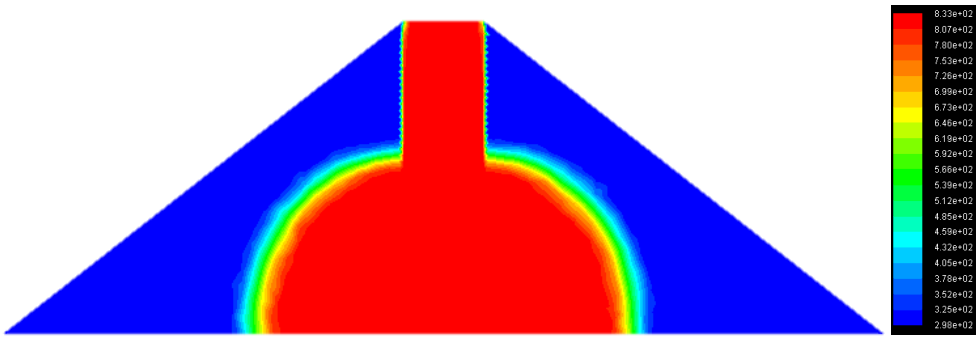

Figure 8.5: Charging temperature profile of the packed bed concept (legend shows temperature in K) (Louw, 2014)

As the thermocline is the only region where heat transfer occurs, the discharge temperature is the same as the charging temperature provided the thermocline does not enter the vertical shaft. The size of the storage system relative to the typical dimensions of the rock particles results in a discharge temperature profile that

remains very close to 560 °C for 16 hours and drops below 530 °C by the 18th hour.

Allen *et al.* (2015) predict the cost for a containment version of this concept to be below \$ 10/kWh$_{th}$ at storage sizes above 100 MWh$_{th}$, a rating sufficient for a 2 MW turbine with 15 hours of storage.

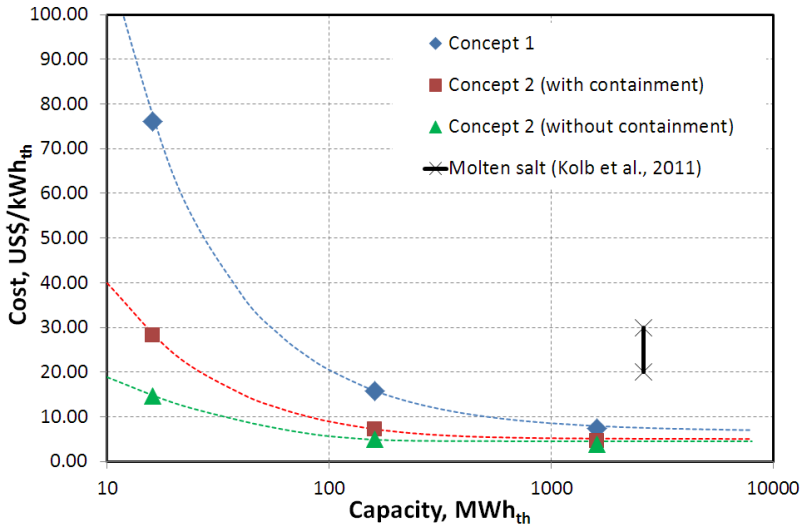

Figure 8.6: Cost estimation of crushed rock thermal storage (Allen et al., 2015)

The SUNSPOT cycle has a number of derivative cycle definitions, one of which (Figure 8.7) is simplified to an air heating loop that changes a rock bed and a steam cycle with a heat recovery steam generator (HRSG), typically used as bottoming cycles in CCGT (Pitot de la Beaujardiere et al., 2016). The HRSG exhaust is recuperated potentially via the thermal storage back to the receiver to improve efficiency. The cycle can be hybridized using a burner or a gas turbine for higher efficiency (Koll et al., 2011).

The configuration is suited to the CSP node model. Assuming both component concepts have equal probability of reaching the stated cost targets, the value of the concept can be tested in relation to the 2030 WWF Vision. Table 8.5 provides cost values for the two additional scenarios: Low cost storage (case 2) and Low cost storage and heliostats (case 3). Both are tested dependent (MDO = 0) and independent of system (MDO = 1).

The CSP node configurations were adjusted for a wide range of node proportioning. Storage size was varied from five to 25 hours and turbine size from 10 MW to 40 MW (with reference to the 20 MW default size of the Gemasolar plant turbine).

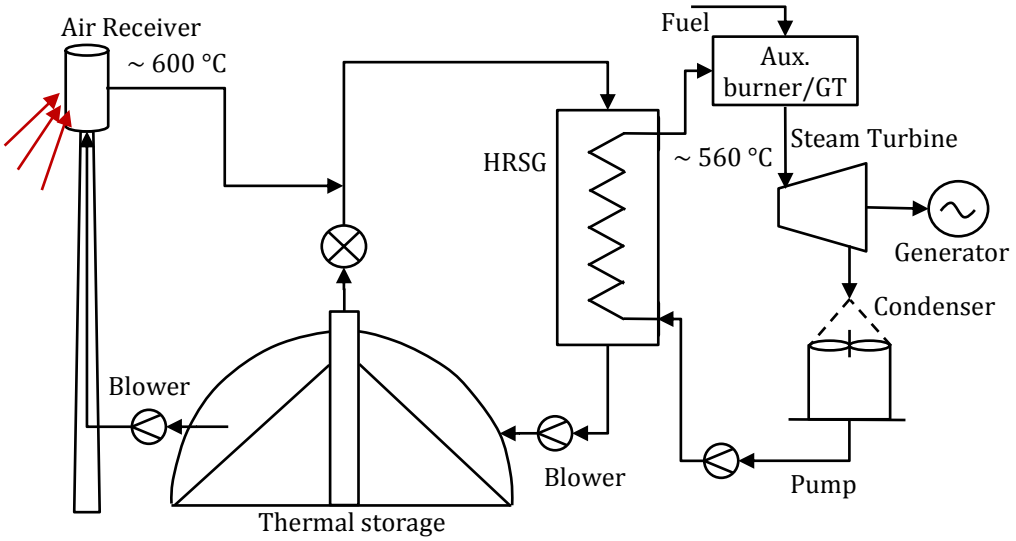

Figure 8.7: Schematic layout of a simplified SUNSPOT CSP plant (own interpretation)

Table 8.5: CSP component costs for SUNSPOT

	Unit	Case 1: WWF Cost	Case 2: Low cost storage	Case 3: Low cost storage and heliostats
Optical	$/m^2	90 – 105 (100)	100	85
Receiver	$/kW$_{th}$	120	120	120
Thermal storage	$/kWh$_t$	30	10	10
Power plant	$/kW$_e$	900	900	900
Steam generator	$/kW$_e$	300	300	300
Balance of plant	-	10	10	10

Figure 8.8 shows the combined results of the three cases for both dependent and independent conditions. The independent axis in all cases represents storage rating. The lines and legend represent turbine rating. The first three rows plot LCOE for the respective cases. The fourth row plots fulfilment, the ratio to which the node satisfies demand, defined in a similar manner to capacity factor.

Case 1 demonstrates that a turbine between 15 MW and 20 MW with 15 storage hours is ideal for LCOE in independent mode. This outcome changes in dependent mode, but rather than discuss lowest cost, it is more important to note that at 15 hours of storage, the 20 MW selection results in the lowest LCOE. Beyond 15 storage hours, all configurations lead to higher cost, likely due to the diurnal frequency.

Case 2 only deviates by switching to the low cost storage solution. Again, the optimal range for the turbine in independent mode is 15 MW to 20 MW, although the low cost storage offers a broader optimal region biased towards the high storage size.

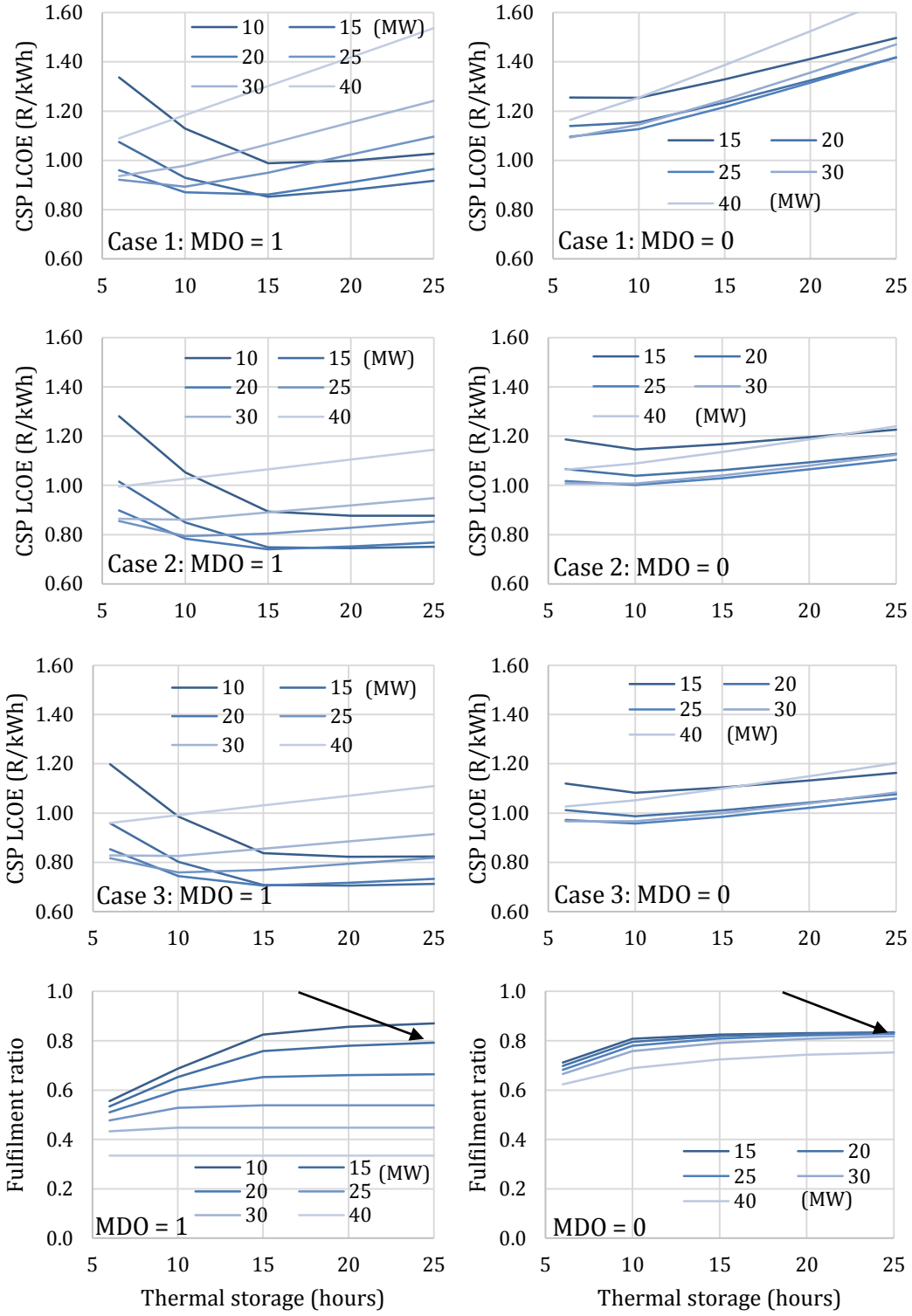

Figure 8.8: Results of low cost components in systems scenarios. Left column represents CSP capacity acting independent; right column represents system dependence. Top three rows plot respective LCOE results. Row four plots fulfilment for the WWF scenario. Legend represents turbine size in MW in each case.

The lower cost storage appears to assist the system dependent mode for high storage cases as would be expected and indeed reduces the LCOE difference between the modes directly and as a ratio.

Case 3 additionally switches to the low cost heliostat which very predictably leads to lower costs almost uniformly, hence not showing it as a separate derivative case.

Additionally, the fulfilment ratio offers insight to the allocation of CSP in the system. The tight range of fulfilment in the dependent system is indicative of CSP serving its role. It is interesting that it never significantly gets beyond 80 % fulfilment, being surprisingly more constrained than the independent mode.

This apparent constraint suggests that CSP in the system is actually struggling to be as useful as it could be. It could be that insufficient CSP capacity exists in a system with too much variability in remaining demand once intermittent renewable generation is removed. This undue variability can be expressed using a residual duration curve, in this case, a CSP demand and supply duration curve as shown in Figure 8.12. Indeed such variability appears to be the problem based on the definition of the system, and the question that arises is how might this change if the proportion of CSP is increased such that all new generating capacity in an adaption of the WWF scenario is CSP with gas as backup.

Figure 8.9 shows a simple system LCOE optimization to determine CSP capacity, assuming that a typical CSP node should have a 15 MW turbine with 25 hour storage. This optimization considers the same capacity of new OCGT and CCGT per the WWF scenario (called Big CSP and Gas) and a reduced amount of gas turbine capacity (called Big CSP and moderate gas).

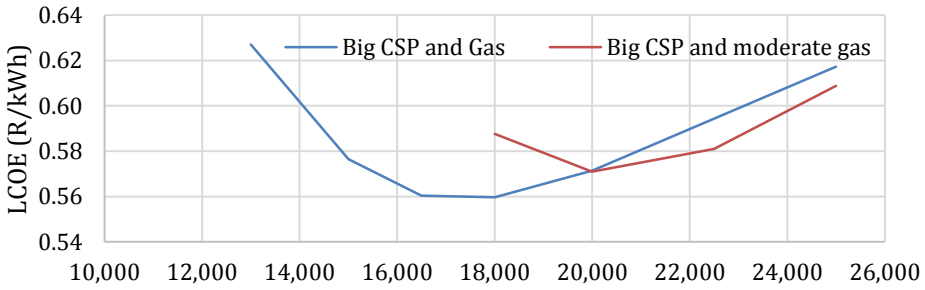

Figure 8.9: Lowest cost of Big CSP & Gas vs. Big CSP with moderate gas

18 GW of CSP with the larger gas turbine capacity was selected due to the extremely low annual consumption of gas and the cost probability model run for the low cost heliostat and storage values. Figure 8.10 shows the Big CSP scenario to be somewhat lower cost (2 % mean value) than the WWF scenario.

The result is not completely unexpected, and it needs to be noted that the scenarios have the differing CSP cost assumptions. The interesting outcome, however, can be shown in the CSP LCOE and fulfilment results in Figure 8.11. Fulfilment rises

significantly in the system dependent mode and easily exceeds the independent mode fulfilment, as it might be expected to do (see pointers), reaching almost 95 %. Also interesting is that the CSP LCOE in the dependent mode reduced by 10 % compared with the lower CSP allocation.

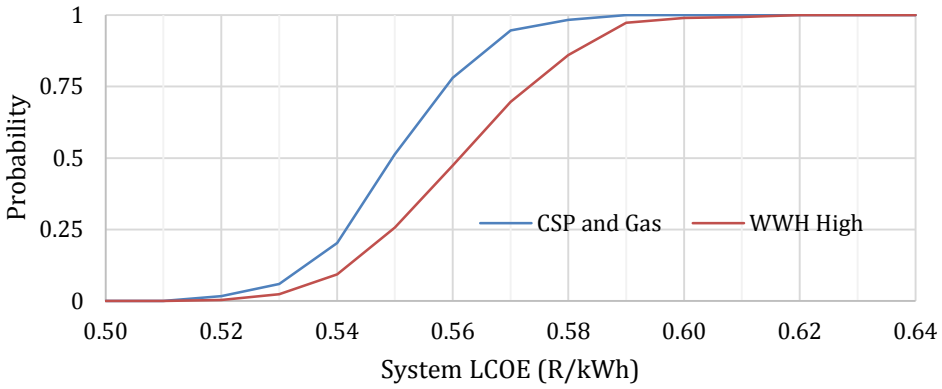

Figure 8.10 Cost probability of Big CSP case (CSP and Gas) compared with the WWF High scenario

The CSP (residual) duration curves in Figure 8.12 confirm the effect and are shown for three cases. CSP in independent mode is shown as "IPP" and can be assumed to have a demand duration of unity. Beyond 4,000 hours, the CSP capacity in the system starts to wane and reaches zero, implying that all possible utilization has occurred from the IPP point of view.

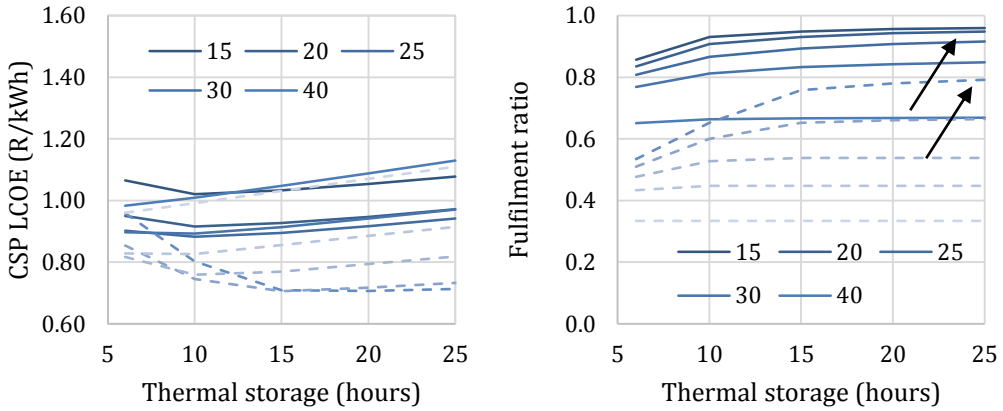

Figure 8.11 CSP LCOE and Fulfilment in Big CSP case; solid lines represent system operation (MDO = 0), broken lines represent IPP operation (MDO = 1)

Demand duration in the WWF scenario is very steep, and while supply exceeds demand, measured by fulfilment, CSP is not capable of fully supporting the system. In the Big CSP case, fulfilment is much improved and isn't significantly less than actual supply from CSP.

Systems analysis using the CSP model demonstrates how CSP cycle and component research could be guided to optimally allocated research funding. In this particular example, the key findings are as follows:

1. Cost reduction of the thermal storage component appears to have a marginal advantage in a lower cost system.
2. Within reasonable estimates of technology advancements in CSP, larger storage sizes assist the system up to the diurnal cycle (24 hours) and thereafter lead to cost increases. Perhaps for this reason, dispatchability of CSP is limited and needs to be balanced with other dispatch power solutions to be most effective as shown by the residual duration.

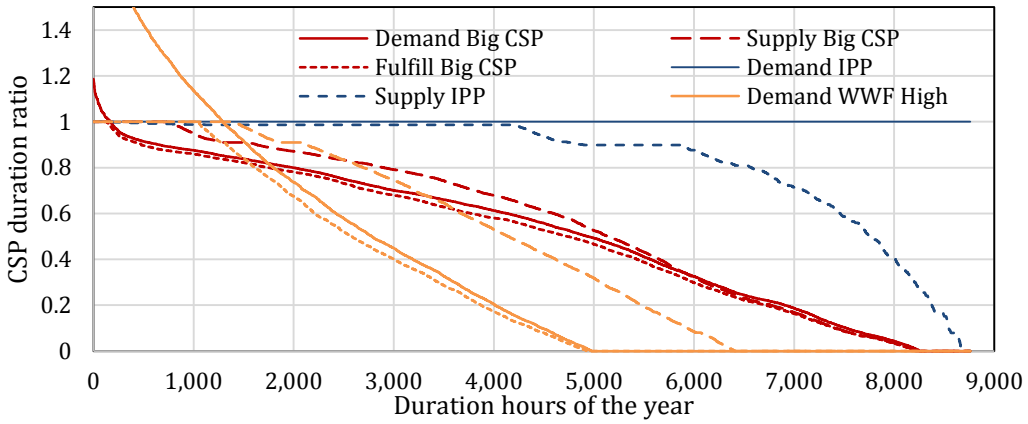

Figure 8.12: CSP residual duration curves

8.4 Industrial and economic potential of CSP in Southern Africa

The results of this dissertation indicate that CSP potentially has immediate marginal value in the South African electricity system and that provided the technology achieves the expected learning rate, the incremental addition of CSP will be economically sensible. The added capacity should in turn play a primary role in the learning rate cost reduction. An important part of the cost and value cycle is the degree to which the technology can be localized and industrialized.

Figure 8.13 is a graphical representation of thirteen power technology attributes in an attempt to present the value proposition of CSP for South Africa (Gauché, Brent & von Backström, 2014). CSP is ranked based on its current status, having a high LCOE but a potential for significant cost reduction and localization. Realizing all techno-economic benefits, however, will likely require substantial policy intervention. The primary intervention is the establishment of a long term annual new capacity allocation exceeding 200 MW in order to trigger industrial investment. Other interventions relate to public support for local R&D and support for commercializing early-stage technology (Ernst & Young & Enolcon, 2013; Grobbelaar, Gauché & Brent, 2014; Sager et al., 2015).

A phased approach is recommended based on the findings of this work. The first phase is recognizing the value of 3 GW of CSP at current technology performance and cost to serve the role in supporting evening peak electricity. While offering a direct marginal value of electricity, this capacity would allow for a sustained decade-long establishment of a CSP industry. During this phase, public investment in R&D should prepare for increased local participation for the second phase. The second phase combines the established local infrastructure with local value from the R&D investments to grow the expansion rate of CSP capacity to serve its full potential in the system and to also provide electricity and plants to the SADC region.

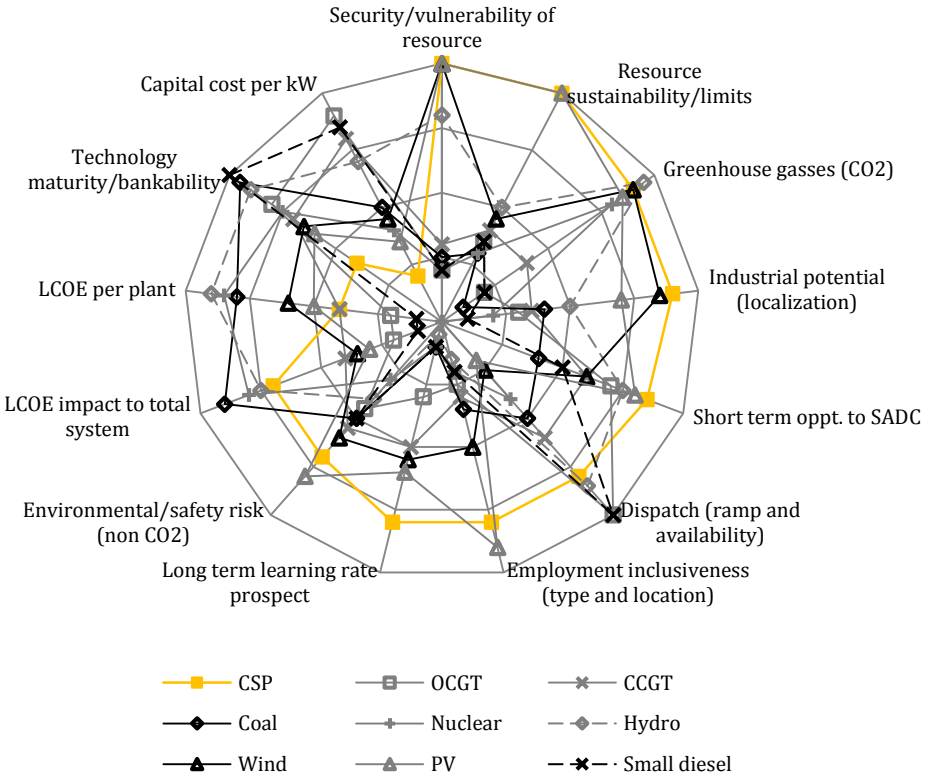

Figure 8.13: Spider diagram for the value of CSP in Southern Africa (Gauché, Brent & von Backström, 2014)

Assuming that capacity growth and industrial participation is achieved, the CSP rollout resolves concerns expressed in Chapter 4 relating to the risk of providing baseload and dispatch power when fossil fuel availability is expected to lead to an increase in their cost. Substantial, well planned CSP capacity will require equally substantial backup capacity, but such a system is likely to consume significantly less fuel while offering resilience to changes in demand.

Lastly, the analysis presented in this dissertation suggests that provided a large-scale adoption of CSP towers is taken seriously and planned well, South Africa can benefit from a more secure and resilient electricity system. The economic opportunity

offered by local industrial and research participation could enhance an economy that itself is not limited by a constrained electricity system. Without the benefit of hindsight and to the extent possible, the propositions regarding CSP in South Africa remain valid.

8.5 Conclusion

The spatial-temporal analysis correlates with Auret's (2015) findings that CSP capacity best serves the electricity system when it is system controlled and not incentivized by a simple tariff. The marginal value of electricity is proposed as a figure of merit and is valued at R 0.48/kWh in the system controlled WWF scenario for 2030.

The system analysis method demonstrates the ability to enumerate the value of R&D activities, in this case demonstrating that very low cost thermal storage offers a significant value in the system. In this example, it is suggested that the WWF scenario can be improved using 18 GW of lower cost CSP in a hypothetical alternative scenario. In all cases, it is clear that some form of backup generation is required.

Conditional on all assumptions, CSP appears to play a pivotal role in the IRP timeframe (to 2030) by providing a marginal cost and performance benefit under all investigated cases.

9 CONCLUSIONS AND RECOMMENDATIONS

The outcomes relating to the objective of the dissertation and the propositions made regarding CSP are presented in this final chapter in the form of findings, conclusions, contributions and recommendations.

9.1 Summary of findings

A method has been developed to quantifiably evaluate the value and potential of CSP central receiver towers for the case of South Africa. Assuming that the method and all associated assumptions are suitable, the method has proved successful and has provided evidence that central receiver tower systems can play a significant role in the timeframe between now and 2030. One particular scenario proposes that a renewable centered approach to new capacity which adds 8 GW of CSP with an average of 12 hours of storage enables South Africa to generate 25 % of its annual power by non-hydro renewable means by 2030, more than doubling current mandated targets.

The methodology required a thorough review of CSP and the energy options available to South Africa during the time horizon of the study in order to set a number of propositions regarding the value of CSP. Climate change and the associated transition away from CO_2 generating power plants is taken for granted in order to focus on energy resource constraints. The literature remains divisive regarding energy resource constraints. At the time of writing, oil and coal are in oversupply, yet concerns regarding resource availability remain part of the national energy planning process.

In the event that fossil and nuclear fuels become scarcer as is forecast in several studies, South Africa could potentially face significant risk in the provision of baseload and dispatchable power. The 2010 IRP appears to be particularly vulnerable in this case per the findings of Chapter 4, and this is reinforced by the systems analysis probabilistic cost modeling as presented in Part 3.

The core of the method was the development of the CSP central receiver model. Within given constraint and environmental ranges, the CSP model provides validated and sensible results for its intended purpose requiring only three environmental parameters (DNI, wind speed and ambient temperature) and three plant configuration parameters (storage size in hours, solar multiple and turbine size). The model is also able to adjust for technology advances fundamentally, rather than in specificity, in order to make future system scenarios more practical. By multivariate probability analysis, the confidence of the model is expressed as being accurate to within 7 % at a standard deviation and the limitations of usage.

The greatest uncertainty identified in the systems model is the treatment of cost, particularly cost related to conventional fuels in the timeframe of the study. The 2013

draft IRP Update presents various scenarios based on the risks, availability and cost of technologies and their associated fuels leading up to 2030. The resulting system definitions in these scenarios differ to such an extent that CSP plays no role in the 'Big gas' scenario up to 2050; whereas, CSP is the primary solution in the 'High nuclear cost' scenario with 13,400 MW in 2030 and 38,100 MW in 2050. This range supports the finding that the appropriate treatment of future scenarios is more important than the technical accuracy of the generation system as a key challenge in energy systems analysis (Pfenninger, Hawkes & Keirstead, 2014b).

For this reason, scenarios have been defined primarily based on expected annual demand and seeded with initial systems definitions such as the 'WWF High' scenario. Each scenario was subjected to a more rigorous probability study of cost ranges considered relevant in the analysis timeframe. In this way, all likely scenarios regarding scarcity of fuels or technologies were handled by a single probability distribution and represented by a comparison of cumulative probability, thus enabling a comprehensive assessment for a more robust outcome. This approach worked well and proved useful at highlighting the virtues of the WWF scenario compared with others. The probability approach might explain why the WWF scenario offers better resilience to demand changes, which would be due to the robustness of the resulting system.

With satisfactory CSP and systems models in place, analysis of various scenarios provides evidence that the IRP is vulnerable; whereas, a plan based on renewables in which CSP plays a potentially pivotal role is the right choice. A well balanced system still relies on backup generation and pumped storage, but very light usage of these results in low cost and a resilient system. The CSP model also proved useful in a separate study, illustrating that in combination with backup, CSP serves a viable baseload role in four regions of world.

The limits of CSP as a technology and in terms of economic activity were explored in various ways. Within reasonable bounds of the expected development of the technology, CSP does not on its own provide a national or regional supply of electricity cost-effectively. Backup power generation, even if sparingly used, is required. This can be done using combinations of backup generators, hybridization of CSP plants, and grid connected storage facilities such as pumped storage. While this evolutionary CSP development view might seem to limit the value of CSP in a system context, systems-based sensitivity and marginal analysis provides significant evidence that when considering cost and resource vulnerability, CSP capacity is a requirement, not an alternative, to a lowest cost electricity system.

The analysis suggests that dependent on technology advancement and propensity to adopt the technology from research to deployment, South Africa can effectively utilize 8–18 GW of CSP capacity by 2030. In all cases studied, well planned deployment of CSP leads to an order of magnitude reduction in the use of fossil or nuclear fuel based capacity.

Key findings from this study provide initial but quantifiable evidence that the tested propositions of Chapter 4 are valid.

- The systems analysis scenarios and cases tested indicate that when conventional resources become scarce for any reason ranging from cost increases to not being able to adapt to demand, CSP offers the ideal sustainable technology required to be part of a well-defined system. CSP on its own does not offer the best solution but it does appear to be the ideal complement to other generation types.
- To a limited extent through a review of the regional capabilities and the experience gained in participation in national R&D planning, the central receiver type of CSP technology appears to be well aligned to South African industry and associated resources.
- The urgency to participate in a large-scale CSP rollout has not been vigorously tested. The outcomes of this study, however, continue to support all aspects of the proposition that South Africa should support research, development and deployment of CSP as a national priority.
- Central receiver technology continues to show the most potential within the contemporary definition of CSP types. While the CSP model developed illustrates the greater efficiency of the technology, no work was done to compare point focus and line focus technology suitability.
- Several publications based on this work strongly support the value of a distributed network of CSP plants in sunny regions. The reliance on backup generation capacity usage is approximately inversely proportional to the degree of distribution of CSP capacity where distribution is loosely defined as spatially-separated by weather event independence. Distributed CSP could reduce transmission line loads and provide value to local communities, but this has not been tested.

9.2 Conclusions

Two general conclusions can be made from the findings in this study:

Firstly, the importance of time-synchronous, spatial-temporal systems analysis in evaluating the role and potential of CSP towers has been demonstrated for multiple scenarios and cases in several publications through the course of this study. The ideal role and behavior of CSP in an electricity network is not suitably represented by techno-economic analysis of a stand-alone CSP plant. Through implicit correlation of supply and demand linked to weather, the methods demonstrate the value of early adoption of CSP through to a large-scale rollout. This value is not just in the ability to size and locate CSP capacity, but to also evaluate the contribution of CSP based on how it is operated. CSP operating optimally in the WWF scenario has a marginal value of R 0.48 /kWh compared with a flat-tariff operation.

Secondly, the preliminary evaluation of CSP in the IRP timeframe suggests that a

large-scale rollout of CSP in a well-balanced system results in potentially the lowest cost electricity system regardless of future fuel costs, but particularly in the event that conventional fuels become more scarce. Unexpectedly, the spatial-temporal method exposed a potentially more important attribute to CSP in a well-balanced system. Backup generation and storage is still required in the system but is seldom used, and in combination with CSP, it offers greater resilience to changes in demand. In other words, CSP with backup offers the electricity system higher reserve margin without significant additional cost.

CSP advocates promote dispatchability as the value of CSP, but the market generally has not responded to this value of the technology. If CSP offers the value and potential that some believe, then a significant opportunity is being missed. The upfront risk and cost of large efficient CSP plants is an Achilles heel that currently holds CSP back. Systems analysis that is able to evaluate CSP appropriately and accurately could provide much better informed information to decision makers in order to balance adoption risk and reward. The results of this study overwhelmingly supports the adoption of CSP in South Africa, not as a final conclusion, but as a call to invest more resources in research to support or refute this outcome.

9.3 Summary of contributions

The spatial-temporal model developed in this study was intended to address a need for a CSP central receiver tower model that did not seem to be generally available. The model generally satisfies the requirements of being variant agnostic, fast to solve, yet sufficiently accurate and sensitive to the key parameters in a CSP plant. While fundamentally developed for central receiver CSP plants, the principles are generally applicable to other CSP types. Within the CSP model, a number of specific contributions have resulted in the development of a fast and predictable model.

- A computationally simple method to determine the performance of the heliostat field.
- A re-analysis of atmospheric attenuation data in order to find a computationally stable and generalized model for attenuation based on fundamental light transmission principles.
- A generalized heat transfer model for central receiver convection and radiation losses without requiring iterative solution techniques.

The significant variance in cost projections for future scenarios resulted in the use of a relatively simple probability analysis for the systems model in combination with the more deterministic technology models applied to generators. Using this analysis results in a single probability distribution for any given physically defined electricity system.

All results of a system scenario ultimately reduces to a single parameter: cost of electricity produced. This includes the cost of unserved electricity, which is included in the model due to the fact that the degree of unserved power is not directly

controlled in the analysis and thus needs to be factored in as a parity penalty. With cost as the final measure, the concept of the MVOE is introduced and has an equivalence to LCOE in order to compare any marginal change within or between scenarios by attributing the system change to the adapted parameter. MVOE can then be used to evaluate the economic impact attributable to a specific technology and, therefore, also could be used as a tool to aid tariff policy as recommended in a short policy brief in Appendix C.

All other contributions are based on the publications already cited in this dissertation.

9.4 Policy value

The objective of this study aims to provide quantitative methods and data as a potential benefit for national planning and policy. A summary of findings relevant to policy are listed with reference to the policy brief in Appendix C.

Cost risk and mitigation

Costs associated with CAPEX and LCOE remain high for CSP and the consequence of thermo-economics where large expensive plants are required to drive down LCOE are likely to remain a barrier for the technology. Based on the positive outcome of this study, CSP is presented as a pivotal technology for South Africa, resulting in a risk vs. benefit dilemma. By continuing to support CSP by providing capacity to IPPs where the upfront cost of projects is not a public risk, CSP will have the opportunity to build evidence of the value and associated cost reduction.

Tariff evolution and CSP incentives

The significant MVOE of R 0.48 /kWh when CSP plants serve the system suggests that tariffs based on time-of-day fluctuation would be required. The MVOE analysis itself can aid development of tariffs. More sophisticated tariff structures are not critical at this time (during the initial adoption) but the residual load duration analysis suggests that system centered CSP capacity needs to be balanced with generators that are not linked to demand sooner rather than later. The MVOE-based tariff proposal in Appendix C. sets a base price competitively to all other power generating options for a base price and provides incentives up to the cost of avoided generators.

Research support

Data is a critical need for good systems analysis. This proposal recommends that IPPs be compelled to share performance data for research purposes in exchange for a license to produce power. In addition to the recommended research support to mitigate CSP cost risk, Section 9.5 outlines recommendations for further research.

9.5 Recommendations for future research

This dissertation forms part of an initial collection of outputs based on a common

sharing of fundamentally open methods rather than the application and adaption of closed or proprietary methods. In support of the policy implications, the following recommendations encourage an ambitious increase in research directed towards future sustainable energy systems rather than incremental items that did not fit into the time or scope of this study.

9.5.1 Independent energy system and grid integration center

Most entities in South Africa resourced to handle grid integration have some form of stake or vested interest making it difficult to openly share information or to establish an independent body of knowledge. An energy modeling alliance has been established (Fouche & van Niekerk, 2014) but without stable and secure funding, has made little coordinated progress.

A nationally funded independent center or alliance is recommended that would provide a coordinated environment for research, data, recommendations, advice and methods. Several specific areas would benefit from resources and coordination:

- Data relating to electricity and energy usage aggregated by geographical region at various scales from sub-municipal to national.
- Technical details relating to the current and future transmission and grid plans.
- Grid transmission models including signal integrity, stability and limits.
- Expansion of solar and weather measuring stations, including support of data quality and organization.
- Establishment of open-source energy systems modeling platforms, including models of components in the system organized as libraries.

9.5.2 CSP research

CSP research in South Africa is as much in its infancy as the deployment of the technology. The status elsewhere is not significantly more advanced. Coupling with the concept of an independent energy systems center, CSP will require significant ongoing research support in order to evaluate the value and contribution of the technology within energy systems.

Notable changes that could improve the CSP model in the shorter-term relate to validation and improved correlations of the primary energy efficiency conversion correlations based on actual CSP plant operation. In particular, refinements to the treatment of thermal storage charging and discharging models would allow for improved accuracy for investigation of longer storage hours.

All components of cost estimating require improvement, from capital cost to maintenance over lifetime of the plant. Operational behavior linking employment and other ongoing operating costs to performance are not yet well understood in South Africa.

REFERENCES

Allen, K., von Backström, T., Joubert, E. & Gauché, P. 2015. Rock bed thermal storage: Concepts and costs. In *SolarPACES 2015*. V. 1734. V. Rajpaul & C. Richter, Eds. Cape Town, South Africa: AIP Conf. Proc. 50003-1–8. DOI: 10.1063/1.4949101.

Auret, C. 2015. Scenario modelling for short to long term rollout of concentrating solar power in South Africa. Stellenbosch University. Available: http://hdl.handle.net/10019.1/96941.

Ayodele, T.R., Jimoh, A.A., Munda, J.L. & Agee, J.T. 2012. Wind distribution and capacity factor estimation for wind turbines in the coastal region of South Africa. *Energy Conversion and Management*. 64:614–625. DOI: 10.1016/j.enconman.2012.06.007.

Ballestrín, J. & Marzo, A. 2012. Solar radiation attenuation in solar tower plants. *Solar Energy*. 86(1):388–392. DOI: 10.1016/j.solener.2011.10.010.

Bañuelos-Ruedas, F., Angeles-Camacho, C. & Rios-Marcuello, S. 2010. Analysis and validation of the methodology used in the extrapolation of wind speed data at different heights. *Renewable and Sustainable Energy Reviews*. 14(8):2383–2391. DOI: 10.1016/j.rser.2010.05.001.

Black & Veatch. 2012. *Cost and Performance data for Power Generation Technologies*.

Blackmon, J.B. 2013. Parametric determination of heliostat minimum cost per unit area. *Solar Energy*. 97:342–349. Available: doi:10.1016/j.solener.2013.08.032.

Blanco, M.J. 2011. *Tonatiuh download*. Available: http://code.google.com/p/tonatiuh.

Bode, S.J. & Gauché, P. 2012. Review of optical software for use in concentrating solar power systems. In *Proceedings of the Southern African Solar Energy Conference (SASEC 2012)*. Stellenbosch, South Africa. 1–8.

Brooks, M.J., du Clou, S., van Niekerk, J.L., Gauche, P., Leonard, C., Mouzouris, M.J., Meyer, A.J., van der Westhuizen, N., et al. 2015. SAURAN: A new resource for solar radiometric data in Southern Africa. *Journal of Energy in Southern Africa*. 26(1):2–10.

Brownfield, M.E., Schenk, C.J., Charpentier, R.R., Klett, T.R., Cook, T.A., Pollastro, R.M. & Tennyson, M.E. 2012. *Assessment of undiscovered oil and gas resources of four East Africa Geologic Provinces: U.S. Geological Survey Fact Sheet 2012–3039*.

Cheang, V.T., Hedderwick, R.A. & McGregor, C. 2015. Benchmarking supercritical carbon dioxide cycles against steam Rankine cycles for Concentrated Solar Power. *Solar Energy*. 113:199–211. DOI: 10.1016/j.solener.2014.12.016.

Cilliers, P. 1998. *Complexity and Postmodernism: Understanding Complex Systems*. Routledge.

Cilliers, P. 2011.

Creamer, T. 2011. *Surging tariffs and interest bill, but also signs of greater stability at Eskom*. Available: http://www.engineeringnews.co.za/article/eskoms-interest-bill-surging-but-funding-plan-advanced-2011-07-08.

Cros, S. & Wald, L. 2003. Survey of the main databases providing solar radiation data at the ground level. In *Proceedings of the 23rd EARSeL Annual Symposium "Remote Sensing in Transition"*. Ghent, Belgium. 491–497. Available: http://hal.archives-ouvertes.fr/docs/00/46/57/89/PDF/earsel03_survey_database.pdf.

CSIR Energy Centre. 2015. Financial benefits of renewables in South Africa in 2014 Actual diesel- and coal- fuel savings and avoided " unserved energy " from the first approximately 1 . 6 GW of wind and PV projects in a constrained South African power system CSIR Energy Centre Dr. (January).

Curzon, F.L. & Ahlborn, B. 1975. Efficiency of a Carnot engine at maximum power output. *American Journal of Physics*. 43:22–24.

Dale, M. 2012. Meta-analysis of non-renewable energy resource estimates. *Energy Policy*. 43:102–122. DOI: 10.1016/j.enpol.2011.12.039.

Denholm, P. & Hand, M. 2011. Grid Flexibility and Storage Required to Achieve Very High Penetration of Variable Renewable Electricity. *Energy Policy*. 39(3):1817–1830. DOI: http://dx.doi.org/10.1016/j.enpol.2011.01.019.

Denholm, P., Hand, M., Mai, T. & Margolis, R. 2012. *The Potential Role of Concentrating Solar Power in Enabling High Renewables Scenarios in the United States*. Golden, Colorado. Available: http://www.nrel.gov/docs/fy13osti/56294.pdf [2013, December 30].

Department of Energy. 2010. *Cost of Unserved Energy (COUE) - IRP 2010 Input Parameter information sheet (Supply input)*.

Department of Energy. 2011. *Integrated Resource Plan for Electricity 2010-2030*. Available: http://www.doe-irp.co.za/content/IRP2010_2030_Final_Report_20110325.pdf.

Department of Energy. 2012. *Renewable Energy Independent Producer Procurement Programme*. Available: http://www.ipprenewables.co.za/ [2015, January 26].

Department of Energy. 2013a. *Renewable Energy IPP Procurement Programme, Bid Window 3 Preferred Bidders' announcement.* Available: http://www.record.org.za/resources/doc_download/79-department-of-energy-list-of-ipp-preferred-bidders-window-3-04nov2013.pdf.

Department of Energy. 2013b. *Integrated Resource Plan for Electricity (IRP) 2010-2030 Update Report 2013*. Available: http://www.doe-irp.co.za/content/IRP2010_updatea.pdf.

Department of Energy. 2013c. *Department of Energy Draft 2012 Integrated Energy Planning Report Executive Summary*.

Department of Minerals and Energy. 2008. *National Energy Act No 34 of 2008*. Available: http://www.energy.gov.za/files/policies/NationalEnergyAct_34of2008.pdf [2014, October 21].

Dobos, A., Gilman, P. & Kasberg, M. 2012. *P50/P90 Analysis for Solar Energy Systems Using the System Advisor Model*. Golden, Colorado. Available: http://www.nrel.gov/docs/fy12osti/54488.pdf [2013, December 30].

Duffie, J.A. & Beckman, W.A. 2006. *Solar Engineering of Thermal Processes.* Third edit ed. Wiley.

Eltrop, L. & Annegarn, H. 2013. *Energy as a Key Element of an Integrated Climate Protection Concept for the City Region of Gauteng*. Available: http://www.enerkey.info/index.php [2015, December 22].

Emes, M.J., Arjomandi, M. & Nathan, G.J. 2015. Effect of heliostat design wind speed on the levelised cost of electricity from concentrating solar thermal power tower plants. *Solar Energy*. 115:441–451. DOI: 10.1016/j.solener.2015.02.047.

Energy Exemplar. 2015. Available: http://energyexemplar.com/software.

ERC. 2013. *Assumptions and Methodologies in the South African TIMES (SATIM) Energy Model*. Available: http://www.erc.uct.ac.za/Research/Otherdocs/Satim/SATIM Methodology-v2.1.pdf.

Ernst & Young & Enolcon. 2013. *Assessment of the localisation , industrialisation and job creation potential of CSP infrastructure projects in South Africa – A 2030 vision for CSP.* Available: http://http//0101.nccdn.net/1_5/1c8/ 164/360/GIZ-CSPStudy-FinalReportJune2013.pdf.

Eskom. 2011a.

Eskom. 2011b. *COP17 Fact sheet: Eskom generation plant mix.* Available: http://www.eskom.co.za/OurCompany/SustainableDevelopment/ClimateChangeCOP17/Documents/GenerationMix.pdf [2014, October 15].

Eskom. 2012. *Environmental footprint*. Available: http://www.eskomfactor.co.za/eskom-factor-environmental.php.

Eskom. 2014. *Generation Connection Capacity Assessment of the 2016 Transmission Network (GCCA-2016)*. Available: http://www.eskom.co.za/Whatweredoing/GCCAReport/Documents/GCCA2016ReportREV2.pdf [2014, October 08].

Fichter, T., Trieb, F. & Moser, M. 2014. Optimized Integration of Renewable Energy Technologies Into Jordan's Power Plant Portfolio. *Heat Transfer Engineering*. 35(3):281–301. DOI: 10.1080/01457632.2013.825183.

Fiksel, A. & Thornton, J.W. 1995. Developments to the TRNSYS simulation program.

Journal of Solar Energy …. 117(5):123–127. Available: http://www.osti.gov/energycitations/product.biblio.jsp?osti_id=78263 [2013, December 30].

Fluri, T.P. 2009. The potential of concentrating solar power in South Africa. *Energy Policy*. 37(12):5075–5080. DOI: 10.1016/j.enpol.2009.07.017.

Fouche, E. & van Niekerk, J.L. 2014. *Towards an Energy Modelling Alliance in South Africa*. Stellenbosch, South Africa.

Fripp, M. 2008. Optimal investment in wind and solar power in California. 251. Available: http://www2.hawaii.edu/~mfripp/papers/Fripp_Dissertation.pdf [2013, December 30].

Gary, J., Turchi, C. & Siegel, N. 2011. CSP and the DOE SUNSHOT Initiative. In *Proceedings of Solar Power and Chemical Energy Systems conference (SolarPACES 2011)*. V. 1. Granada, Spain. 8.

Gauché, P. & Louw, A.D.R. 2014. *Patent No. 2014/03555*. South Africa.

Gauché, P., von Backström, T.W. & Brent, A.C. 2011. CSP Modeling Methodology For Macro Decision Making - Emphasis On The Central Receiver Type. In *Proceedings of Solar Power and Chemical Energy Systems conference (SolarPACES 2011)*. Granada, Spain. 1–8.

Gauché, P., Pfenninger, S., Meyer, A.J. & Brent, A.C. 2012. Modeling dispatchibility potential of CSP in South Africa. In *Proceedings of the Southern African Solar Energy Conference (SASEC 2012)*. V. 2011. Stellenbosch, South Africa. 1–11.

Gauché, P., von Backström, T.W. & Brent, A.C. 2013. A concentrating solar power value proposition for South Africa. *Journal of Energy in Southern Africa*. 24(1):67–76.

Gauché, P., Brent, A.C. & von Backström, T.W. 2014. Concentrating solar power: Improving electricity cost and security of supply, and other economic benefits. *Development Southern Africa*. (July):1–19. DOI: 10.1080/0376835X.2014.930791.

Gauché, P., Rudman, J. & Silinga, C. 2015. *Feasibility of the WWF Renewable Energy Vision 2030 – South Africa*. Cape Town. Available: https://shar.es/1GOrge.

Gauché, P., von Backström, T.W., Brent, A.C. & Rudman, J. 2015. CSP Opportunity and Challenges in a National System : The WWF Renewable Vision for a 2030 South African Electricity Mix. In *SolarPACES 2015*. Cape Town: AIP. 8.

GeoModel Solar. 2012a. *SolarGIS Database version 1.8 satellite-derived solar radiation and meteorological data*. Available: http://solargis.info/doc/_docs/SolarGIS_data_specification.pdf.

GeoModel Solar. 2012b. *SolarGIS iMaps online paid access to high-resolution solar data*. Available: http://solargis.info/imaps/.

GeoModel Solar. 2015. *SolarGIS Solar radiation maps*. Available: http://solargis.info/doc/87 [2015, December 01].

Giglmayr, S. 2013a. Development of a Renewable Energy Power Supply Outlook 2015 for the Republic of South Africa. University of Applied Sciences – Technikum Wien, Vienna, Austria.

Giglmayr, S. 2013b. Development of a Renewable Energy Power Supply Outlook 2015 for the Republic of South Africa. 121.

Giglmayr, S., Brent, A.C., Gauché, P. & Fechner, H. 2015. Utility-scale PV power and energy supply outlook for South Africa in 2015. *Renewable Energy*. 83:779–785.

Gil, A., Medrano, M., Martorell, I., Lazaro, A., Dolado, P., Zalba, B. & Cabeza, L.F. 2010. State of the art on high temperature thermal energy storage for power generation. Part 1—Concepts, materials and modellization. *Renewable and Sustainable Energy Reviews*. 14(1):31–55.

Gilman, P. & Dobos, A. 2012. *System Advisor Model, SAM 2011.12.2: General Description*. Golden, Colorado.

Grobbelaar, S., Gauché, P. & Brent, A. 2014. Developing a competitive concentrating solar power industry in South Africa: Current gaps and recommended next steps. *Development Southern Africa*. 31(3):475–493. DOI: 10.1080/0376835X.2014.891971.

Hagemann, K. 2008. Mesoscale wind atlas of South Africa. UCT.

Hahmann, A.N., Badger, J., Vincent, C.L., Kelly, M.C., Volker, P.J.H. & Refslund, J. 2014. *Wind Atlas for South Africa (WASA): Mesoscale Modeling for the Wind Atlas of South Africa (WASA) Project*.

Hartnady, C. 2010. South Africa's diminishing coal reserves. *South African Journal of Science*. 106(9/10):5. Available: http://www.scielo.org.za/scielo.php?pid=S0038-23532010000500008&script=sci_arttext&tlng=pt [2013, December 30].

Hartnady, C.J.H. 2012.

Heun, M.K. & de Wit, M. 2012. Energy return on (energy) invested (EROI), oil prices, and energy transitions. *Energy Policy*. 40:147–158. DOI: 10.1016/j.enpol.2011.09.008.

Heun, M.K., van Niekerk, J.L., Swilling, M., Meyer, A.J., Brent, A.C. & Fluri, T.P. 2010. Learnable lessons on sustainability from the provision of electricity in South Africa. In *Proceedings of the ASME 2010 4th International Conference on Energy Sustainability ES2010*. Phoenix, Arizona, USA: ASME. 1–11.

Ho, C.K. 2008. *Software and Codes for Analysis of Concentrating Solar Power Technologies*. Albuquerque, NM. Available: http://energy.sandia.gov/wp/wp-content/gallery/uploads/SAND2008-8053.pdf.

Howells, M., Rogner, H., Strachan, N., Heaps, C., Huntington, H., Kypreos, S., Hughes, A., Silveira, S., et al. 2011. OSeMOSYS: the open source energy modeling system: an introduction to its ethos, structure and development. *Energy Policy*. 39(10):5850–5870.

Hubbert, M. 1956. Nuclear energy and the fossil fuel. *Drilling and production practice*. Available: http://www.hubbertpeak.com/hubbert/1956/1956.pdf [2013, December 30].

IEA. 2010. *Technology Roadmap: Concentrating Solar Power*. Paris, France: OECD Publishing. DOI: 10.1787/9789264088139-en.

IEA. 2013. *Key World Energy Statistics 2013*. Available: http://www.iea.org/publications/freepublications/publication/KeyWorld2013.pdf.

IEA. 2014. *Technology Roadmap Solar Thermal Electricity*. DOI: 10.1007/SpringerReference_7300.

IEA. 2015. *2015 Key World Energy Statistics*.

Ineichen, P. 2013. *Long term satellite hourly, daily and monthly global, beam and diffuse irradiance validation. Interannual variability analysis.* Available: http://www.cuepe.ch/archives/annexes-iae/ineichen-2013_long-term-validation.pdf.

IRENA. 2012a. *Renewable energy technologies: Cost analysis series, vol 1: power sector, issue 4/5 Solar Photovoltaics*. Available: http://www.irena.org/DocumentDownloads/Publications/RE_Technologies_Cost_Analysis-SOLAR_PV.pdf.

IRENA. 2012b. *Summary for Policy Makers: Renewable Power Generation Costs*. Available: http://www.irena.org/DocumentDownloads/Publications/Renewable_Power_Generation_Costs.pdf.

IRENA. 2012c. *Renewable energy technologies: cost analysis series: Concentrating Solar Power.* (1). Abu Dhabi, UAE. Available: http://www.irena.org/DocumentDownloads/Publications/RE_Technologies_Cost_Analysis-CSP.pdf.

IRENA. 2015. *Renewable Power Generation Costs in 2014*.

Jorgenson, J., Denholm, P., Mehos, M. & Turchi, C. 2013. Estimating the Performance and Economic Value of Multiple Concentrating Solar Power Technologies in a Production Cost Model Estimating the Performance and Economic Value of Multiple Concentrating Solar Power Technologies in a Production Cost Model. (December).

Kistler, B.L. 1986. *A User's Manual for DELSOL3: A Computer Code for Calculating the Optical PErformance and Optimal System Design for Solar Thermal Central Receiver Plants*. Albuquerque, NM. Available: http://energy.sandia.gov/wp/wp-content/gallery/uploads/SAND86-8018_DELSOL_Users_guide.pdf.

Klein, S.A. et al. 2010. *TRNSYS 17: A Transient System Simulation Program, Solar Energy Laboratory*. Madison, USA. Available: http://sel.me.wisc.edu/trnsys.

Knapp, V., Pevec, D. & Matijević, M. 2010. The potential of fission nuclear power in resolving global climate change under the constraints of nuclear fuel resources and once-through fuel cycles. *Energy Policy*. 38(11):6793–6803. DOI: 10.1016/j.enpol.2010.06.052.

Kolb, G., Ho, C., Mancini, T. & Gary, J. 2011. *Power tower technology roadmap and cost reduction plan*. Albuquerque, NM. Available: http://prod.sandia.gov/techlib/access-control.cgi/2011/112419.pdf [2011, September 21].

Koll, G., Sahraoui, T., Hoffschmidt, B., Khedim, A., Pomp, S., Schwarzbözl, P. & Dillig, M. 2011. ALSOL – Solar Thermal Tower Power Plant Algeria. In *Proceedings of the 17th SolarPACES Conference*. Granada, Spain. 20–23.

Kröger, D. g. 2011. *SUNSPOT: The Stellenbosch UNiversity Solar POwer Thermodynamic cycle*. St. DOI: 10.1007/s13398-014-0173-7.2.

Larmuth, J.N., Landman, W.A. & Gauché, P. 2015. A Top-down Approach to Heliostat Cost Reduction. In *SolarPACES 2015*. Cape Town: AIP. 8.

Leary, P.L. & Hankins, J.D. 1979. *A user's guide for MIRVAL—a computer code for comparing designs of heliostat–receiver optics for central receiver solar power plants*. Albuquerque, NM.

Leonardi, E. & D'Aguanno, B. 2011. CRS4-2: A numerical code for the calculation of the solar power collected in a central receiver system. *Energy*. 36(8):4828–4837. DOI: 10.1016/j.energy.2011.05.017.

Loulou, R. & Labriet, M. 2008. ETSAP-TIAM: the TIMES integrated assessment model Part I: Model structure. *Computational Management Science*. 5(1–2):7–40.

Louw, A.D.R. 2014. Discrete and porous computational fluid dynamics modelling of an air-rock bed thermal energy storage system. Stellenbosch University. Available: http://hdl.handle.net/10019.1/86233.

Meduri, P.K., Hannemann, C.R. & Pacheco, J.E. 2010. Performance Characterization and Operation of eSolar's Sierra SunTower Power Tower Plant. In *Proceedings of Solar Power and Chemical Energy Systems conference (SolarPACES 2010)*. Perpignan, France. 8.

Meyer, A.J. & van Niekerk, J.L. 2011. Roadmap for the Deployment of Concentrating Solar Power in South Africa. In *Proceedings of Solar Power and Chemical Energy Systems conference (SolarPACES 2011)*. Granada, Spain. 9.

Miketa, A. & Merven, B. 2013. *Southern African Power Pool: Planning and Prospects for Renewable Energy*. Available: http://www.irena.org/DocumentDownloads/Publications/SAPP.pdf.

Mileva, A., Nelson, J.H., Johnston, J. & Kammen, D.M. 2013. SunShot solar power reduces costs and uncertainty in future low-carbon electricity systems. *Environmental science & technology*. 47(16):9053–60. DOI: 10.1021/es401898f.

Mills, A. 1995. *Heat and Mass Transfer*. (Irwin heat transfer series). Taylor & Francis.

Mohr, S.H. & Evans, G.M. 2009. Forecasting coal production until 2100. *Fuel*. 88(11):2059–2067. DOI: 10.1016/j.fuel.2009.01.032.

Mortensen, N.G., Hansen, J.C., Kelly, M.C., Szewczuk, S., Mabille, E. & Prinsloo, E. 2012. *Wind Atlas for South Africa (WASA) Observational wind atlas for 10 met. stations in Northern, Western and Eastern Cape provinces*.

Mortensen, N.G., Hansen, J.C. & Kelly, M.C. 2014. *Wind Atlas for South Africa (WASA) Western Cape and parts of Northern and Eastern Cape Observational Wind Atlas for 10 Met . Masts in Northern , Western and Eastern Cape Provinces*.

Murray, J. & King, D. 2012. Oil's tipping point has passed. *Nature*. 481:433–435.

National Planning Commission. 2012. *National development plan 2030 – Our future – make it work.* National Planning Commission, Ed. Available: http://www.npconline.co.za/MediaLib/Downloads/Downloads/NDP 2030 - Our future - make it work.pdf.

Novikov, I.I. 1958. The efficiency of atomic power stations (a review). *Journal of Nuclear Energy (1954)*. 7(1):125–128.

NREL. 2011a. *Gemasolar Thermosolar Plant project overview*. Available: http://www.nrel.gov/csp/solarpaces/project_detail.cfm/projectID=40.

NREL. 2011b. *National Solar Radiation Data Base, 1991- 2005 Update: Typical Meteorological Year 3*. Available: http://rredc.nrel.gov/solar/old_data/nsrdb/1991-2005/tmy3/by_state_and_city.html#C.

NREL. 2011c. *National Renewable Energy Laboratory, SolTrace: Downloads*. Available: http://www.nrel.gov/csp/soltrace/download.html.

NREL. 2011d. *Sierra SunTower project overview*. Available: http://www.nrel.gov/csp/solarpaces/project_detail.cfm/projectID=63.

NREL. 2011e. *Reference Solar Spectral Irradiance: Air Mass 1.5*. Available: http://rredc.nrel.gov/solar/spectra/am1.5.

NREL. 2013. *Concentrating Solar Power Projects*. Available: http://www.nrel.gov/csp/solarpaces/.

NREL. 2014. *Concentrating Solar Power Projects in South Africa*. Available: http://www.nrel.gov/csp/solarpaces/by_country_detail.cfm/country=ZA [2015, December 28].

NREL. 2015a. *NREL: Concentrating Solar Power Projects - Crescent Dunes Solar Energy Project*. Available: http://www.nrel.gov/csp/solarpaces/project_detail.cfm/projectID=60 [2015, December 28].

NREL. 2015b. *NREL: Concentrating Solar Power Projects - Redstone Solar Thermal Power Plant*. Available: http://www.nrel.gov/csp/solarpaces/project_detail.cfm/projectID=4289 [2016, January 09].

Ong, S., Campbell, C. & Denholm, P. 2012. *Land Use Requirements for Solar Power Plants in the United States*. Golden, Colorado. Available: http://www.nrel.gov/docs/fy13osti/56290.pdf [2013, December 30].

Patzek, T.W. & Croft, G.D. 2010. A global coal production forecast with multi-Hubbert cycle analysis. *Energy*. 35(8):3109–3122. DOI: 10.1016/j.energy.2010.02.009.

Pfenninger, S. & Keirstead, J. 2015. Renewables, nuclear, or fossil fuels? Scenarios for Great Britain's power system considering costs, emissions and energy security. *Applied Energy*. 152:83–93.

Pfenninger, S., Hawkes, A. & Keirstead, J. 2014a. Energy systems modeling for twenty-first century energy challenges. *Renewable and Sustainable Energy Reviews*. 33:74–86. DOI: 10.1016/j.rser.2014.02.003.

Pfenninger, S., Gauché, P., Lilliestam, J., Damerau, K., Wagner, F. & Patt, A.G. 2014. Potential for concentrating solar power to provide baseload and dispatchable power. *Nature Climate ….* (June):4–7. DOI: 10.1038/NCLIMATE2276.

Pfenninger, S., Hawkes, A. & Keirstead, J. 2014b. Energy systems modeling for twenty-first century energy challenges. *Renewable and Sustainable Energy Reviews*. 33:74–86. DOI: 10.1016/j.rser.2014.02.003.

Pitman, C.L. & Vant-Hull, L.L. 1984. *Atmospheric transmittance model for a solar beam propagating between a heliostat and a receiver*.

Pitot de la Beaujardiere, J.F.P., Reuter, H.C.R., Klein, S.A. & Reindl, D.T. 2016. Impact of HRSG characteristics on open volumetric receiver CSP plant performance. *Solar Energy*. 127:159–174. DOI: http://dx.doi.org/10.1016/j.solener.2016.01.030.

REN21. 2016. *Renewables 2016 Global Status Report*. Paris. Available: http://www.ren21.net/status-of-renewables/global-status-report/ [2016, June 30].

de Rosa, A.V. 2005. *Fundamentals of renewable Energy Processes*.

Rutledge, D. 2011. Estimating long-term world coal production with logit and probit transforms. *International Journal of Coal Geology*. 85:23–33. Available: http://www.sciencedirect.com/science/article/pii/S0166516210002144 [2013, December 30].

Rutledge, D. 2013. *Energy Supplies and Climate*. Available: http://rutledge.caltech.edu/.

Sager, M., Ellen, D., Ritchken, E. & Osborne, S. 2015. *Concentrated Solar Power: A strategic industrial development opportunity for South Africa*. Cape Town. Available: http://awsassets.wwf.org.za/downloads/concentrated_solar_power_report_final.pdf.

Sandia. 2009. *Sandia National Laboratories, Delsol version 3*. Available: http://energy.sandia.gov/?page_id=6530.

SANEDI. 2015. *Wind resource maps for WASA domain, South Africa*. Available: http://wasadata.csir.co.za/wasa1/WASAData [2015, December 21].

Schell, S. 2010.

Schell, S. 2011. Design and evaluation of esolar's heliostat fields. *Solar Energy*. 85(4):614–619. DOI: 10.1016/j.solener.2010.01.008.

Schwarzbözl, P., Pitz-Paal, R. & Schmitz, M. 2009. Visual HFLCAL-A software tool for layout and optimisation of heliostat fields. In *SolarPACES 2009*. Berlin. 15–18.

Sengupta, M. & Wagner, M. 2012. Atmospheric attenuation in central receiver systems from dni measurements. In *Proceedings of Solar Power and Chemical Energy Systems conference (SolarPACES 2012)*. Marrakech, Morocco. 6.

Silinga, C. & Gauché, P. 2013. Scenarios for a South African CSP peaking system in the short term. In *Proceedings of Solar Power and Chemical Energy Systems conference (SolarPACES 2013)*. V. 0. Las Vegas, Nevada.

Silinga, C. & Gauché, P. 2014. Scenarios for a South African CSP Peaking System in the Short Term. *Energy Procedia*. 49:1543–1552. DOI: 10.1016/j.egypro.2014.03.163.

Stellenbosch University. 2014. *Helio100*. Available: http://helio100.sun.ac.za/ [2016, January 04].

Stine, W.B. & Geyer, M. 2001. *Power from the sun.* Web site e ed. Available: http://powerfromthesun.net/book.html.

Suri, M., Cebecauer, T. & Skoczek, A. 2014a. Cloud Cover Impact on Photovoltaic Power Production in South Africa. *2nd Southern African Solar Energy Conference*. Available: http://geomodelsolar.eu/_docs/papers/2014/Suri-et-al--SASEC2014--Cloud-cover-impact-on-PV-power-production-in-South-Africa.pdf.

Suri, M., Cebecauer, T. & Skoczek, A. 2014b. Cloud Cover Impact on Photovoltaic Power Production in South Africa. In *Southern African Solar Energy Conference SASEC2014*. Skukuza. 8. Available: http://geomodelsolar.eu/_docs/papers/2014/Suri-et-al--SASEC2014--Cloud-cover-impact-on-PV-power-production-in-South-Africa.pdf.

Suri, M., Cebecauer, T., Meyer, A.J. & van Niekerk, J.L. 2015. Accuracy - Enhanced Solar Resou Rce Maps of South Af Rica. In *Third Southern African Solar Energy Conference*. Skukuza.

Telsnig, T., Eltrop, L., Winkler, H. & Fahl, U. 2013. Efficiency and costs of different concentrated solar power plant configurations for sites in Gauteng and the Northern Cape, South Africa. *Journal of Energy in Southern Africa*. 24(1):77–88.

Tomaschek, J., Telsnig, T., Fahl, U. & Eltrop, L. 2015. Integrated Analysis of Dispatchable Concentrated Solar Power. *Energy Procedia*. 69(0):1711–1721. DOI: 10.1016/j.egypro.2015.03.138.

Torresol Energy. 2011. *Gemasolar solar power plant reaches 24 hours of uninterrupted production*. Available: http://www.torresolenergy.com/TORRESOL/NewsTS/gemasolar-solar-power-plant-reaches-24-hours-of-uninterrupted-production.

Trieb, F., Schillings, C., Sullivan, M.O., Pregger, T. & Hoyer-klick, C. 2009. Global Potential of Concentrating Solar Power. In *Proceedings of Solar Power and Chemical Energy Systems conference (SolarPACES 2009)*. Berlin. 1–11.

Trieb, F., Schillings, C., Pregger, T. & O'Sullivan, M. 2012. Solar electricity imports from the Middle East and North Africa to Europe. *Energy Policy*. 42:341–353. DOI: 10.1016/j.enpol.2011.11.091.

Trieb, F., Fichter, T. & Moser, M. 2013. Concentrating solar power in a sustainable future electricity mix. *Sustainability Science*. 9(1):47–60. DOI: 10.1007/s11625-013-0229-1.

Tyner, C. & Wasyluk, D. 2014. eSolar's Modular, Scalable Molten Salt Power Tower Reference Plant Design. *Energy Procedia*. 49:1563–1572. DOI: 10.1016/j.egypro.2014.03.165.

Ummel, K. 2013a. *Planning for Large-Scale Wind and Solar Power in South Africa: Identifying Cost-Effective Deployment Strategies Using Spatiotemporal Modeling.* Washington, DC. Available: http://international.cgdev.org/publication/planning-large-scale-wind-and-solar-power-south-africa-identifying-cost-effective.

Ummel, K. 2013b. *Making Large-Scale Wind and Solar Power a Reality*. Available: bit.ly/1fbQscR.

USA Department of Energy. 2012. *SunShot Vision Study*. Washington, DC. Available: http://www1.eere.energy.gov/solar/pdfs/47927.pdf.

USA Department of Energy. 2015. *Concentrating Solar Power Competitive Awards*. Available: http://www.energy.gov/eere/sunshot/concentrating-solar-power-competitive-awards [2015, December 28].

Viebahn, P., Lechon, Y. & Trieb, F. 2011. The potential role of concentrated solar power (CSP) in Africa and Europe—A dynamic assessment of technology development, cost

development and life cycle inventories until 2050. *Energy Policy*. 39(8):4420–4430. DOI: 10.1016/j.enpol.2010.09.026.

Vignola, F., Grover, C. & Lemon, N. 2011. Building a Bankable Solar Radiation Dataset. In *Proceedings of Solar 2011, American Solar Energy Society*. Raleigh, NC.

Wagner, M. 2008. Simulation and Predictive Performance Modeling of Utility-Scale Central Receiver System Power Plants. University of Wisconsin – Madison.

Wilcox, S. & Marion, W. 2008. *Users Manual for TMY3 Data Sets, Technical Report NREL/TP-581-43156*. Golden, Colorado.

World Nuclear Association. 2011. *Thorium*. Available: http://www.world-nuclear.org/info/inf62.html.

WWF-SA. 2014. *Renewable energy vision 2030 – South Africa*. Cape Town. Available: http://awsassets.wwf.org.za/downloads/a16369_wwf_reip_report_online.pdf.

Young, S. 2011. *Analysis of UK wind power generation*.

APPENDIX A: CONCENTRATING SOLAR POWER MODEL

This appendix covers aspects of the CSP model not included in the main text including foreground matter, assumptions and model details that are of a more general knowledge nature or that offer supporting data and methods.

A.1. Electromagnetic radiation and the sun

The model uses a pillbox approximation for flux distribution, assuming in all cases that the subtend angle is 9.3 mrad (Duffie & Beckman, 2006). Figure A.1 shows basic standard values for average dimensions and temperatures. Figure A.2 is a plot of the spectral distribution outside of the earth's atmosphere and at sea-level. Also shown is the back-body equivalent temperature distribution.

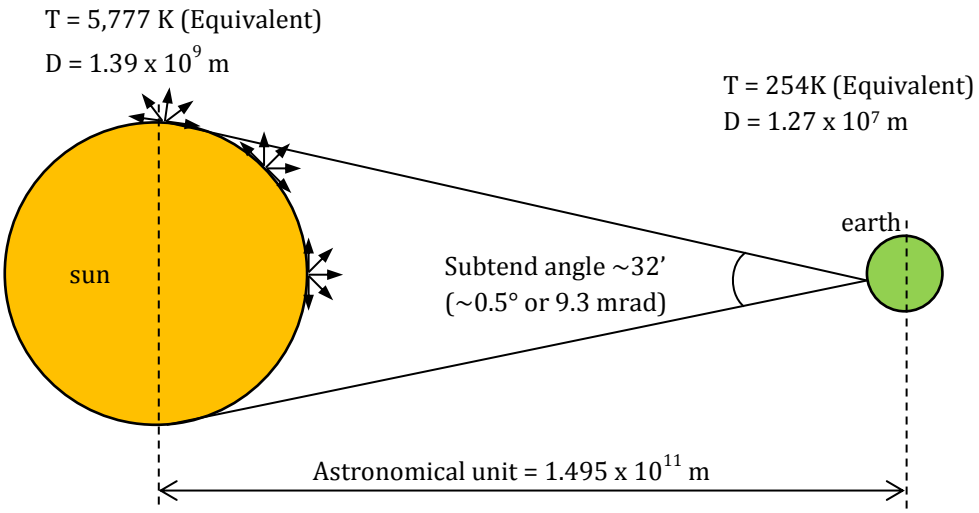

Figure A.1: Basic sun – earth relationships (adapted from Duffie & Beckman (2006))

The elliptic orbit of earth causes small variations in the subtend angle and actual extraterrestrial solar flux. This results in the actual extraterrestrial solar irradiation to range from about 1,412 W/m^2 in late December to 1,322 W/m^2 in late June. While DNI is measured and accounted for in the model, the variance in the subtend angle is not accounted for.

The sea-level standard (AM1.5) spectral distribution in Figure A.2 is a reference distribution for this standard (NREL, 2011e). AM1.5 refers to a typical zenith angle of the sun such that the irradiation travels through the atmosphere 1.5 times more than if the sun were at the zenith. Loss of solar irradiation in the atmosphere is due to scattering, absorption and reflection in the atmosphere. All analysis relating to spectral influences on model parameters made use of the reference AM1.5 distribution. This included background investigations in determining suitability of

locally available glass mirror by integration of the monochromatic transmission and reflection.

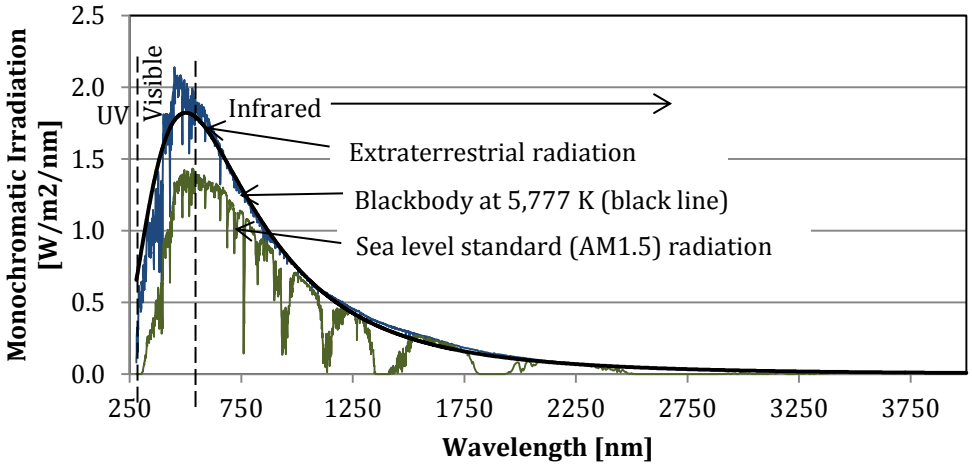

Figure A.2: Solar spectral distribution for extraterrestrial, sea level standard (AM1.5) and blackbody equivalent (adapted from (NREL, 2011e))

Emissivity and absorptivity are equated per monochromatic wavelength and surface temperature.

$$\varepsilon_{(\lambda,T)} = \alpha_{(\lambda,T)} \tag{A.1}$$

The integrated emissivity and absorptivity are simplified to a temperature independent solar absorptivity α_s and a thermal emissivity ε for the receiver radiant surface. No treatment is given to solar irradiation transmission through glazing in the receiver.

Radiation loss from the receiver is a function of the receiver temperature, sky temperature and ground temperature.

$$\dot{Q}_r = \sigma \varepsilon_r A_r \left(F_{r-sky} \left({T_r}^4 - {T_{sky}}^4 \right) + F_{r-ground} \left({T_r}^4 - {T_{ground}}^4 \right) \right) \tag{A.2}$$

where T_r is the effective radiant temperature, T_{sky} is the sky temperature and T_{ground} is the ground temperature. Sky and ground temperatures can be approximated; but assuming that during sunny conditions the ground temperature is elevated above the 2 m ambient temperature, and sky temperature is correspondingly lower with clear skies, the receiver radiant environment is simplified to being a function only of the ambient temperature.

$$\dot{Q}_r \sim \sigma \varepsilon_r A_r \left({T_r}^4 - {T_a}^4 \right) \tag{A.3}$$

where this assumption is further supported by the following conditions and assumptions.

- Solar reflector (heliostat) temperatures are assumed to be the same as the 2 m ambient temperature due to minimal solar absorption and the typical height of reflectors in CSP.
- Thermal radiation is most relevant during times of clear sunny skies where the sky temperature is slightly below ambient (Mills, 1995), and the temperature of the reflector field and ground is similar or somewhat above ambient temperature respectively.
- It is assumed that receivers in CRS are either vertical or tilted to face slightly downward.
- Parabolic trough receivers are horizontally mounted and, at solar noon, are exposed to a view of approximately 50 % sky and 50 % other surroundings. At all other times, the reflector surface begins to block sky view.
- In addition to these geometric arguments, deviation from the ambient temperature has a negligible impact. At a receiver surface temperature of 400 °C and a surrounding temperature of 30 °C, a 1 °C reduction in the surrounding temperature results in an increase in receiver radiant losses of 0.057 % or 6.3 W/m^2. Figure A.3 shows this for a range of receiver temperatures.

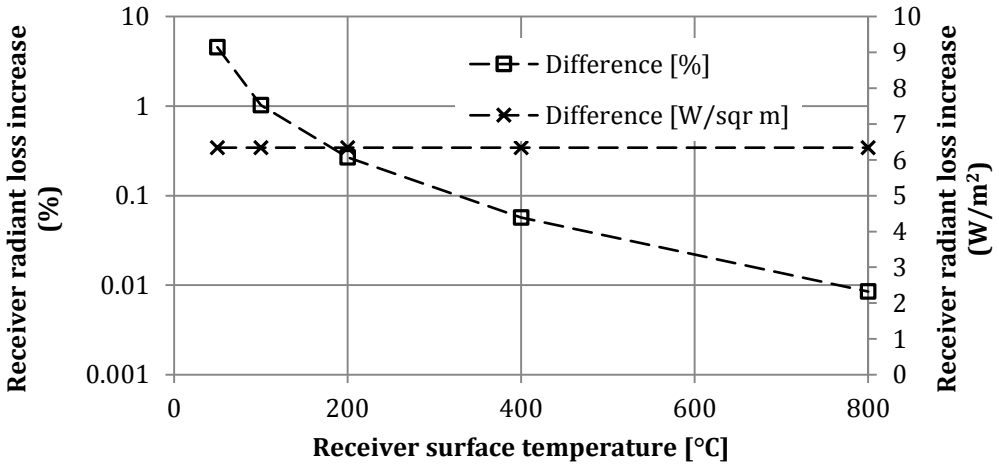

Figure A.3: Receiver thermal loss increase as percentage and flux for a 1 °C reduction in surrounding temperature from a 30 °C ambient

Wagner (2008) made a similar assumption for a central receiver and modeled the sky and ambient separately as having view factors of 0.5 each.

The simplified heliostat beam image in the model is conceptually illustrated in Figure A.4.

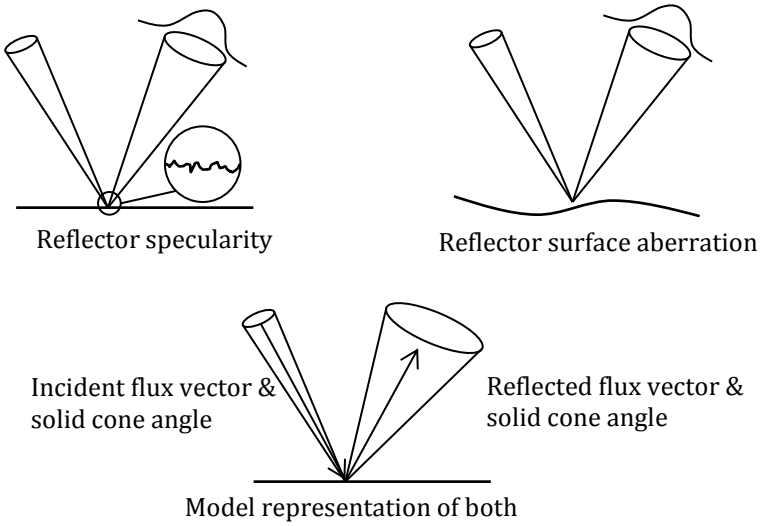

Figure A.4: CSP model representation of specular and macro reflector behavior

A.2. Heliostat-receiver attenuation losses

Attenuation loss models used for comparison in the development of the adapted Lamberts law model (Leary & Hankins, 1979; Pitman & Vant-Hull, 1984; Kistler, 1986; Ballestrín & Marzo, 2012).

Vittitoe & Biggs clear day (visibility 23 km)

$$\tau_a = 0.99326 - 0.1046S + 0.017S^2 - 0.002845S^3 \quad \text{(A.4)}$$

Vittitoe & Biggs hazy day (visibility 5km)

$$\tau_a = 0.98707 - 0.2748S + 0.03394S^2 \quad \text{(A.5)}$$

Used in Delsol (Kistler, 1986) in the form for clear skies

$$\text{Loss}(\%) = 0.6739 + 10.46\,S - 1.7\,S^2 + 0.2845\,S^3 \quad \text{(A.6)}$$

and hazy skies

$$\text{Loss}(\%) = 1.293 + 27.48\,S - 3.394\,S^2 \quad \text{(A.7)}$$

where

$$\text{Loss}(\%) = 100(1 - \tau_a) \quad \text{(A.8)}$$

(Leary & Hankins, 1979) clear day model used in Mirval

$$\text{Loss}(\%) = 0.679 + 0.01176 \times 10^3\,S - 1.97\,S^2 \qquad (S \leq 1\text{km}) \quad \text{(A.9)}$$

$$\text{Loss}(\%) = 100(1 - e^{-0.1106\,S}) \qquad (S > 1\text{km}) \tag{A.10}$$

(Ballestrín & Marzo, 2012) approximation is on data up to 4 km. For clear skies

$$\text{Loss}(\%) = 0.29544 + 15.22128\,S - 1.8598\,S^2 + 0.15182\,S^3 \tag{A.11}$$

and hazy skies

$$\text{Loss}(\%) = 0.77941 + 55.49083\,S - 14.78875\,S^2 + 1.53718\,S^3 \tag{A.12}$$

A.3. Heliostat field parameters

This section includes data specific to the CSP heliostat model used in all cases.

A.3.1. Data tables

Columns indicate zenith angle and rows indicate solar azimuth angle

Table A.1: Combined cosine, blocking and shading efficiencies

	0°	9°	18°	27°	36°	45°	54°	63°	72°	81°	90°
-180°	0.833	0.831	0.825	0.815	0.801	0.782	0.724	0.594	0.401	0.196	0.000
-162°	0.833	0.831	0.825	0.815	0.801	0.782	0.734	0.613	0.422	0.206	0.000
-144°	0.833	0.831	0.825	0.815	0.802	0.783	0.755	0.666	0.488	0.242	0.000
-126°	0.833	0.831	0.825	0.816	0.802	0.784	0.757	0.670	0.490	0.243	0.000
-108°	0.833	0.831	0.826	0.816	0.803	0.785	0.742	0.621	0.422	0.207	0.000
-90°	0.833	0.831	0.826	0.817	0.803	0.785	0.733	0.602	0.402	0.197	0.000
-72°	0.833	0.831	0.826	0.816	0.803	0.785	0.742	0.621	0.422	0.207	0.000
-54°	0.833	0.831	0.825	0.816	0.802	0.784	0.757	0.670	0.490	0.243	0.000
-36°	0.833	0.831	0.825	0.815	0.802	0.783	0.755	0.666	0.488	0.242	0.000
-18°	0.833	0.831	0.825	0.815	0.801	0.782	0.734	0.613	0.422	0.206	0.000
0°	0.833	0.831	0.825	0.815	0.801	0.782	0.724	0.594	0.401	0.196	0.000
18°	0.833	0.831	0.825	0.815	0.801	0.782	0.734	0.613	0.422	0.206	0.000
36°	0.833	0.831	0.825	0.815	0.802	0.783	0.755	0.666	0.488	0.242	0.000
54°	0.833	0.831	0.825	0.816	0.802	0.784	0.757	0.670	0.490	0.243	0.000
72°	0.833	0.831	0.826	0.816	0.803	0.785	0.742	0.621	0.422	0.207	0.000
90°	0.833	0.831	0.826	0.817	0.803	0.785	0.733	0.602	0.402	0.197	0.000
108°	0.833	0.831	0.826	0.816	0.803	0.785	0.742	0.621	0.422	0.207	0.000
126°	0.833	0.831	0.825	0.816	0.802	0.784	0.757	0.670	0.490	0.243	0.000
144°	0.833	0.831	0.825	0.815	0.802	0.783	0.755	0.666	0.488	0.242	0.000
162°	0.833	0.831	0.825	0.815	0.801	0.782	0.734	0.613	0.422	0.206	0.000
180°	0.833	0.831	0.825	0.815	0.801	0.782	0.724	0.594	0.401	0.196	0.000

Table A.2: Shading efficiencies

	0°	9°	18°	27°	36°	45°	54°	63°	72°	81°	90°
-180°	1.000	1.000	1.000	1.000	1.000	0.999	0.952	0.825	0.596	0.314	0.000
-162°	1.000	1.000	1.000	1.000	1.000	1.000	0.965	0.848	0.627	0.331	0.000
-144°	1.000	1.000	1.000	1.000	1.000	1.000	0.993	0.911	0.721	0.388	0.000
-126°	1.000	1.000	1.000	1.000	1.000	1.000	0.993	0.912	0.716	0.383	0.000
-108°	1.000	1.000	1.000	1.000	1.000	1.000	0.969	0.847	0.612	0.320	0.000
-90°	1.000	1.000	1.000	1.000	1.000	0.999	0.958	0.821	0.579	0.302	0.000
-72°	1.000	1.000	1.000	1.000	1.000	1.000	0.969	0.847	0.612	0.320	0.000
-54°	1.000	1.000	1.000	1.000	1.000	1.000	0.993	0.912	0.716	0.383	0.000
-36°	1.000	1.000	1.000	1.000	1.000	1.000	0.993	0.911	0.721	0.388	0.000
-18°	1.000	1.000	1.000	1.000	1.000	1.000	0.965	0.848	0.627	0.331	0.000
0°	1.000	1.000	1.000	1.000	1.000	0.999	0.952	0.825	0.596	0.314	0.000
18°	1.000	1.000	1.000	1.000	1.000	1.000	0.965	0.848	0.627	0.331	0.000
36°	1.000	1.000	1.000	1.000	1.000	1.000	0.993	0.911	0.721	0.388	0.000
54°	1.000	1.000	1.000	1.000	1.000	1.000	0.993	0.912	0.716	0.383	0.000
72°	1.000	1.000	1.000	1.000	1.000	1.000	0.969	0.847	0.612	0.320	0.000
90°	1.000	1.000	1.000	1.000	1.000	0.999	0.958	0.821	0.579	0.302	0.000
108°	1.000	1.000	1.000	1.000	1.000	1.000	0.969	0.847	0.612	0.320	0.000
126°	1.000	1.000	1.000	1.000	1.000	1.000	0.993	0.912	0.716	0.383	0.000
144°	1.000	1.000	1.000	1.000	1.000	1.000	0.993	0.911	0.721	0.388	0.000
162°	1.000	1.000	1.000	1.000	1.000	1.000	0.965	0.848	0.627	0.331	0.000
180°	1.000	1.000	1.000	1.000	1.000	0.999	0.952	0.825	0.596	0.314	0.000

Table A.3: Blocking efficiencies

	0°	9°	18°	27°	36°	45°	54°	63°	72°	81°	90°
-180°	0.924	0.925	0.927	0.931	0.936	0.941	0.945	0.947	0.949	0.952	0.955
-162°	0.924	0.925	0.927	0.931	0.936	0.941	0.944	0.946	0.950	0.953	0.956
-144°	0.924	0.925	0.927	0.931	0.935	0.940	0.943	0.945	0.949	0.953	0.958
-126°	0.924	0.925	0.927	0.931	0.935	0.939	0.943	0.946	0.950	0.955	0.959
-108°	0.924	0.925	0.927	0.931	0.935	0.939	0.944	0.948	0.952	0.956	0.961
-90°	0.924	0.925	0.927	0.931	0.935	0.939	0.943	0.948	0.953	0.958	0.962
-72°	0.924	0.925	0.927	0.931	0.935	0.939	0.944	0.948	0.952	0.956	0.961
-54°	0.924	0.925	0.927	0.931	0.935	0.939	0.943	0.946	0.950	0.955	0.959
-36°	0.924	0.925	0.927	0.931	0.935	0.940	0.943	0.945	0.949	0.953	0.958
-18°	0.924	0.925	0.927	0.931	0.936	0.941	0.944	0.946	0.950	0.953	0.956
0°	0.924	0.925	0.927	0.931	0.936	0.941	0.945	0.947	0.949	0.952	0.955
18°	0.924	0.925	0.927	0.931	0.936	0.941	0.944	0.946	0.950	0.953	0.956
36°	0.924	0.925	0.927	0.931	0.935	0.940	0.943	0.945	0.949	0.953	0.958
54°	0.924	0.925	0.927	0.931	0.935	0.939	0.943	0.946	0.950	0.955	0.959

72°	0.924	0.925	0.927	0.931	0.935	0.939	0.944	0.948	0.952	0.956	0.961
90°	0.924	0.925	0.927	0.931	0.935	0.939	0.943	0.948	0.953	0.958	0.962
108°	0.924	0.925	0.927	0.931	0.935	0.939	0.944	0.948	0.952	0.956	0.961
126°	0.924	0.925	0.927	0.931	0.935	0.939	0.943	0.946	0.950	0.955	0.959
144°	0.924	0.925	0.927	0.931	0.935	0.940	0.943	0.945	0.949	0.953	0.958
162°	0.924	0.925	0.927	0.931	0.936	0.941	0.944	0.946	0.950	0.953	0.956
180°	0.924	0.925	0.927	0.931	0.936	0.941	0.945	0.947	0.949	0.952	0.955

Table A.4: Cosine efficiencies

	0°	**9°**	**18°**	**27°**	**36°**	**45°**	**54°**	**63°**	**72°**	**81°**	**90°**
-180°	0.898	0.896	0.888	0.876	0.859	0.837	0.811	0.781	0.747	0.710	0.670
-162°	0.898	0.896	0.888	0.876	0.859	0.837	0.811	0.781	0.747	0.710	0.670
-144°	0.898	0.896	0.888	0.876	0.859	0.838	0.812	0.782	0.749	0.712	0.672
-126°	0.898	0.896	0.888	0.876	0.860	0.839	0.813	0.784	0.751	0.714	0.675
-108°	0.898	0.896	0.889	0.877	0.860	0.839	0.814	0.785	0.753	0.717	0.679
-90°	0.898	0.896	0.889	0.877	0.860	0.840	0.815	0.786	0.754	0.719	0.681
-72°	0.898	0.896	0.889	0.877	0.860	0.839	0.814	0.785	0.753	0.717	0.679
-54°	0.898	0.896	0.888	0.876	0.860	0.839	0.813	0.784	0.751	0.714	0.675
-36°	0.898	0.896	0.888	0.876	0.859	0.838	0.812	0.782	0.749	0.712	0.672
-18°	0.898	0.896	0.888	0.876	0.859	0.837	0.811	0.781	0.747	0.710	0.670
0°	0.898	0.896	0.888	0.876	0.859	0.837	0.811	0.781	0.747	0.710	0.670
18°	0.898	0.896	0.888	0.876	0.859	0.837	0.811	0.781	0.747	0.710	0.670
36°	0.898	0.896	0.888	0.876	0.859	0.838	0.812	0.782	0.749	0.712	0.672
54°	0.898	0.896	0.888	0.876	0.860	0.839	0.813	0.784	0.751	0.714	0.675
72°	0.898	0.896	0.889	0.877	0.860	0.839	0.814	0.785	0.753	0.717	0.679
90°	0.898	0.896	0.889	0.877	0.860	0.840	0.815	0.786	0.754	0.719	0.681
108°	0.898	0.896	0.889	0.877	0.860	0.839	0.814	0.785	0.753	0.717	0.679
126°	0.898	0.896	0.888	0.876	0.860	0.839	0.813	0.784	0.751	0.714	0.675
144°	0.898	0.896	0.888	0.876	0.859	0.838	0.812	0.782	0.749	0.712	0.672
162°	0.898	0.896	0.888	0.876	0.859	0.837	0.811	0.781	0.747	0.710	0.670
180°	0.898	0.896	0.888	0.876	0.859	0.837	0.811	0.781	0.747	0.710	0.670

APPENDIX B: NATURE CLIMATE CHANGE ARTICLE

nature climate change

LETTERS

PUBLISHED ONLINE: 22 JUNE 2014 | DOI: 10.1038/NCLIMATE2276

Potential for concentrating solar power to provide baseload and dispatchable power

Stefan Pfenninger[1]*, Paul Gauché[2], Johan Lilliestam[3], Kerstin Damerau[3], Fabian Wagner[4] and Anthony Patt[3]

Previous studies have demonstrated the possibility of maintaining a reliable electric power system with high shares of renewables, but only assuming the deployment of specific technologies in precise ratios, careful demand-side management, or grid-scale storage technologies[1,2]. Any scalable renewable technology that could provide either baseload or dispatchable power would allow greater flexibility in planning a balanced system, and therefore would be especially valuable. Many analysts have suggested that concentrating solar power (CSP) could do just that[3–8]. Here we systematically test this proposition for the first time. We simulate the operation of CSP plant networks incorporating thermal storage in four world regions where CSP is already being deployed, and optimize their siting, operation and sizing to satisfy a set of realistic demand scenarios. In all four regions, we show that with an optimally designed and operated system, it is possible to guarantee up to half of peak capacity before CSP plant costs substantially increase.

Greenhouse gas emissions will need to fall substantially over the coming decades if the worst impacts of climate change are to be avoided, a conclusion reflected in mid-century emissions reduction targets of 80% in numerous political jurisdictions, including California and the European Union[9–12]. Given the suite of technologies now available, there is widespread belief that renewable sources of energy, and above all renewable sources of electricity, will have to play an important role in this decarbonization[13,14]. Wind and solar power offer an abundant supply potential, but both are intermittent, with their output determined by diurnal and annual cycles, as well as by local weather conditions[15–17].

Recent studies have used data with high spatial and temporal resolution to study the feasibility of integrating large amounts of wind and solar within a portfolio of renewable energy sources. They have found it to be possible, but that it requires optimizing the system design across several technologies[1,2], and incorporating excess solar and wind capacity of up to twice the peak power demand if the need for grid level storage is to be avoided[18,19]. These factors could make integration difficult in practice, first because of the complexity of optimizing across multiple technologies, and second because the land required for excess renewables capacity may be a binding constraint in densely populated regions, such as Europe or South Asia. Using technologies that either use less land or can be built in remote, sparsely inhabited regions would hence be beneficial[20], as would identifying whether there is a single technology that on its own could offer a high level of reliability, so as to give energy system planners and policy-makers greater flexibility with respect to balancing a decarbonized electricity system. We therefore study the reliability of CSP, which can best be deployed in deserts where land-use limitations do not appear to be a constraining factor, and which offers the promise of overcoming intermittency by making use of short-term thermal storage to bridge the day–night cycle and periods of cloudy weather. Some existing CSP plants can already operate at full capacity around the clock in summer[6,7]. In winter, or when cloudy conditions are prolonged, however, even these CSP plants need to cease power production.

Two well-known strategies can increase the availability of renewable power. First, for all wind and solar technologies, an interconnected fleet taking advantage of anticorrelation between weather at geographically dispersed sites can provide greater availability than a single plant[21–24]. Second, for CSP plants specifically, the size of an individual plant's solar field relative to its power block can be increased, allowing the plant to more rapidly fill its heat storage during sunny conditions. We illustrate the effects of both strategies in Fig. 1 for CSP plants operating in the Mediterranean countries (see Supplementary Fig. 1 for the results in the other regions, Supplementary Fig. 6 for the possible sites and Supplementary Table 2 for plant design parameters). Figure 1a shows hourly generation curves for a hypothetical network of 100 CSP plants in the Mediterranean basin, revealing that there are extended periods in winter when the fleet must operate at or near zero generation. Figure 1b illustrates the effect of including a reserve buffer by doubling the solar collection area of each plant, while maintaining the storage and turbine capacity. This allows individual plants with beneficial conditions at a given time to compensate for adverse weather elsewhere in the system, and improves fleet availability, although as shown in the figure still does not provide 100% reliability. Oversizing comes at a financial penalty because it discards much of the thermal energy collected: assuming 2010 technology costs, the levelized cost of electricity for the case in Fig. 1a is 0.15 USD/kWh, compared to 0.19 USD/kWh in Fig. 1b.

To examine this tradeoff between cost and availability in detail, we next consider actual load curves that the operator of a network of CSP plants might design and operate a system to satisfy. Such load curves would mainly depend on the power demand, but also very much on the power mix; whether, for example, supply contained a great deal of day-only photovoltaic power, volatile wind power, seasonally determined hydro power or flexible gas power. As we cannot predict what the electricity mix might look like at a time when CSP is needed to offer high availability, we consider three extreme cases, which together can provide an indication of possible needs. The first is a flat load curve, meaning that CSP would be required to provide baseload, much like nuclear power does today

[1]Department of Civil and Environmental Engineering and Grantham Institute for Climate Change, Imperial College, London SW7 2AZ, UK, [2]Department of Mechanical and Mechatronic Engineering, Stellenbosch University, Stellenbosch 7602, South Africa, [3]Department of Environmental Systems Science, ETH Zurich, CH-8092 Zurich, Switzerland, [4]Mitigation of Air Pollution and Greenhouse Gases Program, International Institute for Applied Systems Analysis, A-2361 Laxenburg, Austria. *e-mail: s.pfenninger12@imperial.ac.uk

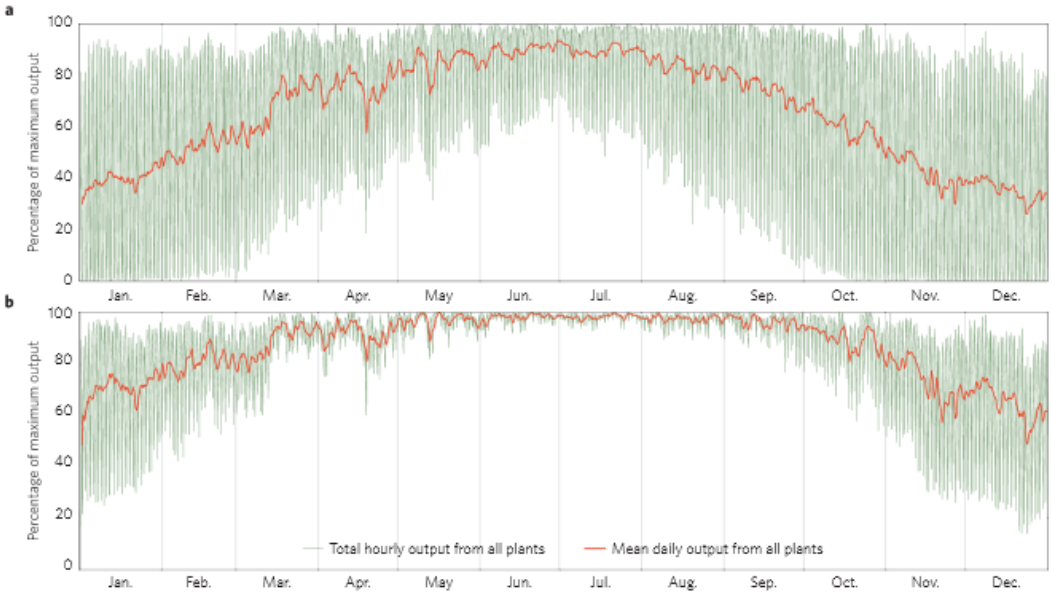

Figure 1 | Total output for the year 2005 from 100 plants spread across locations in the Mediterranean basin. a, The plants are operated without concern for demand or coordination: in each hour, each plant produces as much power as possible. See text for plant dimensions. **b**, The size of the solar field is doubled, while the power block and storage size is kept constant.

in many countries. The second is the load curve for the European Union, meaning that CSP would be required to follow the load of a region that experiences peak demand in winter, and during evening hours after sundown ('winter peak demand'). The third is the load curve for California, a warm industrialized region where peak demand is dictated by air conditioning needs, with the highest demand during summer afternoons ('summer peak demand').

Figure 2 shows the projected levelized costs of satisfying varying levels of availability with a CSP fleet in the ten best sites in the southern and eastern Mediterranean countries, and considering steps taken to optimize the system design around three demand profiles. The curves show the effects on cost of varying availability, expressed as the requirement for dispatchable, non-CSP backup capacity as a fraction of peak load. For the top curve, as in Fig. 1, we do not assume any effort to optimize the siting or operation of plants towards a particular demand curve, and the only control variable is the oversizing of the solar fields across the whole system. The middle set of curves shows the results when one assumes that the entire plant fleet is coordinated, to satisfy a given share of each of the demand curves at the lowest possible cost. Such optimization could include using storage to delay output at one plant, to maintain availability above a particular threshold when another plant in the system is forced to go offline because of poor weather. The relative sizing of individual plants is still not optimized in this case. Finally, the lowest set of curves shows results when adding efforts to optimize the planning of each individual plant by also allowing the optimization to choose the size of each plant's generator, solar field and thermal storage system independent of each other. This allows the model to increase overall system reliability and further reduce costs by optimizing the utilization of each individual plant and the dimensioning of its components (see Supplementary Information for full assumptions in the model, results for other world regions in Supplementary Fig. 2, and comparisons using projected 2030 costs in Supplementary Fig. 7).

The results in Fig. 2 illustrate that it is possible to improve the cost/availability frontier substantially by coordinating and optimizing the design and operation of plants within a system. In the optimized cases, high levels of reliability, 70–80%, can be achieved with practically no cost penalty, and very high levels of reliability with cost penalties of less than 50%, which may be considered modest or affordable. Unsurprisingly, the cost penalty is lowest when the need is to satisfy peak summer demand, and greatest when the need is to satisfy peak winter demand.

A final question concerns whether these qualitative insights gained from Fig. 2 can be generalized to other world regions. Figure 3 shows results for the fully optimized case, illustrating differences across four world regions. It is possible to achieve quite similar levelized costs, across all regions and demand scenarios, when the availability of backup generation is high and the needs for CSP availability correspondingly low. However, the costs for power from CSP generation in the absence of substantial backup capacity vary widely across regions and scenarios. In countries with well-developed power sectors the required dispatchable backup capacity already exists, primarily in the form of fossil-fired plants with fast start-up times. Thus, for an initial deployment of CSP the most sensible cost figures to draw from are well above 50% available backup capacity. However, if the ultimate goal is the decarbonization of power generation with reliable CSP generation, existing backup capacity will need to be relied on less and less. The cost penalties for achieving high CSP reliability are much higher for the United States and India, reflecting less favourable climatic conditions in terms of greater spatial correlation of cloud cover.

Baseload capability or full load-following capability may be an illusive, and unnecessary, goal for any single technology. Nuclear power stations, for example, have an average availability of around 80%, mainly because of maintenance and unforeseen stoppages[25]. Droughts and heat waves can at present force existing wet-cooled thermal power stations to reduce or stop production

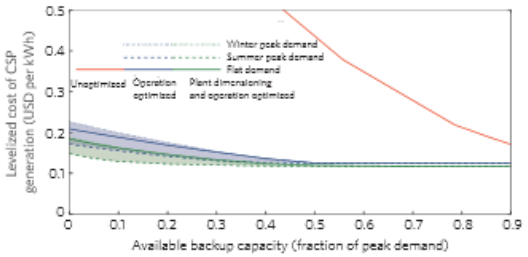

Figure 2 | Costs of guaranteeing to meet various fractions of the load in the three load profiles by CSP plants, for the worst (costliest) year out of the four simulated in the Mediterranean basin.

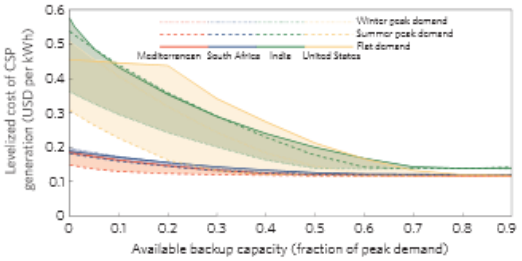

Figure 3 | Costs of guaranteeing to meet various fractions of the load for fully optimized plants (design, location and operation) in the four regions, for the worst (costliest) year out of the four simulated years. The shaded area shows the range of costs resulting from the three different load profiles.

during sustained periods owing to cooling water temperature restrictions, and climate change is likely to reduce water availability and increase surface water temperatures further[26,27]. Our results suggest that a geographically dispersed CSP network, using current thermal storage technology, could be a comparably dispatchable or baseload-capable technology in some parts of the world. This could overcome one of the key perceived barriers to an energy system based primarily on renewables, which may be crucial for successful decarbonization and thus for avoiding severe unmitigated climate change.

This result comes with one condition and two caveats. The condition is that the plants in that system be designed and operated in a coordinated fashion, rather than in a manner where each is as large as possible or is operated without consideration of regional weather conditions and the total fleet output. We have not considered whether the coordination takes place through the actions of a central planner, an appropriately designed power market, or some other mechanism, nor do we make statements concerning how likely such coordination is. We do, however, show that as few as ten geographically dispersed locations are, with coordination, sufficient.

The first caveat is that very high availability of CSP, namely without any need for dispatchable backup capacity, may be economically practical only in some world regions. Of the four regions we examined, the Mediterranean and South Africa offer the promise of very high availability without a substantial cost penalty, whereas the United States and India do not. Progress on high-resolution solar resource modelling will allow future work to investigate these disparities further. In these latter two regions, CSP might still be able to provide a large share of reliable power, but the exact extent would be contingent on specific demand curves and the features of the other technologies in the power mix. This becomes important when deep emissions reductions require that existing dispatchable backup capacity provided by fossil-fired power stations is decommissioned and replaced with emissions-free alternatives.

The second caveat is that CSP is at present more expensive than other technologies. It has yet to experience deployment at a scale comparable to wind or photovoltaics, yet there is reason to believe that should it do so, perhaps driven by its greater degree of reliability, its costs could quickly fall. To assess the implications of this possibility, we ran the fully optimized scenario with estimated 2030 costs (Supplementary Fig. 7). These costs were derived by extrapolating estimated 2020 component costs using IEA estimates for overall CSP plant costs in 2030 (Supplementary Table 3). The results show levelized electricity costs cut by more than half and a narrower range of costs to supply the different demand curves. Because the future costs of CSP, not to mention future options for electrochemical storage, are difficult to estimate, we have not engaged in any detailed analysis comparing dispatchable CSP systems with other systems integrating intermittent generation with grid-level storage. Our results suggest, however, that CSP may be an attractive option, and it is thus possible to consider CSP satisfying a large fraction of a future decarbonized, affordable, and reliable electricity system.

Methods

We conducted our analysis using an existing CSP plant model as described in ref. 28, and extended it by adding an optimization component to consider coordinated plant siting, design and operation. This is a linear programming model specifically designed to run on high-performance clusters to examine a large number of optimization scenarios. The structure and equations of the model are described in greater detail in the Supplementary Information.

The primary input data to run the model comprises hourly data on solar radiation, surface temperature and wind, the latter two to calculate thermal-to-electric conversion efficiency. Radiation data were supplied by satellite observation, whereas temperature and wind were derived from climate model reanalyses. We ran the model based on these data from four world regions: the Mediterranean region (Northern Africa, the Middle East and Southern Europe), South Africa, the United States and India. We selected the regions based on two criteria: there is planned or ongoing use of CSP in the region, and both solar irradiance and weather data were available.

For each region, we performed three sets of model runs. The first set of model runs simulated plants running at their maximum output for as long as possible, and was performed for all sites in the respective region. The second and third sets of model runs expanded this to perform an optimization of plant operation and of plant design and operation, respectively, and were performed for ten sites selected from the initial set of sites in each region, by choosing those ten sites with the highest annual Direct Normal Irradiance (DNI). In these latter two runs we made the model more tractable by resampling the data in three-hour timesteps.

The optimization runs required the specification of demand curves. We selected three alternatives—a typical winter peak demand, a typical summer peak demand and a constant demand—to simulate the widest range of realistic scenarios.

Details on all of our data, including satellite and reanalysis irradiance and weather data, electricity demand data and cost data, are available in the Supplementary Information.

Received 28 March 2014; accepted 21 May 2014; published online 22 June 2014

References

1. Ekman, C. K. & Jensen, S. H. Prospects for large scale electricity storage in Denmark. *Energy Convers. Manage.* **51,** 1140–1147 (2010).
2. Mathiesen, B. V. & Lund, H. Comparative analyses of seven technologies to facilitate the integration of fluctuating renewable energy sources. *IET Renew. Power Gen.* **3,** 190–204 (2009).
3. Usaola, J. Operation of concentrating solar power plants with storage in spot electricity markets. *IET Renew. Power Gen.* **6,** 59–66 (2012).
4. Trieb, F., Schillings, C., Pregger, T. & O'Sullivan, M. Solar electricity imports from the Middle East and North Africa to Europe. *Energy Policy* **42,** 341–353 (2012).

5. Izquierdo, S., Montañés, C., Dopazo, C. & Fueyo, N. Analysis of CSP plants for the definition of energy policies: The influence on electricity cost of solar multiples, capacity factors and energy storage. *Energy Policy* **38,** 6215–6221 (2010).
6. Lilliestam, J., Bielicki, J. & Patt, A. Comparing carbon capture and storage (CCS) with concentrating solar power (CSP): Potentials, costs, risks, and barriers. *Energy Policy* **47,** 447–455 (2012).
7. Fthenakis, V., Mason, J. & Zweibel, K. The technical, geographical, and economic feasibility for solar energy to supply the energy needs of the US. *Energy Policy* **37,** 387–399 (2009).
8. Viehbahn, P., Lechon, Y. & Trieb, F. The potential role of concentrated solar power (CSP) in Africa and Europe. *Energy Policy* **39,** 4420–4430 (2011).
9. McCollum, D., Yang, C., Yeh, S. & Ogden, J. Deep greenhouse gas reduction scenarios for California—Strategic implications from the CA-TIMES energy-economic systems model. *Energy Strategy Rev.* **1,** 19–32 (2012).
10. Lilliestam, J. *et al.* An alternative to a global climate deal may be unfolding before our eyes. *Clim. Dev.* **4,** 1–4 (2012).
11. *EC Energy Roadmap 2050 COM(2011) 885/2* (European Commission, 2011).
12. State of California. *Executive Order S-3-05* (The Governor of California, 2005).
13. Haller, M., Ludig, S. & Bauer, N. Decarbonisation scenarios for the EU and MENA power system: Considering spatial distribution and short term dynamics of renewable generation. *Energy Policy* **47,** 282–290 (2012).
14. IPCC. *Special Report on Renewable Energy Sources and Climate Change Mitigation* (Cambridge Univ. Press, 2011).
15. Delucchi, M. A. & Jacobson, M. Z. Providing all global energy with wind, water, and solar power, Part II: Reliability, system and transmisison costs, and policies. *Energy Policy* **39,** 1170–1190 (2011).
16. Jacobson, M. Z. & Delucchi, M. A. Providing all global energy with wind, water, and solar power, Part I: Technologies, energy resources, quantities and areas of infrastructure, and materials. *Energy Policy* **39,** 1154–1169 (2011).
17. Garrison, J. B. & Webber, M. E. An integrated energy storage scheme for a dispatchable solar and wind powered energy system. *J. Renew. Sustain. Energy* **3,** 043101 (2011).
18. Heide, D., Greiner, M., von Bremen, L. & Hoffmann, C. Reduced storage and balancing needs in a fully renewable European power system with excess wind and solar power generation. *Renew. Energy* **36,** 2515–2523 (2011).
19. Budischak, C. *et al.* Cost-minimized combinations of wind power, solar power and electrochemical storage, powering the grid up to 99.9% of the time. *J. Power Sources* **225,** 60–74 (2013).
20. Arent, D. *et al.* Implications of high renewable electricity penetration in the U.S. for water use, greenhouse gas emissions, land-use, and materials supply. *Appl. Energy* **123,** 368–377 (2014).
21. Patt, A., Komendantova, N., Battaglini, A. & Lilliestam, J. Regional integration to support full renewable power deployment for Europe by 2050. *Environ. Politics* **20,** 727–742 (2011).
22. Battaglini, A., Lilliestam, J., Haas, A. & Patt, A. Development of SuperSmart Grids for a more efficient utilisation of electricity from renewable sources. *J. Cleaner Prod.* **17,** 911–918 (2009).
23. Katzenstein, W., Fertig, E. & Apt, J. The variability of interconnected wind plants. *Energy Policy* **38,** 4400–4410 (2010).
24. Kempton, W., Pimenta, F. M., Veron, D. E. & Colle, B. A. Electric power from offshore wind via synoptic-scale interconnection. *Proc. Natl Acad. Sci. USA* **107,** 7240–7245 (2010).
25. *IAEA Nuclear Power Reactors in the World 2011 Edition* (International Atomic Energy Agency, 2011).
26. Förster, H. & Lilliestam, J. Modeling thermoelectric power generation in view of climate change. *Reg. Environ. Change* **10,** 327–338 (2010).
27. Van Vliet, M. T. H. *et al.* Vulnerability of US and European electricity supply to climate change. *Nature Clim. Change* **2,** 676–681 (2012).
28. Gauché, P., von Backström, T. W. & Brent, A. C. in *17th SolarPACES Conference* 20–23 (2011).

Acknowledgements

Funding for this work was provided by the Grantham Institute for Climate Change, the European Institute of Innovation and Technology via its Climate-KIC program, and derived from the European Research Council, grant number 313533.

Author contributions

S.P., J.L. and A.P. designed the study and drafted the manuscript. S.P. implemented the models and performed all analyses. P.G. contributed the CSP plant model and solar resource data. K.D. performed the site selection and obtained demand data. F.W. contributed to model development and implementation. All authors contributed to editing and discussing the manuscript.

Additional information

Supplementary information is available in the online version of the paper. Reprints and permissions information is available online at www.nature.com/reprints. Correspondence and requests for materials should be addressed to S.P.

Competing financial interests

The authors declare no competing financial interests.

APPENDIX C: POLICY BRIEF

This policy brief is an outcome of a PhD titled: **Spatial-temporal model to evaluate the system potential of concentrating solar power towers in South Africa**. The objective of the PhD was to develop a method to quantifiably evaluate the value and potential of CSP in the future electricity system of South Africa with the intention to provide a better technology perspective for guiding national policy.

C.1. Background

The Integrated Resource Plan (IRP) of South Africa legislates the definition of the national electricity system with a twenty year horizon and intended updates every two years (Department of Energy, 2011). The implementation program of the IRP for renewable energy capacity is the Renewable Energy Independent Power Producer Procurement Programme (REIPPPP) (Department of Energy, 2012). The program, launched in 2011, is an initiative of the DOE that awards bids to applicants according to allocations set per technology. With a good start in terms of the plan and the associated implementation program, updates to the plan have stalled while good progress has resulted in the implementation program.

The 2010 IRP prioritizes nuclear power as a replacement to coal power for reasons relating to uncertainty around the ability of renewables to offer affordable and guaranteed power. Concerns have been expressed regarding the sustainability and security of the 2010 IRP, and arguments are being presented that a renewable focused future is economically more suitable (Department of Energy, 2013b; Gauché, von Backström & Brent, 2013; WWF-SA, 2014).

Reliable and quantifiable evidence using rigorous spatial-temporal analysis and high quality resource data is important, particularly in a transition towards a sustainable electricity system (Pfenninger, Hawkes & Keirstead, 2014b). Auret (2015) recently demonstrates that using these methods, the IRP and variants thereof can be explored for their strengths and drawbacks, particularly with reference to CSP where the lack of a suitable tariff arrangement will not enable the technology to fulfil its promise of dispatch power. The results of this study support these findings.

C.2. Analysis and findings

The study finds CSP to play a potentially pivotal role in South Africa's near-to-mid-term future. The following list summarizes findings relevant to policy advice.

1. In the event of a scarcity risk of fossil or nuclear fuels in future, South Africa's electricity network could be vulnerable in terms of utility baseload or dispatch electricity supply. This risk is considered to be significant and the evolution away from conventional means of power generation is inevitable within a relatively short timeframe.

2. The system model interpretation of the 2010 IRP in the study does not factor in construction time constraints, additional cost uncertainty, or externality factors relating to the addition of 9.6 GW of nuclear power. Yet the model produces quantifiable data suggesting that this nuclear capacity results in a system less capable of adjusting to hourly fluctuations in demand, particularly when the system becomes capacity constrained. Excessive reliance on last-resort generators and the cost of unserved electricity are a result.

3. Assuming a capacity constrained system resulting in excessive use of last-resort generators and unserved electricity, CSP offers an immediate solution at current costs. Provided this CSP capacity is distributed and has sufficient storage, adding 3,300 MW of CSP could result in a lower generation cost regardless of fuel cost escalation. In the margin as excessive use of last-resort generators transition to unserved power, this CSP system would reduce fuel consumption of last-resort generators by 80 %.

4. Within the time horizon of the IRP (up to 2030), a renewable centric electricity capacity expansion containing 8 GW or more of CSP can result in the lowest cost electricity system for most scenarios of the future considering cost and demand uncertainty. This CSP capacity must serve the system somewhat sacrificially by offering increased availability at the expense of capacity factor. Margin cost analysis (MVOE) can inform tariffs.

5. The maturity of CSP remains a problem for the technology. Costs associated with CAPEX and LCOE remain high for CSP, and the consequence of thermo-economics where large expensive plants are required to drive down LCOE is likely the leading adoption hurdle.

C.3. Recommendations

A summary of recommendations is listed per category.

Cost risk and mitigation

1. The thermo-economic challenge of contemporary CSP results in single project costs in the order of $ 1 billion. Assuming that CSP can fulfil its promise, significant increases in CSP R&D expenditure would help to make more informed decisions for a fraction of the cost of a project, thereby reducing risk. Relevant public bodies include DST (Technology R&D), DOE (Energy) and DTI (Industry).

2. Provided competitive tariffs are enforced, the success of the REIPPPP suggests that a greater capacity allocation could be provided to CSP. This program protects the public from the cost of projects, and lower tariffs could result from a lesser constrained allocation. Over-capacitating the system is a possible consequence and would require immediate reconsideration of

alternatives to CSP, notably nuclear, coal and CCGT capacity.

3. CSP is increasingly acknowledged for its local content potential in South Africa. Allocation of capacity to IPPs should provision for sufficient time and information for the participation of local suppliers and service providers. Specific tax and subsidy incentives should also be offered as soon as possible in order to attract local participation.

Tariff evolution and CSP incentives

1. A tariff structure allowing for more competition could accelerate the reduction of CSP costs. Increased competition can result from a greater allocation to CSP and/or allowing CSP to compete for allocation to other generation types. This recommendation calls for the IRP process to evolve from a prescriptive plan to a plan guided by analysis of needs and available technologies but where allocation of power generation is open to the market. However this might take shape, the following specific recommendations for CSP tariffs are a result of the sensitivity study of the PhD.

    a. Tariff level 1: A base tariff for power generation independent on demand or technology. This tariff would follow LCOE of lowest cost options which are presently wind and PV.

    b. Tariff level 2: Adjustments based on CO_2 taxes or other externality costs in order to provide true cost parity from a global point of view.

    c. Tariff level 3: An incentive tariff to produce power during times of high demand as is presently offered in the REIPPPP. This tariff is intended to provide bankability for CSP projects and should be based on the cost of mid-merit or peaking power production. It is assumed that an IPP will strive to achieve an investible NPV (net present value).

    d. Tariff level 4: An additional incentive for low residual demand times which are typically not possible to forecast due to the intermittence of other renewable generators or other contingencies. The tariff level can be linked to the cost of last-resort generators and MVOE analysis. IPPs and DOE (as the centralized decision maker) can use MVOE analysis to determine location, sizing and proportioning of projects that best serve the system.

2. An alternative or additional recommendation is to allocate CSP capacity to Eskom, the national utility. This recommendation assumes that Eskom would automatically implement and operate CSP to result in the lowest cost system. This recommendation excludes consideration for macroeconomics and the merits of independent vs. public enterprises.